NAA-SR-11492
COPY
160 PAGES

MASTER

SNAP 8 PROGRAM REPORT

MAY – JULY 1965

(Title Unclassified)

AEC Research and Development Report

ATOMICS INTERNATIONAL
A DIVISION OF NORTH AMERICAN AVIATION, INC.

DISCLAIMER

Printed in USA Price $3.45 Available from the

U. S. Atomic Energy Commission
Technical Information Extension,
P. O. Box 1001
Oak Ridge, Tennessee.

Please direct to the same address inquiries covering the procurement of other classified AEC reports.

NAA-SR-11492
SNAP REACTOR,
SNAP PROGRAM
M-3679 (41st Ed.)

21,485

SNAP 8 PROGRESS REPORT

MAY – JULY 1965

(Title Unclassified)

D. G. MASON

ATOMICS INTERNATIONAL

A DIVISION OF NORTH AMERICAN AVIATION, INC.
P.O. BOX 309 CANOGA PARK, CALIFORNIA

CONTRACT: AT(11-1)-GEN-8
ISSUED: SEPTEMBER 30, 1965

DISTRIBUTION

SYSTEMS FOR NUCLEAR AUXILIARY POWER
(SNAP)-REACTOR SNAP PROGRAM
M-3679 (41st Ed.)

	No. of Copies
AEC Patent Office	1
Aerojet-General Corporation (NASA)	6
Aerojet-General Corporation, Sacramento	1
Aerojet-General Nucleonics	1
Aerojet-General Nucleonics (NASA)	1
Aeronautical Systems Division	2
Aerospace Corporation	1
Aerospace Test Wing (AFSC)	1
Air Force Headquarters	1
Air Force Surgeon General	1
Air Force Foreign Technology Division	1
Air Force Weapons Laboratory	3
Air University Library	1
AiResearch Manufacturing Company, Phoenix	1
Allison Division-GMC	1
Argonne National Laboratory	1
Army Ballistic Research Laboratories	1
Army Director of Transportation	1
ARO, Inc.	1
Avco Corporation	1
Battelle Memorial Institute	1
Battelle-Northwest	2
Bendix Corporation (AF)	1
Brookhaven National Laboratory	1
Bureau of Naval Weapons	2
Bureau of Ships	2
California Patent Group	1
Central Intelligence Agency	1
Chicago Patent Group	1
Department of the Army	1
Director of Defense Research and Engineering (OAP)	1
Douglas Aircraft Company, Inc., Newport Beach	1
DuPont Company, Aiken	1
DuPont Company, Wilmington	1
Electro-Optical Systems, Inc.	1
General Atomic Division	1
General Dynamics/Astronautics (AF)	1
General Dynamics/Astronautics (NASA)	1
General Dynamics/Fort Worth	1
General Electric Company, Cincinnati	1
General Electric Company (FPD)	2
General Electric Company (MSVD)	1
General Electric Company, San Jose	1
Hughes Research Laboratories	1
Institute for Defense Analyses	1
Jet Propulsion Laboratory	2
Johns Hopkins University (APL)	1
Lockheed-Georgia Company	1
Los Alamos Scientific Laboratory	1
Martin-Marietta Corporation, Denver	1
Minnesota Mining and Manufacturing Company	1
Monsanto Research Laboratory	1
Mound Laboratory	1
NASA Ames Research Center	1
NASA Goddard Space Flight Center	2
NASA Langley Research Center	1
NASA Lewis Research Center	7
NASA Manned Spacecraft Center	1
NASA Marshall Space Flight Center	1
NASA Scientific and Technical Information Facility	3
National Aeronautics and Space Administration, Washington	2
National Reactor Testing Station (PPCO)	4
Naval Air Development Center	1
Naval Radiological Defense Laboratory	1
Naval Research Laboratory	2
Navy Marine Engineering Laboratory	1
New York Operations Office	1
Nuclear Metals, Inc.	1
Nuclear Weapons Training Center Pacific	1
Oak Ridge Operations Office	1
Office of Naval Research	2
Office of the Chief of Engineers	1
Office of the Chief of Naval Operations	3
Office of the Chief of Naval Operations (OP-03EG)	2
Office of the Chief of Transportation	1
Pratt and Whitney Aircraft Division (NASA)	1
Rand Corporation	1
Sandia Corporation	1
Union Carbide Corporation (ORNL)	8
United Nuclear Corporation (NDA)	1
University of California, Livermore	1
Westinghouse Electric Corporation, Lima	1
Westinghouse Electric Corporation, Lima (AF)	1
Westinghouse Electric Corporation (NASA)	1
White Sands Missile Range	2
Division of Technical Information Extension	10
AI Library (Includes 2 copies to CPAO, 2 copies to AEC, Washington, 2 copies to COO)	116

CONTENTS

CONTENTS

CONTENTS

CONTENTS

TABLES

TABLES

TABLES

FIGURES

FIGURES

FIGURES

FIGURES

FIGURES

ABSTRACT

The previous SNAP 8 Progress Report was "SNAP 8 Progress Report, February – April 1965," C. E. Johnson, NAA-SR-11092 (CRD), issued June 15, 1965.

I. PROGRAM OBJECTIVES

The objectives of the SNAP 8 reactor program are to assemble and test the 600-kwt, 1300°F SNAP 8 reactor and to continue the development of technology to provide a reactor capability at thermal power levels up to approximately 1 Mwt for both manrated and instrument-rated space electric power applications. The SNAP 8 reactor program is being performed for the Atomic Energy Commission (AEC). The performance objectives of the reference design SNAP 8 reactor are summarized in Table 1.

TABLE 1
SNAP 8 REACTOR PERFORMANCE OBJECTIVES

Thermal Power	600 kwt
NaK Outlet Temperature	1300°F
Reactor Operating Period	10,000 hours
Reliability	
Instrument-Rated Reactor	>96%
Manrated Reactor	>99%

II. PROGRESS SUMMARY

A. REFERENCE SYSTEM DESIGN

Layouts of 4π shielded manrated concepts were prepared. Various reflector materials, shield cooling concepts, and reactor-reflector-shield mounting concepts were investigated. The use of liquid lead as a primary gamma shield material in the vicinity of the reactor was also investigated. The concepts using liquid lead and a shaped 4π shield showed significant weight savings.

B. FUEL DEVELOPMENT

The NAA-115-1, NAA-115-2, and NAA-117-1 irradiation tests of sublength SNAP 8 fuel elements continued operation at design conditions at Hanford.

A cladding tube chromizing process capability run was successfully completed. This run demonstrated an ability to maintain the chromized layer within required limits.

Process improvement studies have resulted in 100% improvement in penetration variability in the electron-beam-welded S8DS cup-plug closure.

C. COMPONENT DEVELOPMENT

The platinum resistance temperature detector (RTD) being developed for the NaK temperature sensing system has drifted an equivalent of approximately 2°F after over 8500 hours of endurance testing at 1300°F.

Twelve S8DS design actuators have been operating satisfactorily at S8DS design conditions (1025°F and 10^{-6} torr) for more than 3000 hours. Two of the twelve actuators have been delivered to the Battelle Memorial Institute as a part of the HF-10 irradiation capsule.

A developmental test assembly of the S8DS control-drum drive and scram mechanism has successfully completed 170 simulated scrams and over 2600 hours of endurance under simulated S8DS operating conditions.

D. SYSTEM DEVELOPMENT

1. SNAP 8 Experimental Reactor (S8ER)

The secondary coolant system was drained and disassembled. Disassembly of the primary NaK coolant system external to the reactor containment vessel was completed.

The S8ER fuel elements were removed from the core vessel on July 28, 1965 using the unitized core removal method. The core was transferred without incident to the Atomics International Component Development Hot Cell for disassembly and detailed examination.

2. SNAP 8 Ground Prototype (S8DS)

The final assembly of the S8DS reactor was started June 17, 1965 under "clean room" conditions.

Fabrication of the neutron shield was completed.

Five actuators have been manufactured and two have successfully completed acceptance tests. The remaining three are awaiting testing. Ten limit switches have successfully passed acceptance testing and six are in test. Three scram kits were delivered to the assembly area for acceptance testing. Twelve snubbers successfully passed acceptance testing.

All work on Ground Prototype Test Facility (Building 059) modifications to the vacuum system installation was completed.

III. REFERENCE DESIGN

A. DESIGN DESCRIPTION

1. Instrument-Rated System

The SNAP 8 nuclear system for unmanned applications (Figure 1) consists of a shielded compact nuclear reactor moderated by zirconium-hydride and cooled by liquid NaK-78. The reactor is controlled by movable beryllium reflectors which, by their position, control the amount of leakage flux. Each major assembly of the instrument-rated SNAP 8 nuclear system is described in the following paragraphs. Table 2 lists the detailed characteristics, a weight summary is given in Table 3, and the environmental criteria are summarized in Table 4. The design reliability goal for the instrument-rated nuclear system has been tentatively established at 96.3%.

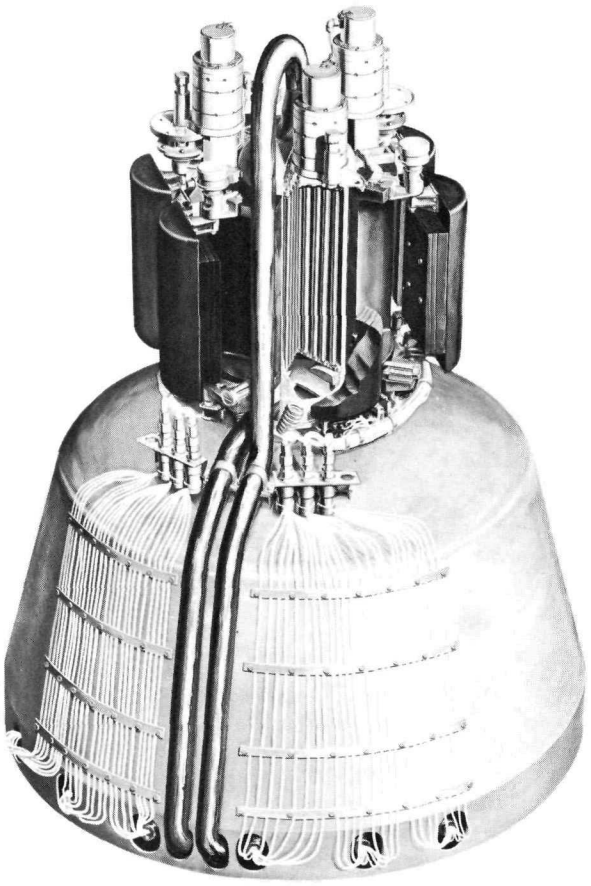

2-9-65 7568-01300-3

Figure 1. SNAP 8 Nuclear System

a. Fuel Elements

The SNAP 8 reactor core contains 211 fuel elements made of Zr – 10.5 wt % U alloy hydrided to a hydrogen content of 6×10^{22} hydrogen atoms/cc of (U-Zr) H_x. The uranium is 93% enriched. The elements are clad in 10-mil-thick Hastelloy-N tubing, coated internally with a hydrogen permeation barrier. The active length of the fuel element is 16.825 in. Other dimensions and characteristics are listed in Table 2.

b. Core Vessel and Internals (less fuel elements)

The core vessel is 0.105-in.-thick stainless steel. The core vessel contains an upper grid plate of 316 SS, a lower grid plate of Hastelloy-C, a coolant baffle plate of 316 SS, internal BeO reflectors clad in 316 SS, and the 211 fuel elements previously descirbed.

c. Instrumentation and Reflector Assemblies

The beryllium control reflector assembly is made in two halves so that it forms a hollow right-circular cylinder completely surrounding the active core length. The beryllium reflector is a nominal 3 in. thick with the ability to shim both positively and negatively 1 in. Each reflector drum is driven by its own drive mechanism. Three reflector drums are used as startup drums and are driven by springs. The other three reflector drums are used as control drums and are driven by long-term bidirectional control-drum actuators. A startup programmer and controller are provided to achieve proper operational sequence of the drums. A platinum resistance temperature sensor is used to measure the coolant outlet temperature.

TABLE 2

SNAP 8 REFERENCE INSTRUMENT-RATED NUCLEAR SYSTEM CHARACTERISTICS

Reactor Design

Fuel Elements	
Number	211
Fuel alloy, wt % U in Zr	10.5
Uranium enrichment, at.% U^{235}	93.15
Degree of hydriding, N_H, 10^{22} a/cm^3	6.05
Fuel rod diameter, in.	0.530
Active fuel length, in.	16.825
Fuel element length, in.	17.145
Cladding material	Hast-N
Cladding ID, in.	0.540
Cladding thickness, in.	0.010
Ceramic barrier material	SCB
Ceramic barrier thickness, in.	0.002
Diametral hydrogen gap, in.	0.006
Source	
Type	Po-Be
Strength, curies	0.1
Location	top head of vessel
Internal Reflectors	
Composition	BeO
Cladding material	316 SS
Cladding thickness, in.	0.030
Inlet Plenum Grid Plate	
Material	Hast-C
Thickness, in.	0.650
Diameter, in.	9.186
Number of coolant holes	372
Diameter of coolant holes, in.	0.156
Pitch of coolant holes, in.	0.570
Outlet Plenum Grid Plate	
Material	316 SS
Thickness, in.	0.850
Number of coolant holes	372
Diameter of coolant holes, in.	0.156
Pitch of coolant holes, in.	0.570
Coolant	
Material	NaK-78
Melting point, °F	12
Core Vessel	
Material	316 SS
Internal diameter, in.	9.214
Thickness, in.	0.105
Length, in.	26.24
Distance between grid plates, in.	17,224
Reflector Control Elements	
Material	Be
Number of startup drums	3
Number of long-term control drums	3
Total number of drums	6
Radius of curvature of drums, in.	4.5
Nominal thickness of drums, in.	3.125
Shimming capability, in.	+1.5, -1.0
Envelope, drums full out, in.	27.6
Overall length, in.	18.5
Drum length, in.	15.375

Reactor Parameters

Design Operating Conditions	
Reactor thermal power, kwt	600
Net electrical power, kwe	35(@ 470 kwt)
Coolant inlet temperature, °F	1100
Coolant outlet temperature, °F	1300
Coolant flow rate, lb/sec	13.6
Operating pressure, psia	45
Core pressure drop, psi	4.8 (@ 600 kwt)
Maximum hot spot fuel temperature °F	1520
Maximum hot spot cladding temperature, °F	1430
Operating lifetime, hr	10,000
Peak heat flux, Btu/hr-ft^2	~100,000
NS pressure drop, psi	<8(@ 600 kwt)
Reactivity Requirements, $	
Xenon	-1.05
Samarium buildup	-1.02
Fission product poison	-1.17
U^{235} burnup	-0.66
Temperature and power defect	-2.15
Hydrogen redistribution	-0.55
Hydrogen loss	-2.00
Contingency	-2.40
Cold Clean Excess Reactivity	*+8.00*
Samarium Burnout	+3.00
Total Control Drum Worth	$21.06
Shutdown Margin	-13.06
Temperature Coefficients, ¢/°F (at design power level)	
Spectrum	-0.01
Axial expansion	-0.048
Upper grid plate	-0.026
Lower grid plate	-0.019
Reflector (prompt, lower plenum)	-0.04
Reflector (prompt, upper plenum)	-0.04
Total isothermal (@1200°F)	-0.20
Total isothermal (@ room temperature)	-0.15
Nuclear Parameters	
Average thermal neutron flux <1 ev, n/cm^2-sec	3 x 10^{12}
Median fission energy, ev	0.21
Mean prompt neutron lifetime, μ-sec	8.4
Uranium loading, kg U^{235}	7.65
Hydrogen reactivity worth, %Δk/k per %Δ H/H	0.50
Volume fractions in core	
Fuel	0.782
Cladding	0.061
NaK	0.123
Ceramic	0.013
Void	0.021
Radial peak to average power	1.22
Axial peak to average power	1.44
Average power density, watts/cc	36.6
Reliability Goals, %	
Overall	96.85
Core assembly	98.96
Reflector assembly	98.50
Shield assembly	99.97
Safety assembly	99.44
Cumulative Probability of Success	
Through launch	99.74
Through startup	98.87
Through 10,000 hours	97.23
Complete mission	96.85
Nonpuncture probability	99.9
Control System Parameters	
Single control drum worth, $	3.90
Full-in drum position, degrees	0
Full-out drum position, degrees	154
Drum movement per step, degrees	0.26
Maximum drum rotation rates, degrees/sec	
Startup drums (simultaneous motion)	0.086
Control drums	0.053
Maximum differential drum worth, ¢/degree (nominal shim)	7.0
Kinetic Parameters	
Number of delayed neutron groups	6
Decay constants, sec^{-1}	
$\lambda 1$	0.0124
$\lambda 2$	0.0305
$\lambda 3$	0.111
$\lambda 4$	0.301
$\lambda 5$	1.13
$\lambda 6$	3.0
Effective delayed neutron fraction	0.0080
Group delayed fractions	
$\alpha 1$	0.0329
$\alpha 2$	0.2194
$\alpha 3$	0.1960
$\alpha 4$	0.3947
$\alpha 5$	0.1150
$\alpha 6$	0.0419
Transport delay times (@ 35 kwe), sec	
Nuclear system to boiler	1.0
Boiler	6.8
Boiler to nuclear system	4.5
Nuclear system	1.7

Typical Shield Parameters

Instrumented Payload Dimensions	
Diameter, ft	20
Axial distance from reactor core center, ft	40
Shield Materials	
Cladding	347 SS
Gamma	W
Neutron	LiH
Shield Dimensions	
Overall shield length, in.	34.3
Neutron shield thickness, in.	33.3
Gamma shield thickness, in.	1.0
Maximum diameter of conical shield, in.	51.5
Minimum diameter of conical shield, in.	39.2
Radiation Levels Due to Reactor Sources	
Fast neutron dose at payload, nvt	1 x 10^{11}
Gamma dose at payload, rads (C)	1 x 10^6
Shield Assembly Weight, lb	
Neutron shield	1365
Gamma shield	115
Shield vessel and structure	450
Total shield assembly weight without armor	1930

7-23-65

7568-01790c

TABLE 3

SNAP 8 NUCLEAR SYSTEM WEIGHT SUMMARY

System Component	Quantity	Weight Per Item* (lb)	Total Weight (lb)	Center of Gravity† (in.)		
				X	Y	Z
Core Assembly	1	-	310.3	26.0	0.0	0.0
Core vessel	1	45.2	45.7	24.5	0.0	
Outlet plenum grid plate	1	5.9	5.9	16.1	0.0	
Fuel elements	211	0.8	193.9	25.1	0.0	
Internal reflectors	42	-	12.0	25.0	0.0	
Inlet plenum grid plate	1	6.5	6.5	33.4	0.0	
Flow baffle plate	1	7.0	7.0	34.6	0.0	
Inlet NaK pipe (16 in. long)	1	1.8	1.8	40.0	13.5	
Outlet NaK pipe (54 in. long)	1	8.4	8.4	25.0	10.0	
NaK in vessel	-	18.7	18.7	26.9	0.0	
NaK in pipe	-	10.4	10.4	27.9	11.2	
Reflector Assembly	1	-	284.6	22.8	+ 0.1	
Control drum actuators	3	20.0	60.0	11.5	0.0	
Startup drum drives	3	0.8	2.4	14.0	0.0	
Reentry actuator assembly	1	6.0	6.0	16.5	-11.2	
Upper drum support assemblies	6	2.0	12.0	16.5	0.0	
Fixed external reflectors	2	22.5	45.0	25.0	0.0	
End-of-life shutdown actuator	1	1.8	1.8	16.5	11.2	
Control and startup drums	6	19.9	119.5	25.0	0.0	
Shear and load lugs	8	1.0	8.0	31.2	0.0	
Drum release actuators	6	0.6	3.6	33.5	0.0	
Lower drum support assemblies	6	2.0	12.0	33.8	0.0	
Reflector ejection springs	4	1.0	4.0	36.0	0.0	
Drum position indicators	3	0.5	1.5	36.4	0.0	
Drum key lock brackets	4	0.9	3.6	15.3	0.0	
Miscellaneous brackets and fittings	-	-	5.2	34.9	0.0	
Shield Assembly	1	1930	1930	58.1	+ 0.3	
Miscellaneous						
Supplemental reflector drum shims	6	6.2	37.1	25.0	0.0	
Environmental cover	1	~65	~65	~44	0.0	0.0
Payload instrumentation	-	~17	~17	-	-	-
Diagnostic instrumentation	-	~50	~50	-	-	-
Interconnecting cables	-	~20	~20	~44	-	-

*Weight expressed to the nearest 0.1 lb

†X axis — is the centerline of the nuclear system. X = 0 is a point 25.000 in. forward of the midpoint between the upper and lower grid plates. The positive direction is toward the nuclear system.

Y axis — is perpendicular to the X axis with the positive direction being toward the side of the reactor where the coolant outlet pipe crosses over the side of the reactor.

Z axis — is orthogonal to the X and Y axes with the positive direction being 90° clockwise from the positive Y axis when viewing the nuclear system from the reactor end.

TABLE 4

SNAP 8 NUCLEAR SYSTEM ENVIRONMENTAL CRITERIA
(Page 1 of 2)

Environment	Ground Handling and Prelaunch*	Launch†	Orbit§
1. Pressure	External pressures: sea level to 50,000 ft with maximum change ±1.25 psi/min.	External static pressure envelope as a function of time. (To be determined)	External pressure: 10^{-12} mm Hg
2. Temperature	+50 to +160°F	-	-
3. Humidity	a. Protected during shipment and storage (RH <70%)** b. During vehicle integration: 6 hr at 65% RH and 106°F; 6 hr of decreasing temperature to 91°F and increasing RH to 100%; 8 hr of decreasing temperature to 81°F with release of 4.4 grains H_2O/ft^3; 4 hr of increasing temperature to 106°F and decreasing RH to 50%	-	-
4. Rain	a. Protected during shipment and storage b. During vehicle integration: Anticipated precipitation Rate (in./hr) / Amount (in.) / Time 0.6 / 7.1 / 12 hr 6 / 0.5 / 5 min 12 / 0.2 / 1 min 0.34 / 4.0 / 12 hr	-	-
5. Sand and dust	a. Protected during shipment and storage b. Applicable components tested with 140-mesh silica flour for 3 hr at 77°F and RH <30%; sand and dust density, 0.1 to 0.25 grams/ft^3, with air velocity = 2500 ± 500 ft/min	-	-
6. Salt spray	a. Protected during shipment and storage b. Applicable components tested to demonstrate ability to withstand exposure to salt spray for 6 wk as experienced at coastal regions of continental U.S.A.	-	-
7. Fungus	Applicable components tested per MIL-E-52720(ASG), Fungus Resistance Tests, Procedure 1.	-	-
8. Shock	Drop of 18 in. measured at either a corner or a surface, onto a concrete surface.	System Three shocks of 18 g's in each of 3 mutually perpendicular axes (18 total) of one of the following pulses: a. Triangular pulse 10 msec b. Half-sine pulse 8 msec c. Rectangular pulse 5 msec Component: Three shocks of 35 g's in each of 3 mutually perpendicular axes (18 total) of one of the following pulses: a. Triangular pulse 10 msec b. Half-sine pulse 8 msec c. Rectangular pulse 5 msec	Nonoperating††: capable of withstanding 3-g shocks on each of 3 mutually perpendicular axes at one of the following wave forms: a. Triangular pulse 10 msec b. Half-sine wave pulse 8 msec c. Rectangular pulse 5 msec Operating: withstand 3-g peak, half-sine wave pulse of one msec at mounting interface

TABLE 4

SNAP 8 NUCLEAR SYSTEM ENVIRONMENTAL CRITERIA
(Page 2 of 2)

Environment	Ground Handling and Prelaunch*	Launch†	Orbit§
9. Vibration	Sweep applied to transportation container on 3(30-min log) mutually perpendicular axes: 2 to 5 cps at 1 in. double amplitude; 5 to 27.5 cps at 2-g peak; 27.5 to 43.5 cps at 0.0517 in. double amplitude; 43.5 to 500 cps at 5-g peak; then a 5-min dwell at each resonant frequency noted at above amplitude	System Sweep from 5 to 16 cps at 0.368 in. double amplitude and 16 to 2000 cps at 5-g peak on each of 3 mutually perpendicular axes; then 5-min dwell at each major resonant frequency at the above amplitude Component 16 to 100 cps at 6-g peak; 100 to 180 cps at 0.0118 in. double amplitude; 180 to 2000 cps at 19-g peak; then dwell at 1/2 above amplitude for 5 min at each major resonant frequency Random Vibration – Components A random vibration sweep test over a frequency interval of 20 to 2000 cps for 5 min in each of 3 mutually perpendicular axes according to the following schedule: 20 to 200 cps at +2 db/oct 200 to 700 cps at 0.64 g^2/cps 700 to 900 cps at -17.5 db/oct 900 to 2000 cps at 0.15 g^2/cps	Capable of withstanding vibrations of 0.25-g peak over a frequency of 5 to 2000 cps for 5 min at the NS mounting interface
10. Wind	Withstand steady-state wind force of 54 mph with wedge-shaped gusts of 75 mph	-	-
11. Storage life	Two years (except source)	-	-
12. Radio frequency generation and interference	-	Designed and tested to MIL-STD-826 (USAF) dated 20 January 1964	Designed and tested to MIL-STD-826 (USAF) dated 20 January 1964
13. Acoustic noise	-	Total integrated sound pressure level of 148 db, Re 0.0002 microbar over a specific frequency spectrum	-
14. Acceleration	-	Longitudinal axis: +7 g for 5 min, -3 g for 5 min; lateral and normal axes: ±4.5 g for 5 min	Operating: +1 g along axis of symmetry and ±1/4 g radially including rotational effects Nonoperating:†† +3-1/2 g along longitudinal axis in combination with ±1 g on any lateral axis for a period of time less than 5 min
15. Magnetic fields	-	-	To be determined
16. Gravitational fields	-	-	To be determined
17. External radiation	-	-	To be determined

*Environment to which the nuclear system may be subjected without any detrimental effects during shipment from Atomics International up to the time of encapsulation in the launch vehicle nose cone
†Environment to which the nuclear system may be subjected without any detrimental effects after exposure to the ground handling and prelaunch environment up to the time of separation from the launch vehicle
§Environment to which the nuclear system may be subjected without any detrimental effects after exposure to the launch environment
**RH = Relative humidity
††Nonoperating: Defined as prohibiting operation of the reflector-control system; i.e., control drums are held stationary

d. Shield

A typical neutron shadow shield designed to limit the dose at the payload is in the shape of a truncated cone whose cone angle completely hides the payload from the reactor assembly. The neutron shield is made of lithium hydride (LiH) cast in a stainless-steel container. Between the neutron shield and the reactor assembly is a circular plate of tungsten designed to limit the gamma dose at the payload. The design parameters for a typical 600-kwt shield are given in Table 2.

e. Safety System

The safety system includes a reentry actuator, reflector ejection springs, a destruct charge, an end-of-life scram actuator, a telemetry scram actuator, a reflector unlocking actuator, and associated circuitry. In addition, void filler blocks and a drum lockout system are furnished as part of the ground handling safety equipment.

The reentry actuator is designed to hold the reflector assembly in place at the top of the core vessel. The actuator is designed and located so that it will be melted by reentry heat. Heating of this actuator allows the reflector ejection springs to remove the reflector assembly from the vicinity of the core vessel.

The destruct charge is a shaped explosive charge surrounding the core vessel. It can be fired prior to reactor startup to preclude reactor criticality in the event of an unsuccessful launch. The destruct charge is optional and its use will be evaluated for each particular mission.

The reflector unlocking actuator is designed to hold the reflector assembly to the core vessel during launch. Thus, it is not necessary for the reentry actuator assembly to hold the reflector assembly under launch conditions.

The void filler blocks are neutron poison blocks designed to be slipped into the cavities in the stationary beryllium reflector normally occupied by the reflector drums when in their full-in position. The drum lockout system is a key-operated locking system designed to prevent reflector drum motion.

An environmental cover is supplied to protect the nuclear system from the natural environments, e.g., rain, sand, and dust. The cover, using a side ejection concept, is supported from the base ring of the shield. View ports are provided for access to the pinpullers and the key locks. The cover is made of 5-mil aluminum honeycomb. The destruct charge, if used, is mounted on the cover and is ejected with the cover once startup is initiated.

B. MANRATED SYSTEM

Design concept studies were continued on both the shadow-shielded and 4π-shielded system concepts. These studies are based on the following basic criteria:

Reactor thermal power	600 kilowatts
Reactor coolant temperatures	Inlet 1100°F, outlet 1300°F
Reactor life	10,000 hours to 3 years
Reactor control method	Rotating control drums
Radiation shadow diameter at payload	60 ft diameter at 150 ft from core
Radiation dose rate	Within shadow zone at payload - 1.5 mrem/hr; elsewhere - 100 rem/hr (4π-shielded cases only).

The goal of these studies is to design a single reactor and reflector system concept which can be used with both shadow-shielded and 4π-shielded system configurations.

1. Shadow-Shielded Concept

The most recent shadow-shielded concept is shown in Figure 2. It is designed for a 10,000-hour life. The major assemblies are described below.

a. Core and Vessel Assembly

The core assembly internals are identical to those of the instrument-rated design. These components are mounted within a 316 stainless-steel vessel. At the upper end of the vessel, four pipes supply NaK at 1100°F which flows toward the shadow shield and out at 1300°F through four pipes connected to the lower end of the vessel. A baffle plate at the inlet provides the proper flow distribution. Also attached to the shield end of the vessel are brackets which support the reflector assemblies.

b. Reflector Assemblies

Eight tapered control drums and eight filler pieces, all made of beryllium, surround the reactor vessel. Each drum is a portion of a truncated cone with a flat surface 1/4 inch from and parallel to its axis. The drum thickness at the core midplace is about 3-1/4 inches. The filler pieces are of irregular cross section as required to fill in the spaces between control drums.

Each control drum is driven by a step output type of actuator in 1/4° increments. These actuators are mounted above the core vessel as shown in Figure 2 to place them in the most favorable position for radiation of their heat to space and to eliminate any interference with the piping at the lower end. To minimize radiation scattering to the payload, the actuators are set inward from the drum axes and drive the drums by a suitable gear train. The actuators are also staggered in height to prevent interference. Built into each actuator is a pneumatically powered override device. In the event of an actuator failure, the override device can be energized to drive the control drum to the full-in position, thus making it possible to obtain the full reactivity contribution of that drum for the reactor operation. Since the control drum actuator is reversible, no "scram" action is provided. Shutdown is accomplished by driving the drums to their full-out position. Shutdown can be accomplished by driving out only four drums.

c. Control Instrumentation

The reference design instrument-rated control concept is used because of its simplicity and inherent reliability. In this concept, reactor coolant outlet temperature is sensed and maintained between preset limits (1280 and 1330°F) by means of an on-off digital control system. In a manrated system, however, the circuitry is simplified by eliminating certain memory functions and made more flexible by the addition of manual overrides.

d. Shield Assembly

The shield must provide attenuation of the gamma and neutron radiation from the reactor to an acceptable level for both equipment and men. Since the shield is the largest contributor to the total weight of the nuclear system, its design and material must be optimized.

The shadow shield is separated into two sections by the primary loop gallery. Primary loop components such as the pumps and heat exchangers will be located in this gallery. The section of the shadow shield nearest the reactor provides the necessary shielding to prevent activation of the secondary loop coolant as it circulates through the equipment in the primary loop gallery. The second section of the shield, together with the first section completes the shielding necessary to protect the spacecraft and astronauts.

Each section of the shadow shield contains two regions, a gamma shield of tungsten or

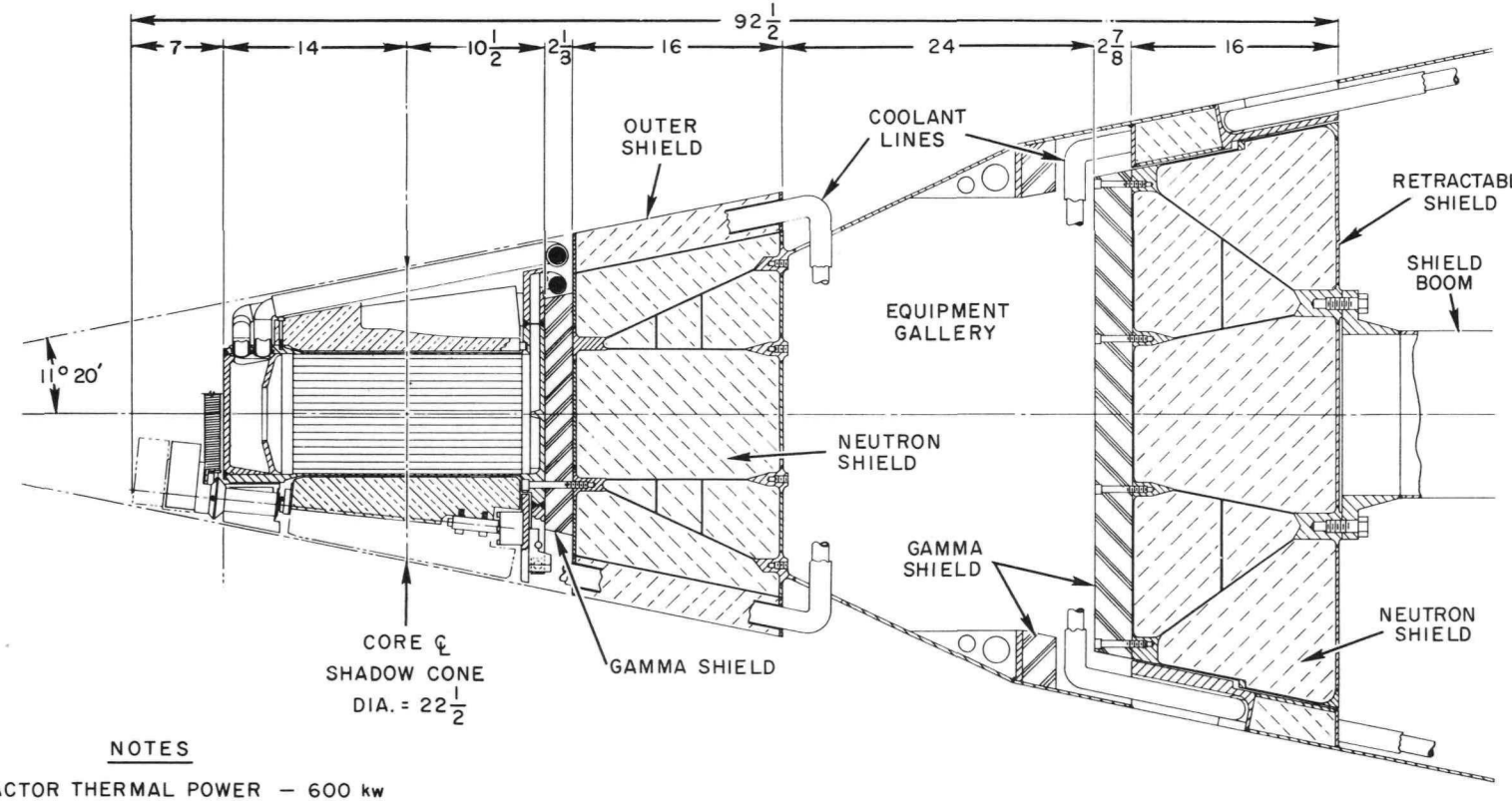

NOTES

1. REACTOR THERMAL POWER — 600 kw
2. RADIATION SHADOW CONE DIA = 60 ft @ 150 ft. FROM CORE ℄
3. RADIATION DOSE RATE = 1.5 mr / hr @ 150 ft FROM CORE ℄

8-2-65

7568-02314

Figure 2. SNAP 8 Manrated Shadow-Shielded Nuclear System Concept

depleted uranium and a neutron shield of lithium hydride. For minimum overall shield weight, the thickness and the material of each gamma and neutron shield region are optimized.

The primary and secondary coolant pipes are routed through the outer periphery of each section. In each case, the outer peripheral portion forms a meteorite protective shell. Thus, the main part of each shield section is well protected from meteorite bombardment. The loss of hydrogen from the outer peripheral portion due to meteorite puncture of the shield skin will not adversely affect the overall shielding capability.

A typical manrated shadow shield assembly weighs approximately 5135 lb. It shields a 60-ft-diameter payload located 150 ft from core center to 1.5 mrem/hr when the reactor is operating at its rated power of 600 kwt.

2. 4π-Shielded Concepts

Since any 4π-shielded nuclear system will be much heavier than a comparable shadow-shielded system there is a larger incentive to increase the design life of the reactor. Current designs are based on a 3-year (26,300 hr) life.

At the present time, two different reflector and control drum designs are being considered concurrently. One design uses conical beryllium drums similar to those used on the shadow-shielded design. The other uses cylindrical, beryllium-oxide, poison-backed drums. Nine different conceptual designs have been made. The two latest ones are shown in Figures 3 and 4. Brief descriptions of the major assemblies of each design are given below.

a. Core and Vessel Assembly

In order to achieve the 3-year operating life, the number of fuel elements has been increased from 211 to 241 and the active fuel length has been increased by about one inch. As noted in Section III-C-1 the spacing of the fuel elements is varied to minimize both the coolant pressure loss and the reactivity loss. Eight pipes carrying 1100°F NaK are connected to the top end of the vessel. A baffle plate in the upper plenum provides the proper flow distribution. The NaK flows downward through the core, into the lower plenum, and out at 1300°F through eight pipes. Heavy fins attached to the inlet (1100°F) NaK pipes surround the entire reflector assembly and form a "cold wall" which absorbs the heat radiated from both the reflector assembly and the inner surface of the shield.

b. Reflector Assemblies

In the conical drum design (Figure 3) the drums and filler pieces are made of beryllium and are similar in shape to those described for the shadow-shielded design. The principal differences are that they are slightly longer and the midplane thickness has been increased to 4 inches.

In the cylindrical drum design the filler pieces are made of beryllium oxide and the 4-inch-diameter drums are composites of 2.8 inches of beryllium oxide, 0.4 inch of nickel alloy (Inconel-X), and 0.8 inch of boron carbide. The drums are clad in metal as a precaution against flaking or powdering resulting from radiation damage.

In both cases, the drums and filler pieces are supported from the reactor vessel. The actuators used are the same as those described earlier for the shadow-shielded design.

c. Shield Assembly

In initial design studies on 4π-shield concepts, either tungsten or depleted uranium were used for gamma shielding. Both of these materials produce a large number of high energy gammas due to neutron capture, resulting in a significant increase in the gamma dose level at the payload. To alleviate the secondary gamma problem, designs using lead contained in

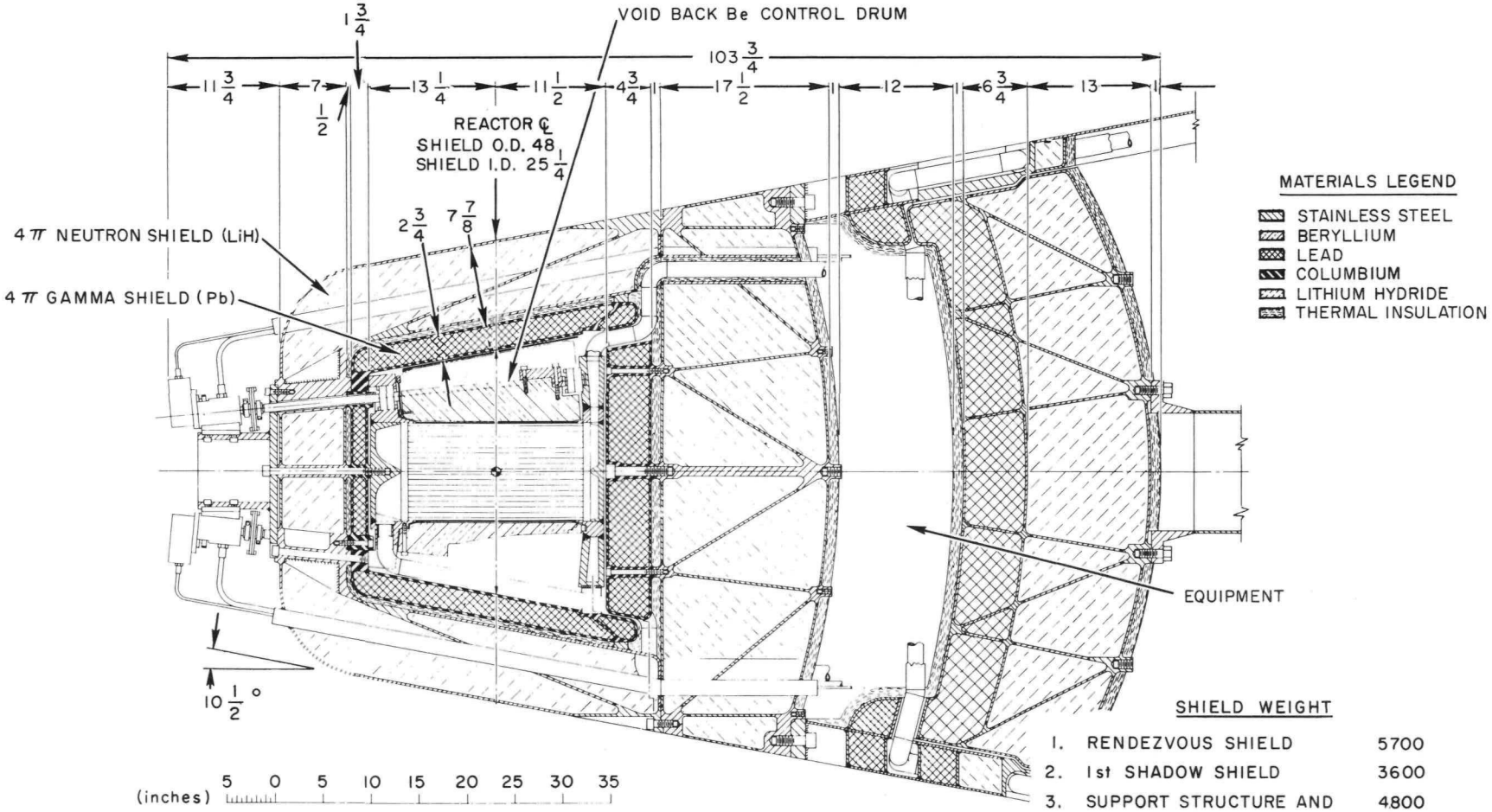

Figure 3. SNAP 8 Manrated 4π-Shielded Nuclear System Concept with Void Back Control Drum

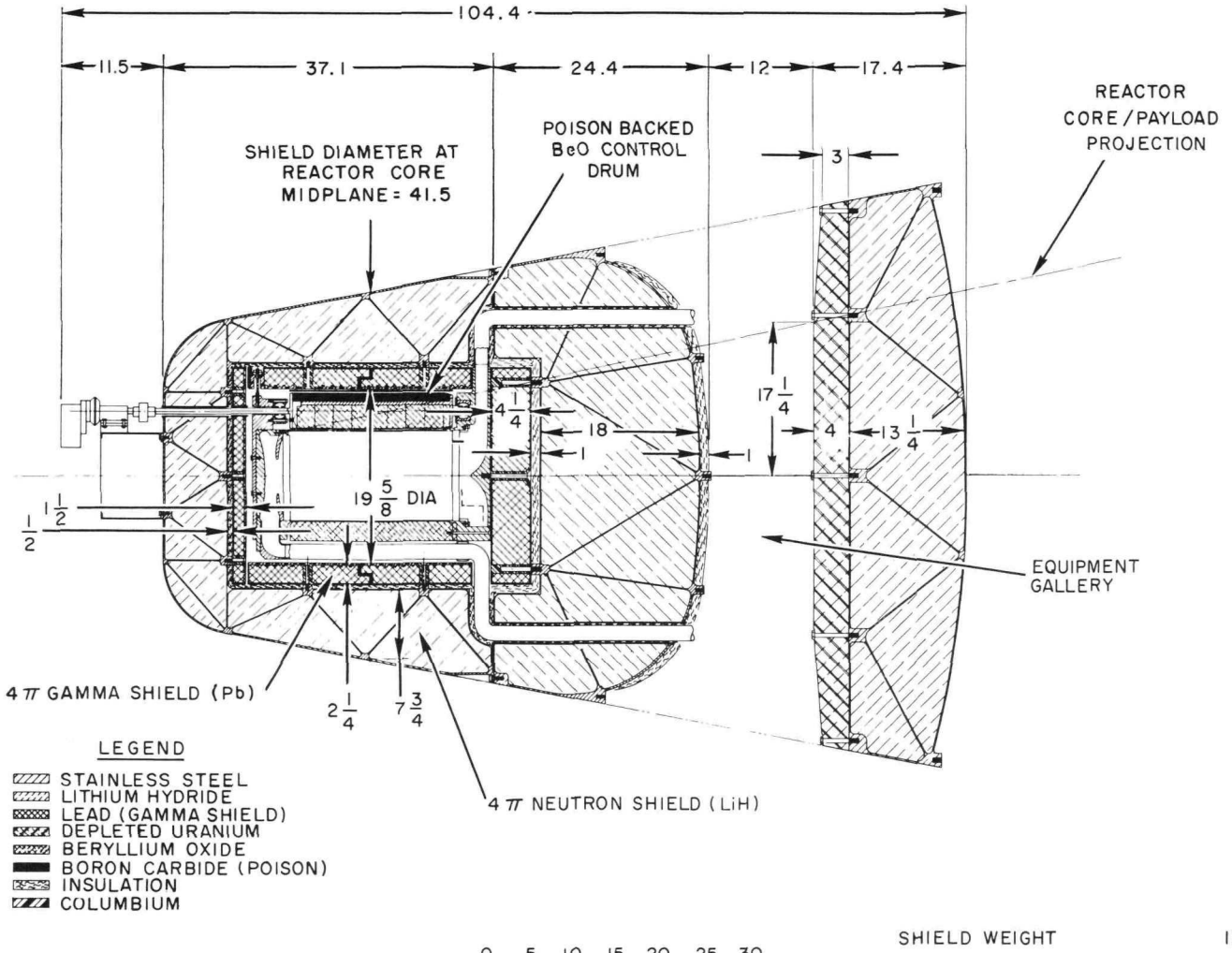

Figure 4. SNAP 8 Manrated 4π-Shielded Nuclear System Concept with Poison-Backed Control Drum

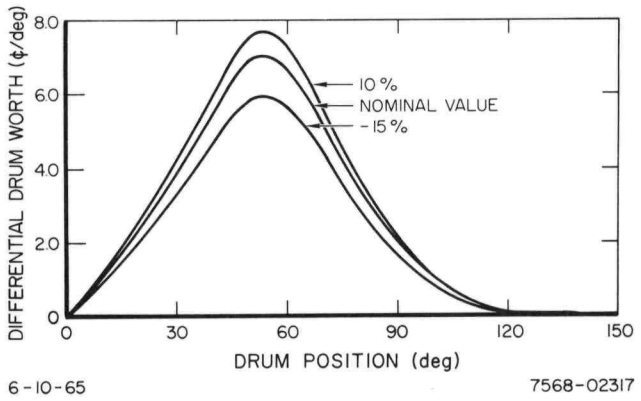

Figure 5. S8DS Differential Drum Worth vs Drum Position, 3.125-in.-Thick Drum

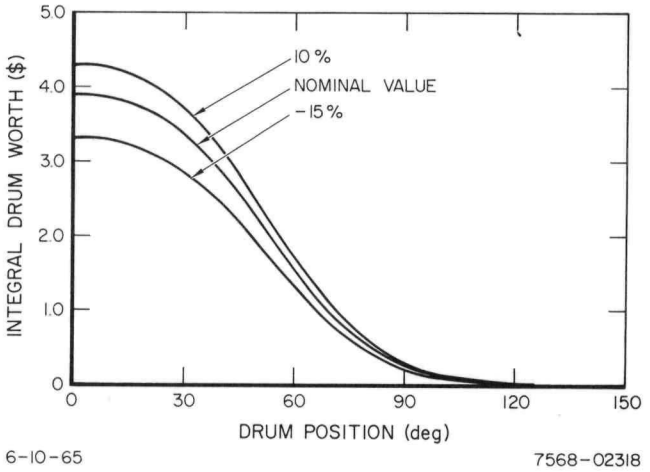

Figure 6. S8DS Integral Drum Worth vs Drum Position, 3.125-in.-Thick Drum

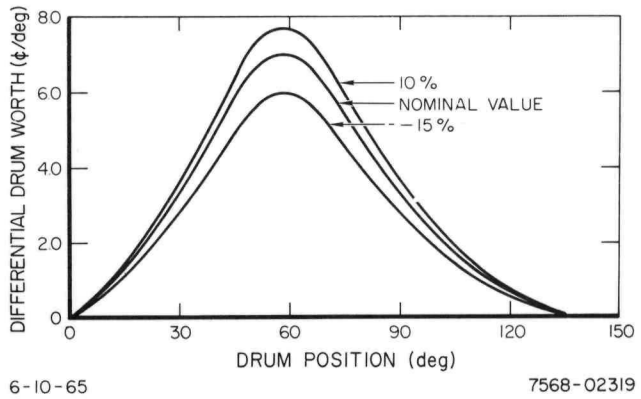

Figure 7. S8DS Differential Drum Worth vs Drum Position, 4.125-in.-Thick Drum

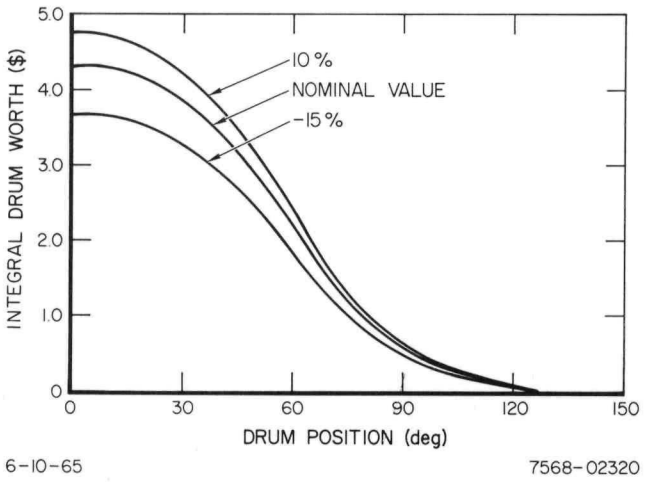

Figure 8. S8DS Integral Drum Worth vs Drum Position, 4.125-in.-thick Drum

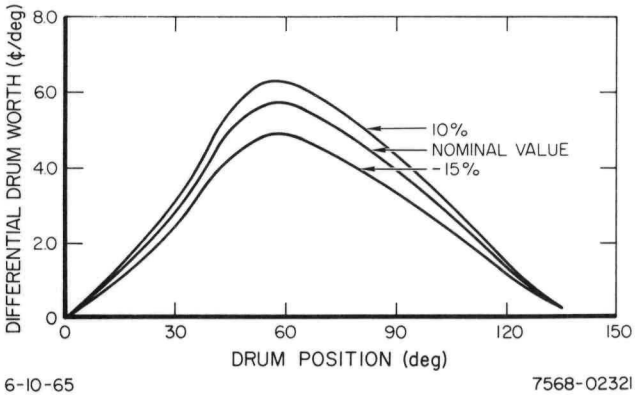

Figure 9. S8DS Differential Drum Worth vs Drum Position 5.125-in.-Thick Drum

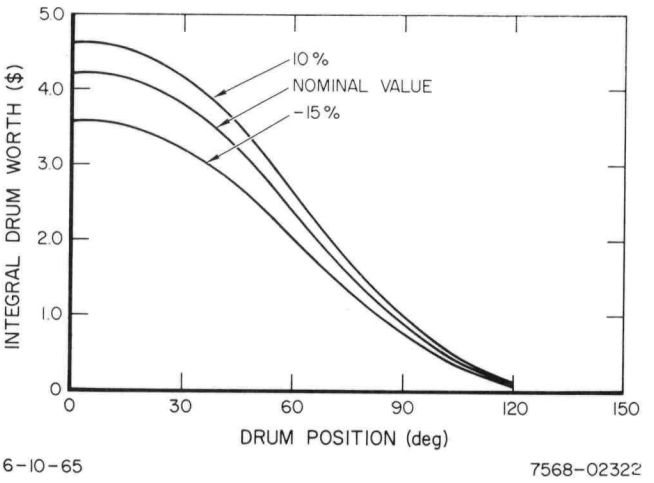

Figure 10. S8DS Integral Drum Worth vs Drum Position, 5.125-in.-Thick Drum

columbium have been investigated. Preliminary results indicate there may be a significant weight saving in this latter 4π-shield design concept.

It will be noted that in the conical drum design the lithium hydride thickness in the side portion of the rendezvous shield is uniform, whereas, in the cylindrical drum design the thickness varies from thick at the bottom to thin at the top. In both cases the shielding is designed for a somewhat arbitrary but reasonable midplane dose rate of 100 rem/hr at 100 ft from the reactor centerline. Since the core neutrons contribute only about 20% of this dose rate, moderate variations in the neutron dose rate resulting from the lithium hydride thickness variation do not affect the preliminary studies.

The temperature of the lead immediately surrounding the reactor is well above its 621°F melting temperature and probably sufficiently high that a columbium (or tantalum) containment shell is required rather than a steel shell that would be adequate at a more moderate temperature. Lithium hydride temperatures are below the melting point of 1270°F.

C. ANALYSIS

1. Nuclear Analysis

a. SNAP 8 Control-Drum Worths

The expected control-drum worths of the S8DS are shown in Table 5 for various possible shim configurations. Calculations were based on measurements obtained from the SNAP Critical Assembly 4A (SCA-4A)* modified to account for geometrical and compositional differences. The values are estimated to have a maximum error band of ±10%.

TABLE 5

SNAP 8 CONTROL-DRUM WORTH FOR VARIOUS SHIM CONFIGURATIONS

Drum Thickness (in.)	Drum Worth ($)
3.125	3.90
4.125	4.31
5.125	4.20

Experimentally obtained integral and differential drum worths as a function of drum position for the three shim configurations are shown in Figures 5 through 10.

b. Effect of Nickel in Stationary Reflectors (Manrated System)

Calculations were made to determine the reactivity loss associated with using a structurally stronger material for the stationary reflector pieces to strengthen the reflector. Substitution of nickel for canned BeO in the stationary reflector pieces of a tapered drum design concept results in a loss of $2.50 in reactivity.

c. Relative Worths of Various Reflector Materials (Manrated System)

The relative worth of various reflector materials for manned applications; e.g., nickel, beryllium, and varying densities of canned beryllium oxide was determined. Unclad beryllium was found to be the most effective reflector for all thicknesses of interest. Nickel was found to be the least effective and beryllium oxide of intermediate value. Although previous studies have shown pure BeO of full theoretical density to be superior to beryllium, the studies revealed that the canned BeO of lower density is less effective than beryllium. The results are shown in Figure 11.

*NAA-SR-11092, C. E. Johnson, "SNAP 8 Progress Report, February-April 1965," June 15, 1965, pp 23-25

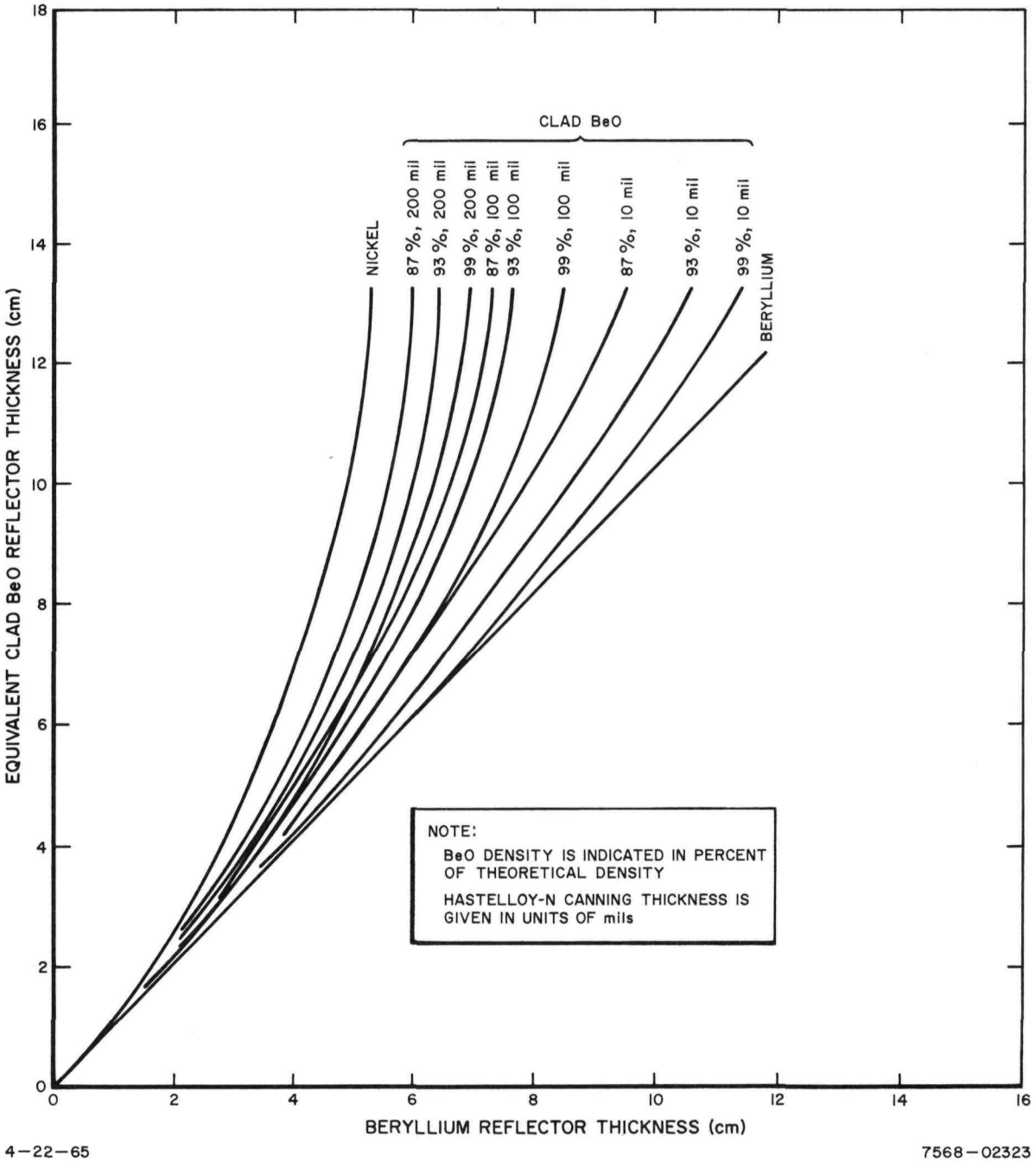

Figure 11. Clad BeO Reflector Thickness vs Thickness of Beryllium Reflector with Equal Reactivity

d. Fuel Element Spacing in Manrated SNAP 8 System

The reactivity penalty associated with increasing the fuel element spacing to decrease the NaK pressure drop across the core was calculated. The reactivity loss as a function of fuel element spacing is shown in Figure 12. Because of the amount of reactivity loss, a study was made with 30-mil spacing in the inner five rings of fuel elements and 10-mil spacing in the outer three rings. The resultant reactivity penalty was -$1.27. The same reactivity loss would be associated with a uniform spacing of about 20 mils throughout the core.

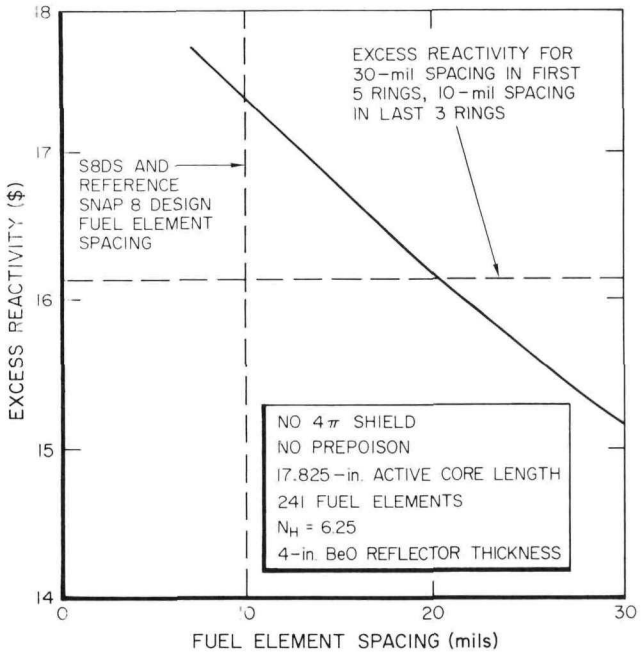

Figure 12. Excess Reactivity of Manrated SNAP 8 Reactor vs Fuel Element Spacing

e. Reactivity Requirements for Manrated SNAP 8 System

The reactivity requirement for a manrated 600-kwt SNAP 8 reactor for a lifetime of three years has been calculated to be $17.15. The system utilized a tritium-helium inherent shutdown device. Table 6 shows the contributions to the required reactivity.

TABLE 6

REACTIVITY REQUIREMENTS OF THE MANRATED SNAP 8 REACTOR FOR A 3-YEAR LIFETIME AT 600 kwt

Hydrogen Loss	$ 4.15
Tritium-Helium Shutdown	2.50
Xenon Buildup	0.90
Samarium Buildup	1.20
Fission Product Buildup and Uranium Burnout	3.85
Hydrogen Redistribution	0.60
Temperature and Power Defect	2.15
Minimum Contingency	1.80
Total	$17.15

f. Worth of Manrated 4π Shield

The reactivity worth of the 4π shield proposed for the manrated SNAP 8 reactor was calculated using a combination of one-dimensional-transport-theory calculations and an albedo technique. The maximum worth of the shield was found to be $1.50 when placed against the reflector. This is in general agreement with experiments performed on the SNAP Critical Assembly (SCA-4A). The variation of the shield worth as it is moved away from the reactor is shown in Figure 13. The two curves in the figure were calculated using geometrical view factors for an infinite cylinder and a sphere. Both curves are normalized to a total shield value of $1.50. It is expected that the actual worth would be within the values shown by the two curves.

g. Worth of Poison-Type Control Drums for Manrated SNAP 8 System

A control-drum configuration of eight poison-backed beryllium control drums has been found to provide adequate control for a manrated 4π shielded SNAP 8. Preliminary calculations showed the eight drums to be worth $15.50. B_4C was selected as the poison material for studies of the optimum ratio of poison thickness to drum diameter.

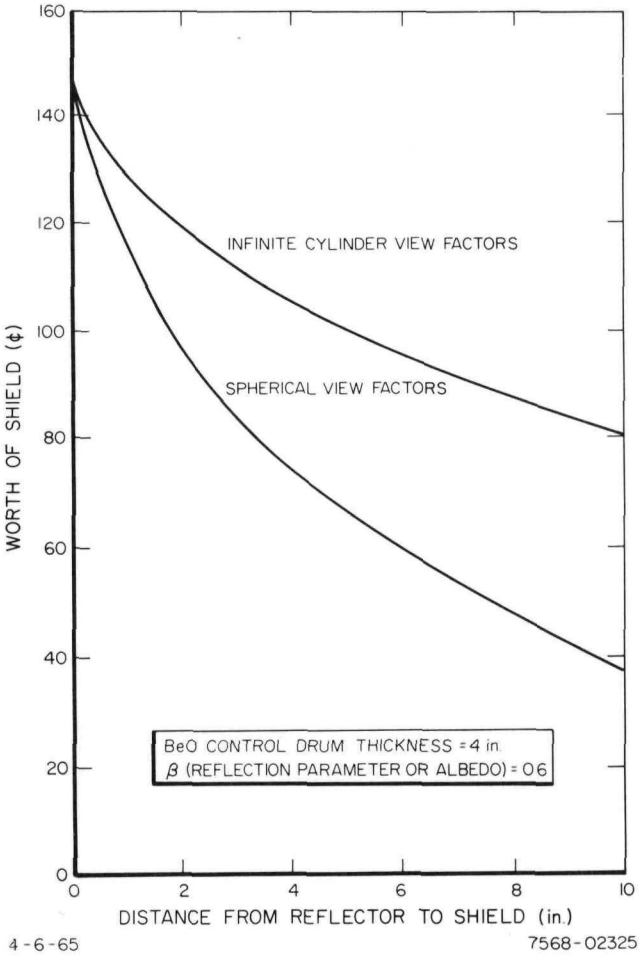

Figure 13. Variation of 4π Shield Worth with Location

2. Thermal Analysis for Manrated 4π-Shielded SNAP 8 System

The steady-state operating temperatures of the SNAP 8 manrated 4π-shielded system was determined. Figure 14 shows a typical design. The design point of reactor operation is 600 kwt with 1100°F inlet and 1300°F outlet coolant temperatures. The neutron control drum contains BeO and B_4C in a Inconel container. The tungsten gamma shield generates ~80 to 90% of the heat released in the shield. The LiH neutron shield temperature limitation was set at 1000°F to provide an adequate margin from its 1270°F melting temperature. Thermal insulation separates the high temperature tungsten from the LiH.

Cooling of the shield is accomplished by routing the primary coolant through pipes, containing aluminum fins, located between the neutron control drums and the tungsten shield as shown in Section A-A of Figure 14. In Figure 15, the expected maximum neutron reflector temperatures for the reactor operating at design conditions are indicated. With the tungsten thermally insulated from the LiH neutron shield, the maximum LiH temperature for 600-kwt core operation in a nominal zero °F space temperature is about 800°F. This maximum temperature occurs at the centerline of the first shadow shield nearest the reactor.

3. Control Analysis

The UPSTART digital system simulation program is being developed for analysis of the transient characteristics of reactor systems. The program is composed of self-contained modules which simulate the dynamics of each major component of the reactor and process loops. These components include the reactor core, the controller, the safety system, a liquid-to-liquid counterflow heat exchanger, a three-region boiling coolant heat exchanger, a liquid-to-space-and/or-air heat exchanger, a parasitic load resistor, a thermoelectric pump, and piping segments.

The reactor simulation includes the neutron kinetics and the thermal kinetics of the fuel cladding, and coolant. Two 6-group neutron kinetics calculations are available. The first is an "exact" calculation using the conventional mono-energetic kinetics equations. This calculation would be used for relatively rapid changes in neutron flux levels such as those which would occur in incidents which involve large reactivity insertions. The second neutronics calculation uses an approximation to the exact equations. This approximate equation, which reduces computer time, can be used in slower transients

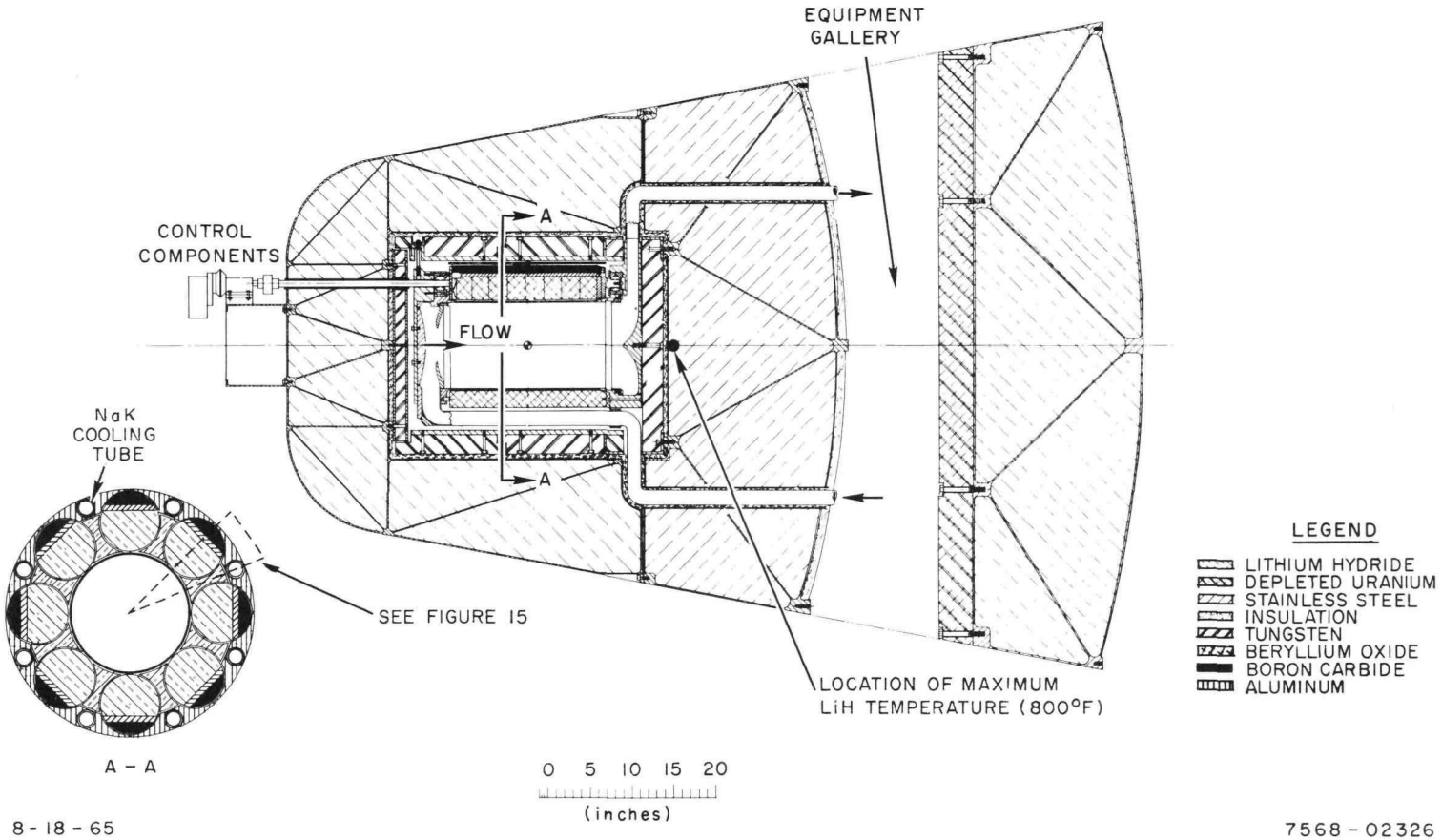

Figure 14. SNAP 8 Manrated 4π Shield Design

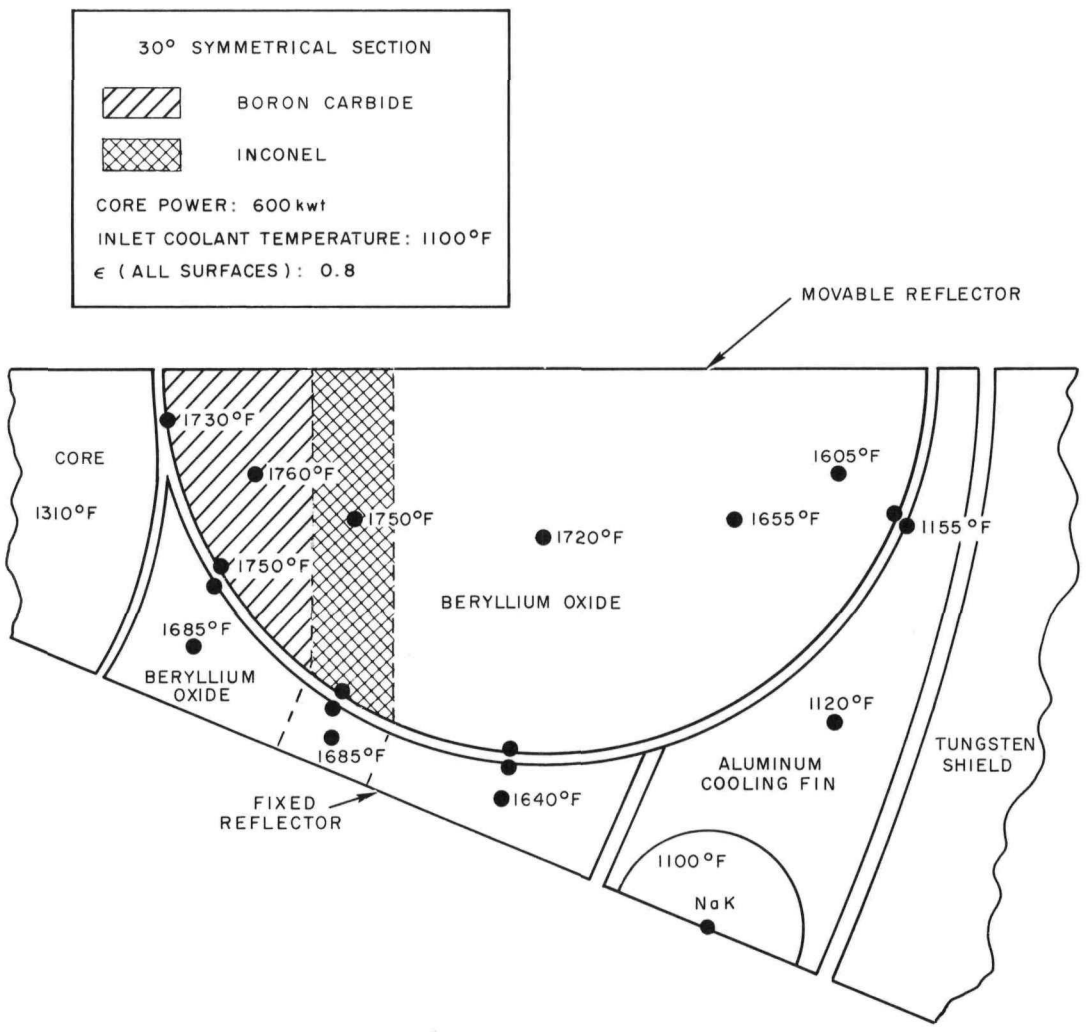

Figure 15. SNAP 8 Manrated 4π Shield, Poison-Backed Control Drum Detail

such as those induced by changes in temperature, flow, and small reactivity insertions. The reactor thermal kinetics simulation consists of differential-difference equations*,† describing the fuel, fuel cladding, and flowing coolant. As many as 20 axial nodes may be used in the fuel, fuel cladding, and coolant.

The controller simulation is a flexible, general purpose module which contains the logic of the control system. The decisions made in the controller determine the direction and rate of drum movement which may be either continuous or movement in discrete steps. Up to seven changes in the rate of drum movement are available during a transient. The rate changes are initiated when preselected reference points of two system variables are exceeded; e.g., drum angle and coolant temperature. Current systems use the reactor outlet coolant temperature as the controlled parameter, however,

*R. W. Winson, "Thermal Model of a SNAP Reactor Core with Flowing Coolant," NAA-SR-9443, November 26, 1963
†R. W. Winson, "Thermal Model for Use in SNAP System Simulation," NAA-SR-10961, March 2, 1965

any variable may be used. It is possible to simulate unidirectional or bidirectional deadband control with a zero or finite deadband width. Control concepts not using reflector drums could be easily simulated.

The safety system is represented by the simulation of a sensor and actuator. There are four variables which are sensed to determine if the safety system will override all other modes of control. One of these variables is flow and the other three are arbitrary. When the safety system is in control of the reactor, the drum movement may be continuous or discrete at any preset rate with an arbitrary reactivity worth as a function of angular drum position. This safety system simulates scram action, setback action, or hold action during any transient.

The three heat exchanger simulations and the parasitic load resistor simulation are described by differential-difference equations for flowing coolant similar to those used in the reactor core model.*,† The heat exchanger simulations are flexible and may be used with any system configuration.

The liquid-to-liquid heat exchanger model consists of a single axial node and two radial nodes while the boiler model consists of three axial nodes and two radial nodes. These axial boiler nodes represent the preheating region (liquid-to-liquid), the boiling region (liquid-to-2 phase), and the superheat region (liquid-to-vapor).

The thermoelectric pump simulation consists of three major components: a d-c electromagnetic pump, thermoelectric elements, and heat transfer fins. The simulation§ of these three components is accomplished by solution of the equations describing heat flow, electrical current flow, and pressure-momentum flow.

The piping segments are simulated using the differential-difference equations describing flowing coolant,† pipe wall, and pipe heat losses. These piping segments are the connecting links between the component modules of the program.

All component modules have been checked individually with respect to conservation of energy and with respect to transients obtained by other models.**,†† In addition, the SNAP 10A and SNAP 8 systems have been simulated and transient and steady-state calculations have agreed very well with test data and data from other models.**,††

The computer time required for an average nuclear startup transient covering ~8000 seconds is about one minute.

The modularization of the program makes it possible to simulate any arbitrary system by simply connecting the system modules in a closed loop(s). This type of system simulation has the advantage that a minimum amount of programming time is required and that the system modules are virtually unchanged from one system to another.

*R. W. Winson, "Thermal Model of a SNAP Reactor Core with Flowing Coolant," NAA-SR-TDR-9443, November 26, 1963

†R. W. Winson, "Thermal Model for Use in SNAP System Simulation," NAA-SR-TDR-10961, March 2, 1965

§R. W. Winson and P. M. Magee, "Thermoelectric Pump Digital Simulation," NAA-SR-TDR-11409, May 27, 1965

**C. E. Johnson, "SNAP 8 Progress Report, November 1964-January 1965," NAA-SR-10792 (CRD), March 15, 1965

††C. E. Johnson, "Progress Report, SNAP 8, August-October 1964," NAA-SR-10492 (SRD), December 23, 1964

4. Shielding Analysis

a. Instrument-Rated System

A preliminary analysis was made to determine the significance of gamma-ray scattering in the instrument-rated reference design. Included was scattering from the lithium-hydride shadow shield as a result of photons which bypass the gamma shield and from NaK pipes and electrical cable assemblies which lie outside of the LiH shadow shield. These results show that for 600-kwt operation, scattering from the LiH will produce at the 20-ft-diameter payload (located 40 ft from the reactor) a relatively uniform pattern of approximately 5×10^5 rads in 10,000 hr or about 50% of the tolerance dose of 10^6 rads/10^4 hr. When added to the contribution of scattering from the NaK pipes and electrical cables, the total gamma scattered dose will approach 7 to 8 x 10^5 rads near the outer radius of the 20-ft-diameter payload.

b. Manrated System

Previous 4π shield designs have used tungsten or depleted uranium as gamma shield material. Use of these materials resulted in doses comprised mainly of secondary gamma radiation.* In order to reduce the primary-secondary dose imbalance, lead was investigated for use as a gamma shielding material. Secondary gamma radiation from lead is 5 to 10 times less than that from tungsten or depleted uranium. Table 7 shows comparable thickness and weight saving possible with lead for two typical shadow shield designs. The shields are designed for a dose rate of 1.5 mrem/hr at 150 ft from the reactor.

Nuclear heating rates for a number of reflector and shield configurations were determined. These results are shown in Figures 16 through 20 as described below:

1) Figure 16 shows nuclear heating rates in the neutron shield portion of the first shadow shield section vs distance into the neutron shield. The neutron shield begins immediately below the 2-1/2-in. tungsten gamma shield.

2) Figures 17 and 18 show nuclear heating rates vs reactor radius in 4-in.-diameter BeO-B_4C poisoned control drums surrounded by a 4π shield composed of 2-1/2 in. W and 12 in. LiH. The drums are composed of 3-1/2 in. BeO, 1/2 in. Ni, and 1 in. B_4C.

TABLE 7

TYPICAL SHADOW SHIELD DESIGNS

	Design 1 (W, U^{238}, LiH)			Design 2 (Pb, LiH)		
	Thickness (in.)	Material	Relative Weight	Thickness (in.)	Material	Relative Weight
1st gamma shield	2.7	W	-	4.5	Pb	-
1st neutron shield	22	LiH	-	17.4	LiH	-
2nd gamma shield	4.1	U^{238}	-	6.5	Pb	-
2nd neutron shield	12.5	LiH	-	13.2	LiH	-
Relative weight	-	-	1.0	-	-	~0.875

*C. E. Johnson, SNAP 8 Progress Report, February-April 1965," NAA-SR-11092 (CRD), June 15, 1965

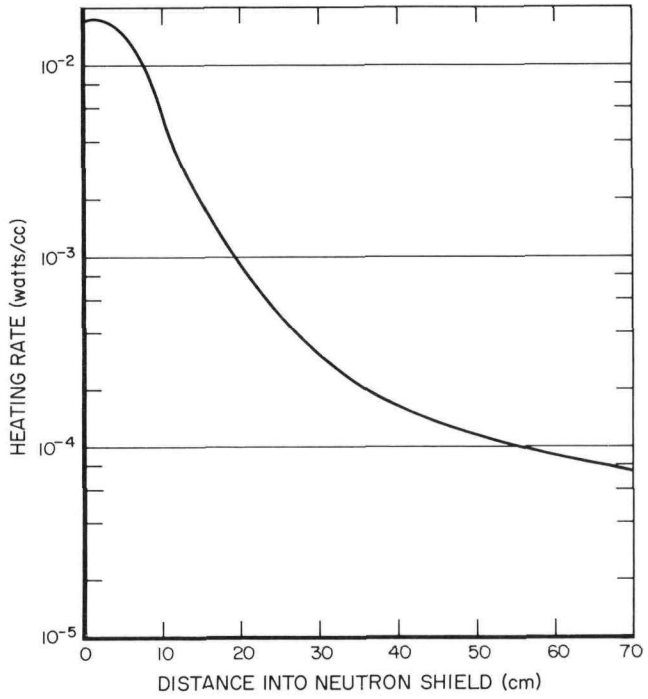

Figure 16. Nuclear Heating in Shadow Shield

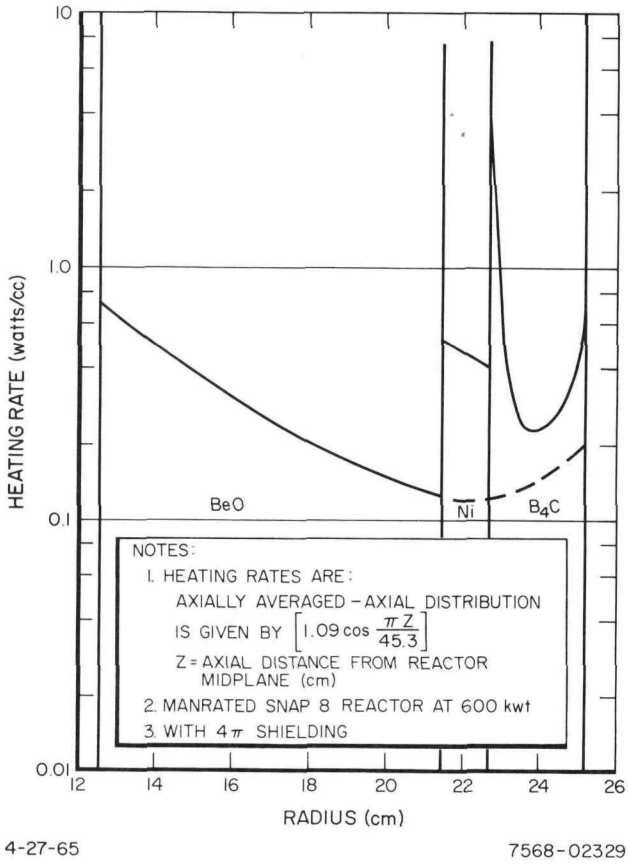

Figure 17. Nuclear Heating Rates in Poison-Backed Control Drums, With the Control Drum In

Drums-in (poison out) and drums-out (poison in) conditions are shown in Figures 17 and 18, respectively. The values shown are averages taken over the core length. The dashed lines show the heating rates in the BeO cusp regions between the drums.

3) Figure 19 shows nuclear heating rates vs reactor radius in a 4 in. beryllium reflector surrounded by a 4π shield composed of 2-1/2 in. W and 12 in. LiH. The values shown are again averages taken over the core length.

4) Figure 20 shows nuclear heating vs radius in a 4π shield composed of 6 cm W and 30 cm LiH. The shield encloses a reactor core and 4-in. beryllium reflector.

Also investigated was the nuclear heating in the liquid lead region of a Pb-LiH 4π shield. The 4π shield investigated enclosed a reactor core and a reflector with 4-in. poison-backed drums. The maximum heating rate in the lead was determined to be 0.9 watts/cc and the integrated heat load in the cylindrical annulus surrounding the reactor was determined to be ~12 kw.

5. Stress Analysis

The acceleration response of the SNAP 8 DRM-1 components to the Apollo vibration environment has been calculated. The calculations were based on the simplified equations of motion simulated from the S8DRM-1 experimental data and predicted random vibration spectra of the Apollo spacecraft.

The predicted power spectral density of Apollo random vibration input for a system whose mass is relatively large is 0.001 g^2/cps

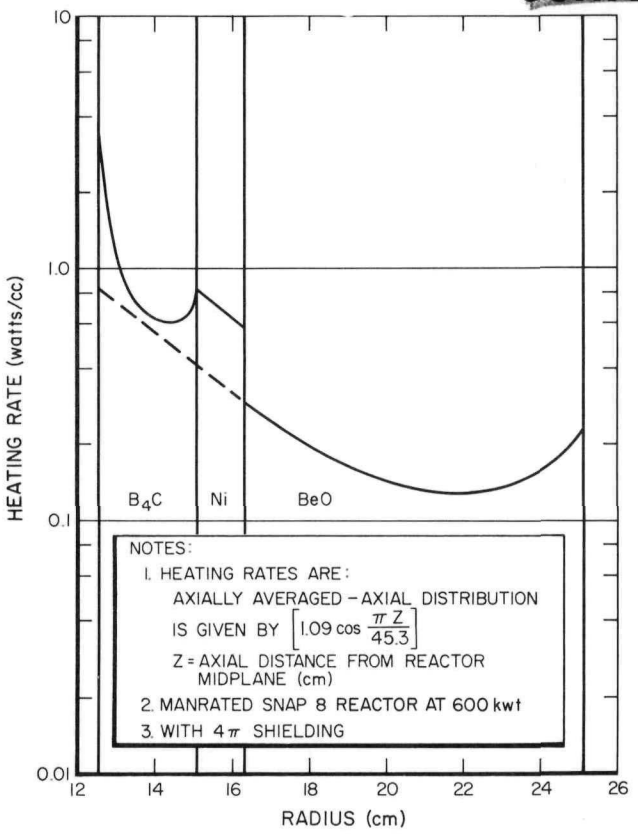

Figure 18. Nuclear Heating Rates in Poison-Backed Control Drums, With the Control Drum Out

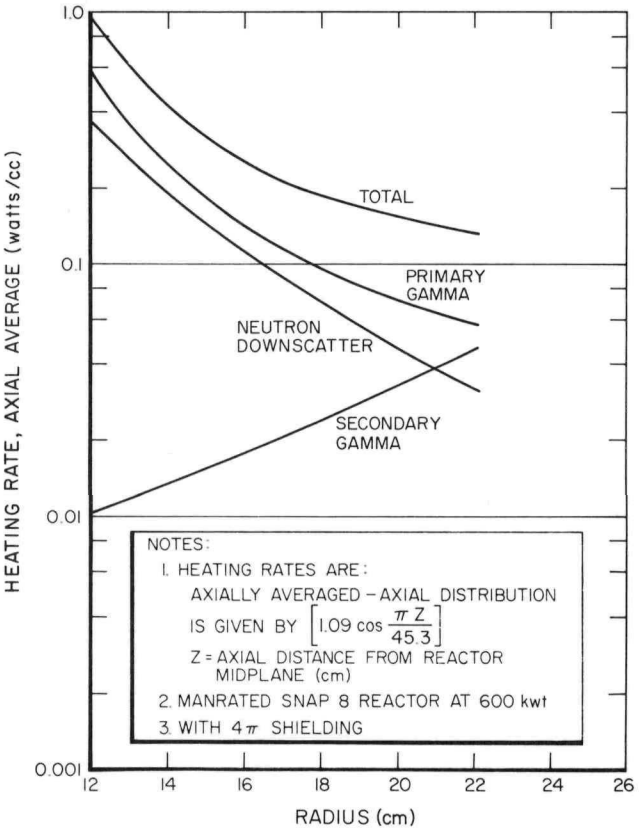

Figure 19. Nuclear Heating in 4-in. Tapered Beryllium Reflector

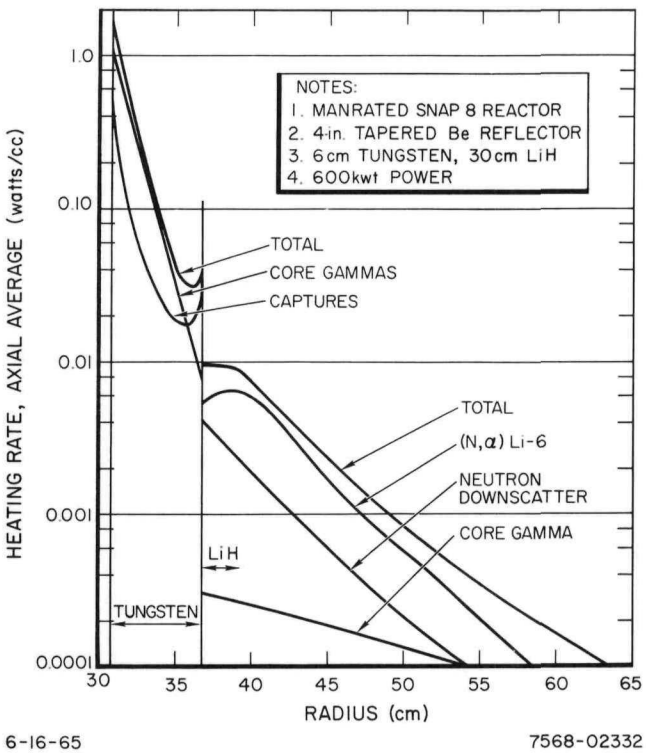

Figure 20. Nuclear Heating in a 4π Shield

TABLE 8

ACCELERATION LOADING ON MAJOR STRUCTURAL COMPONENTS DUE TO COMBINED APOLLO RANDOM VIBRATION ENVIRONMENT

Component	Axis	Acceleration	
		g_{rms}	g_{max} (Operating)
Reactor Top	Y	7.95	23.85
	Z	7.32	21.96
Reactor Center of Gravity	Y	3.06	9.18
	Z	3.52	10.56
Reactor Base	X	5.65	16.95
Upper Grid Plate	X	5.00	15.00
Lower Grid Plate	X	1.96	5.88
Reflector Top	X	3.07	9.21
Reflector Center of Gravity	Y	3.42	10.26
Control Drum Top	X	2.05	6.15
	Z	2.37	7.01
Control Drum Center of Gravity	Y	4.67	14.01
	Z	4.86	14.58
Startup Drum	X	3.04	9.12
Control Drum Actuator	X	5.65	16.95

from 10 to 2000 cps in three mutually perpendicular directions. This input applied at the base of the reactor will produce acceleration loading on the structural elements of the reactor system. This resultant loading is predicted by the relationship

$$g_{rms} = \sqrt{\int_{W_1}^{W_2} \omega_{\ddot{x}}(W) \left| H(W) \right|^2 dw}$$

where

$\omega_{\ddot{x}}(W)$ = power spectral density of the random vibration input,

$H(W)$ = transmissibility function,

W = frequency, and

g_{rms} = root-mean-square output acceleration.

Since g_{rms} represents the standard deviation (1σ value) of the output acceleration, the maximum acceleration will be taken to be $3\ g_{rms}$ (3σ value). Combined loading was assumed to assure a worst case analysis.

Table 8 reveals the predicted response of major system components. The axis indicated is the direction of the resultant loading due to combined loading.

Analog simulation of a longitudinal sinusoidal vibration test, longitudinal random vibration test, and a longitudinal shock test has been completed for a typical SNAP 8 manrated 4π shield system. A modal search indicates that the lowest two natural frequencies in the longitudinal direction are 61 cps and 193 cps. The maximum shock transmissibility in the longitudinal direction is 1.2 and in the lateral direction, 1.9.

Midpoint deflection of the SNAP 8 manrated poison-backed control drum with an Inconel-X cylindrical cladding (4 in. diameter) has been calculated for the following conditions: drums-in position, power level of 600 kw, and cladding temperature variation only in the direction of an axis of symmetry. The centerline deflection of the Inconel-X cladding due to the thermal gradient and radial expansion is 0.079 inch including a factor of safety of 1.4. Allowing for the outward creep of the vessel wall (0.2% in 3 years) and the total inward deflection of the drum, the initial gap between the vessel wall and the drum should be greater than 0.095 inch.

6. Reliability

The reliability goal of the unmanned SNAP 8 nuclear system is $R_s = 0.962$. This objective includes the probability that the system will not fail due to the penetration of the critical subsystems by meteoroids during flight. That is:

$$R_s = [P_s(o)][R]$$

where

$R_s = 0.962$, the total nuclear system goal,

$P_s(o)$ = probability of nonpenetration by meteoroids, and

R = reliability of system not including meteoroid nonpenetration.

The probability of no critical damage due to meteoroid penetration is a function of the modulus of elasticity, the density, the exposed area, and the thickness of the armor and the length of time of exposure of the subsystems to meteoroid hazard. An analysis has been completed optimizing the system probability of no critical damage due to meteoroid penetration with minimum armor weight. The armor material is the same as the external material of the component in each case. The components, however, function in different temperature environments which

TABLE 9

SYSTEM OPTIMIZATION ANALYSIS

Subsystem	Surface Area, A_i (ft^2)	Design Temperature (°F)	Density, ρ_{t_i} $\left(\frac{lb}{ft^3}\right)$	Young's Modulus, E_{T_i} $\left(\frac{lb}{in.^2} \times 10^6\right)$	Thickness for $P_s(o) = 0.999$ (in.)
Neutron Shield					
Top	6.2	1000	485.6	20.6	0.2751
Side	26.8	800	488.7	22.1	0.2695
NaK Piping					
Inlet	2.1	1150	483.3	19.4	0.2800
Outlet	3.7	1350	480.2	17.7	0.2876
Core Upper Plenum	1.0	1350	480.2	17.7	0.2876
No. 1 Actuator and Brake Housing Assembly	0.4	1000	485.6	20.6	0.2751
No. 2 Actuator and Brake Housing Assembly	0.4	1000	485.6	20.6	0.2751
No. 3 Actuator and Brake Housing Assembly	0.4	1000	485.6	20.6	0.2751

Total weight for above conditions = 454.25 lb

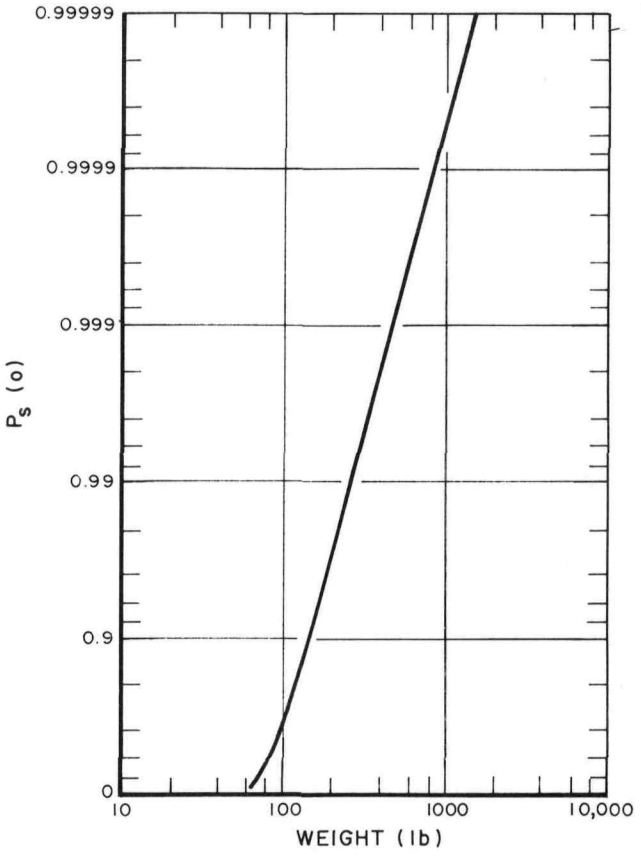

Figure 21. Armor Weight vs Probability of Nonpenetration of Meteoroids

influence the density and Young's modulus of the system. Table 9 is a listing of the SNAP 8 components considered, the value of the parameters involved in the study, and the respective armor thickness required for each component using the criteria dictated by the analysis for a probability of nonpenetration $P_s(o) = 0.999$. Figure 21 is a graph representing the total system armor weight as a function of the probability of nonpenetration. The change in the system reliability requirements for any change in the total armor weight can be determined. For example, the 110 lb increase in the armor weight from 345 to 455 lb improves the $P_s(o)$ from 0.997 to 0.999. This improvement of $P_s(o)$ due to the increase in the weight of armor will decrease the reliability requirement for the system operation by 5.7%.

For $P_s(o) = 0.999$, $R' = 0.963$, and for $P_s(o) = 0.997$, $R'' \approx 0.965$,

$$\frac{R'' - R'}{1 - R''} = \frac{0.965 - 0.963}{1 - 0.965} = \frac{0.002}{0.035}; \frac{0.002}{0.035} \times 100 = 5.7\%$$

where

R' = reliability requirement for system operation when $P_s(o) = 0.999$, and

R'' = reliability requirement for system operation when $P_s(o) = 0.997$.

BLANK

IV. FUEL ELEMENT DEVELOPMENT AND FABRICATION

A. INTRODUCTION AND SUMMARY

The objective of the fuel element program is to develop fuel elements for the 600-kwt SNAP 8 reactor that meet the following performance requirements:

1) A peak power density of the fuel of approximately 5.0 kwt/ft of fuel rod length at a peak central temperature of 1550°F. A peak fuel burnup of about 0.3 metal atom percent in 10,000 hours.

2) Hydrogen loss from the fuel elements of less than 5% of that in the fuel alloy during 10,000 hours of reactor operation. The hydrogen barrier coating and closure seal must withstand thermal and mechanical checkout of the reactor, thermal shock during startup, and a peak cladding operating temperature of 1450°F. The fuel element cladding also must resist corrosion in the NaK environment and maintain dimensional integrity over the life of the core.

3) A fuel element with 99% reliability at the 50% confidence level of meeting these performance goals. Redundant fuel elements are provided in the core so that failure of the hydrogen barrier in a few elements will still permit successful operation of the reactor.

Significant improvements were demonstrated in S8DS fuel element chromizing and closure welding processes. Processes were developed for chromizing lots and for chromizing virgin tube assemblies. S8DS core production capability for chromizing and straightening cladding tube assemblies was demonstrated. Machining methods were established for improving the fit-up and cleanliness of S8DS cup-plug closure weldments. Significant improvements in welding yield and process capability for weld penetration were achieved.

In nondestructive test development, the feasibility of an eddy-current test for determining hydrogen distribution in fuel rods was established. A new x-ray technique was developed for quality assurance of S8DS closure weldments.

Performance tests of developmental S8DS fuel elements continued to demonstrate a substantial improvement in S8DS performance over the S8ER fuel elements.

The NAA-115-1 and NAA-117-1 fuel element irradiations continued at Hanford. Assembly of the NAA-115-2 fuel element was completed and the irradiation test commenced. Fabrication of the NAA-121 fuel element test continued. Hot cell preparations for the S8ER core screening examination were completed.

B. FUEL ELEMENT DEVELOPMENT

1. Fuel

a. Fuel Nondestructive Testing

Eddy-current techniques have been developed for measuring the relative incremental hydrogen content of fuel elements in the S8ER core. Special annular coils were fabricated for making hydrogen measurements of the fuel elements in the hot cell before removal of the cladding. Experiments have shown that the presence of cladding causes no significant difference in relative eddy-current response in the fuel. In practice, the S8ER core fuel elements will be traversed axially through one coil while a reference fuel element of known hydrogen content will be placed in the second or standard coil.

Experiments on the stability and linearity of the neutron scatter method of measuring hydrogen in fuel elements were continued. New BF_3 neutron detectors were procured and successfully tested. Eight SNAP 8 fuel rods which were hydrided to various percentages were tested.

An average of six separate counting periods was determined for each rod. This average was then subtracted from the background count, which is the average count rate with no fuel rod interposed between the neutron source (Pu, Be – 1 curie) and the BF_3 detection chamber. A lower value of the difference between average count rate for a rod and the background count rate indicates a lower hydrogen content in the rod.

Figure 22 shows the linear relationship obtained between count rate difference and weight percent hydrogen for each fuel rod tested; i.e., the fuel rod weight gain after hydriding. Data taken with two different BF_3 counters, F-1058 and F-1060, for the same eight fuel rods are plotted in Figure 22.

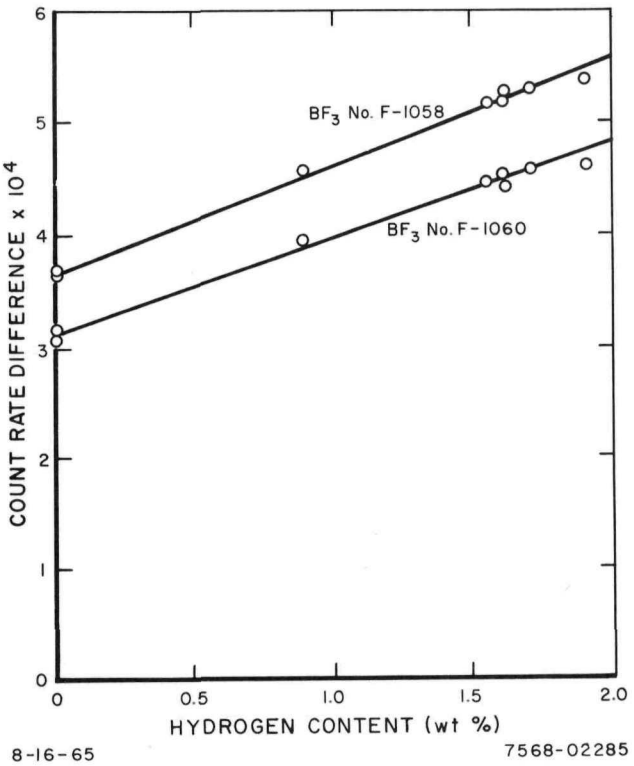

Figure 22. Neutron Scatter Experimental Data

b. Physical Property Measurements

The fuel tensile-creep program has been completed. It was concluded that:

1) At operating temperatures of 1300 and 1400°F and stress levels of 3000 and 4000 psi, fuel material with a hydride composition of 1.72 H/Zr is more resistant to creep than either the 1.60 H/Zr or 1.80 H/Zr fuel.

2) The strain-time relationship for the 1.80 H/Zr fuel material exhibits a parabolic creep curve in comparison to a linear relationship observed for the 1.60 H/Zr fuel. This behavior suggests that the mechanism of creep changes with composition. This change is attributed to the crystallographic differences between the face-centered-cubic delta phase (1.60 H/Zr) and the highly twinned face-centered tetragonal epsilon phase (1.80 H/Zr).

Tensile creep tests were completed on nine specimens of 1.60 H/Zr – SNAP fuel. The carbon levels investigated were 0.05 and 0.30 wt %. Tests were conducted at two stresses: 3000 and 4000 psi, and three temperatures; 1400, 1500, and 1600°F. Creep rate data calculated from the strain-time curves for each specimen are summarized in Table 10. These data are presented as Arrhenius plots in Figures 23 and 24 for the 3000 and 4000 psi stress levels, respectively. The 0.15 wt % carbon addition exhibits the best creep resistance at both stress levels.

Mechanical tests in the beta-delta two-phase region were continued. Tests were conducted in which an axial temperature gradient was imposed on the test specimens, similar to that experienced in an operating fuel element. It was reasoned that in a thermal gradient, the two phases would segregate into distinct regions. Since the beta phase has a higher density than

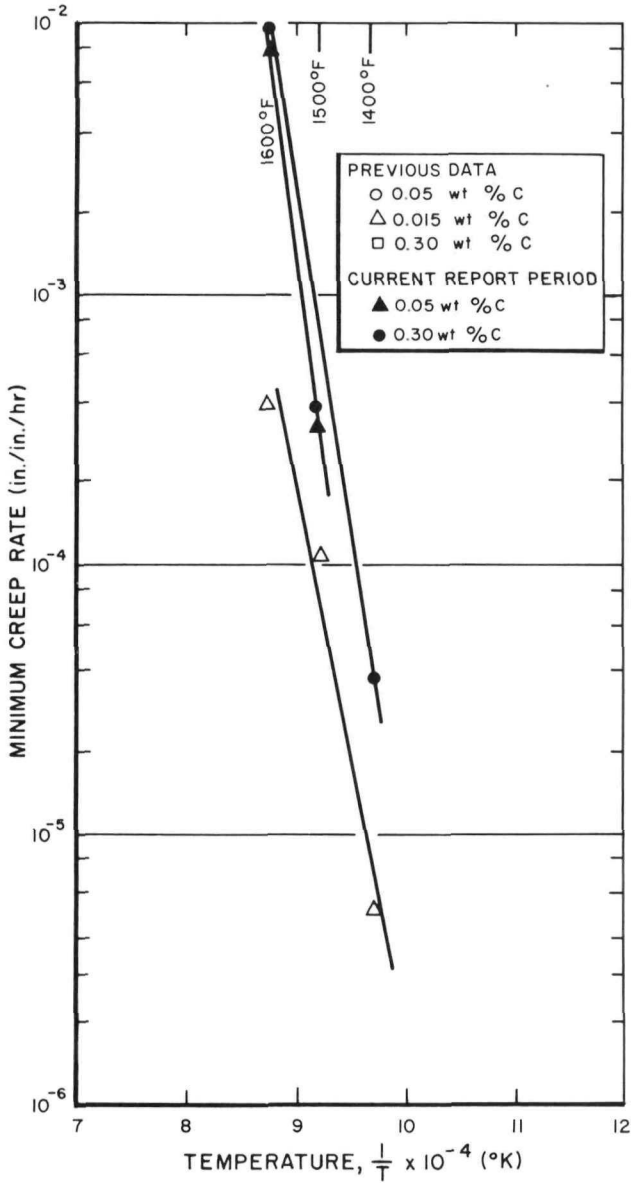

Figure 23. Minimum Creep Rate vs Reciprocal Absolute Temperature for 1.60 H/Zr SNAP Fuel at an Applied Stress of 4000 psi

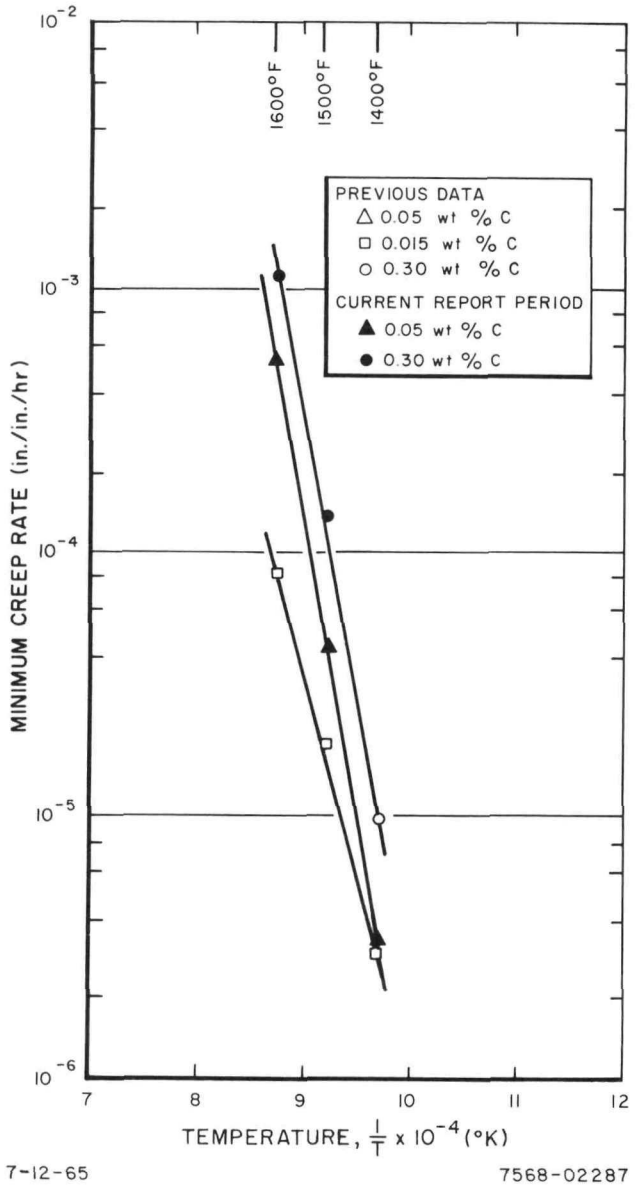

Figure 24. Minimum Creep Rate vs Reciprocal Absolute Temperature for 1.60 H/Zr SNAP Fuel at an Applied Stress of 3000 psi

TABLE 10

TENSILE CREEP DATA FOR 1.60 H/Zr FUEL

Test Number	Composition		Temperature (°F)	Stress (psi)	Strain (in./in.)	Average Minimum Creep Rate (in./in./hr)
	H/Zr	Carbon (wt %)				
21122	1.60	0.05	1400	3000	0.0039	3.4×10^{-6}
21132	1.60	0.05	1500	3000	0.0135	4.4×10^{-5}
21142	1.60	0.05	1600	3000	0.0169	5.5×10^{-4}
21141	1.60	0.05	1600	4000	0.0220	8×10^{-3}
23121	1.60	0.30	1400	4000	0.0072	3.9×10^{-5}
23131	1.60	0.30	1500	4000	0.0433	4×10^{-4}
23132	1.60	0.30	1500	3000	0.0289	1.4×10^{-4}
23142	1.60	0.30	1600	4000	0.0597	1×10^{-2}
23141	1.60	0.30	1600	3000	0.0360	1.1×10^{-3}

delta, it was postulated that high internal stresses could develop to cause cracking of the fuel at the beta-delta interface.

The temperature profile of the test specimens was adjusted to obtain a longitudinal temperature gradient as shown in Figure 25. The center of the test specimens was held at 1400°F, while the ends were about 100°F cooler. The hydrogen pressure in the retort was then adjusted to place the beta-delta equilibrium temperature within the test length. As seen in Figure 25, the hotter portion of the rod was beta phase, while the colder ends were delta phase.

After equilibrium was reached, the samples were placed in tension and strained at a constant rate to failure. The failure occurred at the hottest point of the beta phase material and the ultimate tensile strength was 4250 psi. The samples elongated about 36%, with all of the elongation occurring in the beta phase material. Metallographic examination of the post-test specimens indicated that the beta-delta interface was positioned as predicted in the pressure-temperature relationships (Figure 25).

Conclusions reached from these tests are: (1) The beta phase material is quite ductile as compared to delta phase. (2) The beta-delta interface is stronger than the beta phase material.

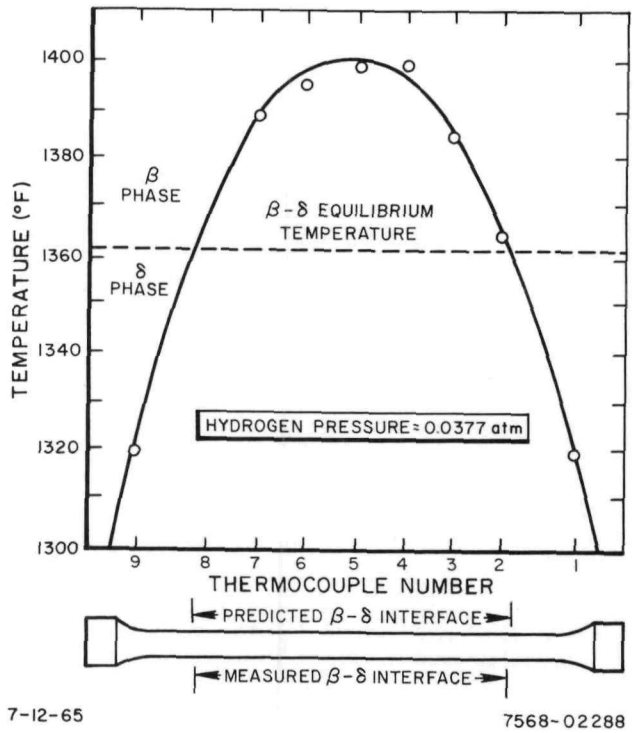

Figure 25. Temperature Profile for Beta-Delta Interface

c. Fuel Coating Interaction Studies

Previous studies on the fuel-coating interaction have included a machining operation to allow insertion and removal of the fuel rod between permeation tests. In addition to the possibility of mechanical damage to the coating, opening the cladding resulted in exposure of the coating to air. The air might destroy any reactive film on the coating produced when the fuel rod was present. A new testing procedure was adopted to eliminate this uncertainty in the fuel-coating interaction studies. A double length membrane was employed whereby the fuel rod was located in the unheated zone of the membrane during the initial permeation testing. Then, after the initial membrane permeation tests, the fuel rod was slid into the heated test zone of the membrane by a magnetic coupling device without opening the membrane or removing it from the test apparatus. The fuel rod can also be removed from the test area in the same manner.

Hydrogen permeation tests were conducted with the fuel rod withdrawn to the unheated zone (equivalent of empty membranes) at 1200, 1300, and 1400°F and hydrogen pressures of 1 to 6 atm. Normal pressure relationships were observed ($p^{1.0}$) for the SCB coating material. Activation energies were determined for comparison with the fueled portion of the experiment. One data point has been obtained on the membrane with the fuel rod in place at 1400°F and 6 atm H_2. The hydrogen permeation results with and without a fuel rod are:

$$\varphi \text{ (fuel)} = 1 \times 10^{-2} \text{ cc/hr-cm}^2 \text{ and}$$

$$\varphi \text{ (without fuel)} = 2.8 \times 10^{-3} \text{ cc/hr-cm}^2.$$

This behavior is consistent with previous tests where the fuel rod was inserted by cutting open the membrane.

2. Hydrogen Barrier

a. Coating Endurance Tests

Three SCB-coated cladding tubes have been tested for 17,500 hours at 1500°F in 1 atm hydrogen, internal pressure. Hydrogen permeation rates through the membranes have been monitored continuously as an average of the three membrane cluster. The permeation history is shown in Figure 26. Each membrane has also been permeation tested individually. The results are compared with the initial permeation values in Table 11. The permeation rates of all three membranes have increased over their initial values. This increase is attributed to a slow crystallization of the coating during endurance test.

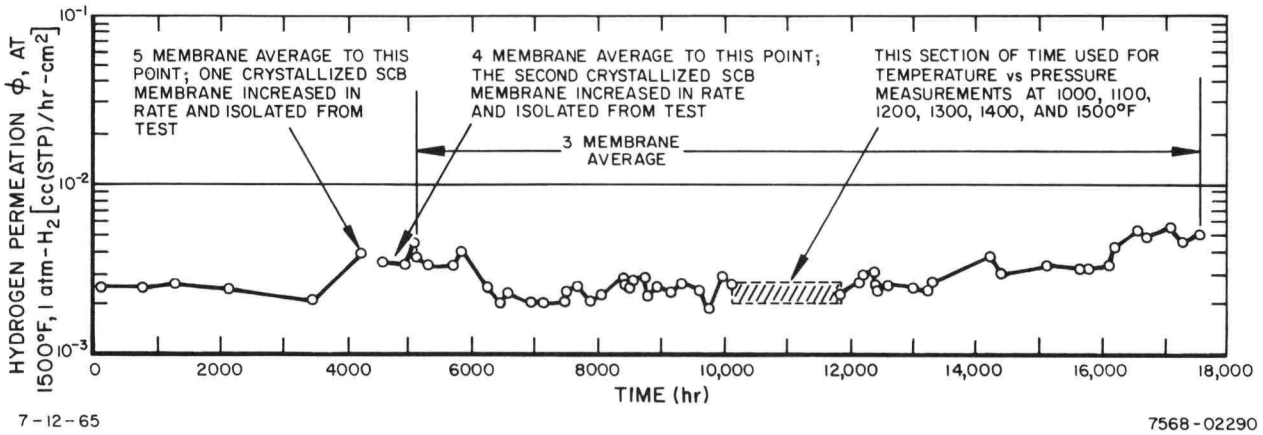

Figure 26. Average Permeation Rate vs Time for Five Membranes Tested at 1500°F

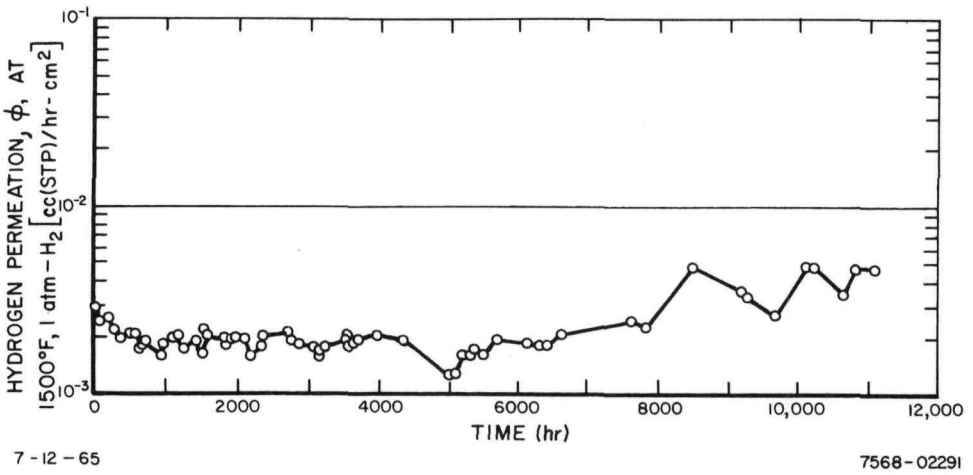

Figure 27. Average Permeation Rate vs Time for Five Membranes Tested at 1500°F (fabricated with short firing cycle for SCB coating)

TABLE 11

INDIVIDUAL PERMEATION RATES OF LONG-TERM TEST MEMBRANES, LONG FIRING CYCLE – SCB, 3-MEMBRANE CLUSTER

Membrane Number	Present Rate, φ, at 1500°F, 1 atm [cc(STP)/hr-cm^2]	Time (hr)	Initial Rate, φ, at 1500°F, 1 atm [cc(STP)/hr-cm^2]
E-835	5.87×10^{-3}	↑	1.2×10^{-3}
E-848	3.94×10^{-3}	15,345	1.7×10^{-3}
E-809	3.25×10^{-3}	↓	2.5×10^{-3}

TABLE 12

INDIVIDUAL PERMEATION RATES OF LONG-TERM TEST MEMBRANES, SHORT FIRING CYCLE – SCB-1, 5-MEMBRANE CLUSTER

Membrane Number	Present Rate, φ, at 1500°F, 1 atm H_2 [cc(STP)/hr-cm^2]	Time (hr)	Initial Rate, φ, at 1500°F, 1 atm H_2 [cc(STP)/hr-cm^2]
2092	6.5×10^{-3}	↑	0.81×10^{-3}
2052	4.89×10^{-3}		1.0×10^{-3}
RD-86	3.09×10^{-3}	8,922	1.5×10^{-3}
RD-14	3.36×10^{-3}		1.24×10^{-3}
2308	4.15×10^{-3}	↓	3.0×10^{-3}

A five-membrane cluster of SCB-coated cladding tubes, processed by the short firing cycle (S8DS process), has exceeded 10,000 hours on endurance test at 1500°F and 1 atm hydrogen, internal pressure. The permeation history of this cluster is given in Figure 27. Individual permeation rates were measured on each tube and the results are given in Table 12. Again, the permeation rate of each tube has increased over the initial value before endurance test. The average permeation rate was a factor of three higher as a result of devitrification.

b. Coating Process Development

(1) In-House Chromizing

During this report period, the development effort was directed toward improvement and better control of the chromizing process for S8DS cladding tubes. Efforts to develop a process for salvaging vendor-chromized cladding tube assemblies by rechromizing were deferred to permit concentration on the development of a capability for chromizing virgin cladding material. During the last half of the report period, efforts were exclusively directed toward scaling the process up to a production capacity for chromizing five tubes in each furnace charge.

Experimental results of development of a capability for chromizing virgin Hastelloy-N cladding tubes are presented in Tables 13 through 16. The majority of the chromizing experiments were conducted at two temperatures for varying periods of time; e.g., 12 to 90 min at 2135°F and 120 min at 1900°F.

Results of the chromizing experiments at 1900°F are tabulated in Table 13. Ceramic adherence after chromizing was satisfactory in most cases, but nonuniform over the length of the tube from the open end to the closed end of

TABLE 13

CHROMIZING OF WHOLE VIRGIN TUBES AT 1900°F

Run Number	Tube Number	Chromizing Time (min)	Chrome Layer Thickness (mils)	Total Indicated Reading (TIR) (mils)				Adherence* Number of Flexes up to 11 (or) until 50% of Coating Lost					Remarks
				As Received	After Chromizing	After Straightening	After Coating	1	2	3	4	5	
1	3190	120	0.3	19	75	3	16	7	5	7	4	11	Cup plug coating pulled away. Permeation reading was off-scale
2	454-1	120	0.3	25	52	8	13	1	2	2	<1	<1	-
3	3192	90	0.31	11	75	-	-	<1	<1	<1	5	11	-
	459-3	90	0.55	27	53	-	24	<1	<1	<1	<1	<1	-
4	3197	60	0.31	61	44	-	54	<1	<1	<1	<1	<1	Heat-Treated 2 hr, 1900°F
	465-3	60	0.47	41	64	-	85	<1	<1	<1	<1	<1	
5	3963	120	0.28	-	83	15	10	3	5	<1	<1	-	-
	3965	120	0.20	-	58	7	3	1	<1	<1	<1	-	-
6	3962	120	0.20	27	97	8	23	11	-	-	-	-	-
	3964	120	0.20	-	81	10	14	11	-	-	-	-	-
7	3974	120	0.35	28	66	6	2	11	7	6	7	-	-
	3975	120	0.35	20	160	11	14	11	<1	<1	<1	-	-
	3976	120	0.24	20	81	11	13	7	1	1	1	-	-
8	3977	120	0.30	02	21	2	10	3	2	<1	3	-	-
	3978	120	0.20	16	75	1	9	11	3	<1	11	-	-
	3979	120	0.20	0	97	3	6	4	<1	1	4	-	-

*Columns refer to measurements made along the tube from the open to the closed end.

TABLE 14

INITIAL CHROMIZING OF WHOLE VIRGIN TUBES AT 2135°F

Run Number	Tube Number	Chromizing Time (min)	Chrome Layer Thickness (mils)	Total Indicated Reading (TIR) (mils)				Adherence** Number of Flexes up to 11 (or) until 50% of Coating Lost					Permeation, φ [cc(STP)/hr]	Remarks
				As Received	After Chromizing	After Straightening	After Coating	1	2	3	4	5		
1	889-2	30*	0.79	—	250	4	23	3	<1	1	5	<1	1.54	
2	3189	90	0.63	—	66	—	60	7	—	—	—	—	—	
	3200	90	0.80	—	122	6	10	11	<1	5	3		—	Crazing of Surface
3	3933	90	1.34†	46	81	—	—	5	11	11	11	11	—	Quenched in Water
	3936	90	1.26	99	250	5	28	11	<1	<1	<1		—	Crazing of Surface
4	3947	90	1.26	17	341	19	18	5	—	—	—	—	—	Quenched in Water
	3951	90	1.26	12	289	16	26	11	—	—	—	—	—	Quenched in Water
5	3959	20	0.80§	32	29	—	24	1	<1	<1	4	3	—	Chromized on Inside only
6	3960	30	—	12	110	5	4	11	—	—	—	—	—	Chromized on Inside only
7	3934	12	0.70	55	22	10	21	4	8	5	6		—	Cooled slowly (3 hr)
	3961	12	0.70	14	35	9	15	5	—	—	—	—	—	to 1200°F

*Temperature, 2100°F
†Sandblasted down to 1.02
§Sandblasted down to 0.47
**Columns refer to measurements made along the tube from the open to the closed end.

TABLE 15

CHROMIZING OF WHOLE VIRGIN TUBES AT 2135°F FOR 12 MINUTES

Run Number	Tube Number	Chrome Thickness (mils)	Total Indicated Reading (TIR) (mils)				Adherence† Number of Flexes up to 11 With Less Than 50% of Coating Lost					Permeation, φ [cc(STP)/hr]		Furnace
			As Received	After Chromizing	After Straightening	After Coating	1	2	3	4	5	1st	2nd	
1	3950	0.32	25	120	32	—	8	—	—	—	—	0.46	0.49	Electric
	3952	0.32	36	62	12	—	2	—	—	—	—	0.45	0.47	
2	3948	0.31	41	120	—	—	3	—	—	—	—	0.47	0.46	Electric
	3949	0.31	14	79	—		2	11	<1	3	3	—	—	
3	3957	0.29	14	240	—	—	6	—	—	—	—	1.39	1.38	Electric
	3958	0.31	6	75	—	—	2	—	—	—	—	0.37	0.41	
4	300-1	0.39	42	68	13	16	<1	<1	<1	8	*	—	—	Gas
	473-2	0.40	32	93	7	4	11	11	<1	8	*	—	—	
	417-6	0.36	13	192	4	7	5	—	—	—	—	—	—	
5	377-1	0.41	12	75	3	5	11	*	4	4	*	—	—	Gas
	261-1	0.40	21	91	12	9	<1	3	<1	5	*	—	—	
	417-4	0.41	24	149	16	16	<1	<1	3	6	*	—	—	
6	4068	0.32	8	173	9	17	<1	<1	5	11	*	—	—	Gas
	4069	0.30	35	43	2	18	<1	<1	2	5	*	—	—	
	4070	0.39	32	62	13	16	<1	<1	1	3	*	—	—	

*No adherence specimen with this number.
†Columns refer to measurements made along the tube from the open to the closed end.

the tube (the adherence values are given in Table 13). The present testing method consists of manually bending a split tube sample over a mandrel of the same diameter as the cladding tube until 50% of the ceramic coating is lost. It is interesting to note that exposure of chromized tubes to a 2-hr heat treatment at 1900°F resulted in poor adherence, confirming data previously obtained on a short specimen.

Results of the chromizing experiments at 2135°F are summarized in Table 14. As expected, a thicker chromized layer resulted in these experiments than in the lower temperature runs of equal duration. At first, a great amount of difficulty was experienced in straightening these tubes due to their extreme hardness. More rapid cooling from the chromizing temperature, achieved by using individual retorts of small diameter, reduced the hardness and greatly improved the ductility of the chromized tubes. Quenching of the chromized tubes in water was attempted with the expectation that the quenching would make the tubes softer; however, this procedure resulted in increasing the total indicated reading (TIR) of the tubes and was therefore discontinued.

In one 2135°F chromizing run, the tubes were slowly cooled to 1200°F in order to determine whether the increased hardness was due to either precipitation of intermetallic compounds or a transition from a disordered to an ordered phase. Since no difficulty was experienced in straightening these tubes, it was concluded that the precipitation of intermetallics was not occurring. From this experiment and the improved ductility obtained by rapid cooling, it is believed that the improved ductility was brought about by the suppression of the ordered $CrNi_3$ phase, i.e., rapid cooling is required only through the critical temperature range of approximately 1000°F for the Cr-Ni system.

Though the ductility of the tubes was improved by rapid cooling, the chrome layer was too thick and this resulted in crazing or cracking of the surface during the straightening operation. It was decided to maintain the chromizing temperature at 2135°F but to shorten the time at temperature in order to decrease the chromized layer thickness to approximately 0.4 mil. No crazing or cracking was observed with this diffusion layer thickness. Table 15 presents the results of experiments conducted under these conditions in both electric and gas-fired furnaces. In six experiments with a total of 15 tubes, the chromized layer thickness averaged 0.35 mil with a range of 0.12 mil from minimum to maximum thickness.

Based on these results, effort was initiated to scale the process up to core production capacity. Table 16 presents results which show that a chromized layer thickness of 0.4 ±0.15 mils can be obtained under production conditions.

In order to explore in more detail the differences in the chromized layer obtained under different conditions, numerous samples of tubes and cup plugs chromized at Atomics International have been analyzed with an electron microprobe. The most important preliminary result is that the chromium content of the AI-chromized material is much higher on the surface. It runs approximately from 70 to 85%, compared to 30 to 40% for the vendor material.

(2) Vendor Chromizing

During the previous reporting period, preliminary work by Vendor C on a tube chromizing process with 4-in. open-end tubes was very promising. This work was continued on full-scale, closed-end membranes. Four separate lots of membranes (six 20-in. closed-end membranes per lot) were produced, three with CrI_2 as pack material and one with $CrCl_3$.

Of the three pilot runs made by the vendor using the CrI_2 process, one run was lost because of a leak which developed in the retort, another displayed acceptable coating performance but poor adherence, and the third was successful from the standpoint of both coating and adherence behavior. Table 8 summarizes the results of these pilot runs.

The pilot run using a $CrCl_3$ pack mix was unsuccessful and all tubes were rejected because of excessive flaking of the ceramic coating at or near the blind ends of the tubes (see Table 17).

Neither process developed by the vendor met the chromized layer thickness specification of 0.40 ±0.15 mil. These processes could conform to the thickness specification with improved processing parameters.

This chromizing work was conducted to provide a backup process for the in-house effort. In this respect, the objectives were met.

(3) Effects of Pre-Annealing on Chromized Structures

Two separate tests were conducted to determine the effects of a solution anneal on the subsequent deposition and structure of the chromium diffusion layer on Hastelloy-N tube and

TABLE 16

CHROMIZING OF VIRGIN TUBES AT 2135°F FOR 12 MINUTES USING A RACK IN A GAS-FINNED FURNACE

Run Number	Tube Number	Position on Rack	Average Temperature of Run (°F)	Chrome Thickness (mils)	Total Indicated Reading (TIR) (mils)				Remarks
					As Received	After Chromizing	After Straightening	After Coating	
6	4107	13	2115	0.33	49	78	3	-	Research Organic Chem. Corp. $CrCl_3$ used
8	4055	3	2120	0.37	9	73	4	-	
	4060	7		0.35	7	91	6	-	Fisher's $CrCl_3$ used
	4065	9		0.35	16	72	8	-	
	4066	12		0.50	8	161	9	-	
	4094	14		0.34	10	38	4	-	
9	4109	3	2100	0.26	17	61	8	-	Fisher's $CrCl_3$ used
	4110	7		0.25	5	10	-	-	
	4111	9		0.36	16	40	11	-	Research Organic Chem. Corp. $CrCl_3$ used
	4106	12		0.33	11	136	13		

TABLE 17

ADHERENCE AND PERFORMANCE OF ENAMEL COATINGS TO SNAP 8 MEMBRANES CHROMIZED BY VENDOR C

Pilot Run	Chromizing Process			Adherence Indicies						Coating Performance
				Rechromized Tubes			Chromized Tubes			
	Type of Pack	Time (hr)	Temperature (°F)	Open End	Center	Blind End	Open End	Center	Blind End	
1	CrI_2	7	2000	Retort Leaked; Tubes not Processed						
2	CrI_2	12	2000	35	38	63	35	63	53	6 of 6 Acceptable
3	CrI_2	8	2050	1	12	63	1	36	39	5 of 6 Acceptable
4	$CrCl_3$	10	1850	3	2	3	62	48	56	6 of 6 Rejected

end sections. Both annealed and unannealed tube sections were sent to Vendor B for chromizing. After chromizing, the tube sections were coated and tested for adherence. The results of these tests were inconclusive, as both poor and good adherence indices were obtained in both cases.

(4) Effect of Chromized Substrate Composition on Ceramic Adherence

Difficulties in obtaining acceptable degrees of adherence of ceramic coatings to cup-plugs were experienced at various times during the past year. The ceramic adherence was found to be excellent in some lots of cup plugs, while others exhibited extensive chipping on the rim and the sides.

To determine the effect upon coatability of compositional differences of the substrate sections from five different lots of plugs were selected for study by x-ray fluorescence and electron microprobe techniques. The chromium layer thicknesses and degrees of coatability of the five different lots of cup plugs selected are shown in Table 18.

The outside surfaces of a cup plug from each lot (two from Lot 0603) were scanned for Ni and Cr in several places with an x-ray fluorescence spectrometer and the Cr/Ni ratios were computed on the basis of the peak intensities obtained. Based on these data, those plugs exhibiting Cr/Ni ratios between 0.56 and 1.24 were found to have the best coatability. Plugs with Cr/Ni ratios above these values appeared to exhibit the poorest performance (see Table 19). Each plug was subjected to electron microprobe analysis for Cr, Ni, and Mo. The Cr, Ni, and Mo contents for three of the cup plugs (F1, M2, and E1) at maximum densities were found to total less than 100%. Since such deficiencies were believed to be the result of discrepancies in techniques of measurement or specimen preparation, the data were normalized on the basis of a 100% alloy composition.

Metallographic and microprobe examinations revealed a laminar-type structure in the chromized region composed of a chromium-rich layer varying from 0.03 to 0.64 mil in depth and a nickel-rich layer varying in depth from 0.43 to 2.70 mils. Five of the six cup-plugs exhibited this laminar structure, while the sixth was characterized by a globular or agglomerated appearance.

The chromium content on the edges of these cup-plugs was found to vary from 37 to 90%. Based on these data, cup-plugs with Cr/Ni ratios of about 1.5 were found to exhibit the

TABLE 18

CHROMIUM LAYER THICKNESS AND PERFORMANCE DATA FOR FIVE LOTS OF END PLUGS

Lot Number	Sample Number	Chrome Layer		Number Coated	Yield (%)		
		Thickness (mils)	Structure		Perfect	Acceptable	Rejects
MT	T	0.25	Laminar	5	100	-	-
M0201	M2	0.40	Laminar	8	100	-	-
M0302	M3	0.50	Laminar	10	-	100	-
0603	F1	0.53	Laminar	9	-	40	60
0603	E1	0.76	Laminar				
M0101	M1	0.80	Agglomerated	14	-	-	100

TABLE 19

Cr/Ni RATIOS OF CUP-PLUGS AS DETERMINED BY X-RAY FLUORESCENCE

Sample Number	Cr/Ni Ratios		Yield (%)		
	Average	Range	Perfect	Acceptable	Rejects
T	0.89	0.56 to 1.24	100	-	-
M2	0.66	0.65 to 0.66	100	-	-
M3	0.81	0.80 to 0.82	-	100	-
F1	2.49	2.19 to 2.81		40	60
E1	5.31	4.91 to 5.75			
M1	0.38	-	-	-	100

best coatability. Cup-plugs with chromium content above and below this value appeared to exhibit the worst performance.

c. Nondestructive Tests Related to Coating

(1) Chromized Coating Measurements

Additional evaluation of the x-ray fluorescence method of measuring the quantity or thickness of chromized coatings has continued. The x-ray fluorescence method utilizes a standard laboratory instrument with rotating sample holder into which end caps or tube samples are placed. The calculated ratios of the amplitudes of the chromium and nickel lines are indicative of the quantity of chromium diffused into the surface of the Hastelloy-N components. This has been verified with microprobe readings and metallography. To provide an indirect group of reference standards, a group of end caps was electroplated with varying thicknesses of chromium.

(2) Burnable Poison Analysis

The precision of the neutron activation analyses method of measuring the total and incremental burnable poison content of coated cladding tubes has been steadily improved. This has been in anticipation of the use of this method to routinely inspect S8DS coated cladding tubes. To date, all dynamic irradiations have been performed in the L-77 laboratory reactor operating at 10 watts. The linear rate through the reactor has been 18 in./hr. Approval to perform dynamic irradiations in the AE-6 reactor has been obtained. Static irradiations show that this reactor may be operated at 500 watts with tubes being drawn through the core at a linear rate of about 6 in./min. Radiation levels will be about 10 times those obtained in the L-77 which will permit more accurate radiation measurements to be made in a fraction of the time required with the L-77 irradiated tubes. Because of the increased neutron exposure, special radiation safety precautions are being planned for personnel handling irradiated tubes from the AE-6 reactor. Preliminary radiation surveys of tubes taken 2 hours after irradiation indicate that contact measurements as high as 300 millirem/hr (β, γ) may be expected. After 24 hours, the radiation level has dropped to 5 millirem/hr (β, γ), indicating that no hazard to counting personnel should be expected (samples are counted about 24 hours after irradiation to permit the decay of short-lived isotopes in the cladding and slip).

Development of the pre-irradiated slip method of nondestructively measuring burnable poison has been initiated under the SRIP Program. Poison-containing slip is to be irradiated to activate the Sm^{153} prior to coating the cladding tubes. While some radiation safety

precautions are anticipated, the method shows promise of being more rapid, more accurate, and less costly than the present analytical methods.

d. Advanced Coating Development

The objective of this program is to develop improved hydrogen permeation barrier materials as developed from the SNAP 8 reference barrier material (SCB). Three approaches to this problem have been under study:

1) Crystalline oxides are being introduced into the slip during the frit milling operation. The effectiveness of this approach depends on the relative hydrogen permeation properties of the mill addition oxide and of the matrix material, on the volume fraction of the crystalline oxide that can be added to the slip, and on any change in the hydrogen permeation properties of the matrix glass that may result from the dissolution of the crystalline oxide in the glass during the firing operation.

2) The composition of the frit is being adjusted in an effort to suppress crystallization of the coating material and thereby extend the long-time high-temperature use capability of the coating.

3) Methods for improving the adherence of the coating to the cladding are being developed.

These studies have resulted in a new coating, identified as SCB-2, with improved properties; and a method for improving SCB-1 or SCB-2 coating by adding 10 wt % Al_2O_3 during milling of the frit. The properties of the new coating materials are listed in Table 20 and 21.

TABLE 20
IMPORTANT PROPERTIES OF NEW COATINGS MATERIALS

SCB	Composition (wt %)				Color*	Thermal Expansion Coefficient ($\times 10^6$/°F)	Softening Temperature† (°F)	Relative Fusion Flow§	Incipient Crystallization Temperature** (°F)	Firing Temperature (°F)	Remarks
	SiO_2	BaO	Al_2O_3	Modifier							
1	46.7	32.7	7.5	TiO_2 13.1	Amber	3.1	1480 ± 20	1.0	1625	2100	S8DS reference hydrogen permeation barrier
2	44.0	45.0	11.0	none	none	3.7	1435	0.6	none	≥2150	Resists devitrification; TiO_2-free; higher coefficient expansion
3	38.2	39.1	9.6	TiO_2 13.1	Amber	ND††	ND	0.4	1800	~2100	NS§§: Contains TiO_2, too refractory
4	53.7	37.7	8.6	none	none	3.0	1475	0.2	none	ND	NS: Too refractory
6	51.7	36.3	12.0	none	none	ND	ND	0.0	1600	ND	NS: Too refractory
8	50.0	35.0	8.0	TiO_2 7.0	none	3.2	1400	0.0	1600	ND	NS: Too refractory
9	41.8	42.8	10.4	CaO 5.0	Green	3.9	1500	0.0	1800	ND	NS: Too refractory
10	39.6	40.4	10.0	CaO 10.0	Green	4.1	1500	0.2	1800	ND	NS: Too refractory
11	43.6	44.5	10.9	CaF_2 1.0	Green	ND	ND	0.6	none	~2100	NS: Too refractory
12	42.7	43.6	10.7	CaF_2 3.0	Green	2.5	1360	0.9	none	~2100	NS: Expansion coefficient too low
13	43.0	45.0	11.0	B_2O_3 1.0	Green	ND	ND	0.8	none	>2100	NS: Could not be applied to a cladding assembly
14	39.0	45.0	11.0	B_2O_3 5.0	Green	3.5	1475	1.4	none	>2100	NS: Could not be applied to a cladding assembly
15	43.0	44.0	10.8	B_2O_3 2.2	Green	ND	ND	1.0	none	2100	NS: Could not be applied to a cladding assembly
16	44.0	44.1	11.0	BaF_2 1.0	none	3.6	1500	0.6	1900	ND	NS: Too refractory
17	43.8	42.2	11.0	BaF_2 3.0	none	3.6	1460	0.8	1900	ND	NS: Too refractory
18	39.0	45.0	11.0	V_2O_5 5.0	Green	3.9	1485	0.4	1750	ND	NS: Too refractory
19	29.0	45.0	11.0	V_2O_5 15.0	Green	3.9	1450	0.0	1400	ND	NS: Too refractory
20	43.8	40.5	11.0	BaF_2 5.0	none	3.6	1400	0.9	ND	ND	NS: All were satisfactory but SCB-23 had the best firing properties. The use of these coatings is pending compatibility tests. The fluorine content may have undesirable effects on the fuel-coating system
21	43.7	38.5	11.0	BaF_2 7.0	none	ND	ND	0.9	ND	ND	
22	43.5	35.6	10.9	BaF_2 10.0	none	ND	ND	1.1	ND	ND	
23	43.7	39.5	11.0	BaF_2 6.0	none	3.5	1400	1.0	1900	2100	

*All materials were transparent glasses.
†Softening temperature is defined as the maximum on the thermal expansion vs temperature curve.
§At 2100°F: Based on SCB-1 as unity.
**After annealing in air for 5 hr in a 1400 to 2200°F gradient.
††ND = not determined.
§§NS = not suitable.

TABLE 21

PROPERTIES OF HYDROGEN BARRIER MATERIALS MILL ADDITIONS

Basic Coating Material	Mill Additions		Firing Temperature (°F)	Softening Point* (°F)	Coefficient of Thermal Expansion (x 10^6/°F)	Specimen Number	Hydrogen Permeation Rate at 1500° and 1 atm Pressure [x 10^{-3} cc(STP)/cm^2-hr]
	Amount (wt %)	Oxide					
SCB-1	none	none	2100	1480	3.1	-	1.6†
SCB-1	10	Al_2O_3	2100	>1900	3.3	3103	2.0
						3157	2.0
SCB-1	20	Cr_2O_3	2150	1800	3.1	2296	0.7
						3159	1.6
						3175	4.0
SCB-1	20	CeO_2	2100	1835	3.9	3107	1.5
						3153	10.0
						3181	3.0
SCB-2	none	none	2150	1435	3.7	3145	6.0
						3148	0.6
						3152	0.9

*Softening point is defined as the temperature at the maximum of the thermal expansion curve.
†Average for many tests.

TABLE 22

RELATIVE DEVITRIFICATION TENDENCY OF SCB-1 AND SCB-2 GLASSES

Glass	Temperature at Which Initial Surface Crystallization is Observed (°F)			Thickness of Crystalline Rind Forming at the Surface at 1800°F (in.)			Temperature at Which Initial Internal Crystallization is Observed (°F)		
	After 5 Hours	After 20 Hours	After 24 Hours	After 5 Hours	After 20 Hours	After 24 Hours	After 5 Hours	After 20 Hours	After 24 Hours
SCB-1	1625	1625	-	0.001	0.005	-	1700	>1650, <1700	-
SCB-2	None	-	1760	None	-	Insignificant	None	-	None

SCB-2 represents an improvement over SCB-1, the S8DS reference coating, for three reasons. The most important reason is that it is much more resistant to devitrification than SCB-1 material (see Table 22). Resistance to devitrification is important since it has been found that devitrified SCB-1 coating has a permeation rate a factor of 2 higher and is less resistant to thermal shock after long-term aging than vitreous SCB-1 coatings. SCB-2 material also has a higher thermal expansion coefficient which reduces stresses during cooling. Finally, SCB-2 material does not contain TiO_2 while the other SNAP reference coatings (S14-35A, AI-8763D, and SCB-1) contain about 10 wt % of this constituent. Since TiO_2 may be partially reduced by hydrogen at 1500°F under certain conditions, it may contribute to the fuel-coating reaction observed in fuel elements.

Some of the material properties obtained with mill additions to SCB-1 are noted in Table 21. Al_2O_3 mill additions improved the SCB-1 coating by increasing the softening temperature more than 400°F without a corresponding increase in the firing (application) temperature. A higher softening temperature range is believed to indicate that the coating will be significantly more viscous during service and the higher viscosity may reduce the rate of undesirable diffusion processes (e.g., devitrification or chemical reactions).

The initial permeation rates for membranes coated with these new materials are generally comparable to or better than the rates for SCB-1-coated membranes as noted in Table 21. The permeation rates for three SCB-2-coated membranes tested at 1400°F and 2 atm pressure were 0.6, 0.9, and 6.0×10^{-3} cc(STP)/cm^2-hr. For comparison, the rates for two membranes coated with SCB-1 + 10% Al_2O_3 were 1 and 2 cc(STP)/cm^2-hr and the average rate for SCB-1-coated membranes is 1.6×10^{-3} cc(STP)/cm^2-hr.

As a part of the work on development of ceramic hydrogen barrier materials, limited tests of alternate cladding materials were performed. These alternate claddings included Hastelloy-X and Hastelloy-X-285.* The adherence and appearance of SCB-1 coating to samples machined from Hastelloy-X bar stock and to Hastelloy-X sheet materials were excellent. Furthermore, these properties did not deteriorate after 4,000 hours aging at 1500°F in hydrogen at 1 atm pressure (see Table 23).

Excellent adherence of SCB-1 coatings to Hastelloy-X-285 was obtained but only after precoating oxidation of the substrate. Some of the precoating oxidation treatments used and the results obtained are shown in Table 24. Adherence test results along the length of two full-length closed-end membranes are presented in Table 25. Short sections of SCB-1-coated Hastelloy-X-285 were aged at 1500°F in hydrogen at 1 atm pressure for 1,000 hours without deterioration of the adherence or appearance of the coating.

*Hastelloy-X-285 meets published composition requirements for Hastelloy-X-280; however, it has been found that the concentration of the elements manganese, phosphorus, tungsten, sulphur, carbon, and silicon are unusually low due to the vacuum melting practice employed. As a result, certain performance characteristics of the alloy, such as welding behavior, have been altered relative to those of Hastelloy-X or Hastelloy-X-280.

TABLE 23

ADHERENCE OF SCB-1-COATED HASTELLOY-X AFTER AGING IN HYDROGEN AT 1500°F

Substrate Configuration	Aging Time (hr)	Coating Adherence	Remarks
1 in. by 2 in. by 0.015 in. sheet	0	Excellent	Many flexes were required to break off the coating. The exposed metal was covered with adherent glass (or oxide) fragments.
	500	Excellent	
	1500	Excellent	
	2400	Excellent	
	4000	Excellent	
S8DS	0	-	*
Cup-plugs	1000	-	†
Welded 5/8 in. tubing	0	Excellent	No coating was broken off after flexing 11 times around a 1/2-in.-diameter mandrel.
	500	Excellent	
	1500	Excellent	

*There is no adherence test for cup-plugs, but the coating will spall if adherence is poor.
†No change in appearance except in color. It is normal for the color to change from green to dark grey.

TABLE 24

PREOXIDATION STUDY DATA OF HASTELLOY-X-285* COATED WITH SCB-1

Pre-oxidation†		Oxide		Metal Grain Size		SCB-1 Coating Adherence	Remarks on Adherence
Temperature (°F)	Time (hr)	Appearance§	Weight Gain (10^4gm/cm^2)	Before Coating (ASTM)	After Coating (ASTM)		
-	-	-	-	5	4	none	Less than one flex** was required to break off 50% of the coating.
1900	1/2	U	1.6	4	4	Excellent	Eight flexes were required to break off 50% of the coating.
1900	1	U	2.2	4	5	Excellent	Eight flexes were required to break off 50% of the coating.
1900	2	U	2.6	3	4	Excellent	No coating broke off after 11 flexes
2000	1/2	U	3.8	4	5	Excellent	No coating broke off after 11 flexes
2000	1	U-NU	3.9	3	4	Excellent	No coating broke off after 11 flexes
2000	2	NU	5.8	4	5	Excellent	No coating broke off after 11 flexes
2100	1/2	NU	5.5	4	4	Excellent	No coating broke off after 11 flexes
2100	1	NU	5.7	4	4	Excellent	No coating broke off after 11 flexes
2100	2	NU	7.8	3	4	Excellent	No coating broke off after 11 flexes

*Specimens were 8-in. double-open-end tubes.
†Specimens were pre-oxidized in air at a flow rate of 110 cm^3/min with a dew point of 32°F.
§U = uniform, NU = not uniform.
**One flex consisted of bending a 3/4-in.-long section around a 1/2-in.-diameter mandrel.

TABLE 25

ADHERENCE OF SCB-1 ON PRE-OXIDIZED* HASTELLOY-X-285 SNAP 8 MEMBRANES

Specimen Number	Distance from Blind End (in.)	Remarks on Adherence
X-23-4	1/2	Excellent - No coating broke off after 11 flexes†
	4	Excellent - No coating broke off after 11 flexes
	8	Excellent - No coating broke off after 11 flexes
	12	Excellent - No coating broke off after 11 flexes
	15-1/2	Excellent - 50% of the coating broke off after 9 flexes
	17-1/2	Excellent - 50% of the coating broke off after 9 flexes
X-40-1	1	Excellent - No coating broke off after 11 flexes
	17-1/2	Excellent - 50% of the coating broke off after 6 flexes

*Membranes were oxidized by inserting a quartz probe extending to within one inch of the blind-end and purging with bottled air at a flow rate of 110 cc/min and a dew point of 32°F.
†One flex is a complex bend around a 1/2-in.-diameter mandrel.

3. Closures

a. Closure Development and Testing

Five S8DRM-1 closure seals have been on thermal endurance test for approximately 16,990 hours. The cluster permeation rate is 0.79 cc(STP)hr at 1300°F and 2 atm for an average of 0.16 cc(STP)hr/sample. This is an increase of 0.05 cc/hr from the rate reported at the end of the previous reporting period but represents no change within experimental error.

Five S8DS closure seals have accrued 14,563 hours on thermal endurance test. The cluster permeation rate is 0.37 cc(STP)/hr at 1400°F and 2 atm for an average of 0.07 cc(STP)/hr.

b. Closure Welding

Process improvement studies were conducted to improve the S8DS closure weld process capability. While the current process had been qualified for core production and yield had been acceptable, metallographic examination of rejected closure welds indicated that the chrome substrate on the cladding decreased weld yield.

Chromium has a melting point approximately 1000°F higher than the Hastelloy-N cladding and has a comparatively high vapor pressure. The presence of the chrome substrate in the weld zone tends to inhibit melting of the parent metal and probably enhances bubble defects or porosity.

Mockup welds were made in which the chrome-rich substrate was machined from the cup-plug weld joint surfaces. Metallographic evaluation of the mockup welds showed that the process variability was reduced by a factor of 2 for average weld penetration. These welds also showed an improved surface condition as indicated by dye penetrant tests. These tests indicate that a 90% yield of S8DS closure welds may be expected.

c. Nondestructive Tests Related to Closures

A new commercially available, high resolution, single emulsion x-ray film has made it feasible to inspect closure welds for fit-up prior to welding, and possibly to inspect for weld penetration after welding. S8DS butt weld mockups were radiographed both before and after welding. The before-welding radiographs, Figure 28, show evidence of mismatch and incorrect fit-up, which were not defined during visual examination.

Measurements have been made of weld penetrations of both butt welds and the edge weld which is being evaluated for SNAP fuel elements.

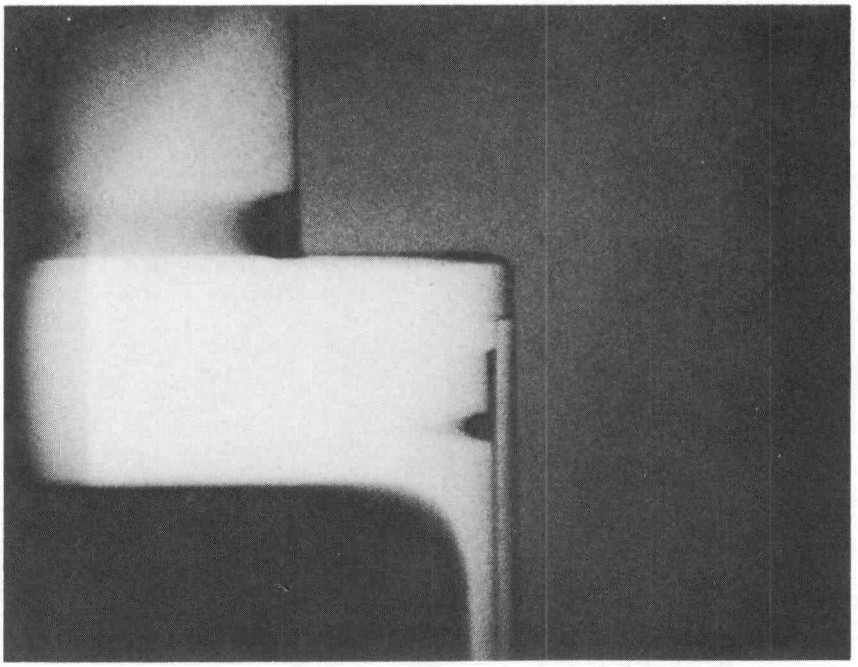

(a)

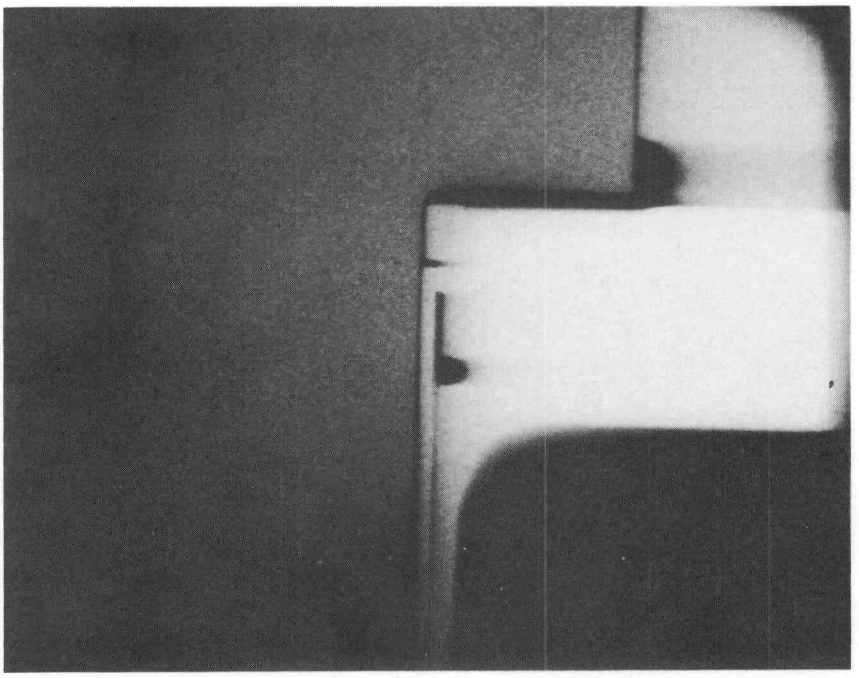

8-19-65 (b) 7568-02292

Figure 28. Butt Weld Joint Radiographed Prior to Welding to Determine Weld Fit-up. The upper radiograph (a) shows a 0.005-in. mismatch between cladding tube and end cap. Radiograph (b) shows a 0.006-in. gap between end of cladding tube and end cap shoulder.

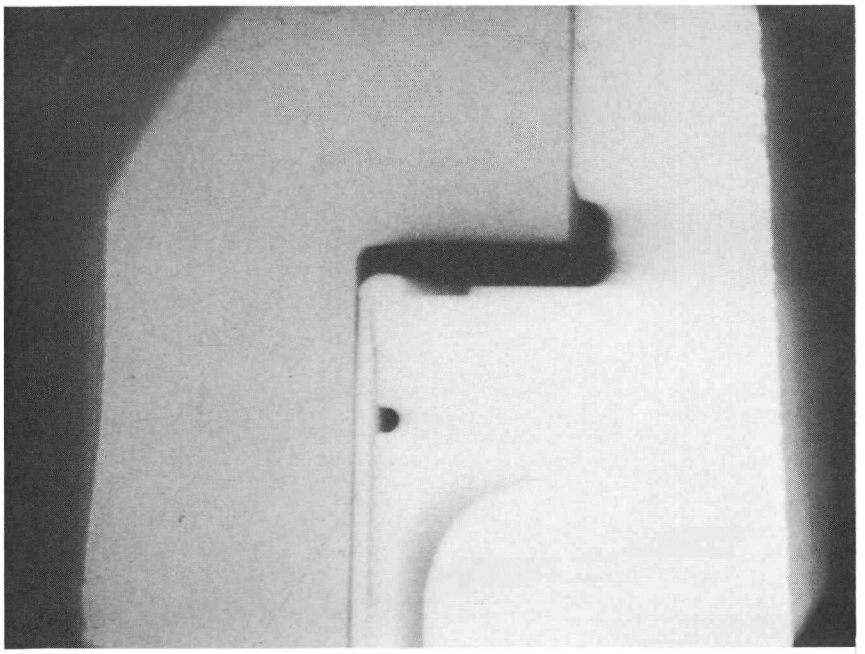

8-19-65 7568-02293

Figure 29. Edge Weld Radiographed with Correction Form. Weld penetration and cladding wall thinning are readily measurable whenever there is a slight radial gap between cladding tube and end cap. Weld penetration is 0.015 in. and the cladding wall thickness has been reduced to 0.006 in.

Whenever a radial gap greater than 0.001 in. is present, sufficient x-rays will penetrate this gap to produce an image as shown in Figure 29. At present, films are examined and measurements are made with a 10X microscope equipped with a micrometer eyepiece. Measurements can be made to the nearest 0.001 in.

Correlation studies between weld measurements made by the radiographic technique and subsequent metallographic examination are in progress. Preliminary data show good correlation between the two methods, demonstrating the accuracy of the nondestructive radiographic technique.

4. Performance Tests

a. S8ER Fuel Elements

During this report period, nonnuclear performance tests (qualification and environmental) of fuel elements of the S8ER design were concluded. Data obtained prior to this report period have been discussed previously.* These data led to the following conclusions:

1) Hydrogen permeation rates increased during pre-endurance tests (damage), decreased during endurance test (generally as a function of pressure), and increased during testing after endurance (additional damage).

*C. E. Johnson, "SNAP 8 Progress Report February-April, 1965, "NAA-SR-11092 (SRD), June 15, 1965, pp 61-67

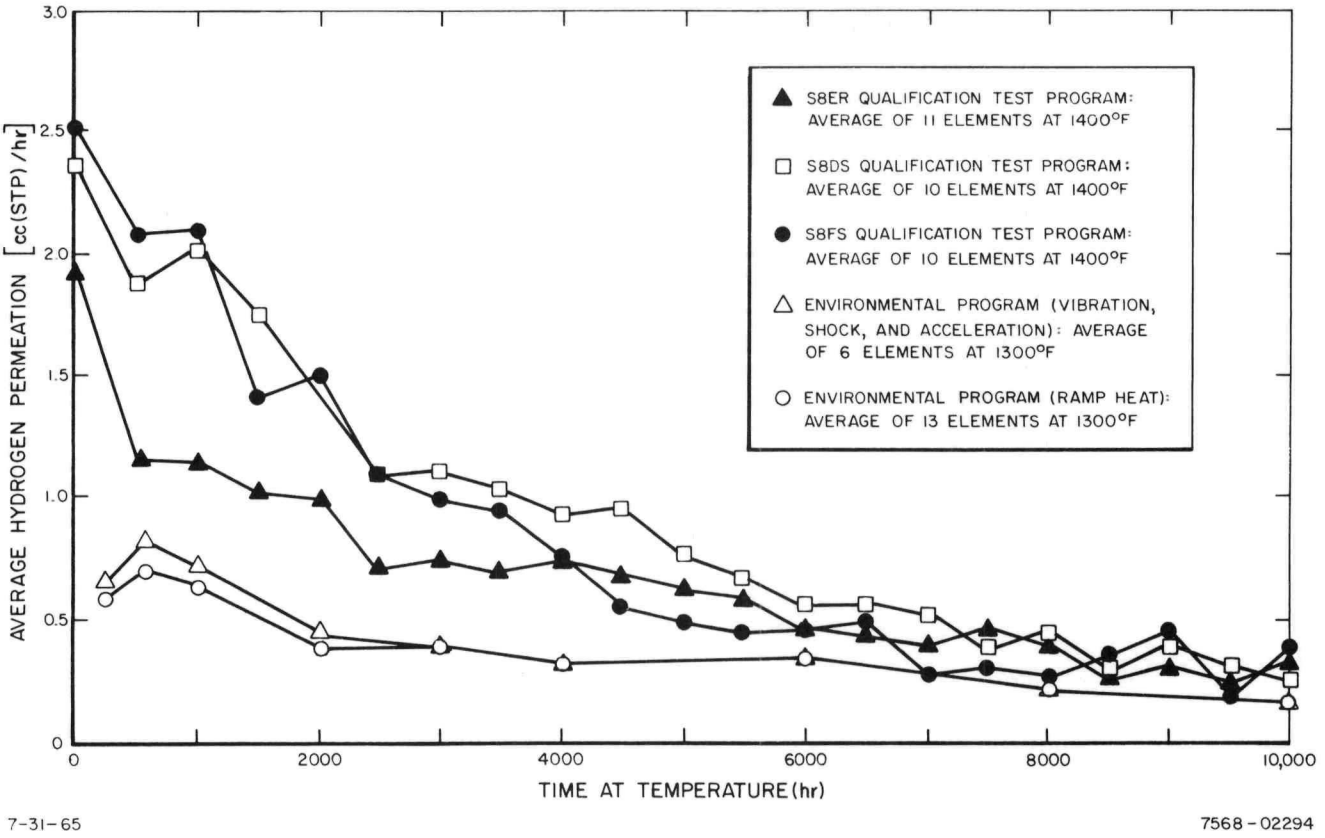

Figure 30. Average Hydrogen Permeation Rates of S8ER Design Fuel Elements During Thermal Endurance Test

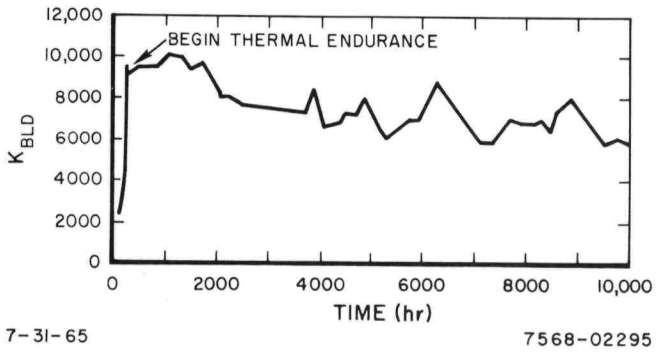

Figure 31. Average K_{BLD} vs Time at 1300°F for 18 Environmental S8ER Design Fuel Elements

TABLE 26

PERMEATION SCAN DATA OF SEVEN S8ER FUEL ELEMENTS

Element Number	Hydrogen Flow (%)			Total Hydrogen Permeation in Scanner [cc(STP)/hr]
	1-1/8-in. Closure End	12-in. Center Section	1-1/8-in. Blind End	
E-814-N	55	20	25	2.6
E-960-N	66	14	20	2.4
E-916-N	44	37	19	1.6
E-884-N	72	7	21	2.5
E-972-N	46	16	38	1.9
E-963-N	51	22	27	2.8
E-1017-N	46	35	19	2.4
Average	54	22	24	2.3

2) The greatest hydrogen loss is from the closure end of the fuel element.

3) Fuel element dimensions increased slightly during performance testing due to the relief of residual stresses incurred during production straightening of the cladding tubes.

Additional data obtained during this report period are discussed in the following paragraphs.

Thermal endurance tests results for the qualification and the environmental elements are summarized in Figure 30. Six of the environmental elements had previously been subjected to high levels of vibration, shock, and acceleration while the remaining 13 environmental elements had previously received high rates of ramp heating. The data shown in Figure 30 for these two groups of elements indicate that the relative effects of these two tests were almost identical. In comparison, initially there is a wide range in the performance of the three groups of qualification elements; however, this variation was reduced to a minimum value with continued testing at 1400°F.

The reduction in hydrogen permeation with time for both the qualification and the environmental elements was not entirely due to the reduction in hydrogen dissociation pressures. Part of the permeation decrease was due to an apparent improvement in the hydrogen barrier, indicated by a decreased K_{BLD} (Figure 31). This decrease in K_{BLD}, a parameter which describes the relative worth of hydrogen barrier, implies an improved ceramic. A similar decrease in K_{BLD} for the qualification elements was shown previously.*

Seven additional fuel elements were tested in the permeation scanner. The data, given in Table 26, support the second conclusion above. Further confirmation was found by testing four fuel elements at gradient temperature. The data from these tests, shown in Figure 32, indicate that higher permeation rates generally occur when the closure end is at the higher temperature while lower permeation rates occur when this end is cooler.

Upon completion of the permeation tests of the fuel elements in the qualification and environmental test programs, all elements were disassembled. Dimensional and weight measurements were taken on each fuel rod prior to performing dissociation pressure tests. Table 27 presents a comparison of the hydrogen loss of the 31 qualification elements during testing based on (a) integrated permeation-time data, (b) weight loss of the fuel during testing, and (c) final hydrogen content based on pressure measurements. For each calculation, the initial amount of hydrogen present is based on quality assurance data which included the initial weight and wt % of hydrogen in the fuel rod. The initial wt % hydrogen was based on chemical analyses. Comparable data for the 19 environmental elements are listed in Table 28.

There is, generally, good agreement between the average values of hydrogen loss as calculated by the three methods for both the qualification and the environmental elements. The largest inconsistencies observed were for three environmental elements, E-1011-N, E-1000-N and E-1054-N. The qualification elements, which were tested at 1400°F, had an average hydrogen loss over 10,000 hours of 14%. In comparison, the environmental elements, which were tested at 1300°F, had an average hydrogen loss over 10,000 hours of about 6%.

Residue was observed when the fuel rods were removed from the cladding assemblies during disassembly. The quantity of residue varied considerably: little was found in the

*Ibid, p. 62

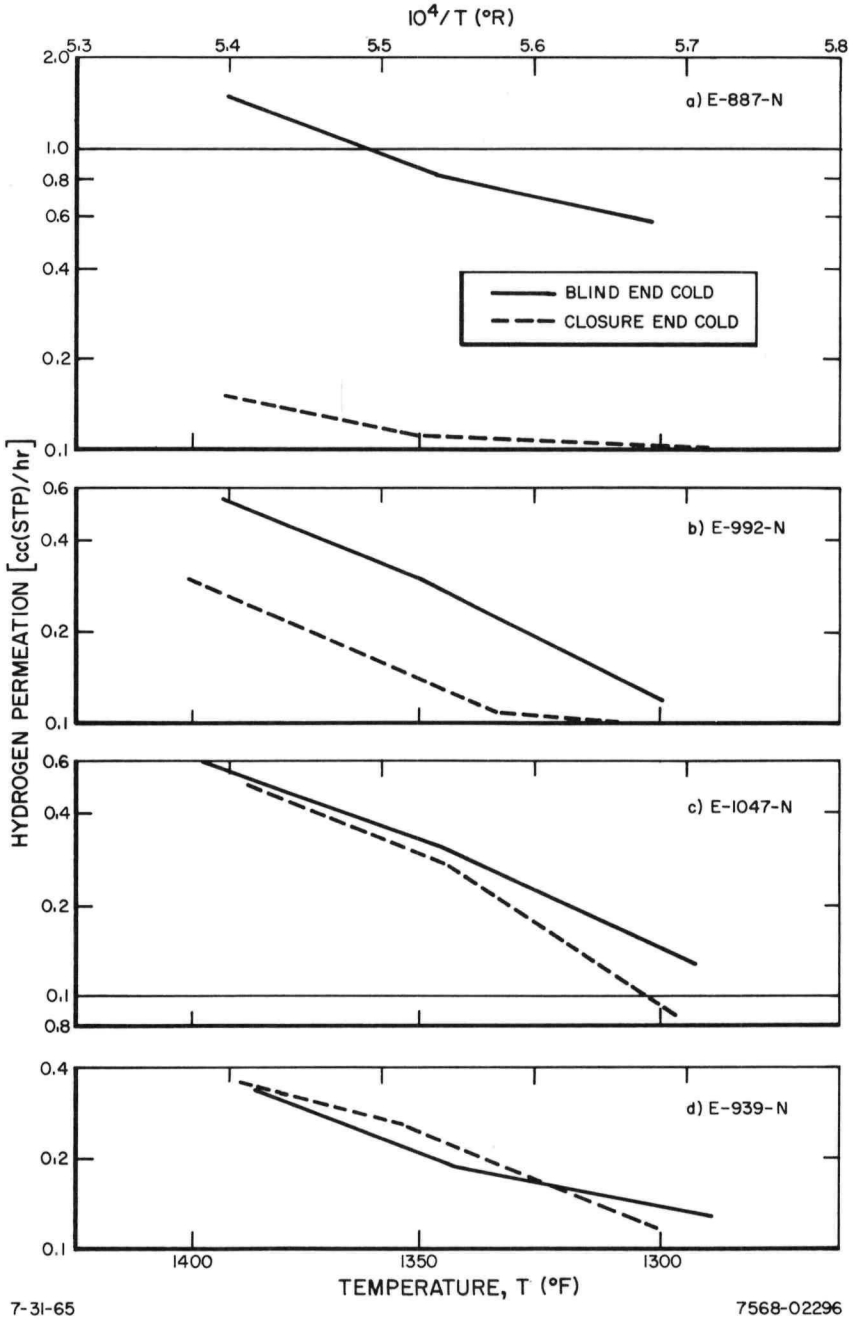

Figure 32. Permeation-Gradient Temperature Relationships

TABLE 27

HYDROGEN LOSS OF 31 QUALIFICATION ELEMENTS

Element Number	Initial Hydrogen (wt %)	Fuel Weight (gm)		Hydrogen Loss at 1400°F* (%)			
		Initial	Final	Through 10^4 Hours (Method 1)†	Through Post-End Testing		
					Method 1†	Method 2§	Method 3**
E-760-N	1.655	308.889	307.780	9.8	11.6	21.7	15.5
E-811-N	1.680	308.638	307.808	18.0	18.4	17.0	16.1
E-881-N	1.640	309.570	308.872	12.3	-	13.7	11.2
-802	1.640	309.190	308.610	10.6	-	11.4	10.6
-886	1.670	309.820	309.120	15.9	-	13.5	14.1
Retort Average	1.650	309.527	308.867	12.9	14.0	12.9	12.0
E-804-N	1.710	309.020	308.101	8.3	-	15.7	14.6
-821	1.710	308.678	307.958	9.9	-	13.6	14.2
-897	1.700	309.122	308.329	11.4	-	15.1	17.9
Retort Average	1.707	308.940	308.159	9.9	11.3	14.8	15.6
E-880-N	1.695	308.912	308.119	8.4	-	15.1	13.4
-841	1.680	308.970	308.383	8.6	-	11.3	12.0
-810	1.690	307.578	307.018	12.8	-	10.8	12.9
Retort Average	1.688	308.487	307.840	9.9	10.8	12.4	12.8
E-939-N	1.705	308.851	307.750	18.3	-	20.9	18.8
-858	1.705	308.243	306.898	18.9	-	25.6	17.8
-887	1.690	309.035	307.962	12.6	-	20.5	15.8
Retort Average	1.700	308.710	307.537	16.6	17.6	22.3	17.5
E-960-N	1.680	308.642	307.833	11.2	-	15.6	16.9
-962	1.675	308.679	307.304	21.7	-	26.6	16.6
-814	1.685	308.663	307.658	15.6	-	19.3	15.7
Retort Average	1.680	308.661	307.598	16.2	16.9	20.5	16.4
E-916-N	1.680	309.415	308.719	15.6	15.8	13.4	13.1
E-870-N	1.680	309.146	308.474	15.0	15.7	12.9	14.3
E-951-N	1.685	309.685	308.969	16.5	-	13.7	16.9
-918	1.680	309.349	308.414	14.9	-	18.0	16.9
Retort Average	1.682	309.517	308.692	15.7	16.8	15.9	16.9
E-861-N	1.710	304.711	304.005	13.6	-	13.5	16.6
-884	1.715	305.081	304.390	15.8	-	13.2	17.4
-1012-N	1.705	304.938	304.161	16.6	-	14.9	16.4
Retort Average	1.710	304.910	304.185	15.3	16.1	13.9	16.8
E-1007-N	1.695	305.376	304.614	13.7	14.8	14.7	17.4
E-972-N	1.715	305.130	304.182	17.5	-	18.1	18.4
-987	1.715	304.770	303.920	14.6	-	16.3	19.2
-992	1.710	304.881	303.982	17.8	-	17.2	18.2
Retort Average	1.713	304.927	304.028	16.6	17.1	17.2	18.9
E-963-N	1.685	305.096	304.385	12.2	-	13.8	16.0
-1047	1.695	305.072	304.256	9.7	-	15.8	13.8
-1017	1.695	304.806	303.872	16.5	-	18.1	17.6
Retort Average	1.692	304.991	304.171	12.8	13.3	15.9	15.8
Total Element	1.689	307.676	306.837	14.0	15.0	16.1	15.7

*Initial hydrogen present is based on the weight of the hydrided final-machined fuel rod and the weight % hydrogen. The final hydrogen present is determined as follows:

† Method 1. Integration of permeation - time data.

§ Method 2. Measured fuel rod weight after decanning. Weight loss is all attributed to hydrogen loss.

**Method 3. Final hydrogen composition based on isochore data (assuming a one-to-one carbon to zirconium combination).

TABLE 28

HYDROGEN LOSS OF 19 ENVIRONMENTAL ELEMENTS

Element Number	Initial Hydrogen (wt %)	Fuel Weight (gm)		Hydrogen Loss at 1300°F (%)			
		Initial	Final	Through 10^4 Hours (Method 1)	Through Post-End Testing		
					Method 1	Method 2	Method 3
E-947-N	1.69	308.184	307.656	-	-	10.0	7.5
-1011	1.70	309.230	308.936	-	-	1.2	9.4
-1009	1.69	308.332	308.119	-	-	4.0	2.6
Retort Average	1.69	308.582	308.237	6.3	6.3	5.1	6.5
E-996-N	1.65	309.431	309.103	-	-	6.3	5.8
-1000	1.66	309.594	309.577	-	-	0.3	4.4
-1029	1.67	309.906	309.548	-	-	6.8	6.2
Retort Average	1.66	309.644	309.409	7.0	7.4	4.5	5.5
E-990-N	1.66	309.529	309.176	-	-	6.7	6.6
-1019	1.67	309.288	308.960	-	-	6.7	5.4
-1033	1.66	309.926	309.750	-	-	3.4	3.4
Retort Average	1.66	309.581	309.295	5.6	6.5	5.6	5.1
E-1001-N	1.68	309.863	309.312	5.7	5.7	10.4	6.7
E-1054-N	1.68	308.891	309.856	-	-	0.6	3.5
-1008	1.68	309.541	309.205	-	-	6.4	7.0
-907	1.68	309.592	309.182	-	-	7.7	8.0
Retort Average	1.68	309.341	309.081	5.9	6.6	4.9	6.2
E-993-N	1.68	309.529	309.171	-	-	6.8	5.3
-904	1.67	309.752	309.361	-	-	7.4	6.2
-940	1.66	310.212	309.961	-	-	4.8	3.6
Retort Average	1.67	309.831	309.498	6.5	6.5	6.3	5.0
E-984-N	1.64	309.708	309.301	6.5	6.5	7.9	6.4
E-1032-N	1.72	308.207	307.860	6.6	7.8	6.4	6.1
E-1052-N	1.69	308.304	307.940	6.3	7.6	6.9	6.2
Element Average	1.67	309.316	308.998	6.3	6.6	5.8	5.8

environmental elements (1300°F tests), whereas it appeared that the majority of the ceramic of all the qualification elements had spalled from the cladding (1400°F tests).

The typical appearance of the environmental element components after test completion is shown by Figure 33. Discoloration of both the fuel rod and the ceramic was noted although no significant amount of spalled ceramic was observed. This discoloration and a dark colored powder material were found on both the environmental and qualification elements. The result of ceramic spalling is illustrated in Figure 34, which shows a section of cladding from a typical qualification element. Equally significant is the fact that none of the disassembled environmental elements had claddings which exhibited "bare metal." This difference in ceramic adherence is further illustrated by photomicrographs of cladding sections from environmental and qualification elements (Figures 35 and 36, respectively). Except for discoloration, there was little apparent change in the ceramic of the environmental elements. Also, the ceramic-metal bond appears to be relatively unchanged due to 1300°F testing.

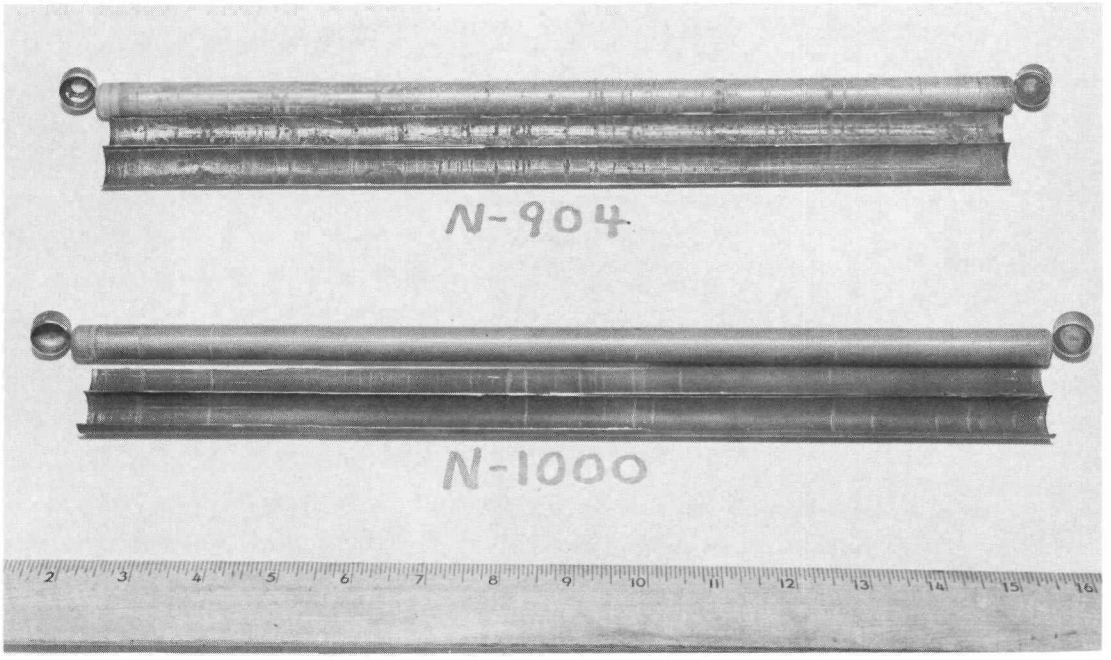

5-17-65 7568-51534CN

Figure 33. Fuel Element Components After Completion of Environmental Testing

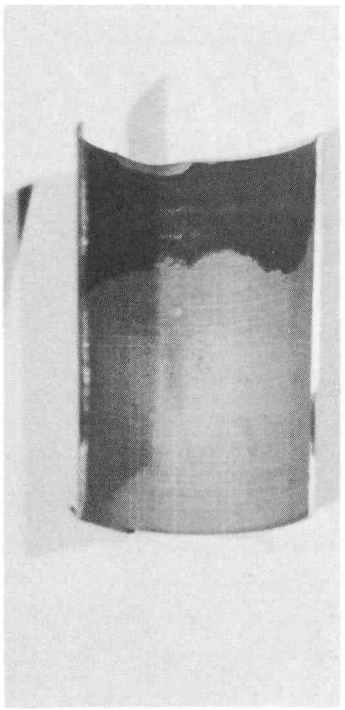

7-31-65 7568-02289

Figure 34. Cladding Section from a Qualification Element (E-810-N)

Photomicrographs of two sections from a qualification element are shown in Figure 36. The first is a cladding section which shows an absence of ceramic. The second shows a cladding section to which some ceramic had adhered. This latter section shows signs of a weakened ceramic-metal bond.

Besides ceramic, the qualification elements also yielded some thin, brownish, translucent flakes. These flakes were not found upon disassembly of the environmental elements. Some of the translucent flakes from the qualification elements were covered on one side with an adherent silvery, metallic-like film. Careful decanning revealed that the silvery film was formed against the ceramic barrier while the brownish, translucent flakes were formed against the fuel rods. Testing of these flakes revealed that the brownish side was electrically nonconducting while the silvery side showed signs of electrical conduction. Both film and

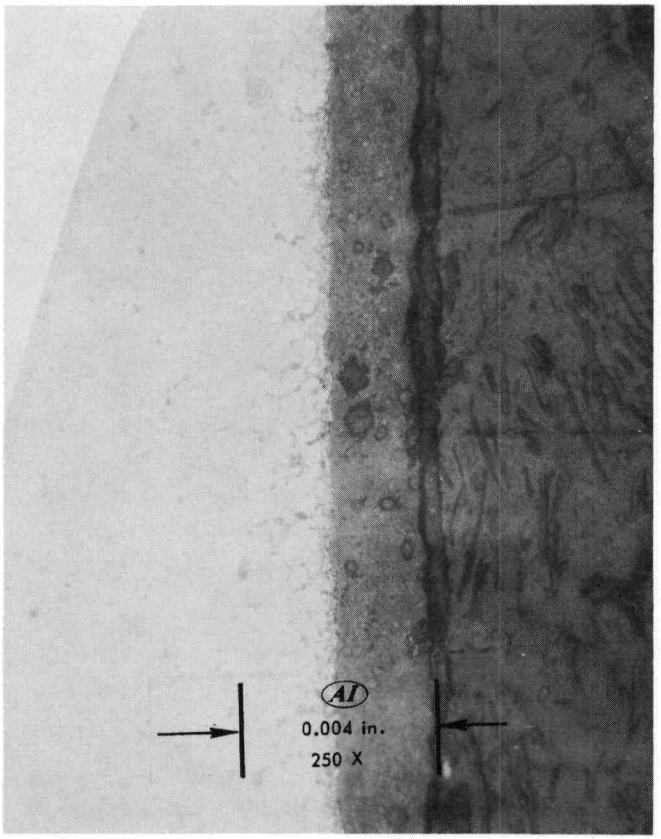

1. HASTELLOY-N TUBE
2. CERAMIC
3. VOID
4. MOUNTING MATERIAL

250 x
MARBLES REAGENT

7-31-45

7568-02297

Figure 35. Cladding Section from an Environmental Element (E-904-N)

a) WITHOUT CERAMIC

b) WITH CERAMIC

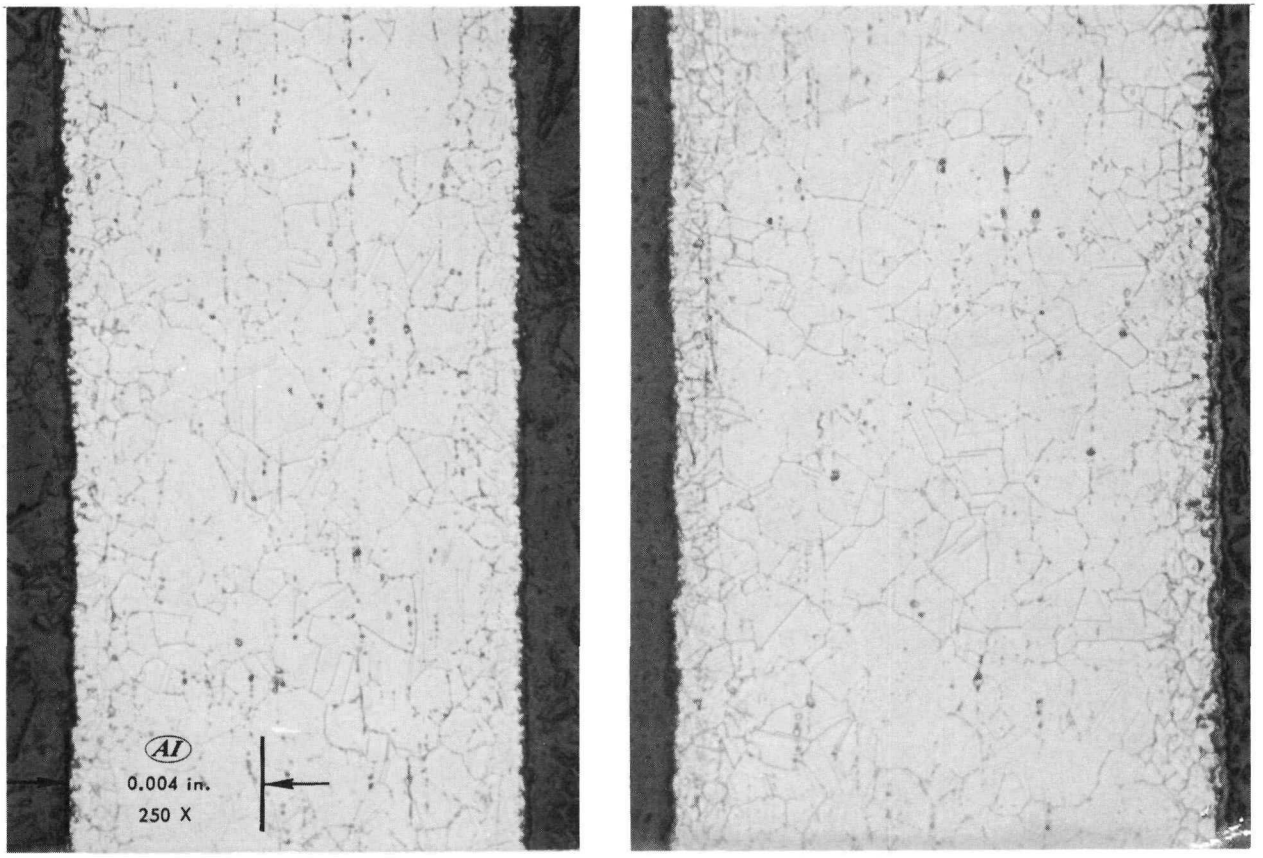

1. HASTELLOY-N TUBE
2. CERAMIC
4. MOUNTING MATERIAL

250x
MARBLES REAGENT

7-31-65

7568-02298

Figure 36. Cladding Section from a Qualification Element (E-811-N)

flakes were stable when heated in air to approximately 1500°F. Chemical analysis revealed that the translucent flakes are predominantly zirconium oxide (ZrO_2) exhibiting both tetragonal and monoclinic structures. X-ray fluorescence indicated that the major constituent of the silvery film is silicon, while spectrographic analysis showed it to be high in zirconium content. In examination by x-ray fluorescence, the ceramic flakes exhibited no significant difference from the original AI-8763D ceramic. Results of the spectrographic analysis (wt %) are shown in Table 29. All metals are in the oxide form.

TABLE 29

SPECTROGRAPHIC ANALYSIS OF RESIDUE FROM DECANNED S8ER FUEL ELEMENTS

Element	Residue (wt %)		
	Ceramic	Translucent Flakes	Metallic Film
Al	3		
B	0.001		
Ba	30	T	T
Ca	2		
Cr	2	T	T
Cu		T	T
Fe	0.2	T	T
Mg	0.3		
Mn	1		
Ni	0.03		
Pb		T	T
Si	25	T	S
Ti	8	T	T
Zr	4	M	M

T = a trace constituent
S = a minor constituent
M = a major constituent
All metals are in the oxide form.

b. S8DS Fuel Element Evaluation Tests

Testing of 61 S8DS developmental fuel elements was continued. In addition, testing of 37 fuel elements, which were fabricated for process verification, was begun. The tests, conducted to evaluate fuel element performance, include:

1) Vibration at different input levels

2) Ramp Heating

Type A: 300°F/min to 850°F, 150°F/min to 1400°F, cooled to 200°F at 50°F/min. This sequence represents one ramp heat cycle.

Type B: 300°F/min to 1400°F maximum, cooling (about 270°F/min peak) to 200°F. This sequence represents one ramp heat cycle.

3) Thermal endurance – continuous operation at isothermal temperatures (1300, 1350, 1400, 1350, 1400 or 1450°F).

4) Destructive analysis – post-test examination of the fuel element components.

The effect of any one test, or series of tests, on fuel element performance is measured by the resultant change in hydrogen permeation (loss) rate at a reference temperature, normally 1400°F. Each element received a permeation test prior to and after completing each of the described tests. In addition, permeation measurements were taken periodically while the elements were undergoing thermal endurance.

Results of tests performed through this report period are summarized in the following sections.

(1) Pre-Endurance Tests

Fourteen S8DS developmental fuel elements were subjected to thermal soak, ramp heating, and thermal cycle tests. Permeation test results are listed in Table 30. The overall result

TABLE 30

THERMAL TEST EFFECTS ON HYDROGEN PERMEATION OF 14 S8DS DEVELOPMENTAL FUEL ELEMENTS

Element Number	Hydrogen Permeation at 1400°F [cc(STP)/hr]			
	Pre-Thermal Soak	Post-Thermal Soak	Post-Ramp Heat (50 Cycles, Type A)	Post-Thermal Cycle
RD-17	0.53	0.48	0.47	0.51
RD-2211	0.18	0.11	0.17	0.30
RD-2241	0.55	0.42	0.35	0.55
RD-33	0.52	0.47	0.53	0.57
RD-2267	0.60	0.39	0.41	0.65
RD-2271	0.33	0.35	0.40	0.75
RD-2443	0.31	0.33	0.41	0.43
RD-94	0.46	0.49	0.64	0.32
RD-97	0.25	0.20	0.17	0.30
RD-3323	0.95	0.57	0.73	0.67
RD-54	0.46	0.24	0.33	0.39
RD-3302	0.42	0.40	0.42	0.40
RD-3309	0.45	0.46	0.61	0.59
RD-2269	0.35	0.52	0.61	0.66
Average	0.45	0.39	0.45	0.51
Average Δ		-0.06	+0.06	+0.06

of these tests was a 13% increase in permeation, a smaller increase than generally has been observed for elements which had received similar tests. For example, 34 previously tested S8DS developmental elements increased in permeation rate from 0.39 to 0.82 cc(STP)/hr at 1400°F after completing a similar thermal test series.* No satisfactory correlation has been determined to explain the variation in the performance of these elements.

(2) Thermal Endurance Tests

After completion of the thermal test series, the 14 fuel elements (listed in Table 30) were loaded into thermal endurance furnaces for testing. Similar tests were also begun on the 34 S8DS developmental fuel elements previously mentioned. Half of the elements from each group were tested at 1300°F for 1400 hours. The remaining elements were tested at 1350°F, also for 1400 hours. After the 1400-hour tests, the temperature of all elements was increased to 1400°F. After 900 hours at 1400°F, the temperature was increased to the present 1450°F test temperature. The average of the permeation rates measured during this sequence of testing is shown in Figure 37. The permeation rates shown for time zero were measured just prior to loading the elements into the endurance furnaces.

*Ibid., p. 56

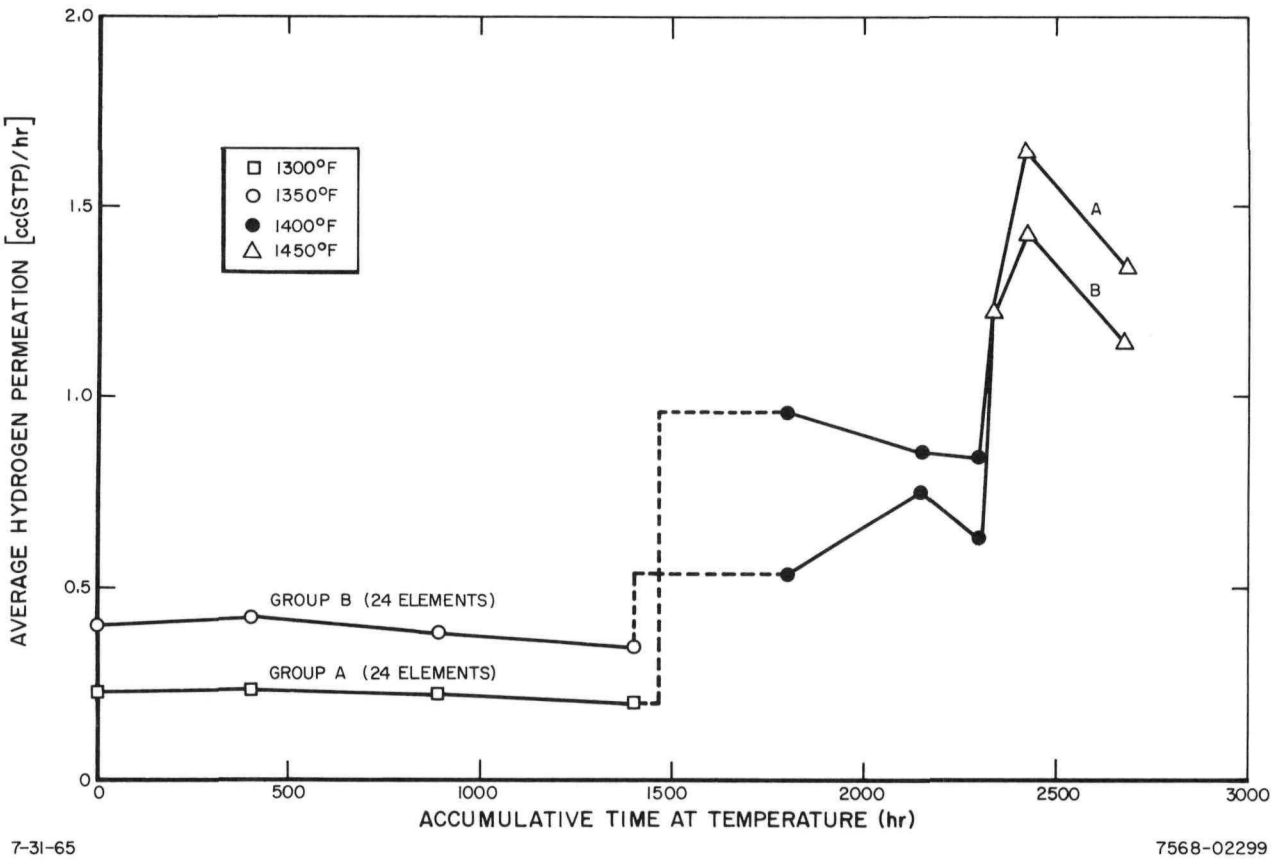

Figure 37. Average Hydrogen Permeation of 48 S8DS Developmental Elements During Thermal Endurance Test

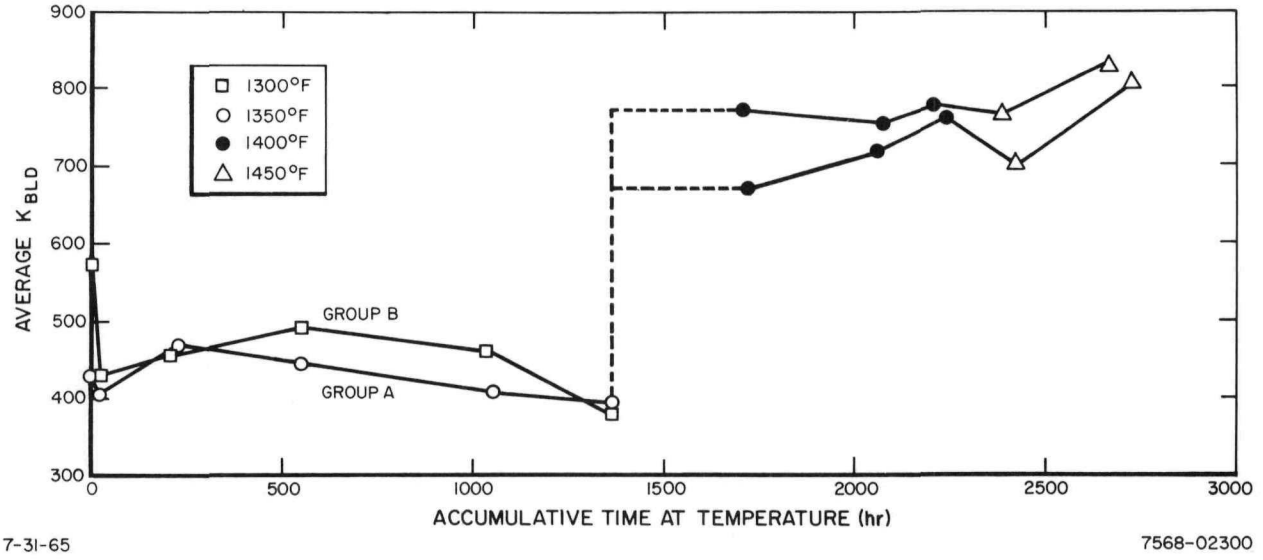

Figure 38. Average K_{BLD}

As indicated by the data of Figure 37, performance after the first 1400 hours of testing is independent of the first test temperature, either 1300°F or 1350°F. A better comparison of the fuel element performance can be made by observing the change in the parameter, K_{BLD}.* This parameter is a calculated quantity which adjusts for the variations in fuel dissociation pressure and/or test temperature. More simply, it is an inverse function of the effectiveness of the hydrogen barrier of the elements. A plot of average K_{BLD} values as a function of time during endurance test is shown in Figure 38. If the effectiveness of the hydrogen barrier were unaffected by the endurance testing, K_{BLD} would remain constant with time. If the barrier effectiveness decreased, K_{BLD} would increase. If the barrier improved, K_{BLD} would decrease. The data plotted in Figure 38 indicate that endurance testing at either 1300 or 1350°F had little effect on the hydrogen barrier. Subsequent endurance testing at 1400°F, however, caused a relatively large initial increase in K_{BLD} for both element groups — indicating decreased efficiency of the hydrogen barrier or a temperature dependency of K_{BLD}. Testing at 1450°F has not as yet produced indications of increased K_{BLD}.

In comparison, data obtained during endurance testing of 12 other SNAP 8 fuel elements (Figure 34) showed a similar increase in K_{BLD} after the temperature was increased from 1300 to 1400°F. In addition, the magnitude of the K_{BLD} values is approximately the same (at equal temperature) for both groups of elements.

Thermal endurance tests were continued on three groups of S8DS developmental fuel elements. A description of the fuel elements and a tabulation of the pre-endurance data were reported earlier.† These fuel elements received only pre-endurance permeation tests prior to beginning thermal endurance. One group of five fuel elements was fabricated with a spacer assembly between the fuel rod and the blind end cap. These 5 fuel elements were tested, in single retorts, at 1400°F for 10,600 hours. The permeation rates measured during this test are presented in Figure 39, which shows hydrogen permeation as a function of time at 1400°F. These data were fit to the equation:

$$\ln L = K_1 + K_2 T \quad ,$$

where

L = permeation rate [cc(STP)/hr],

T = time (hr), and

K_1 and K_2 are constants.

The resulting equations are shown with the respective permeation-time curves of Figure 39.

Thermal endurance data of a second group of five fuel elements are shown in Figure 40. These five fuel elements were fabricated in May 1964 to S8DS fuel element specifications. After 2900 hours of testing at 1400°F, the fuel elements were removed from the endurance furnace, permeation tested, ramp heated for five cycles (Type A), then given another permeation test. The remaining data resulting from this sequence of tests were reported in an earlier progress report.§ The overall average permeation of the fuel elements increased from 0.55 to 0.74 cc(STP)/hr during this series of tests. Immediately after the endurance tests were resumed, the average rate dropped to 0.63 cc(STP)/hr. Subsequent permeation measurements indicated a continued reduction in permeation, as shown in Figure 40.

*The derivation of K_{BLD} was presented in a previous progress report: C. E. Johnson, "SNAP 8 Progress Report, November 1964 — January 1965," NAA-SR-10792 (CRD), March 15, 1965, p. 73

†Ibid., p. 67

§C. E. Johnson, "SNAP 8 Progress Report, February-April 1965," NAA-SR-11092 (CRD), p. 57

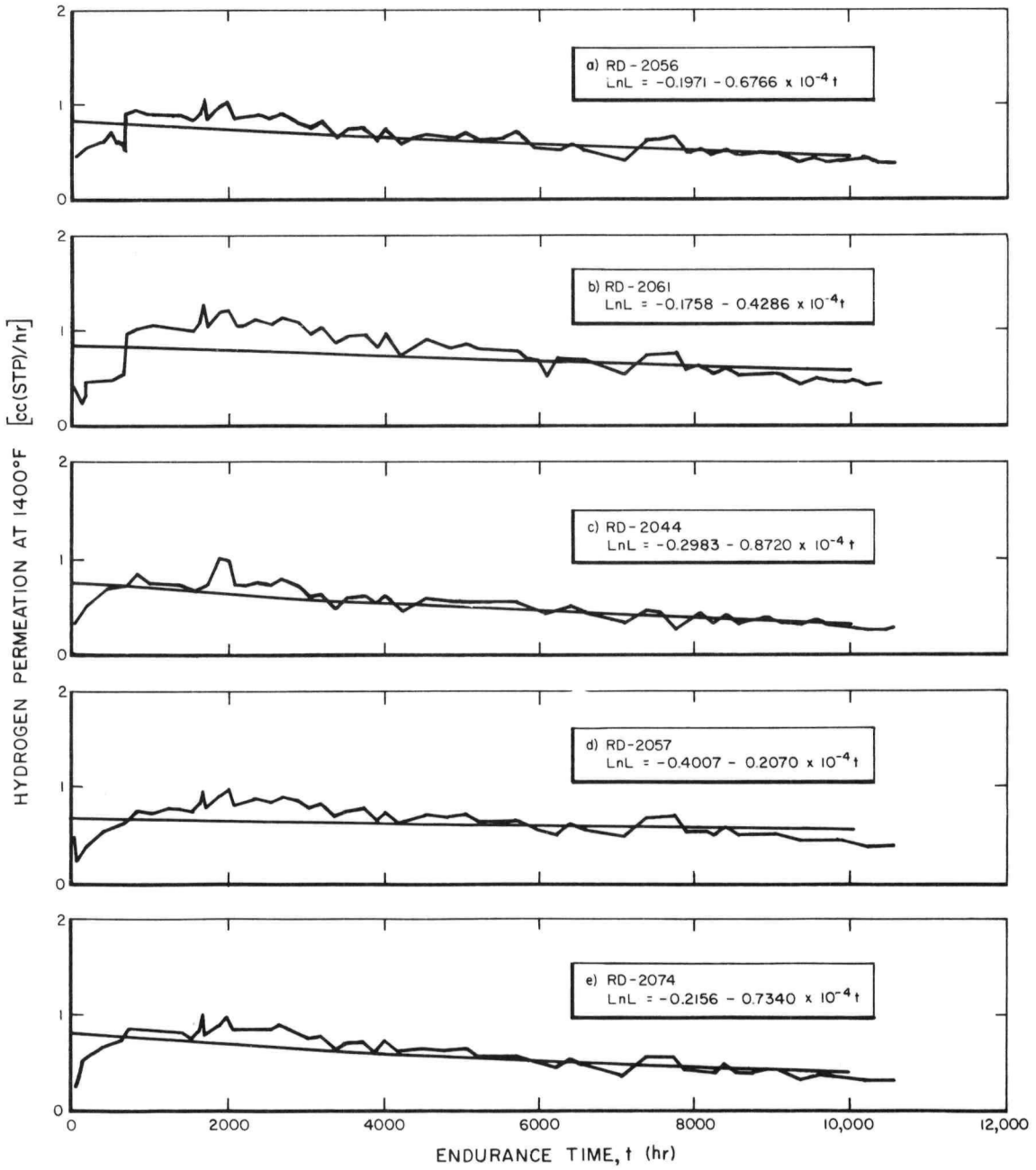

Figure 39. Hydrogen Permeation of Fuel Elements With Spacers During 1400°F Endurance Test

The third group includes three special S8DS design fuel elements with the fuel nickelplated to inhibit possible ceramic-fuel reaction. The endurance data for these elements are shown in Figure 41.

Average K_{BLD} values for each of the three groups of fuel elements are shown as a function of time in Figure 42. Apparently, the three special S8DS elements with nickelplated rods have the best hydrogen barrier tending to substantiate the concept of an intermediate barrier for suppression of fuel coating interaction.

(3) Vibration Tests

Work was continued to determine: (a) if low-level vibration tests should be included with the existing acceptance testing and (b) vibration failure threshold.

Previous fuel element performance data show that the fuel elements, after passing all acceptance tests, covered a range in performance (permeation rate) during subsequent testing. Therefore, it was desirable to establish a test wherein fuel elements which would not perform as well as others could be culled from the remaining elements. Such a test, low-level vibration (see Table 31), had been indicated by the data obtained from the testing of 13 S8DS pilot fabrication fuel elements built in February 1965.* This work was resumed, using 32 fuel elements which had been fabricated in June 1965, primarily for a quality check of a modified chromizing process. Test results of these elements should indicate: (a) if vibration testing is an applicable culling test and (b) if the modified chromizing process affected fuel element performance. Testing of the latter group is in progress.

TABLE 31

LOW LEVEL VIBRATION INPUT*

Magnitude	Frequency (cps)
3/16 in. double amplitude	5 to 13
3.4 g	13 to 400
5 g	400 to 2000

*Vibration inputs were the same for each of three mutually perpendicular axes, with a constant octave sweep rate requiring 5 minutes for each axis.

Another group of five weld verification elements was subjected to multiple permeation tests prior to low-level vibration tests. These are developmental elements with standing-edge closure welds. Available data for these elements are listed in Table 32. Apparently, thermal effects due to permeation testing caused a gradual increase in permeation until, after the eighth test, the average rate was about twice the initial value. After vibration testing, Element N-3297 exhibited extreme hydrogen barrier damage. These elements are being subjected to Type B ramp heat inputs.

Fourteen S8DS elements manufactured prior to March 1965 are being subjected to vibration tests for determining the input level at which significant hydrogen barrier damage occurs. Eight of these elements are the previously mentioned pilot production elements which received low-level vibration, ramp heating, and permeation tests. The remaining six elements were from initial S8DS core production and had received only permeation tests. To factor out possible effects of these previous tests, the elements are grouped as shown in Table 33.

Vibration tests at the levels indicated are being repeated for each group of elements. After each test, x-rays are taken to determine fuel rod damage. This examination is followed by two permeation tests of the element. This test procedure should

*Ibid., p. 71-73

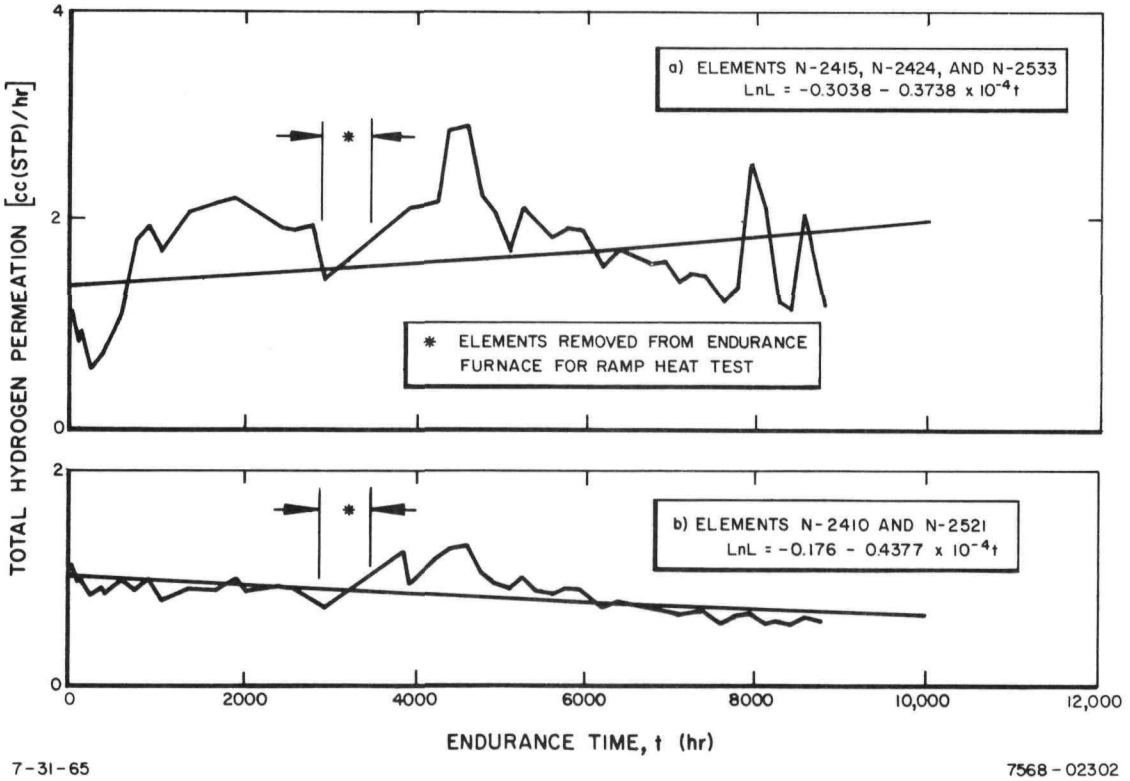

Figure 40. Hydrogen Permeation of Five S8DS Reference Design Fuel Elements During 1400°F Endurance Test

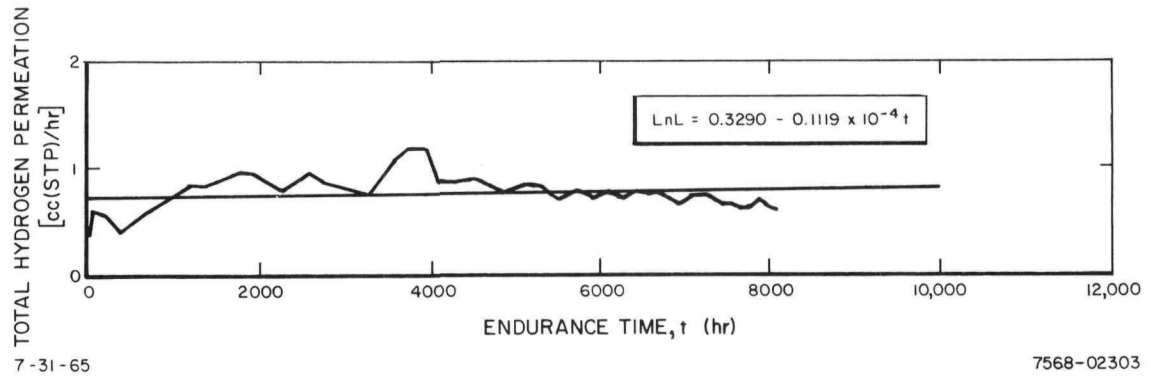

Figure 41. Hydrogen Permeation of 3 Fuel Elements With Nickelplated Fuel Rods During Endurance Test at 1400°F

TABLE 32

MULTIPLE PERMEATION TEST RESULTS OF FIVE S8DS FUEL ELEMENTS
(Chromizing Verification)

Element Number	Hydrogen Permeation at 1400°F [cc(STP)/hr]									
	Pre-Low Level Vibration								Post-Low Level Vibration	
	1	2	3	4	5	6	7	8	1	2
N-3297	0.55	0.59	0.71	0.79	0.86	0.94	0.96	1.1	5.8	5.5*
N-3320	0.60	0.66	0.77	0.78	0.78	0.83	0.84	0.86	0.91	-
N-3307	0.25	0.30	0.37	0.45	0.44	0.46	0.47	0.57	0.69	0.73
N-3256	0.56	0.60	0.63	0.65	0.71	0.74	0.73	0.87	0.92	-
N-3328	0.30	0.34	0.35	0.35	0.37	0.38	0.45	-	0.56	-
Average	0.45	0.50	0.57	0.60	0.63	0.67	0.69	0.8	1.8	

*Post-ramp-heat permeation test gave a rate of 5.8 [cc(STP)/hr] at 1400°F.

TABLE 33

PERMEATION DATA OF S8DS ELEMENTS UNDERGOING VIBRATION FAILURE THRESHOLD TESTING

Element Number	Hydrogen Permeation, φ, at 1400°F [cc(STP)/hr]											
	Before 1st Vibration Test		Low Level Vibration*	After Low Level Vibration		After Ramp Heat (25 cycles of Level A)		1st Vibration Level† (%)	After 1st Vibration		2nd Vibration Level† (%)	After 2nd Vibration
	1	2		1	2	1	2		1	2		1
N-2712§	0.37	0.43	Yes	0.94	0.78	0.87	1.0	125	0.93	-	-	-
N-2789	0.24	0.67	No	-	-	-	-	125**	0.93	-	-	-
N-2724§	0.31	0.38	Yes	0.43	0.39	0.50	0.52	150	0.63	0.80	150	0.76
N-3525	0.23	0.19	No	-	-	-	-	150	0.34	0.56	150	0.60
N-3246§	0.74	0.86	Yes	1.0	0.85	1.1	1.3	150	1.5	1.7	150	1.6
N-2748§	0.44	0.40	Yes	0.72	0.62	0.64	0.76	165	0.77	-	-	-
N-2808	0.21	0.37	No	-	-	-	-	165	0.61	-	-	-
N-2882	0.37	0.38	No	-	-	-	-	165**	1.2	-		-
N-2992§	0.33	0.39	Yes	0.61	0.56	0.72	0.76	175**	0.65	0.79	-	-
N-2733§	0.30	0.30	Yes	0.39	0.36	0.46	0.48	175	0.52	0.61	-	-
N-3534	0.40	0.56	No	-	-	-	-	175††	0.83	0.61	-	-
N-3222§	0.40	0.50	Yes	0.70	0.66	0.72	0.79	185	0.91	-	-	-
N-2941§	0.29	0.27	Yes	0.28	0.25	0.30	0.35	185	0.56	-	-	-
N-3528	0.36	0.48	No	-	-	-	-	185	0.70	-	-	-

*Inputs for low-level vibration test are given in Table 34.
†Refers to percentage of vibration level as given in NASA Specification 417-2.
§Pilot production elements.
**X-ray examination indicated loose material present in the closure axial gap.
††Fuel rod chipped at closure end.

TABLE 34

CHANGE IN FUEL ROD DIAMETER DUE TO HYDROGEN LOSS

Element No.	Initial $(H/Zr)_{eff}$	Initial Diameter (in.)	Δ Diameter (in.)	$\Delta H/Zr$*	Final $(H/Zr)_{eff}$
RD-2074	1.777	0.529	-0.002	-0.106	1.671
RD-2044	1.757	0.529	-0.003	-0.159	1.598
RD-2057	1.704	0.529	-0.003	-0.159	1.545
RD-2056	1.652	0.529	-0.003	-0.159	1.493
RD-2061	1.782	0.529	-0.003	-0.159	1.623

*Calculated from the equation $\Delta(H/Zr) = \frac{100(\Delta D/D_i)}{3.57}$

TABLE 35

HYDROGEN LOSS OF FUEL ELEMENTS WITH SPACERS DURING ENDURANCE TESTING

Element Number	Initial H_2 (wt %)	Fuel Weight (gm)		Hydrogen Loss Through 10,600 Hours at 1400°F* (%)			
		Initial	Final	Method 1	Method 2	Method 3	Method 4
RD-2074	1.71	348.327	346.874	6.1	9.4	Not Calculated	7.0
RD-2044	1.69	348.034	345.245	9.7	8.3		10.6
RD-2057	1.64	348.600	346.040	9.8	10.4		8.5
RD-2056	1.59	348.898	346.895	10.0	10.1		8.2
RD-2061	1.71	348.757	347.249	9.2	11.7		14.6
Average	1.67			9.0	10.0		9.8

*Initial hydrogen content is based on the weight of the hydrided, final-machined fuel rod and the weight % hydrogen. The final hydrogen content is determined as follows:

Method 1. By dimensional change of the fuel rods.
Method 2. Integration of permeation-time curves.
Method 3. Measured fuel rod weight loss.
Method 4. Based on isochore data, assuming a one-to-one carbon to zirconium combination.

provide the data necessary for determining hydrogen barrier degradation as a function of vibration level and accumulative time at that level.

The data listed in Table 33 show that none of the elements have suffered catastrophic hydrogen barrier damage to date. The fuel rod of Element N-3534 was badly chipped at the closure end after completion of vibration tests at 175% of the NASA 417-2 level. Nevertheless, subsequent permeation tests of this element indicate no severe damage to the ceramic.

(4) Destructive Analysis

After completing the endurance tests described in Section IV-B-4-b-(2) above, the five elements with spacer assemblies (endurance data in Figure 42) were disassembled for component analysis. Some residue, in the form of flakes and powder, was observed when the fuel rods were removed from the cladding assemblies. Analysis of the residue indicated the flakes were of a composition similar to the S8ER ceramic hydrogen barrier (AI-8763D). The powder was predominantly zirconium dioxide (ZrO_2). Visual examination failed to reveal any bare metal present in any of the cladding assemblies. Four of the assemblies have been made into membranes for additional permeation tests. The fifth assembly was cut into sections for microscopic examination. Figure 43 shows a photomicrograph of a typical section taken from the cladding of Element RD-2074. This figure shows the ceramic to be relatively unchanged from its initial appearance. Also, there appears to be an excellent bond between the ceramic and the metal tube.

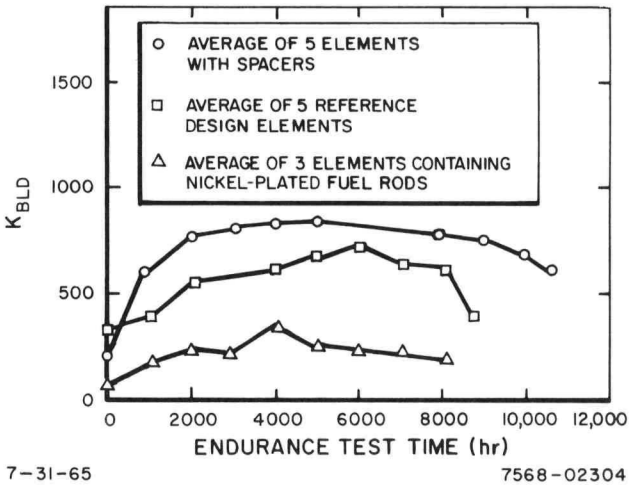

Figure 42. Average K_{BLD} Values of Fuel Elements During Thermal Endurance Test at 1400°F

Dimensional and weight measurements were taken on the fuel rods from the disassembled elements. Fuel rod diameter measurements are listed in Table 34, with the observed decrease in diameters being attributed to hydrogen loss. With these data and the equation,

$$\Delta(H/Zr) = \frac{100(\Delta D/D_i)}{3.57}$$

where

ΔD = change in diameter,

D_i = initial diameter, and

$\Delta H/Zr$ = change in effective hydrogen to zirconium ratios,

it was possible to calculate the total hydrogen present in each fuel rod.

Three additional methods are available for determining hydrogen content. The results of calculating hydrogen loss by these methods are listed in Table 35 along with results from dimensional change calculations. Fuel rod weight measurements were not used to determine hydrogen loss for these elements because of additional machining of the fuel rods after the final hydriding weight measurement.

(5) Input Simulation

Ten S8DS fuel elements, chromized by Vendor B, are undergoing thermal endurance testing at 1400°F. These fuel elements have accrued 1944 hours of a scheduled 5000-hour thermal endurance test per Step 11 of Table 36.

Table 37 shows the hydrogen permeation rates of these fuel elements from acceptance through the 1944 hours of thermal endurance. Although the average permeation rates increase after each input prior to endurance, the increase is less than that found for S8ER elements.* The behavior trend of these fuel elements during thermal endurance is similar to the S8ER fuel elements. This is, the rates generally decrease with extended time at temperature. The increase in hydrogen permeation rates prior to this endurance testing indicates some hydrogen barrier degradation.

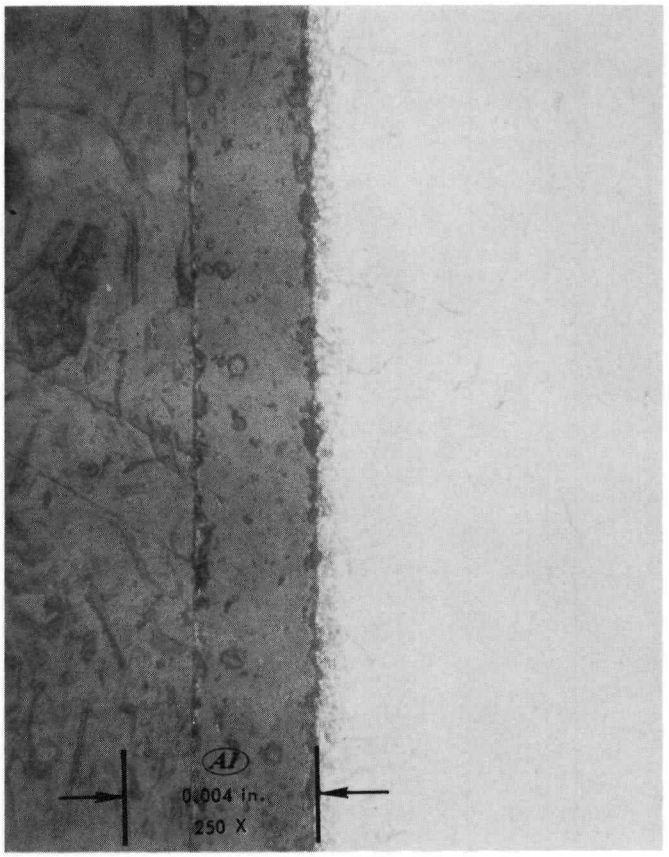

1. MOUNTING MATERIAL
2. CERAMIC
3. HASTELLOY-N TUBE

NOTE: ETCHED WITH MARBLES REAGENT

7-31-65

7568-02305

Figure 43. Photomicrograph of a Typical Section from the Cladding Tube of Element RD-2074

*T. G. Parker, Jr. and S. J. Veeck, "Performance Testing SNAP 8 Experimental Reactor Fuel Elements: Interim Report," NAA-SR-9896 (SRD), August 15, 1964

TABLE 36

SEQUENCE OF TESTS FOR SIMULATION OF S8DS REACTOR OPERATION

Test	Condition
1. Permeation Test	1400°F
2. 5 Thermal Soaks	Heat at 300°F/hr from 400 to 1300°F. Dwell at 1300°F for 10 hr, cool at 300°F/hr to 400°F.
3. Permeation Test	1400°F
4. Ramp Heat (25 cycles)	Heat at 300°F/min from 400 to 850°F, at 150°F/min from 850 to 1400°F. Cool at 50°F/min from 1400 to 400°F
5. Permeation Test	1400°F
6. Thermal Endurance	1400°F for 1000 hr
7. Permeation Test	1400°F
8a. Ramp Heat (same as above)	1 cycle
8b. Thermal Cycle I (2 cycles)	1400 to 1350°F at 300°F/min 1350 to 1450°F at 150°F/min 1450 to 1400°F at 300°F/min
8c. Thermal Cycle II (12 cycles)	1400 to 1450 to 1400°F at 50°F/min. Cool 1400 to 400°F at 50°F/min
9. Perform Step 8	15 times
10. Permeation Test	1400°F
11. Thermal Endurance	1400°F for 5000 hr
12. Permeation Test	1400°F
13. Repeat Step 8	10 times
14. Thermal Endurance	1400°F
15. Thermal Endurance	1400°F for 5000 hr
16. Permeation Test	1400°F
17. Destructive Analyses	

TABLE 37

PERMEATION RATES OF S8DS FUEL ELEMENTS

Element Number	Permeation Rate, φ [cc(STP)/hr]						
	Acceptance	Pre-Thermal Soak	Post-Thermal Soak	Post-Ramp Heat	Post-Thermal Endurance (1000 hr)	Post-Thermal Cycle	Thermal Endurance*
N-2679	0.60	0.56	0.69	0.63	0.75	0.92	-
N-2807	0.57	0.69	0.80	0.61	0.98	1.4	-
N-2815	0.49	0.65	0.64	0.76	0.60	0.70	-
Cluster Total	1.7	1.9	2.1	2.0	2.3	3.0	1.36
N-2827	0.35	0.61	0.52	0.49	0.51	0.47	-
N-2831	0.59	0.72	0.79	0.84	0.96	1.0	-
N-2833	0.32	0.48	0.60	0.38	0.48	0.64	-
Cluster Total	1.3	1.8	1.9	1.7	2.0	2.1	1.64
N-2835	0.39	0.48	0.29	0.49	0.55	0.70	-
N-2914	0.35	0.41	0.46	0.43	0.39	0.65	-
N-2918	0.62	0.71	0.89	0.96	1.0	1.2	-
Cluster Total	1.4	1.6	1.6	1.9	1.9	2.6	1.49
N-2939	0.45	0.66	0.73	0.76	1.1	1.5	0.74
Average	0.47	0.60	0.63	0.64	0.74	0.93	0.52

*Average of last 3 readings during thermal endurance (final reading taken at 1944 hours). Schedule is for 5000 hours of thermal endurance.

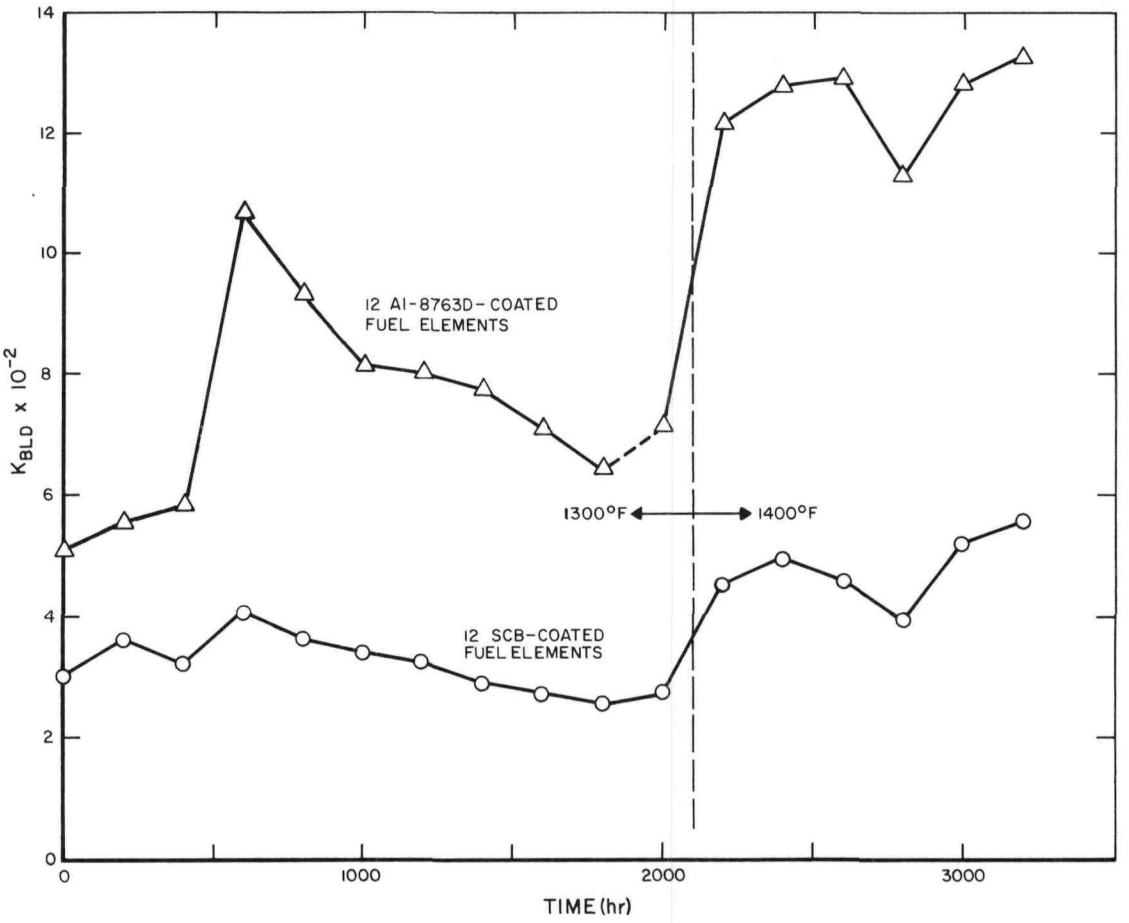

7-31-65

7568-02306

Figure 44. Average K_{BLD} of 24 Fuel Elements Undergoing Endurance Test

(6) Other Tests

Twenty-four fuel elements of the S8DS design, 12 with AI-8763D coating and 12 with SCB coating, are undergoing thermal endurance test. These elements (0.56 in. OD x 14.63 in. long, excluding end pins) were built for S8DRM-1 testing and had previously been subjected to the following pre-endurance inputs:

1) Acceptance permeation test (1400°F);

2) Thermal soak (1300°F);

3) Vibration, shock, and acceleration on a core mockup on a shake table;

4) Ramp heat (1300°F);

5) Thermal cycle (1350°F);

6) Squib firing (6 AI-8763D and 7 SCB); and

7) Reactor assembly vibration and shock (6 AI-8763D and 7 SCB).

The data from these inputs were discussed in a previous progress report.*

The initial endurance test temperature was 1300°F. The hydrogen permeation stabilized at 1300°F in 2100 hours and the temperature was then increased to 1400°F. A total of 3300 hours at temperature have been accrued with 1200 hours at 1400°F.

The hydrogen permeation data during the 1300°F testing show that the 12 SCB-coated fuel elements have remained relatively stable with a normalized axial hydrogen permeation rate (1300°F and 1 atm hydrogen dissociation pressure) of about 0.25 cc(STP)/hr. The normalized average permeation rate of the 12 AI-8763D-coated fuel elements increased from about 0.4 to a maximum of about 0.7 cc(STP)/hr after 650 hours, and then stabilized at about 0.5 cc(STP)/hr. Prior to the increase in test temperature, the 12 SCB-coated fuel elements demonstrated excellent performance based on the near zero average slope of K_{BLD} vs time, as shown on Figure 44. Although the data from the 12 AI-8763D-coated fuel elements are biased upward due to one relatively high leaking fuel element, examination of test results (even excluding the data from the high leaking fuel element) still shows that the SCB-coated fuel elements are performing better than the fuel elements with AI-8763D coating. The increase in K_{BLD} with time as shown on Figure 44 (for the AI-8763D-coated fuel elements from the start of endurance test, and for the SCB-coated fuel elements after the increase in test temperature) indicates fuel element damage. The immediate increase in K_{BLD} exhibited when the test temperature was raised to 1400°F may indicate a temperature dependency of K_{BLD} based on the present theoretical hydrogen permeation equations. Substantiation of this theory will be attempted by lowering the test temperature to 1300°F for a short period of time and comparing past and present 1300°F values of K_{BLD}.

5. Irradiation Tests

a. Materials Irradiation

(1) NAA-116 Series, Low-Temperature Fuel Materials Irradiation

The objective of the low temperature fuel materials irradiation program is to provide irradiated fuel samples for use in the correlation of post-irradiation annealing studies with inpile performances at higher temperatures. The purpose of the annealing tests is to study the swelling behavior of the fuel as a function of annealing temperature and time and as a

*C. E. Johnson, "SNAP 8 Progress Report, February – April 1964," NAA-SR-11092 (CRD), June 15, 1965, pp 68-70

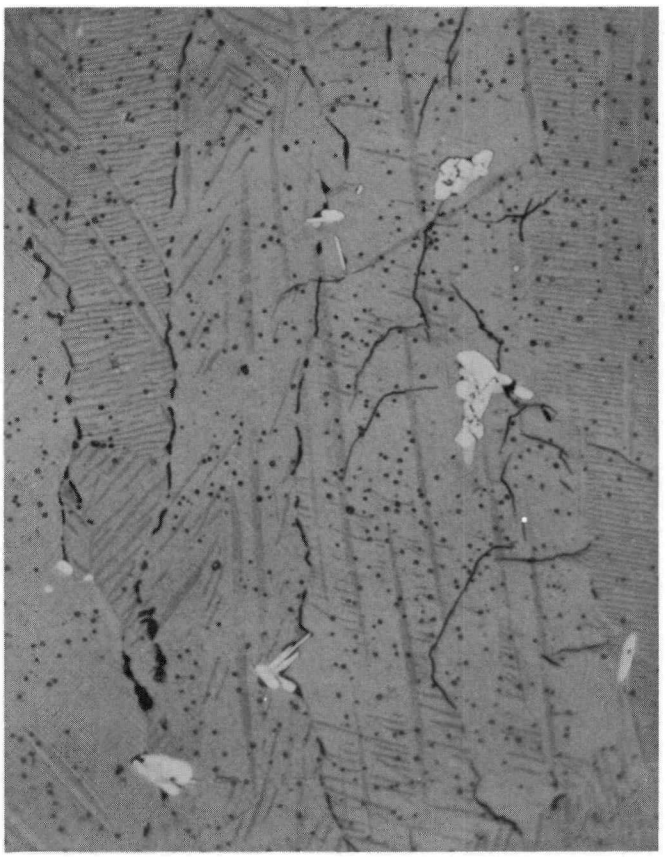

7-30-65 7568-02307

Figure 45. Microcracks in Thermally Cycled SNAP 8 Fuel (1000X)

Note that the cracks appear to follow and join the larger uranium precipitates which are in the grain boundaries. This is in agreement with the hypothesis that the alpha uranium growth acts as stress risers causing the zirconium matrix to crack.

TABLE 38

POST-IRRADIATION ANNEALING RESULTS OF NAA-116-2 MATERIAL

Sample Number	Density (gm/cm^3)		Change,* $\Delta\rho/\rho_2$ (%)
	Post-Irradiated (ρ_1)	Annealed (ρ_2)	
24	5.857	5.880	-0.39
26	5.853	5.842	+0.19
28	5.812	5.774	+0.66†
32	5.794	5.768	-0.42

*Percent change has been expressed as $\Delta\rho/\rho_2$ in compliance with previous results where $\Delta V/V_1$ could be compared directly.
†Sample lost hydrogen from 1.80 to 1.32 wt %

TABLE 39

NAA-116-2 HYDROGEN LOSSES

Sample Number	Hydrogen Content (wt %)	
	Pre-Annealed	Annealed
24	1.71	1.58
26	1.63	1.62
28	1.80	1.32*
32	1.70	1.68

*Probable leak that developed at temperature

TABLE 40

DIMENSIONAL CHANGES OF THERMALLY CYCLED FUEL

Fuel Slug Number	Density (gm/cm^3)		Change, $\Delta\rho/\rho 1$ (%)
	Before Cycling ($\rho 1$)	After Cycling ($\rho 2$)	
624D3-1	6.291	5.548	-11.8
624D3-2	6.064	5.424	-10.5
628B2-3	5.846	5.218	-10.7

function of the metallurgical parameters of the materials. These data are also expected to yield information on the breakaway swelling behavior of the fuel.

Annealing studies were concluded on the materials from the NAA-116-2 capsule (0.4 met. at. % burnup). This consisted of heating the fuel to 1650°F for 50 hours. The resulting density changes are shown in Table 38.

Hydrogen analyses were completed to determine if hydrogen losses had occurred since this could also result in a density change (see Table 39). With the exception of an approximate 2% density change in fuel sample No. 28, the hydrogen losses were negligible in terms of affecting density changes.

Small density changes were expected and probably result from the cancelling effect of two actions, namely:

1) Density increase due to collapse of subsurface microcracks as reported in early lower temperature post-irradiation annealing studies, and

2) Density decrease due to fuel swelling resulting from coalescence of fission gases as a result of the higher annealing temperatures.

In an effort to explain the unusual swelling behavior of the NAA-116 fuel materials (10 to 15 vol % as normalized to 1 met. at. % burnup), thermal cycling studies were conducted out-of-pile to determine whether alpha uranium growth could be responsible. Cycling parameters leading to maximum growth were taken from the literature and adapted to existing equipment capabilities. The cycle chosen was:

1) Heat from 50 to 590°C at 17°C/min,

2) Hold for 20 min at 590°C,

3) Quench to 50°C (490°C/min),

4) Hold for 2 min at 50°C, and

5) Repeat.

The test was terminated after completing 518 cycles; the fuel material had experienced a density decrease of approximately 11% (see Table 40). Metallographic examinations of the cycled fuel revealed the presence of microcracks that were not present before thermal cycling (see Figure 45). Though the results are not conclusive, these density changes are a strong indication that alpha uranium growth can take place at conditions of low-temperature irradiations. The fuel samples from the thermal cycling test will be annealed at 1300°F for 200 hours to determine whether the density can be recovered since this was the observed behavior with the fuel samples from the NAA-116-1 capsule. The fuel will then be examined metallographically to see if the microcracks are collapsing.

(2) NAA-77 Series, Inpile Permeation Tests

The NAA-77 capsule series was designed to measure hydrogen permeation rates of barrier materials during reactor operation. Advantages of this approach are: (1) the rate of radiation damage to the hydrogen permeation barrier material, if any, can be readily determined and (2) the effect of ionizing radiation field on the permeation rate can be measured.

Studies of the effect of reactor radiation on the performance of SCB-1 permeation barrier material have been completed. Four capsules (NAA-77-1 through -4) containing SCB-1-coated membranes have been irradiated and destructively examined in the hot cell. The post-irradiation examination of NAA 77-2 and -3 experiments was completed.

The irradiation history of the four capsules is summarized in Table 41. The conclusions drawn from the NAA-77 irradiation experiments are:

TABLE 41

NAA-77 SERIES IRRADIATION HISTORY

Capsule	Irradiation		Membrane Temperature (°F)	Total Time (hr)	Neutron Dosage		Fission Fragment Dosage/Element-Inch
	Started	Ended			Estimated	Dosimetry	
NAA-77-1	8-63	6-64	1500	4,343	2.56×10^{21}	1.54×10^{21}	-
NAA-77-2	3-64	2-65	1300	4,638	1.39×10^{21}	1.78×10^{21}	1.44×10^{18}
NAA-77-3	3-64	2-65	1500	4,638	1.39×10^{21}	1.44×10^{21}	1.44×10^{18}
NAA-77-4	6-64	6-64	1700	100	~6×10^{19} 13×10^{19}	not measured	7×10^{16} (membrane ruptured)
SNAP 8 Design Parameters, 600-kwt core			~1400	10,000	1.4×10^{21}		7.6×10^{17}

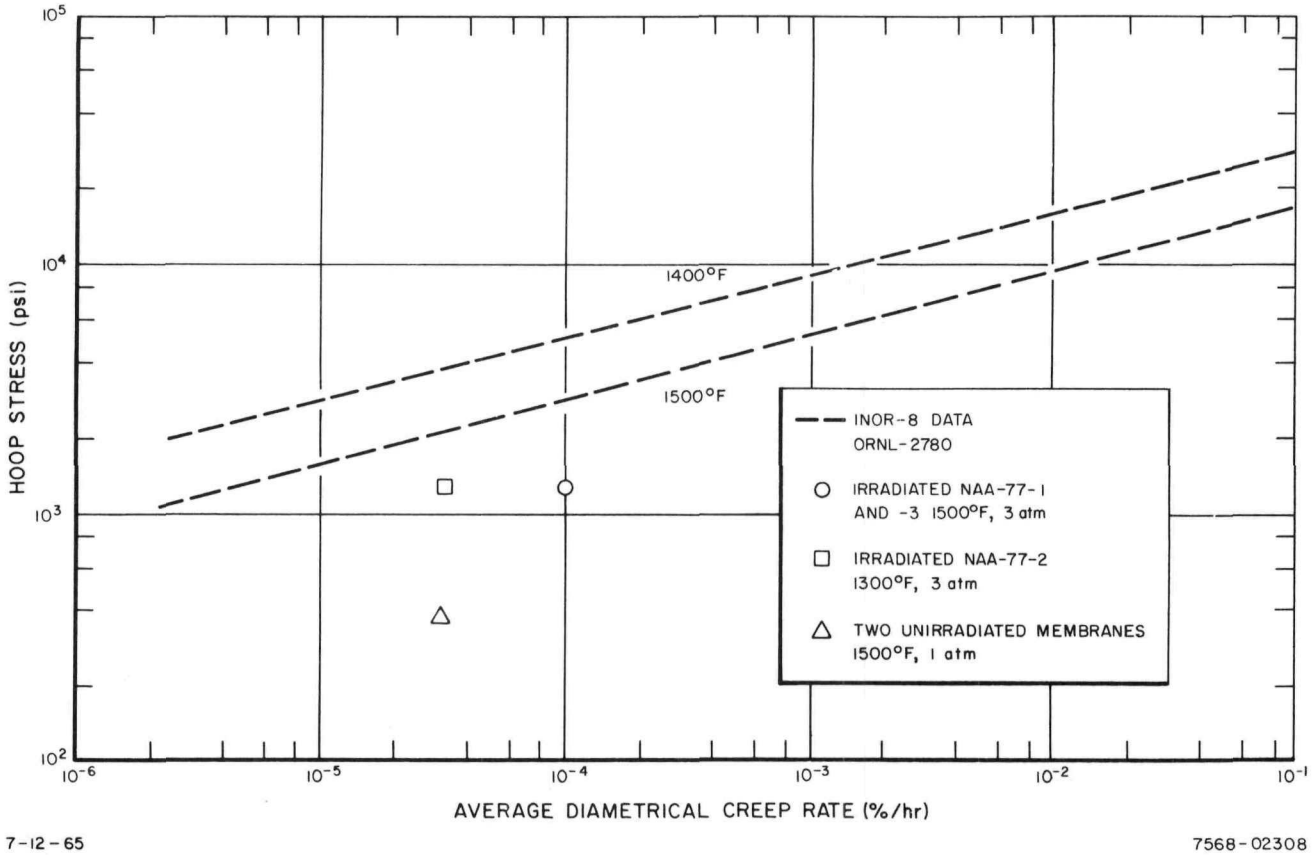

Figure 46. Creep Studies of Irradiated and Nonirradiated SNAP 8 Cladding Assemblies

TABLE 42
ADHERENCE TEST RESULTS OF NAA-77-2 AND -3

Membrane Section	Irradiation Temperature (°F)	NAA-77-2		NAA-77-3	
		General	Index*	General	Index*
Top	>500	Poor	>7	Poor	>7
Middle	1500	Excellent	77+	Excellent	77+
Bottom	1400	Excellent	77+	Excellent	77+

*77+ means no coating spalled off after 11 bends over a 1/2-in.-diameter mandrel.

1) The ionizing radiation field in a reactor does not significantly alter the hydrogen permeation through SNAP 8 fuel cladding assemblies.

2) Radiation appears to accelerate the devitrification process in the SCB-1 hydrogen barrier material, presumably by enhancement of self-diffusion. Inpile annealing of SCB-1-coated membranes caused the activation energy for the permeation process to change from 25,000 ±2000 cal/mole to about 14,000 ±2000 cal/mole. This change has also been observed in out-of-pile annealing treatments.

3) Inpile annealing of SCB-coated membranes does not alter the pressure dependence for hydrogen permeation. The pressure dependence remains directly proportional after either inpile or out-of-pile annealing within limits of the pressure range studied.

The post-irradiation examination of NAA-77-2 and -3 revealed an accelerated Hastelloy-N creep rate similar to that observed with NAA-77-1. Figure 46 shows that the creep rates for NAA-77-1 and -3 were identical (10^{-4}%/hr for a hoop stress of approximately 1200 psi and temperature of 1500°F). The creep rate for NAA-77-2 was 3.3×10^{-5}%/hr for a hoop stress of approximately 1200 psi and a temperature of 1300°F. Thus the irradiated samples show that the creep rates for membranes tested at low stresses for long time periods are accelerated compared to extrapolated creep values obtained from high stress short-term tests.

The disassembly of NAA-77-2 and -3 was routine except that NAA-77-3 had to be "worked" out of the thermal expansion joint. Visual examination of NAA-77-3 showed that some of the SCB coating from the capsule gamma heater was bonded to the outer surface of the membrane in the thermal expansion joint. Since the temperature in the thermal expansion joint was below 700°F, the transfer of the SCB coating is believed to have been accelerated by the radiation. This observation is in agreement with that made on the NAA-77-4 capsule where "freezing" of the membrane in the thermal expansion joint led to premature rupture of the membrane.

Adherence test samples shown in Figure 47 were cut from the top, center, and bottom sections of each membrane. The results of the adherence tests are shown in Table 42 and demonstrate that the SCB coating adherence improved during the irradiation. The top section of the membrane was irradiated at 500°F and exhibited the adherence rating of SCB coating that existed in the as-fired condition.

Figure 48 shows the SCB coating porosity at the blind end of the membrane. The large bubble at the surface is a typical pit defect that develops during the firing of the SCB coating. Table 43 shows the thickness of the SCB coating

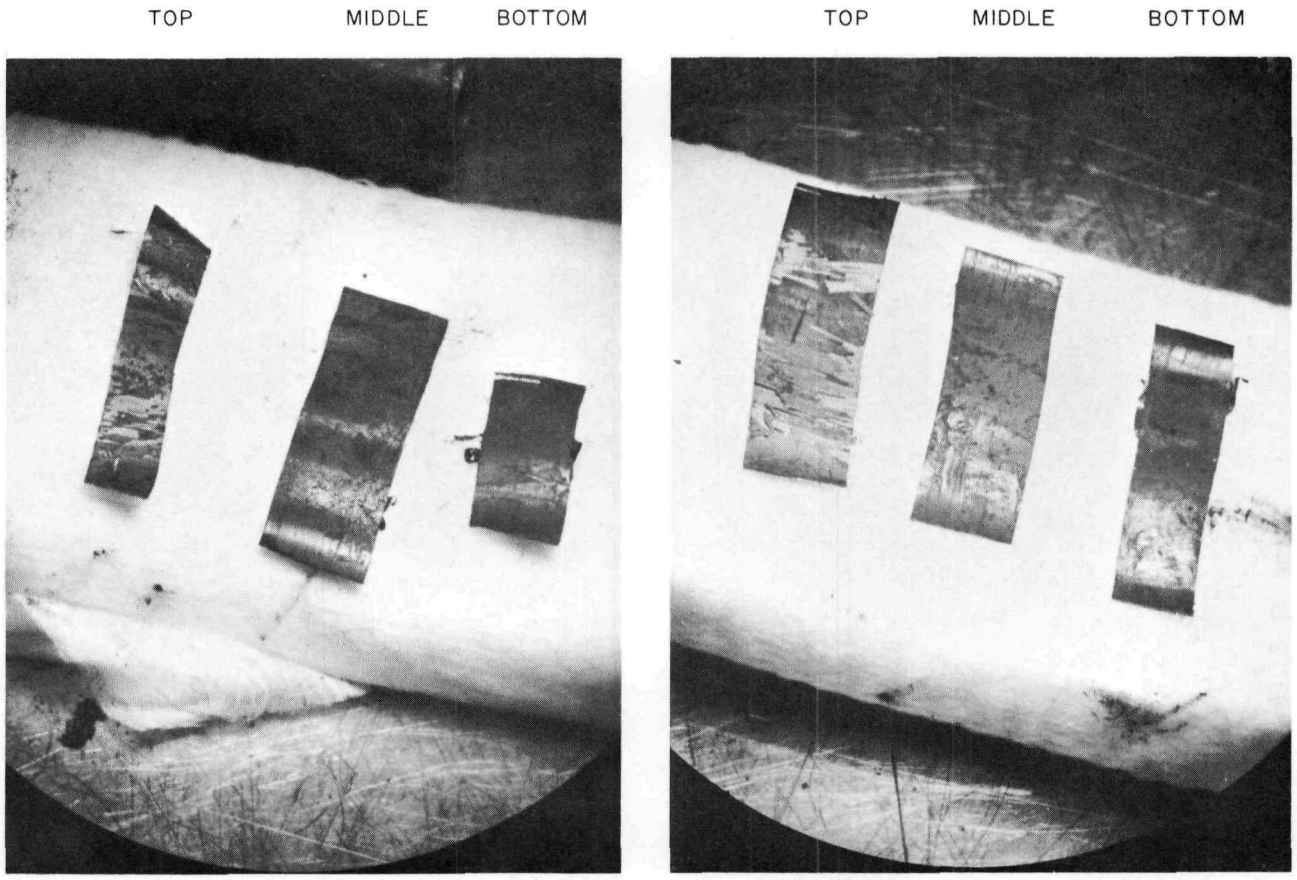

a) NAA 77-2 ADHERENCE SAMPLES

b) NAA 77-3 ADHERENCE SAMPLES

7-30-65

7568-02309

Figure 47. Irradiated Cladding Samples after Adherence Testing

TABLE 43

SCB COATING THICKNESS MEASUREMENTS
FOR NAA-77-2 AND -3 MEMBRANES

Membrane Section	Coating Thickness			
	NAA-77-2		NAA-77-3	
	Average (mils)	Range (mils)	Average (mils)	Range (mils)
Top	2.6	2.0 to 3.1	2.3	2.2 to 2.5
Middle	1.9	1.6 to 2.8	2.2	—
Bottom	1.1	0.6 to 1.6	1.1	0.8 to 1.7

IRRADIATED

NAA 77-2 MEMBRANE COATING

THREE 15-MINUTE COATING FIRINGS

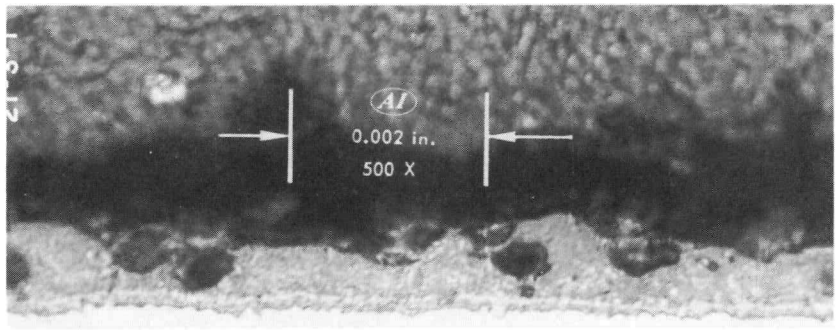

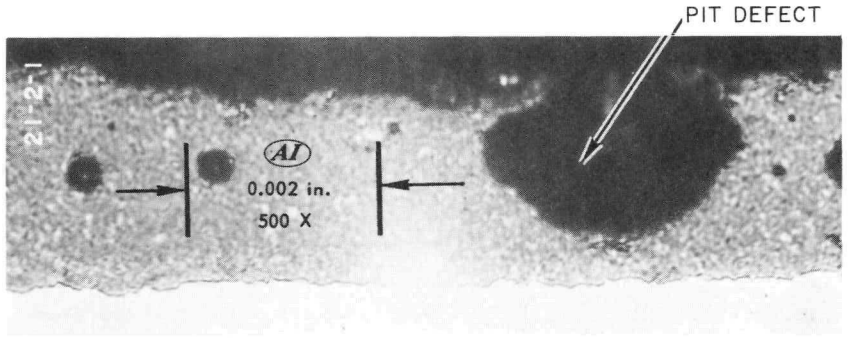

UNIRRADIATED

MEMBRANE COATING

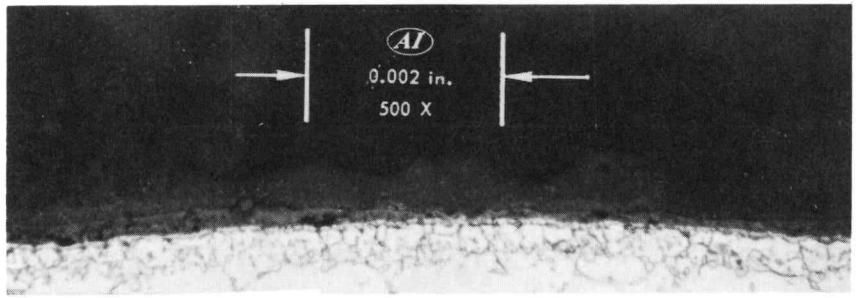

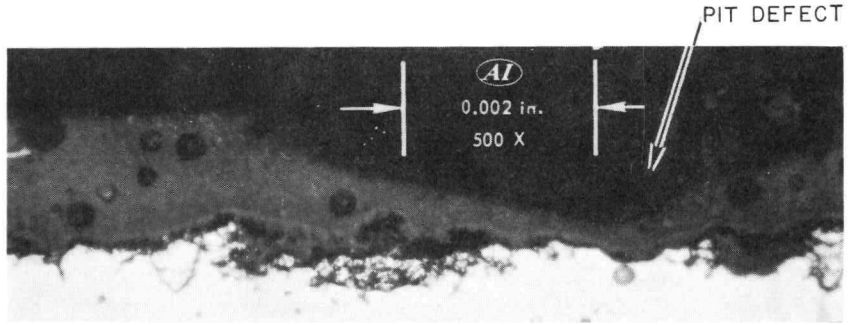

THREE 15-MINUTE COATING FIRINGS

THREE COATING FIRINGS: 2-1/2, 2-1/2, AND 5 MINUTES

7-12-65

7568-02310

Figure 48. SCB-1 Coating Porosity in Irradiated and Unirradiated Membranes

for the two capsule membranes. The coating thickness for NAA-77-2 and -3 was less than the specified minimum requirement for production fuel elements of 1.0 mil in the blind end.

Figure 49 shows the precipitates that were formed during TIG welding of the blind end cap to the tube for both irradiated and unirradiated membranes. Tubes E-822 and E-808 in Figure 50a and b, and in Figure 51 show the normal grain structure, while that seen in Figure 49 for NAA-77-2 and -3 is rather unusual. The five weld zones shown in Figures 49, 50, and 51, show the normal variation in cladding thickness at the TIG weld zone.

The conclusions from the NAA-77 irradiation experiments are:

1) The SNAP 8 cladding assemblies coated with SCB operated satisfactorily in an irradiation environment at 1500°F for over 4600 hours.

2) The hydrogen barrier material suffered slight radiation damage during the irradiation to a neutron exposure of 1.4×10^{21} nvt ($E_n > 1$ Mev) and fission fragment bombardment of 1.44×10^{18} FF/element-inch (1.31×10^{17} FF/cm^2). The permeation rate at 1500°F and 1 atm H_2 pressure increased for NAA-77-2 from 1×10^{-3} to 2.8×10^{-3} cc(STP)/hr and for NAA-77-3 from 0.88×10^{-3} to 2.7×10^{-3} cc(STP)/hr. The pressure dependence remained the same throughout the irradiation.

3) Metallographic examination of the SCB hydrogen barrier material did not reveal evidence of deterioration of the coating due to the irradiation. The adherence of the ceramic to the Hastelloy-N ranged from poor in the 700°F irradiation temperature zone to excellent in the 1400 and 1500°F irradiation temperature zones.

4) The low stress creep deformation of both irradiated and unirradiated membranes was found to be significantly greater than would be predicted from high stress test results.

5) The Hastelloy-N grain boundaries became decorated with a precipitate as a result of long time thermal annealing.

6) No evidence was found to indicate acceleration of grain growth in the Hastelloy-N due to irradiation. The bulk of the membranes, however, contained grains with diameters of 0.005 inch or greater after the SCB coating firing cycle.

b. Engineering Irradiations

The engineering irradiation tests are designed to evaluate the effects on fuel element performance of fuel compositional variables, power density, temperature, and burnup. The tests are statistically designed in an array of parameter levels which span the 600-kwt, 1300°F, 10,000-hour, SNAP 8 core parameters. The program includes both sublength and full-scale fuel element irradiation tests and post-test evaluation of ground test reactor cores.

The irradiation test plan includes redundant parameter levels to assure maximum test reliability. Design details have been presented in previous progress reports. The NAA-115-1 and NAA-117-1 fuel element irradiations continued irradiation at Hanford. Irradiation of the NAA-115-2 fuel element test was begun. Fabrication and assembly of the NAA-121 test was initiated. Final hot cell preparation continued for the post-test evaluation of the S8ER core.

(1) NAA-115-1 Fuel Element Engineering Irradiation

The NAA-115-1 irradiation assembly contains twelve sublength fuel elements in six separate

a) NAA-77-2 WELD ZONE

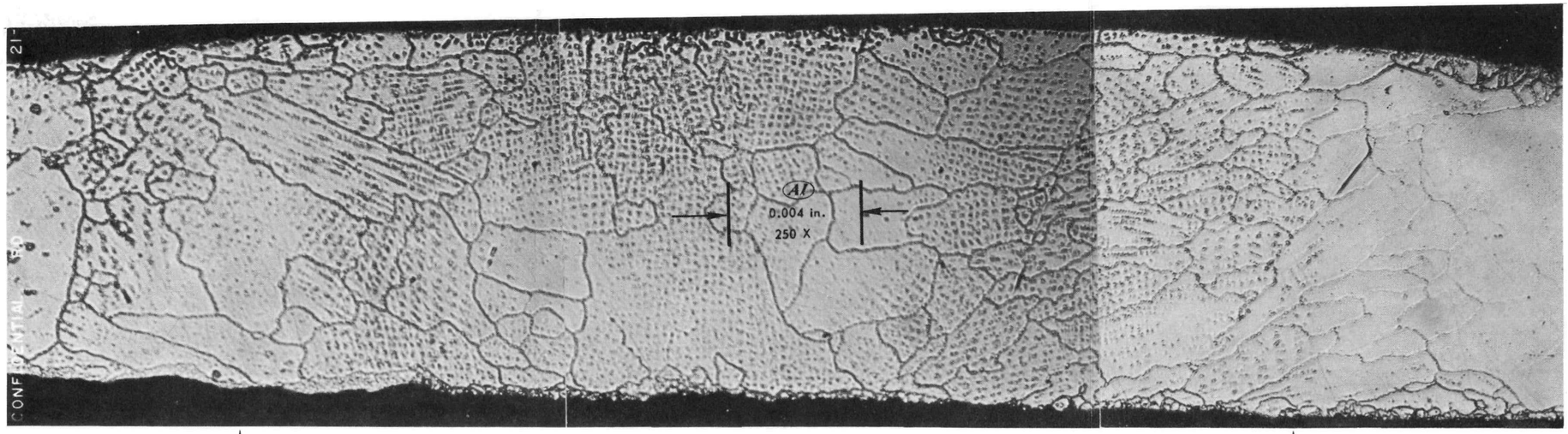

HASTELLOY-N TUBING

HASTELLOY-N BAR STOCK

(b) NAA-77-2 WELD ZONE

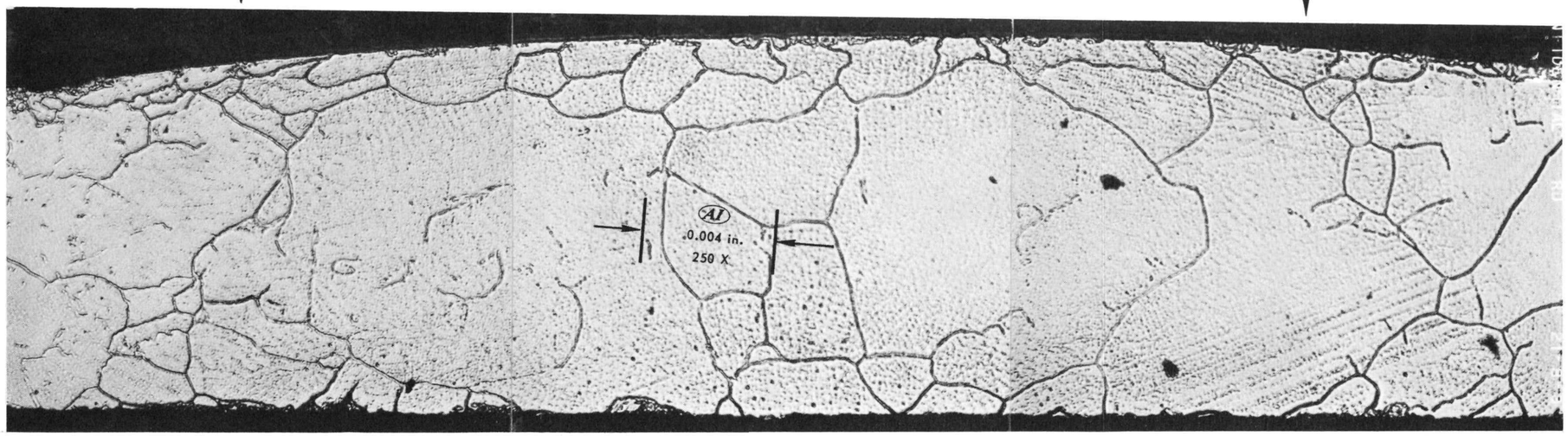

7-12-65 7568-02311

Figure 49. Precipitates in TIG Weld Area of Irradiated NAA-77-2 and NAA-77-3 Membranes

BLANK

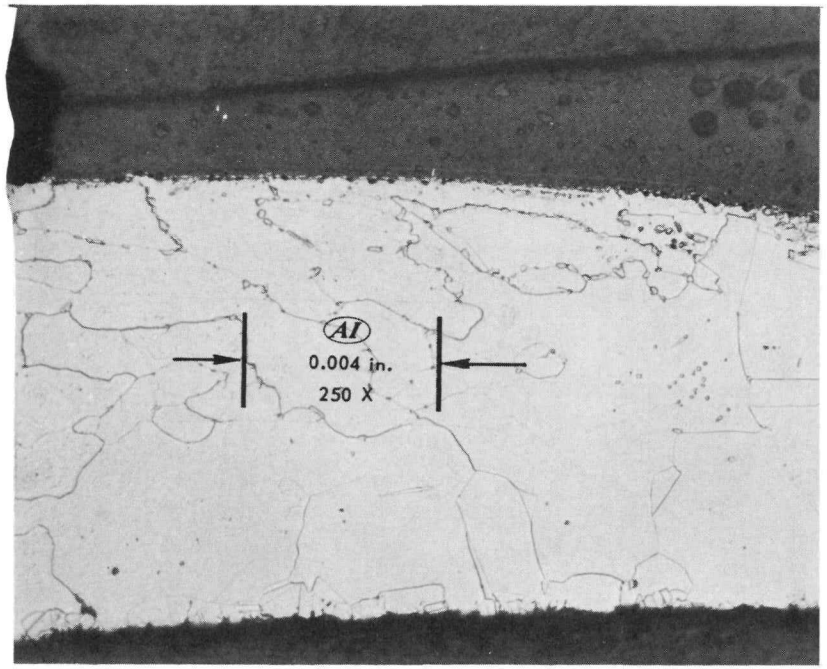

a) TUBE E-822

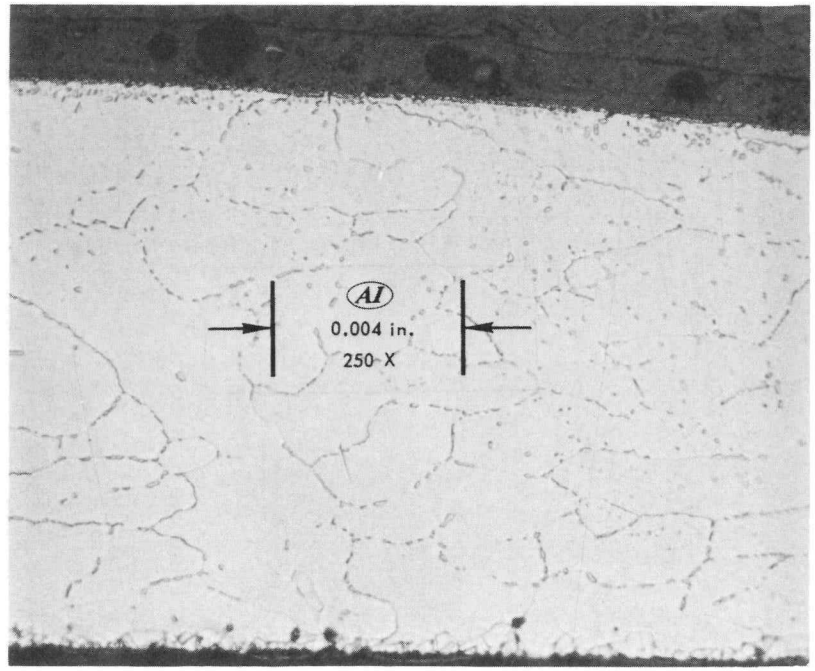

b) TUBE E-808

TIG WELD ZONES OF AGED UNIRRADIATED HASTELLOY-N TUBING

SCB COATING APPLIED OVER CHROMIZING IN A 45-MINUTE TOTAL FIRING (THREE 15-MINUTE FIRED COATS).
BOTH TUBES WERE AGED FOR 14,000 HOURS AT 1500°F WITH 1 ATM. INTERNAL PRESSURE.

7-12-65

7568-02312

Figure 50. Precipitates Formed in TIG Weld Area of Unirradiated SNAP 8 Cladding Tubes

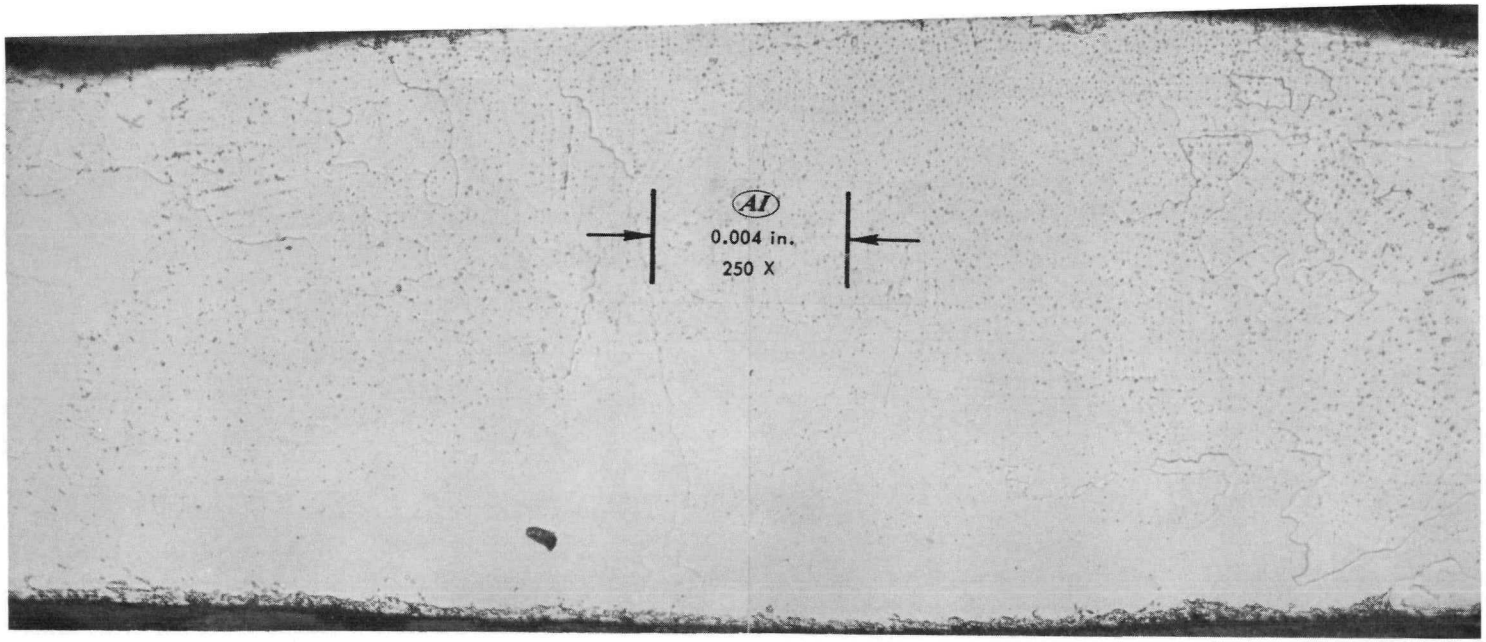

TIG WELD ZONE OF SCB-COATED HASTELLOY-N TUBING

TWO 5-MINUTE FIRINGS: TOTAL = 10 MINUTES AT 2100°F

7-12-65

7568-02313

Figure 51. Precipitates Formed in TIG Weld Area of Unirradiated SCB-Coated Hastelloy-N Tubing

CONFIDENTIAL

temperature-controlled capsules. This test is designed to achieve the equivalent burnup of the SNAP 8 core operating at 600 kwt for 10,000 hours. Data obtained from this test will be used in the S8ER core performance evaluation and will provide detailed data on fuel element performance capability.

During this report period, temperatures were reduced on two of the 12 test fuel elements after thermocouple anomalies were detected. These two elements are now operating at peak fuel temperatures of 1100 and 1150°F. The 10 remaining fuel elements continued operation at design conditions. Because of the redundancy in the experimental plan and the fact that the irradiation is nearing completion, it is estimated that at least 95% of the test objectives will be achieved. Thirty of the original 38 thermocouples in NAA-115-1 continued to demonstrate satisfactory performance.

(2) NAA-115-2 Fuel Element Irradiation Experiment

The NAA-115-2 irradiation test plan includes the same parameters as the NAA-115-1 except that NAA-115-2 contains sublength S8DS fuel elements and it will be irradiated to the equivalent of two years of S8DS operation.

The NAA-115-2 irradiation assembly is identical with the NAA-115-1 assembly but includes improved thermocouples. The thermocouples used in this experiment were fabricated to a specification which was developed as a part of the engineering irradiation program. Details of the thermocouple reliability improvement effort have been presented in previous progress reports.

During this report period, the assembly of the NAA-115-2 was completed and the experiment was inserted in the reactor at Hanford. Startup and operating data indicate that the experiment, the gas control system, and the data acquisition system are functioning as designed. Initial performance data for the assembly shows that all six experiments are operating within 5% of design power. Figure 52 shows a typical fuel element used in the NAA-115-2 experiment. Figure 53 shows a typical single-fuel-element capsule and Figure 54 shows a typical 4-fuel-element capsule. Two of the 4-element type and four of the single-element type experiments were assembled into an experimental train, 32 ft long exclusive of the flexible lead harness. Figure 55 shows the complete assembly as it was prepared for shipment to the reactor.

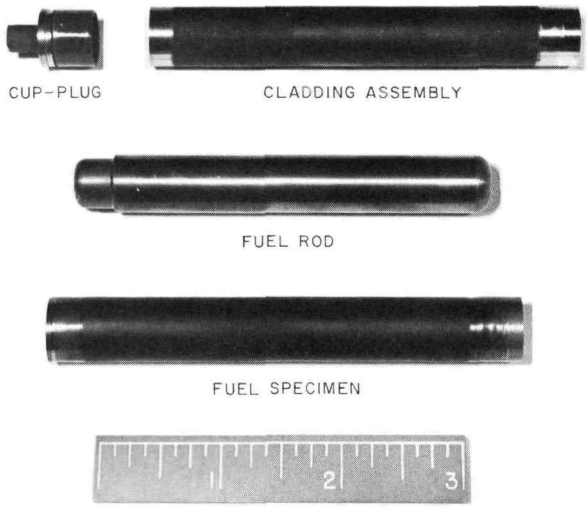

Figure 52. Typical Fuel Specimen Used in NAA-115-2 Irradiation Experiment

(3) NAA-117-1 Fuel Element Engineering Irradiation

The NAA-117-1 irradiation test plan is designed to evaluate the effect of increased power density on fuel element performance over a range of temperature and fuel compositional parameters. The 16 sublength fuel elements continued irradiation at Hanford toward the equivalence of two years of SNAP 8 reference design operation at 1.2 Mwt. Irradiation of the

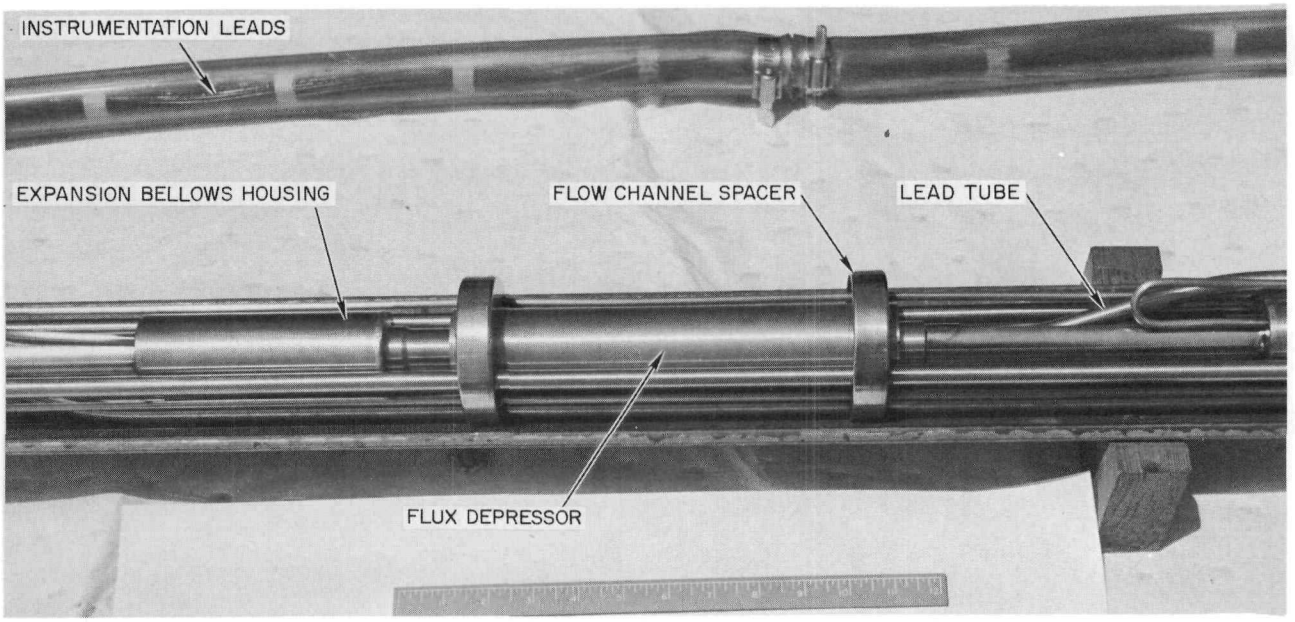

8-19-65 7568-51562CNA

Figure 53. Typical Single-Fuel-Element Experiment, NAA-115-2

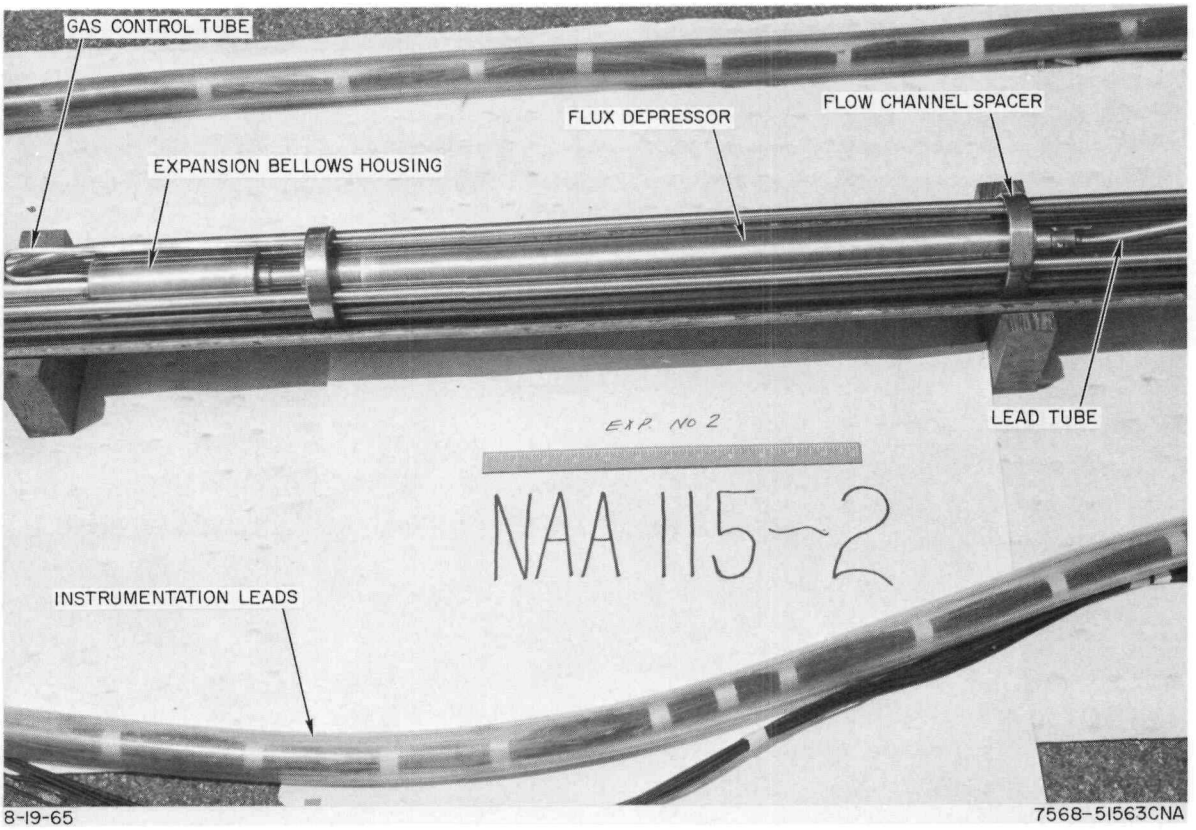

Figure 54. Typical 4-Fuel-Element Experiment, NAA-115-2

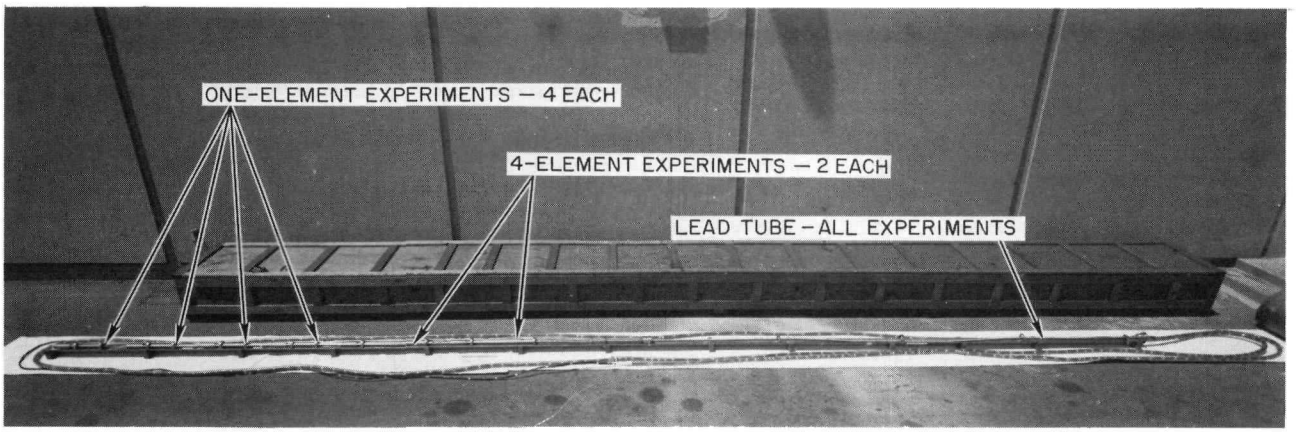

9-9-65 7568-51568CNB

Figure 55. NAA-115-2 Experiment, Complete Assembly

test continued at Hanford with all fuel elements within 2% of design temperature. All thermocouples continued to demonstrate satisfactory performance. Detailed resistance and emf data, measured periodically through the long irradiation period, indicate that thermocouple reliability improvement has been achieved.

(4) NAA-121-1 Prototype Fuel Element Irradiation

Prototype full-scale fuel element performance will be simulated in these experiments which are designed for irradiation in the Hanford production reactors. Details of the experiments have been described in previous progress reports.

The heat transfer analysis of this experiment has been completed. All of the design drawings have been completed with the exception of the reactor installation drawing which is in process. Fabrication of capsule parts continued.

(5) S8ER Post-Irradiation Evaluation

Effort has been concentrated on hot-cell preparations for the S8ER core examination with emphasis on the development of capabilities which are required for screening the 211 fuel elements for detailed examination. Selection of elements for detailed examination is to be based upon:

1) Visual inspection to determine surface condition;

2) Eddy-current inspection to indicate the degree of hydrogen loss and distribution; and

3) Precise measurement of elements to reveal significant changes, if any, in cladding dimensions.

Elements will be visually screened using conventional hot-cell equipment such as periscope, cameras, stereo magnification, and window viewing. In-cell installation of the stereo equipment and the periscope is complete. Fabrication of tooling and fixtures required to support the core disassembly and visual screening operation has been completed. This equipment is composed of holding fixtures, remote transfer tools, positioning and marking tools, and special tools for separation of grid plates and disassembly of the core.

Additional tests were conducted to evaluate an eddy-current technique for determining hydrogen distribution in the fuel elements. Tests were completed with an instrumentation unit matched to this application and with specially wound coils which closely fit the fuel element. The tests were conducted with several non-irradiated clad fuel samples, accurately hydrided to ratios of H/Zr ranging from 0.50 to

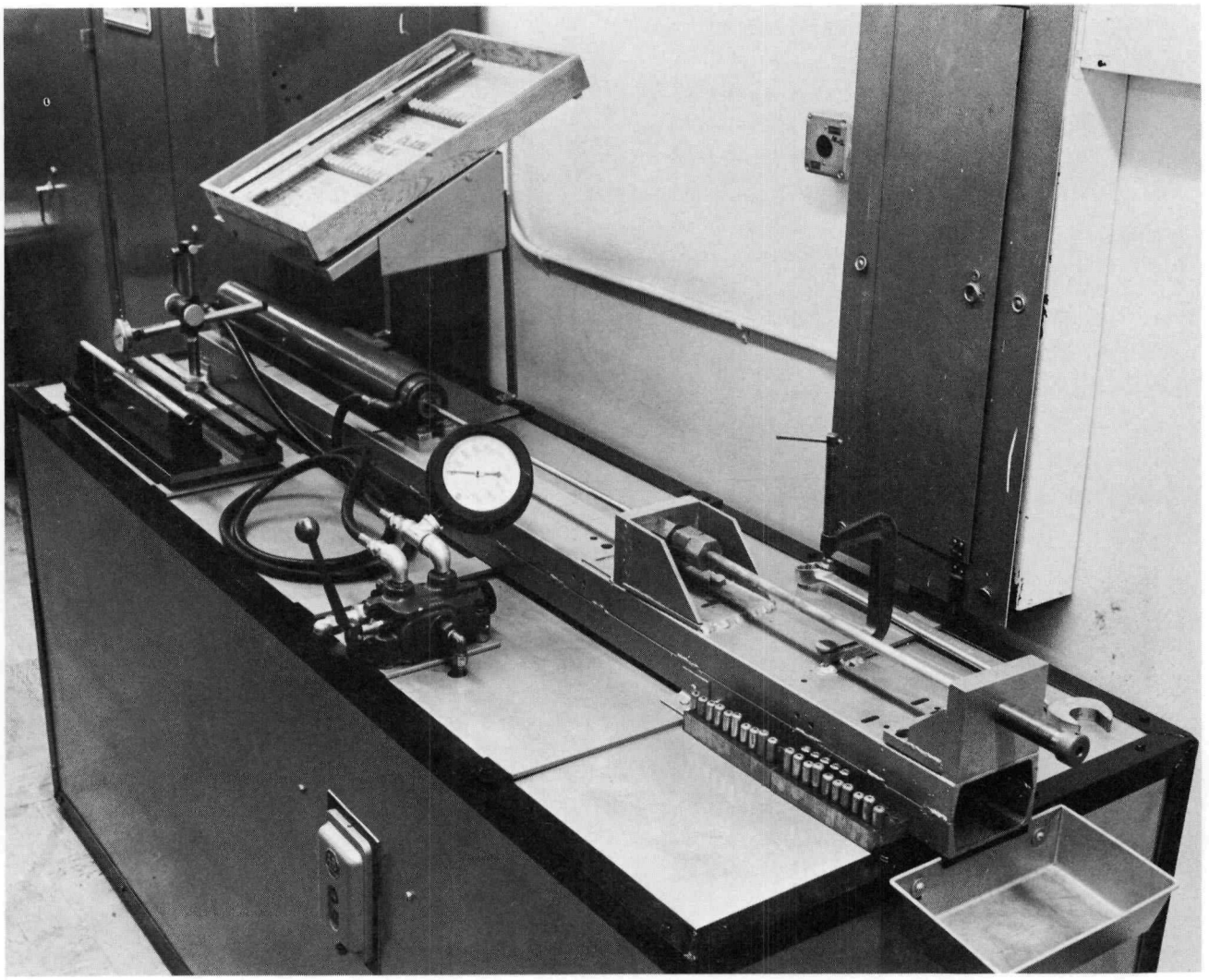

6-29-65 7568-18700

Figure 56. Tube Straightening Equipment

1.85. A nonirradiated clad fuel rod with an axial H/Zr gradient was also tested. Results indicate a linear relationship of eddy-current response to H/Zr with a change of slope at points of phase change. It was demonstrated that the test results are reproducible. The tests also showed that the presence of the cladding does not significantly alter the eddy-current response of the fuel rod.

C. S8DS FUEL ELEMENT FABRICATION

A group of elements was produced from cladding tubes chromized by Vendor B which had been rechromized in-house. During this program, an in-house tube straightening capability was developed and qualified for production. A tube chromizing process specification was issued, equipment and processing refinements were completed, and the tube chromizing process capability run was initiated at the close of the reporting period.

The rechromizing procedure was an extension of the technology developed to chromize cup-plugs (reported in the previous progress report). Various parameters were examined to attain improved coating adherence on the rechromized tubing [Section IV-B-2-b-(2)]. The recommended parameters were 2100°F for 30 minutes. A group of tubes was processed through the production facility to the recommended electropolishing and rechromizing specification. Ten of these tubes were assembled into normal uranium fuel elements and permeation tested. Pertinent data is tabulated in Table 44. It is significant to note that all ten elements had acceptable permeation rates and that the coating adherence was definitely improved over that obtained from vendor-chromized material.

TABLE 44

FUEL ELEMENT DATA – RECHROMIZED TUBING

Element Number	End Sample Adherence Index	End Sample Chrome Thickness (in.)	Permeation Rate at 1400°F [cc(STP)/hr]	
			1st Test	2nd Test
2981	7	0.00055	0.54	0.53
3422	35	0.00034	0.69	0.62
3483	35	0.00055	0.57	0.55
3487	21	0.00071	0.87	0.94
3432	49	0.00091	0.93	0.97
3438	35	0.00106	0.82	1.00
3439	49	0.00080	0.44	0.47
3444	21	0.00060	0.89	0.93
3476	-	0.00111	0.57	0.73
3477	35	0.00083	0.32	0.33
		Average	0.66	0.71

1. Tube Straightening

The tube rechromizing process produced bowed tubing which required straightening prior to application of the ceramic coating. This was not a new condition in that vendor chromized tubing also required straightening. An in-house straightening process was developed after vendor-supplied processes failed to produce the required tube assembly straightness.

The new straightening process consisted of inserting a tungsten-carbide mandrel into the tube to enlarge the inside diameter to 0.5405 in. A full-length mandrel, precision ground to 0.5395 in., was then placed inside the tube assembly. A load was applied from a hydraulic ram stretching the tube beyond the yield point and down over the straightening mandrel. The straightening equipment is shown in Figure 56.

Early lots of in-house chromized cladding tube assemblies were more difficult to straighten because of an extremely hard, thick, chrome layer. Subsequent refinements in the chromizing process reduced the chrome thickness and improved the ductility of the tubing. With these changes the straightening process was capable of producing high quality material on a repetitive basis. For a typical group of tubing samples, the TIR ranged from 0.042 to 0.253 in. in the as-chromized condition. After straightening the TIR's ranged from 0.001 to 0.010 in. which

TABLE 45

FUEL ELEMENT DATA – INITIAL PROCESS CAPABILITY

	Element Number	End Sample Adherence Index	End Sample Chrome Thickness (in.)	Permeation Rate at 1400°F [cc(STP)/hr]	
				1st Test	2nd Test
Capability Study Tubing	4002	15	0.00023	0.34	0.33
	3996	-	0.00017	0.68	0.67
	4014	7	0.00035	0.26	0.28
	4026	28	0.00064	0.39	0.50
	4042	<7	0.00075	0.44	0.47
	4032	20	0.00051	0.27	0.32
	4035	<7	0.00044	0.53	0.63
	4003	7	0.00018	0.22	0.29
	4006	17	0.00030	7.48	-
	4011	23	0.00046	0.26	0.25
Post-Capability Tubing	4034	-	-	0.41	0.35
	4038	<7	0.00042	0.35	0.33
	4039	<7	0.00043	0.96	1.02
	4036	10	0.00046	0.44	0.50
	4037	14	0.00039	0.30	0.35
	4014	7	0.00035	0.26	0.28
	4026	28	0.00064	0.39	0.50
	4042	<7	0.00075	0.44	0.47

is well within the 0.015 in. specified for S8DS fuel elements.

2. Chromizing

Based on results of the development program a preliminary specification was issued for chromizing virgin S8DS cladding tube assemblies. A process capability study was designed to evaluate control of the chrome layer thickness, level of coating adherence, and fuel element performance. A group of 45 tubes was chromized. Each tube was in an individual tubular retort, and five retorts were fired per furnace load. The firing parameters were 2135°F for 12 minutes. The 12-minutes-at-temperature requirement was translated to a total furnace cycle time of 28 minutes, and all 45 tubes were tested in this manner.

The 45 tubes were subjected to extensive evaluation, including taking 381 coating adherence test samples and 66 samples for chrome thickness examination. Statistical analysis of the data produced the following conclusions:

1) At the 90% confidence level, 99% of the tubes processed in this manner would have an inside diameter chrome thickness of 0.0001 to 0.0007 in.

2) The chrome thickness produced was uniform down the length of the tube.

3) Significant variability was noted from furnace load to furnace load.

4) No correlation existed between the end sample coating adherence and coating adherence down the length of the tube.

Evaluation of these results and results obtained in developmental chroming experiments indicated that the process capability could be significantly improved by closer control of the processing temperature and time. The process specification was revised and equipment and instrumentation refinements were initiated to achieve the required process control.

A furnace loading device was constructed to permit all five chromizing retorts to be preassembled into a rack outside the furnace. The rack loading pattern was designed to be compatible with the optimum furnace temperature profile conditions.

The improved chromizing process is a two-step operation to achieve better temperature uniformity. The furnace temperature is set at 1960°F and the retort loading rack is charged into the furnace. When all five retorts have equilibrated at 1900°F, the furnace temperature is rapidly brought up to 2150°F. After all retorts fall in the range of 2135 ± 50°F, the 12-minute time cycle begins, after which the rack is withdrawn from the furnace and the retorts are rapidly cooled. Checkout operations have demonstrated that the process can be followed on an accurate, repetitive basis and a formal process qualification program has been initiated to achieve a chromized layer of 0.00040 ±0.00015 in.

3. Fuel Element Fabrication

A group of 18 normal uranium fuel elements were assembled from tubing chromized during the initial tube chromizing capability study. Ten of the tubes were chromized during the study; the remaining eight were chromized immediately after the study, but to the same process. Pertinent data for these elements is shown in Table 45.

BLANK

V. COMPONENT DEVELOPMENT

A. CONTROL-DRUM DRIVE AND SCRAM MECHANISM

Performance mapping and design verification tests will be conducted on three control-drum drive and scram units of the S8DS design under simulated operating conditions of vacuum and temperature.

Design verification testing is continuing on one scram drive mechanism (SN 001). The unit is mounted on a test fixture which simulates the S8DS control drum and bearings, as shown on Figure 57. Results of the bench test which showed successful mechanical and electrical performance were reported previously.*

An environmental performance test on unit SN 001 has been underway for 1900 hours at 1×10^{-5} to 1×10^{-7} mm Hg and a controlled electromagnetic-clutch temperature of 775°F. The clutch temperature is controlled to maintain the predicted S8DS operating temperature since it is considered the most critical functional part in the control-drum drive and scram system. Figure 58 is a map of the actual measured temperatures of SN 001 with the clutch temperature controlled at 775°F. Due to the limitations of test fixture and heater design, the effects of gamma heating cannot be exactly simulated. Consequently the critical component, the clutch, is controlled and temperatures of other parts are controlled by varying the thermal reflector to achieve the best compromise.

Ten successful thermal cycles from 775°F to ambient and back to 775°F have been performed during this report period with 140 total scram cycles being recorded. All scram times have been less than the maximum allowable system design requirement of 2 sec for 109° drum rotation and 0.5 sec for 23° drum rotation at environmental conditions. Actual measured scram times for the critical shutdown angular rotation (23°) range from 169 to 210 millisec.

A counterclockwise drive unit (SN 002) has been assembled prior to bench performance and environmental testing.

Manufacturing processes for fabrication of the clock-type scram power spring were developed. This spring is a spiral of flat nickel chrome alloy strip (Rene´ 41) and is designed with limits on output torque characteristics to assure reliable, repeatable scram performance. A 0.001-in. tolerance on the material thickness is required to control the output torque which varies as the 3rd power of thickness. Since the nominal tolerance of standard stock† is 0.006 in., the required thickness and tolerance are obtained by re-rolling thicker material. The process developed consists of slitting 0.090-in.-thick by 4 ft by 8 ft sheet along the major axis, progressively rolling down in thickness, and annealing before the final 0.004- to 0.007-in. reduction in thickness. The strip formed is then finish-ground along the slit edges to remove any cracks formed in the slitting and rolling operations. The strip is then wound into a spring and the length cut to achieve the required torque characteristic.

Three developmental springs have been fabricated using this technique and are being used in the three design verification test units. Adaptation of this process to production units was initiated and S8DS system springs are now in fabrication.

*C. E. Johnson, "SNAP 8 Progress Report, February-April 1965," NAA-SR-11092 (CRD), June 15, 1965

†AMS5545 plate, sheet, and strip alloy nickel base – solution heat treated

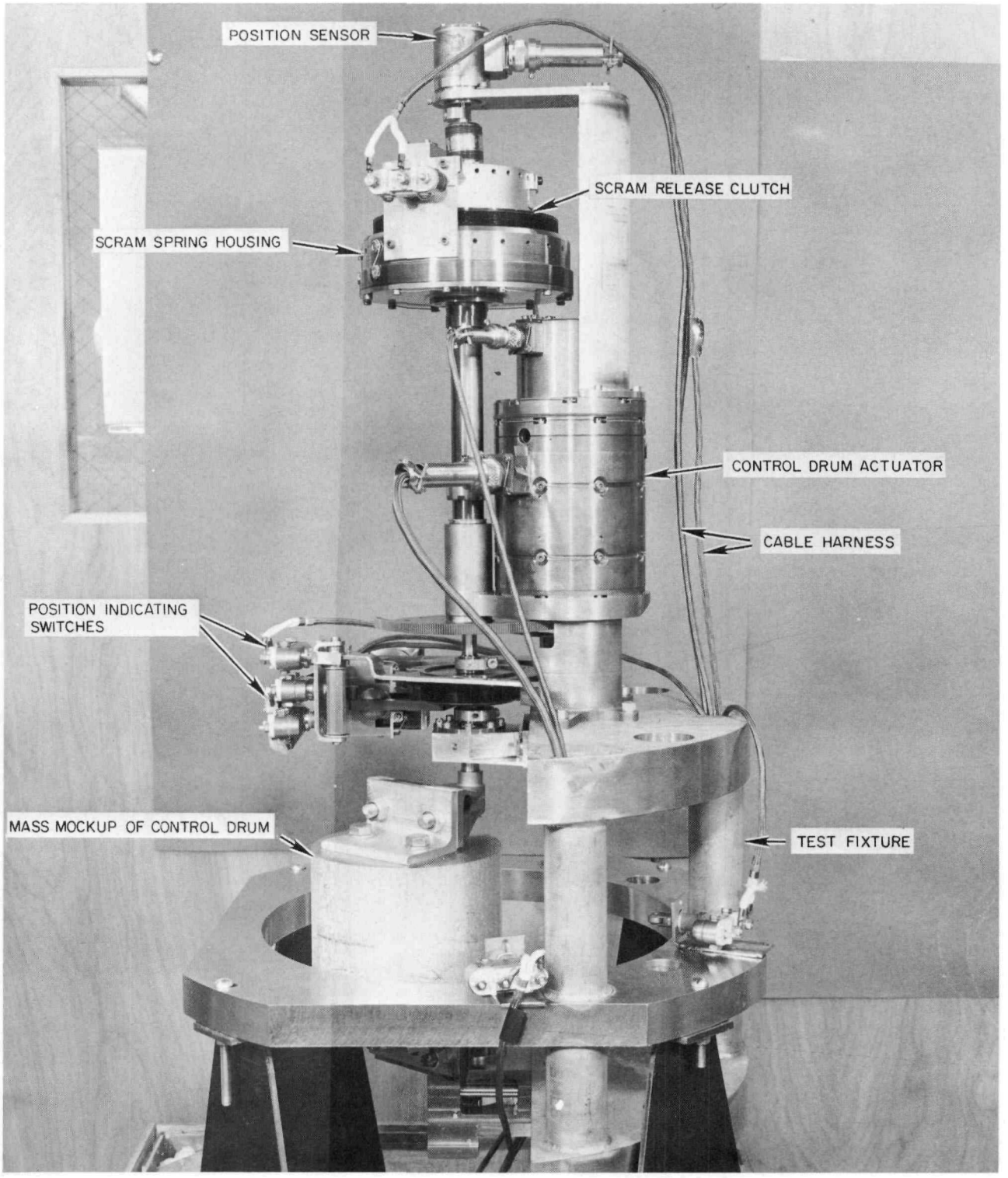

7-7-65

7568-551501A

Figure 57. S8DS Scram Drive Mechanism Test Assembly

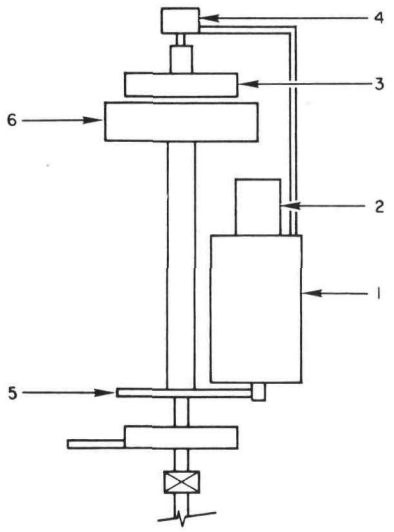

	TEST TEMPERATURE (°F)	EXPECTED OPERATING TEMPERATURE (°F)
1. ACTUATOR STATOR CASE	945	975
2. ACTUATOR BRAKE HOUSING	960	850
3. CLUTCH COIL HOUSING	775	775
4. POSITION SENSOR	490	600
5. DRIVE GEAR	930	930
6. DRIVE BELLOWS HOUSING	870	950

7-16-65 7568-02279

Figure 58. S8DS Scram Mechanism Unit No. 1 Temperature Map

B. CONTROL-DRUM ACTUATORS

The SNAP 8 reactor is controlled by rotating the external beryllium control drums to increase or decrease the fraction of leakage neutrons. The control-drum drive is mechanically connected to an electromagentic actuator which rotates and positions the reflector drums in 0.26° steps through a gear train upon command from a controller. The actuator incorporates a built-in mechanical brake which locks the control drum during the nonoperational period. The release of the brake and the actuator operation are sequenced to prevent free wheeling of the control drum.

The reference design S8DS actuator is a direct-current, variable-reluctance stepping motor. The motor is energized with d-c voltages in discrete pulses which cause the rotor to turn in steps of 1.8°. The rotation may be in either direction as required. The controller is designed to produce two actuator steps of 1.8° or a total of 3.6° for each operation. The geared drive reduces the 3.6° actuator output to 0.26° control-drum rotation. The teeth on the braking surface, Figure 59, serve to provide accurate position alignment after each stepping sequence.

1. Bench Test and Assembly

Thirteen developmental and three S8DS actuators have been successfully assembled and bench tested. The output torque test data, Figure 60, verify that the actuators can provide repeatable torque outputs when manufactured in accordance with rigid dimensional and quality standards. The torque output exceeds the design requirements with an adequate margin of safety and is in agreement with design calculations.

2. High-Temperature and Vacuum Tests (Insulation and Endurance)

Several actuators are presently in various stages of long-term endurance and evaluation tests. A typical high-temperature and vacuum test stand and fixture is shown in Figure 61. The load is a fixed weight which may be rotated through 360° during a continuous series of stepping sequences. The maximum load will occur

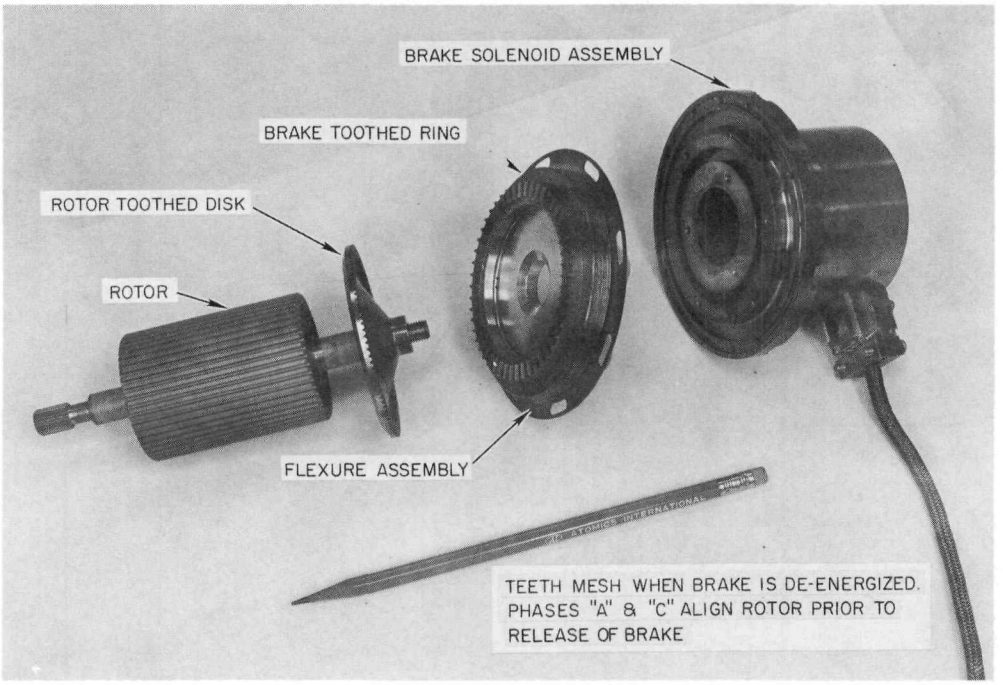

7-16-65 7568-551413A

Figure 59. S8DS Rotor and Brake Assembly

when the weight passes through the 90° or 270° positions. The minimum current and voltage required to step the load is measured at these positions to monitor the torque output. Minimum current to release the brake is also measured as a means of monitoring brake spring force.

a. Nonoperation or Dwell

Two actuators were subjected to long-term periods of nonoperation in the high-temperature and vacuum environment to investigate the effect of long-term dwell. This was done after the first 1000 hours of operation on actuator SN 001 and 640 hours of operation on actuator SN 002. After 500 hours of dwell, actuator SN 001 stepped and performed as required with no change in performance or characteristics. This unit is presently undergoing additional long-term dwell.

b. Coil and Insulation Resistance

There has been no indication of change in coil or phase resistance as a result of the long-term exposure to the 1025°F environment on the actuators tested to date.

There have been, however, changes in the insulation resistance-to-ground. The maximum and minimum phase resistance-to-ground vs time, is shown for three actuators in Figure 62. The curve for actuator SN 001 illustrates the characteristic behavior of the insulation resistance with time at temperature. The initial rapid increase in resistance is attributed to outgassing of the insulation. The steep degradation slopes after the initial increase are due to the carbonization of the surface contamination of the connector pin insulator and the lead insulation. The contamination is due to slight backstreaming of vacuum pump oil into

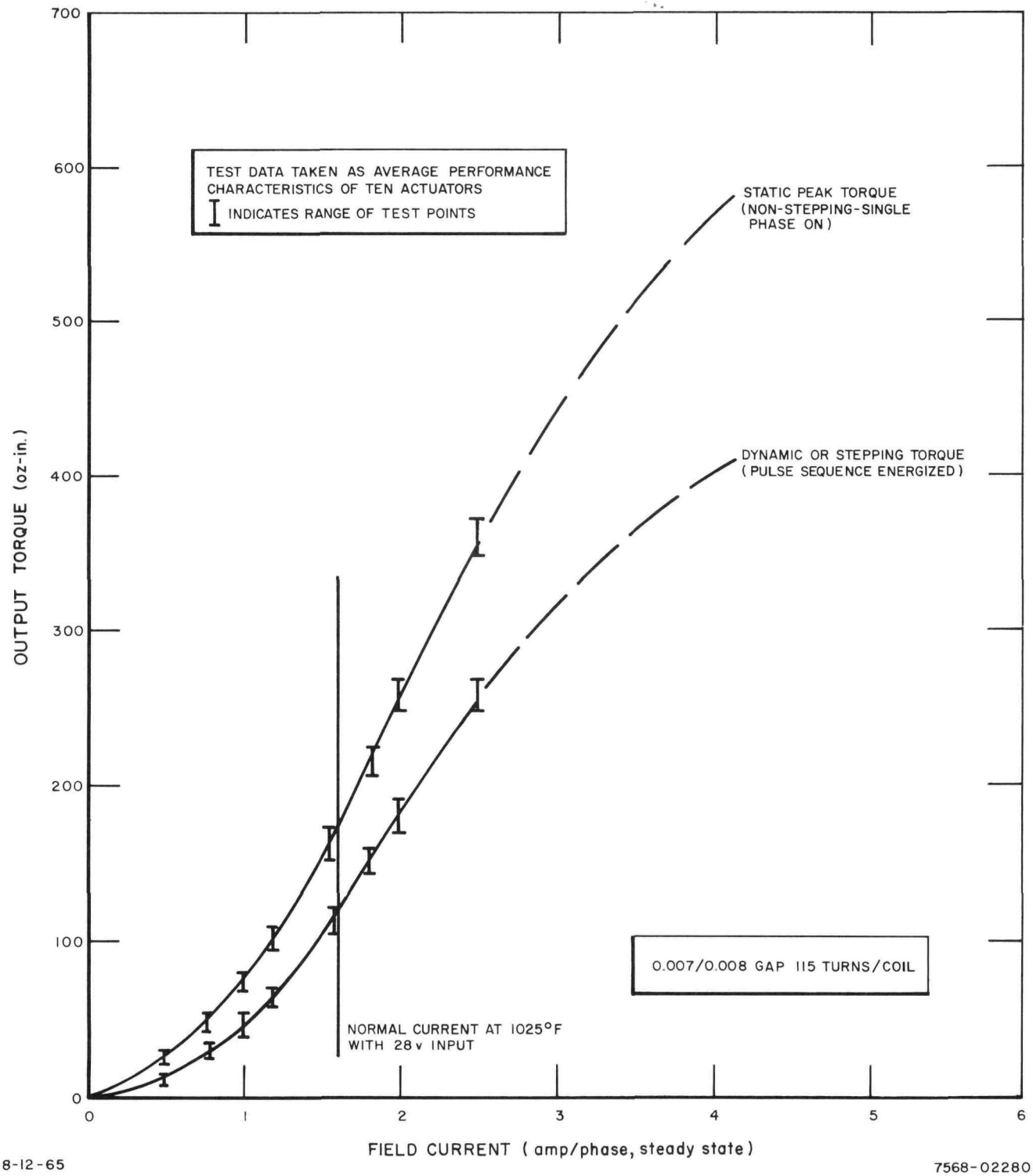

Figure 60. Static and Dynamic Torque vs Field Current for S8DS Design Control-Drum Actuator

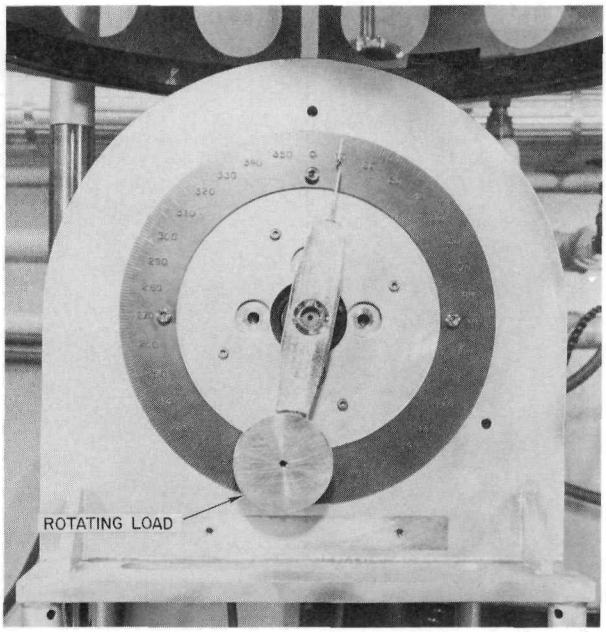

7-16-65 7568-551276A

Figure 61. View of S8DS Control-Drum Actuator High-Temperature and Vacuum Test Stand Showing Rotatable Load

the vacuum environment. The spread between phases and actuators may be attributed to the wiring and lead arrangement within the stator, wherein the leads of one phase are physically closer to ground than in another phase.

Actuator SN 006 was contaminated by oil backstreaming due to failure of the test system during initial vacuum pumpdown. Its performance has demonstrated that actuators perform satisfactorily with the low values of insulation resistance. The steep insulation degradation slope is again an indication of insulation contamination.

c. Consecutive Startup and Thermal Cycle Test

The startup cycle is the most severe condition under which an actuator must perform. The actuator must step with 28 volts applied continuously for 1863° of rotation (135° of drum rotation). The extremely high current density in the wire as well as the rapid internal temperature increase is conducive to the formation of internal hot spots and wire burnouts. After the full-in stepping cycle, the actuator windings are subjected to the externally induced temperature rise caused by nuclear irradiation.

These conditions are simulated and combined in the consecutive startup and thermal cycle test. The cold actuator is stepped with 28 volts applied for a period of time equivalent to the startup. Within 90 minutes after completing the simulated startup stepping cycle, the actuator is raised to 1025°F with external heat. After several hours at this temperature, the actuator is again operated for two complete revolutions with 28 volts applied. This test is conducted during the day with a cooling period at night. Figure 63 illustrates the temperature increase of the coil during the startup test in vacuum at 85 and 1000°F ambients. One test actuator has completed 25 startup and thermal cycles with no significant change in the output torque, brake release current, coil resistance, or insulation resistance.

C. ELECTRICAL COMPONENTS

1. Cable Harness

The objective of the cable harness development program is to test, evaluate, and recommend cable material and associated hardware for use in an integrated harness which is capable of transmitting power and electronic signals between various components of the system.

Methods for termination and fabrication of the S8DS high-temperature cable harnesses have been revised to include the continuous welded circuit concept.* Figure 64 shows a short cable length being welded to an S8DS control drum actuator. The other end of this cable

*C. E. Johnson "SNAP 8 Progress Report, February-April 1965," NAA-SR-11092 (CRD), June 15, 1965

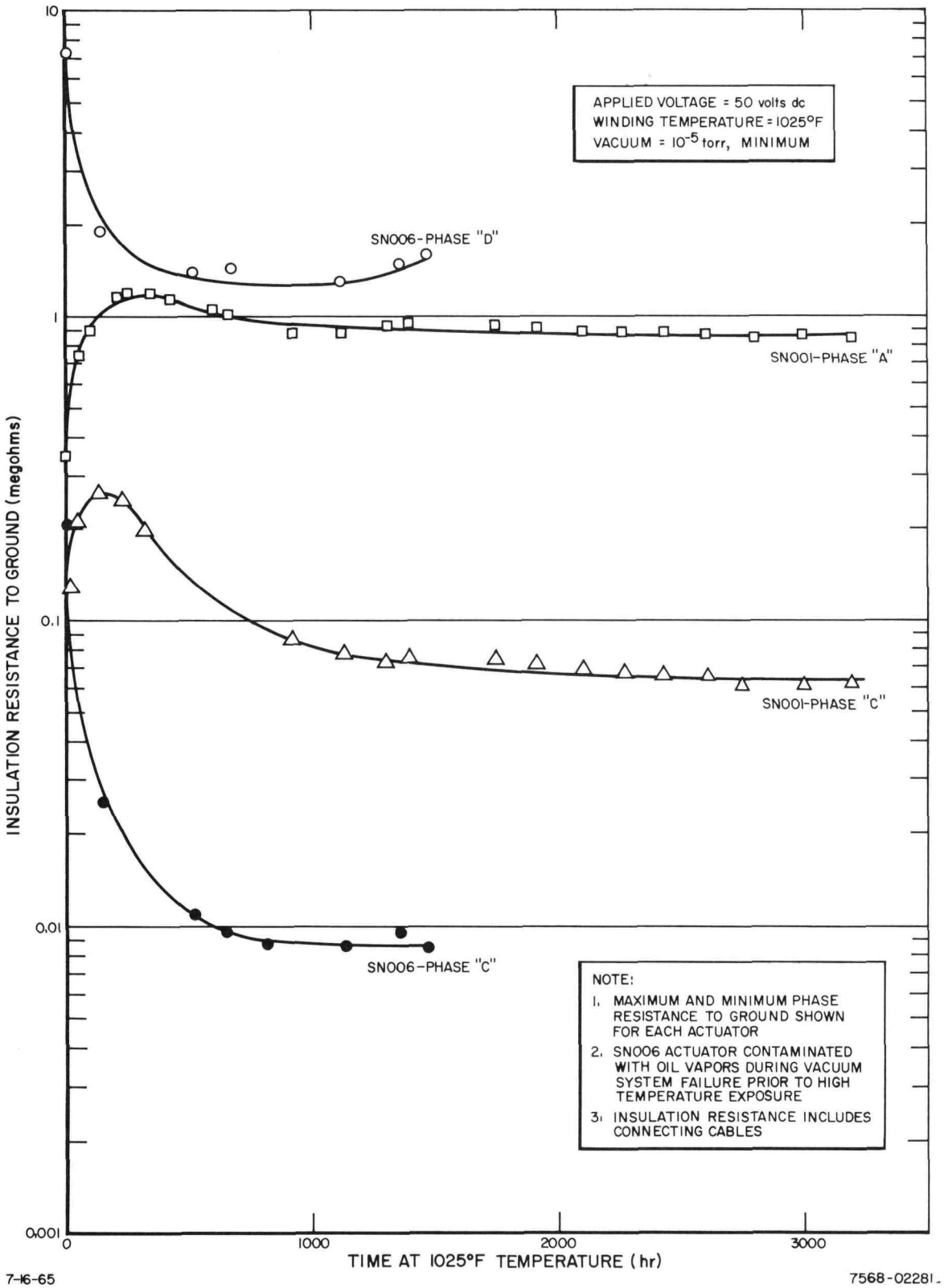

Figure 62. Phase Insulation Resistance-to-Ground vs Time for S8DS Design Control-Drum Actuators

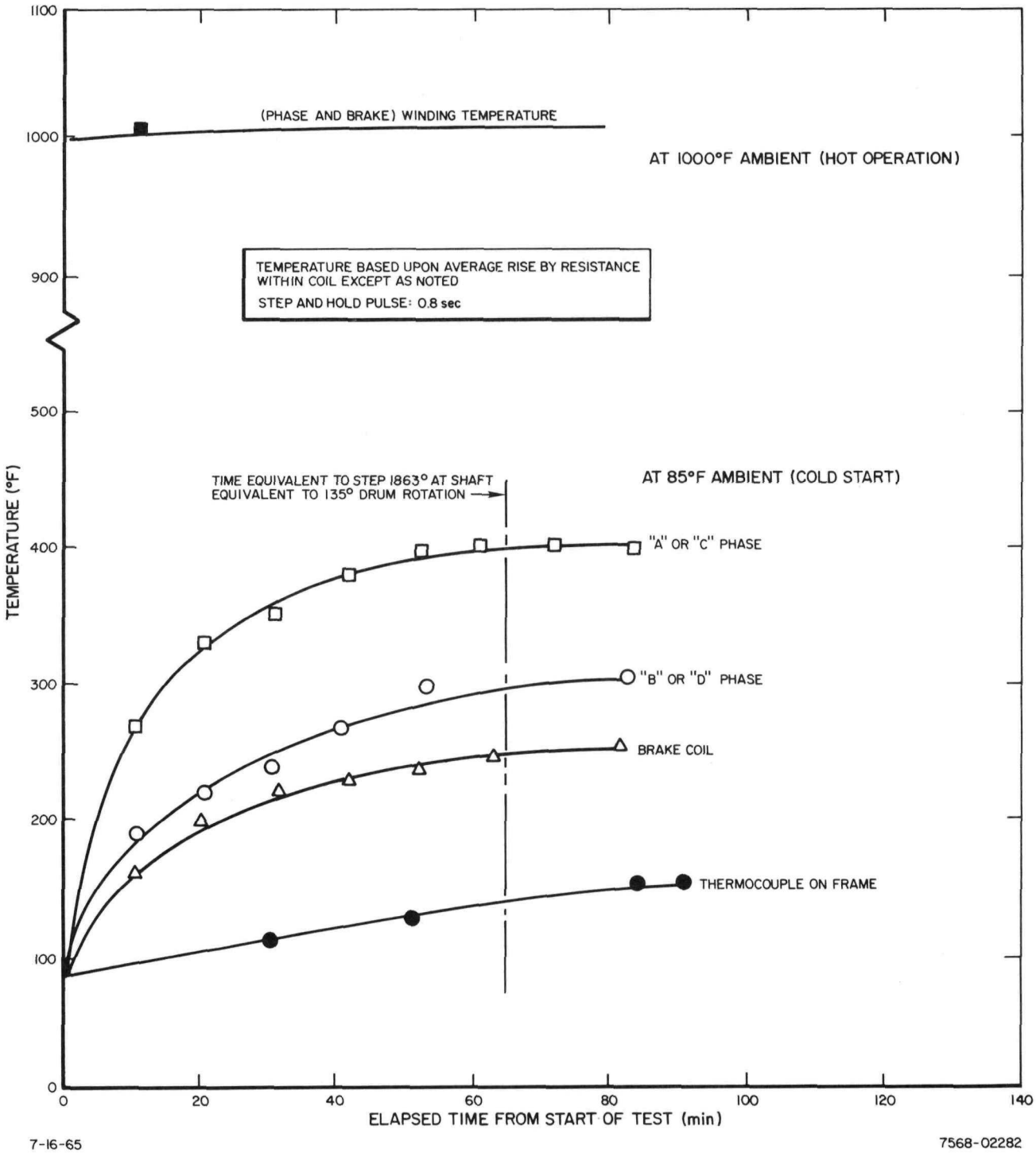

Figure 63. Temperature Rise During Startup Operation of S8DS Design Control-Drum Actuator

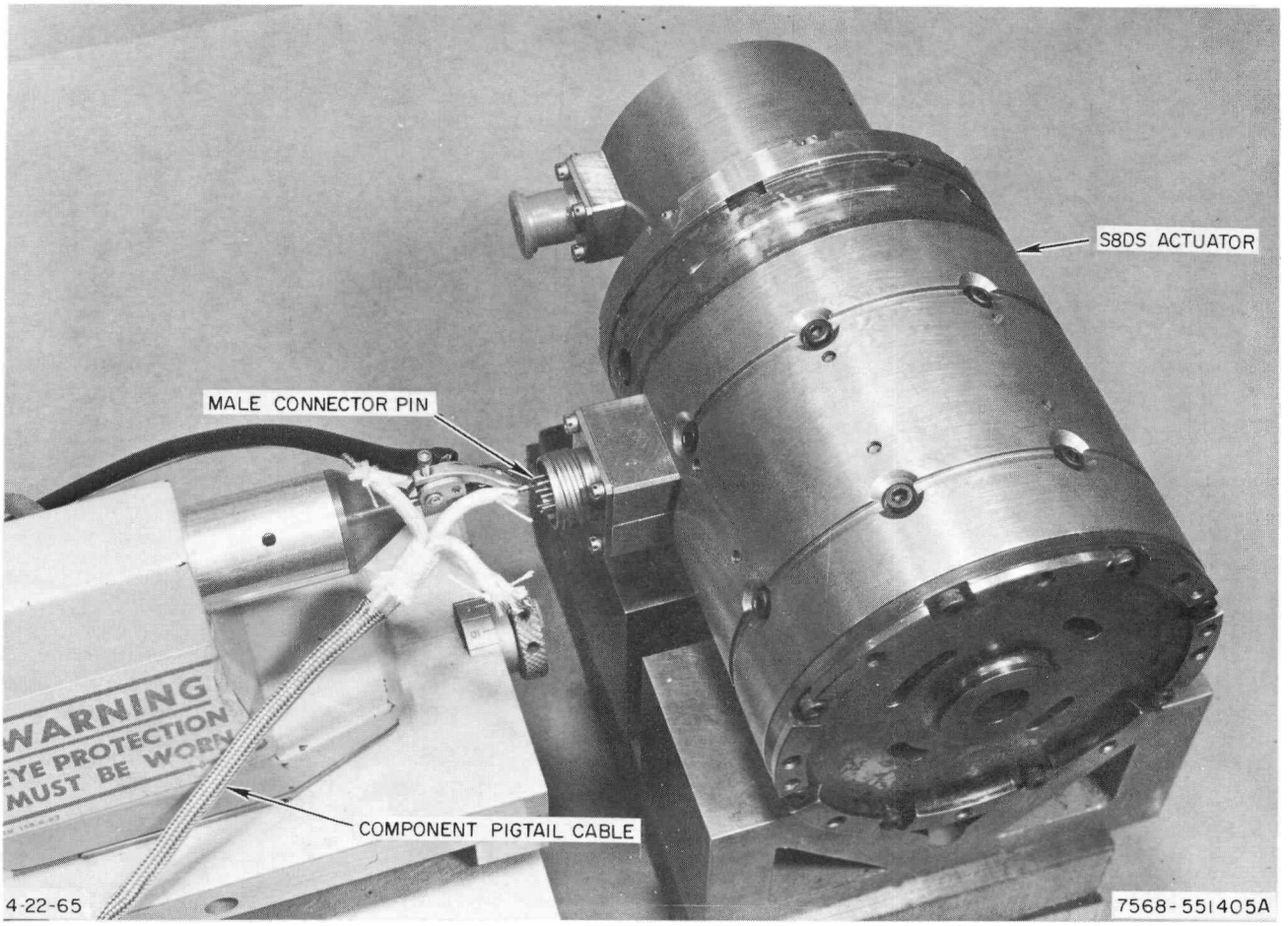

Figure 64. Welding of Pigtail Cable to Component Connector

is terminated to ring lugs (Figure 65) for connection to a terminal block. The terminal block joins the component cable to the reactor cable harness.

On two occasions components have failed to operate in test because of high connector-spring-contact resistance. The heat cleaning process for the harness assembly (800°F in air)* was suspected of causing the high resistance. Tests verified the increase in contact resistance up to 7 ohms. The increase was attributed to oxidation of the contact. This problem was resolved for S8DRM-1 by revising the termination process to provide for assembly of the connector to the harness after the harness is heat cleaned. An S8DRM-1 harness termination with the backshell removed is shown in Figure 66. Heat cleaning is not a problem on the S8DS harness since the spring contact connectors are not used. The cable conductors are welded to male connector pins and ring lugs.

The reliability of the high-temperature cable harness assembly was improved by changing the material of the insulation clamping sleeve. The previous sleeve contained 15 to 20% zinc which, under the harness operating environment, could sublime and deposit on the cable insulation thereby reducing its electrical resistance. A new stainless-steel sleeve is used for insulation clamping (Figure 65).

*C. E. Johnson, SNAP 8 Progress Report, November 1964-January 1965," NAA-SR-10792 (CRD), March 15, 1965

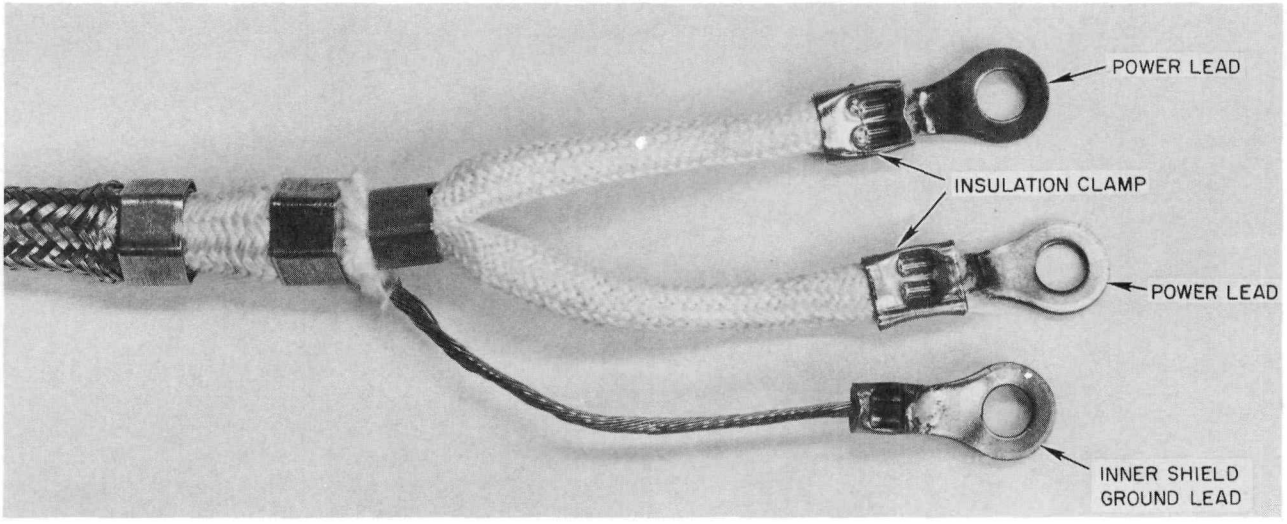

6-29-65 7568-551480A

Figure 65. Component Pigtail Cable End

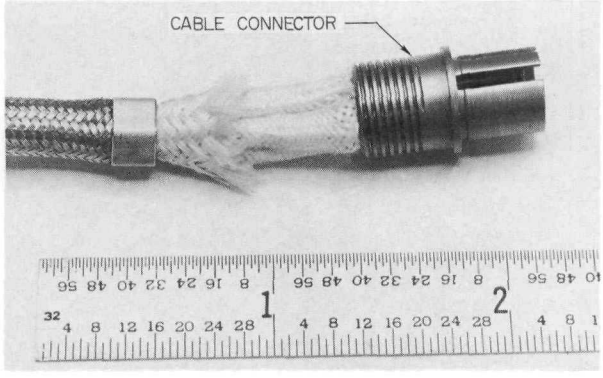

8-30-65 7568-551365a

Figure 66. Cable Harness with Connector (S8DRM-1 design)

The entire termination process was verified by making more than 80 high-temperature cable assemblies of various types including more than 400 wire terminations. These cables are used in high-temperature and vacuum testing of developmental S8DS control-drum actuators, position sensors, limit switches, and complete scram-kit assemblies. They are also used in the HF-10 irradiation capsule test assembly of actuators, position sensors, and limit switches.

2. Coil Techniques

Metal bobbins with an inorganic insulation coating* are being considered for use on SNAP electromagnetic coils. The metal bobbins are designed to increase the strength properties of the coil assembly.

Two additional coatings have been evaluated at 1000°F and 10^{-8} torr, flame-sprayed aluminum oxide and sprayed Allen PBX Cement.† The insulation resistance was monitored daily on three samples of each coating at 50, 100, 300, and 500 vdc at 1000°F. The values of insulation resistance ranged between 1 and 10 megohms at 50 vdc. The resistance decreased at higher voltages. At 500 vdc the resistances were approximately 60% of the 50-vdc values. The PBX coating has advantages, in that (1) it is easier to apply than the aluminum oxide which must be applied by a flame- or plasma-arc-spraying process, and (2) it is less susceptible to chipping than the aluminum oxide.

*C. E. Johnson, "SNAP 8 Progress Report, November 1964-January 1965," NAA-SR-10792 (CRD), March 15, 1965

†C. E. Johnson, "SNAP 8 Progress Report, February-April 1965," NAA-SR-11092 (CRD), June 15, 1965

Electromagnetic coils were produced using previously developed*, § and improved† wet-winding techniques and installed in S8DS position sensors. Initially, problems were encountered with the physical configuration of the sensor housing which resulted in shorting of the coil lead wires. The configuration was modified to provide additional space for routing the lead wire from the coil to the connector pins. No further problems have been encountered subsequent to these revisions. These design modifications have been incorporated in the S8DS position sensor.

D. MECHANICAL COMPONENTS

1. Springs

The spring development program provides design verification of reactor spring design, establishes spring characteristics at elevated temperatures and reactor environments, and generates spring material data for design optimization. Tests are being conducted to evaluate load loss as a function of operating temperature and time, to permit estimates of safe operating stresses and relaxation behavior at the SNAP 8 environmental temperature and irradiation dose level.

Load-relaxation tests of three 88% Ta – 12% W alloy springs (Stauffer-880) in vacuum environment were terminated after 2350 hours of test at temperature. Preliminary results are summarized in Table 46. These tests were conducted at the same loads and temperatures as three similar springs which have completed inpile irradiation tests. Detailed comparison of the inpile and out-of-pile test data has been started to determine the effect of irradiation dose rates on spring relaxation behavior.

A 3000-hour spring comparison test has been completed. In this test, René 41 and Stauffer-880 springs were subjected to identical stress, temperature, and irradiation ($\sim 3 \times 10^{19}$ nvt_f). The René 41 and Stauffer-880 springs were loaded in series and the total combined spring length was kept constant throughout the test. Because the springs were not individually maintained at constant length, and because temperatures were allowed to vary from 400 to 900°F, the test was qualitative and the data obtained cannot be compared with standard spring load-relaxation tests. Three nonquantitative conclusions may be drawn:

1) René 41 helical compression springs were superior to (exhibited less load relaxation than) identical Stauffer-880 springs after 3×10^{19} nvt_f neutron irradiation at $\sim$ 700°F in vacuum.

2) The amount of relaxation was significantly greater for both materials than was

TABLE 46

LOAD RELAXATION TEST DATA, STAUFFER-880 SPRINGS IN VACUUM

	Spring A* (S/N 26)	Spring B† (S/N 28)	Spring C§ (S/N 27)
Test Temperature (°F)	1075	1150	1050/670**
Initial Stress (psi)	40,000	40,000	40,000
Initial Load (lb)	33.1	32.0	32.6
Final Load at 2350 Hours (lb)	29.64	12.98	31.01
Load Relaxation at 2350 Hours (%)	10.45	28.2	4.87

*Spring A – Wire diameter 0.125 in. with seven active coils, 0.818 in. mean diameter; total length 2.065 in.
†Spring B – Wire diameter 0.125 in. with seven active coils, 0.808 in. mean diameter; total length 2.075 in.
§Spring C – Wire diameter 0.125 in. with seven active coils, 0.815 in. mean diameter; total length 2.050 in.
**Temperature variation simulated conditions experienced in HF9 irradiation capsule.

*C. E. Johnson, "SNAP 8 Progress Report, November 1964-January 1965," NAA-SR-10792 (CRD), March 15, 1965
†C. E. Johnson, "SNAP 8 Progress Report, February-April 1965," NAA-SR-11092 (CRD), June 15, 1965
§C. E. Johnson, Progress Report, SNAP 8, August-October 1964," NAA-SR-10492 (SRD), December 23, 1964

expected based on previous out-of-pile tests. The increased degradation is attributed to the radiation environment.

3) Under these test conditions the initial relaxation rate was greater for René 41 than for Stauffer-880, but within 3,000 hours the relaxation rate and total relaxation of Stauffer-880 exceeded that of René 41.

2. Bearings

The S8DS ground test reactor will operate in the slightly oxidizing atmosphere of 10^{-5} torr pressure for over 10,000 hours. Three control-drum bearings sets of different materials combinations are being evaluated at 1150°F and 10^{-5} torr pressure.

Two of the bearing sets have carbon-graphite bushings and Inconel-X monoballs coated with Al_2O_3 on the spherical diameter. The third bearing set has solid carbon-graphite monoballs.

The Al_2O_3-coated surface of one bearing set was coated with a dry-film lubricant, sodium-silicate-bonded molybdenum disulphide plus graphite. This set has been tested for 2144 hours. A maximum torque value of 2.2 in.-lb was measured during the test with the average value being approximately 1.2 in.-lb. Maximum design torque for the bearing is 2.5 in.-lb.

The second Al_2O_3-coated Inconel-X monoball bearing set was tested without a dry-film lubricant for 5050 hours. Torque values were ~1.5 in.-lb.

The test of the solid carbon-graphite monoball bearing set was terminated after 2230 hours of successful testing. Maximum torque was 1.6 in.-lb.

A bearing set with dry-film lubricant on the Al_2O_3-coated Inconel-X is being tested under conditions similar to those above,* except that the vacuum level is 4×10^{-9} torr. This set has accumulated 2250 hours and shown a maximum torque value of 1.4 in.-lb. The average running torque is approximately 1.0 in.-lb.

These tests confirm the performance of the SNAP 8 bearing design and show that if the dry film is lost, which does occur to some degree by sublimation, the bearings function within design torque limits.

3. Gear Mockup Tests

The reference design for the SNAP 8 control-drum drive system specifies a pinion gear train to transmit actuator torque to the reflector drums.

In a space environment, the phenomenon of surface adhesion might occur where these "clean" surfaces are in contact under load and at elevated temperature. The nature of the adhesion can be by diffusion, chemical reaction of intermetallic formation, and/or mechanical interlock. Therefore, it is necessary to prevent the occurrence of these conditions, or if they should occur, the type of interface bond formed should be so weak that shearing can readily occur with a minimum of surface damage.

The approach to the solution of this problem has been to use known dry-film lubricants such as graphite, MoS_2, $MoSe_2$, and mixtures of these which are sodium-silicate bonded so that a low vapor pressure, low shear strength, surface-coating system is achieved.

A test program to evaluate the performance of specific dry-film lubricants at gear operating environments is in progress. In these tests, 300 series stainless-steel specimens, coated with the lubricant, slide against one another at 1150°F and 10^{-5} to 10^{-8} torr pressure. Normal load on the specimens is 40 psi. The test

*C. E. Johnson, "SNAP 8 Progress Report, February-April 1965," NAA-SR-11092 (CRD), June 15, 1965

procedure is to load the surfaces and initiate the vacuum pumpdown and the heatup. When the test environment is stabilized, the sliding action between the samples is initiated at a rate of 7 in./min over 0.5 in. travel. Approximately 70 in. of travel in 140 strokes are accumulated each hour. The total test time is approximately 150 hours.

Tests were conducted to determine the cause for high starting friction encountered when friction surfaces were heated to test temperature under load. Methods of reducing the high starting friction were sought. It had previously been established that an outgassing treatment and burnishing reduced the starting friction of MoS_2 + graphite-coated stainless steel.

Test 9US, MoS_2 + graphite-coated stainless steel vs MoS_2 + graphite-coated stainless steel, was given an outgassing cycle of two hours at 10^{-7} torr pressure and 1150°F. The test specimens were then cooled to room temperature, installed in the friction test system, and brought to 1150°F and 10^{-7} torr. The sliding could not be started automatically because the coefficient of friction was greater than 1 (due to limitations of the equipment). After manual initiation of sliding, the test operated successfully.

Test 10US, a similar combination except that only the slider was coated with MoS_2 + graphite, was next initiated. It also had to be started manually because the coefficient of starting friction exceeded 1, after which it operated satisfactorily.

A similar high starting friction condition was experienced in Tests 11US and 12US. Test 11US used a $MoSe_2$ dry film on both pieces and 12US used a modified MoS_2 + graphite on both pieces. Test 13US was prepared using MoS_2 + graphite coat on stainless-steel specimens. This sample was installed in the test rig and burnished by sliding the samples under load at room temperature in air for three minutes. The test specimens were then removed, blown clean with dry nitrogen, reinstalled, brought to 10^{-7} torr and 1150°F, and sliding initiated. The maximum value of both the starting and dynamic coefficients of friction was 0.45. These values decreased to the 0.3 to 0.4 range during the test.

Test 16GS, a similar system to 13US, was processed identically including the burnishing. The test conditions were also similar except that test pressure was 10^{-5} torr. It also exhibited a starting coefficient of friction of about 0.45 and a dynamic coefficient of 0.25 to 0.35 throughout the test.

From these tests, and from tests that were run earlier in the program, it is concluded that pre-test outgassing is not required but that burnishing of the dry-film lubricant will minimize high starting friction. Table 47 summarizes gear mockup tests performed during this reporting period.

A pattern of behavior was discovered from results of the tests of MoS_2 + graphite coating on stainless steel at 10^{-7} torr and 1150°F. The weight loss of the dry-film lubricant is dependent on the total sliding travel and independent of the test time. Approximately the same weight losses were recorded on two tests in which the same total sliding travel (~23,000 in.) were obtained in 210 hours and 785 hours.

Three 10,000-hour tests were initiated for design verification of the S8DS control-drum drive gear, consisting of Hiperco 27 sliding against Inconel-X, both surfaces coated with MoS_2 + graphite. Two of the tests have been discontinued due to vacuum system failure. Data for these tests as well as for the third test, which is continuing, are given in Table 48.

TABLE 47

DRY-FILM LUBRICANT EVALUATION TESTS

Test Number	Base Metal (SS)	Dry-Film Coating	Test Temperature (°F)	Test Pressure (torr)	Distance Traveled (in.)	Time at Test (hr)	Remarks
9US	316/316	MoS_2 + graphite	1150	1×10^{-7} to 7×10^{-7}	21,876	340	Samples outgassed before run, not burnished. Manual start necessary. Test terminated when coefficient of friction <1.
10US	316/303	MoS_2 + graphite	1150	9×10^{-7}	70	0.1	Only slider coated – not burnished. Manually started, test terminated due to stick-slip operation. 303 used unintentionally, not discovered until test completed.
11US	316/316	$MoSe_2$	1150	1×10^{-7}	0	71	Not burnished. Test could not be started due to excess friction.
12US	316/316	Modified MoS_2 + graphite	1150	2×10^{-8} to 8×10^{-7}		748	Automatic disconnect actuated, indicating coefficient of friction <1. No burnishing.
13US	316/316	MoS_2 + graphite	1150	2×10^{-8} to 9×10^{-8}	22,505	210	Coating burnished by sliding at room temperature. Sliding continued for 8-hr periods, large travel, minimum time.
11GS	316/316	$MoSe_2$	1150	1×10^{-5}	6,089	215	Burnished test, terminated when vacuum failed.
12GS	316/316	MoS_2 + graphite	1150	1×10^{-5}	10,100	170	Not burnished. Test had to be started manually. System cooled, exposed to air, evacuated and reheated. It then started automatically.
13GS	316/316	MoS_2 + graphite	1150	1×10^{-5}	34,020	552	Hand burnished. Test terminated when coefficient of friction exceeded 1.
16GS	316/316	MoS_2 + graphite	1150	1×10^{-5}	10,100	170	Burnished by operating at room temperature. Test discontinued after programmed cycle.

TABLE 48

DESIGN VERIFICATION TEST OF S8DS DRIVE GEAR LUBRICANT

Test Number	Base Material	Dry-Film Coating	Test Temperature (°F)	Test Pressure (torr)	Distance Traveled (in.)	Time at Test (hr)	Remarks
8R	Hiperco 27 / Inconel X	MoS_2 + graphite	1000	9×10^{-8} to 6×10^{-7}	146	3796	Hand burnished. Test aborted due to vacuum failure.
9R	Hiperco 27 / Inconel X	MoS_2 + graphite	1000	2×10^{-8} to 8×10^{-8}	180	4647	Hand burnished. Test aborted due to vacuum failure.
10R	Hiperco 27 / Inconel X	MoS_2 + graphite	1000	4×10^{-8}	198	4761	Hand burnished. Test continuing.

Metallographic examination of the samples is underway and to date, it has been established that a surface reaction at the interface did occur in the Inconel-X, but not with the Hiperco 27. This is being further investigated.

E. SENSORS AND INSTRUMENTATION

1. Instrumentation

a. Drum Position-Sensing System

The drum position-sensing system measures the reactor control-drum angular position and provides an output signal for diagnostic purposes. The desired system accuracy is ±1% of full scale. Since the sensor is mounted on the reflector assembly, it must be capable of operating in the reactor environment throughout the 10,000-hour life of the nuclear system.

(1) Transmitter

A rotary variable-reluctance (differential transformer) type of sensor is being developed for this application. The stator contains one primary and two secondary windings. The magnetic sensor rotor is shaped so that the coupling to one secondary winding, hence its output voltage, is at a maximum when the output voltage from the other secondary winding is at a minimum. The demodulator is designed in such a manner that the output voltages are added in series-bucking, changing polarity at the center of the range of rotation.

Fabrication and pre-irradiation testing was completed on two sensors (SN 006 and SN 008). These two sensors will be operated in a high temperature-vacuum-radiation environment (HF-10 capsule).

Insulation resistance of the two sensors was somewhat higher than that of the first two. The lowest resistance-to-ground, measured at 800°F in vacuum, was 200 megohms. Shaft torque was 0.7 oz-in. and was not affected by the thermal vacuum cycling. Limited measurements of sensor output vs shaft angle were made. The general characteristics were very similar to those shown in the previous progress report* for sensor SN 2702, including the temperature sensitivity associated with one stator pole. The sensitivity to temperature of one pole is equivalent to 10° of arc over the range of 100 to 800°F. The output associated with the other stator pole has practically no change over the temperature range. Tests have been initiated on other sensors to pinpoint the cause for this unsymmetrical temperature sensitivity. The output change vs temperature is repeatable, hence may be accounted for by calibration at operating temperature.

The design of a spring-loaded shaft side loading device was completed. This device is designed to improve the ability of the sensor to measure small motion (~6 minutes of arc), a requirement for the precision drum-position indicating system.

The critical bearing assembly process was perfected during fabrication of sensors SN 006 and SN 008, and was used on the remaining six sensors which are in various stages of fabrication and assembly. The amount of interference between the graphite bushing OD and the retainer ID was modified when difficulties were encountered during the shrink-fitting process. The tolerances on the bearing parts had to be held to ±0.0002 in. Special gages were developed to measure graphite bearing dimensions to the required tolerances. Improved methods of assuring proper alignment and seating during shrink-fitting were developed. Since the bearing shrink-fitting process requires that the retainers

*C. E. Johnson, "SNAP 8 Progress Report, February-April 1965," NAA-SR-11092 (CRD), June 15, 1965

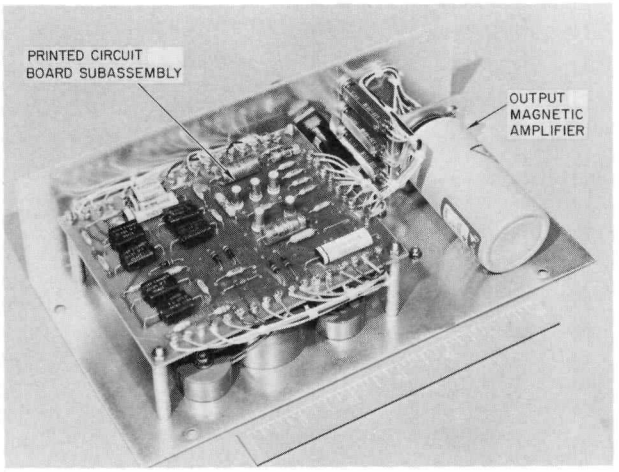

7-21-65 7568-551460A

Figure 67. Internal Construction of S8DS Prototype Demodulator

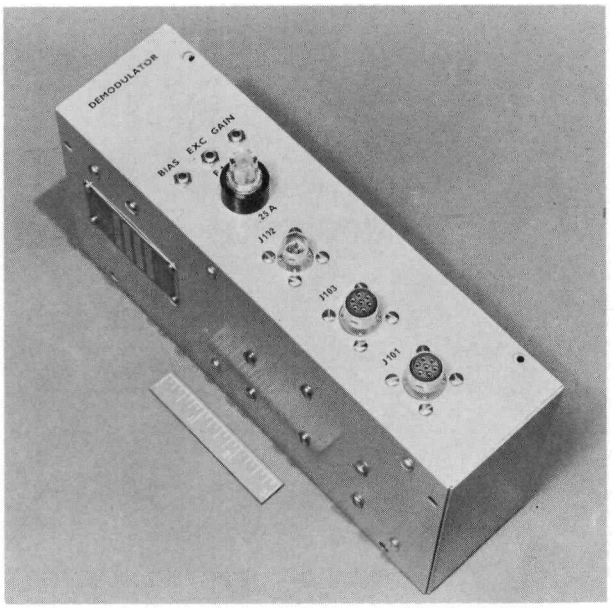

5-6-65 7568-551446

Figure 68. S8DS Prototype Demodulator, Packaged Unit

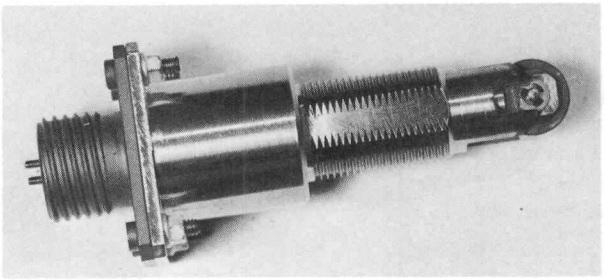

6-8-65 7568-551462CN

Figure 69. S8DS Shorting-Bar Limit Switch

be heated to 1300°F prior to inserting the graphite bearings, the process must be carried out in an inert atmosphere. Drybox procedures and equipment were perfected; e.g., dependable oxygen removal and oxygen warning devices.

(2) Demodulator

Two development demodulators of the S8DS design were assembled for use with the sensors to be tested in the HF-10 irradiation capsule. The S8DS design is electrically identical to the prototype* but differs mechanically as follows: (1) The package dimensions and mounting provisions were modified for compatibility with the S8DS system instrumentation installation. (2) Internal circuitry utilizes a printed circuit board for most connections, instead of round wire. (3) Leads were brought out from the regulator output to the sensor primary and from the demodulator output ahead of the filter to provide signals to be used in the S8DS step counting and verification system (see Section V-E-2 below). Figures 67 and 68 are photographs of an S8DS demodulator.

The HF-10 sensor-demodulator systems were calibrated and then subjected to various tests. Typical results are listed below:

Linearity	±2%
Line regulation with ±5% input variation	0.2%
Short-time output stability	1 millivolt
Long-term repeatability (4 days), maximum deviation from mean output	10 millivolts (0.2% full scale)

Assembly of subcomponent parts on the printed circuit boards for nine S8DS demodulator units has been started.

b. Limit Switch

Static thermal-vacuum tests continued on four developmental model shorting-bar switches. Three units have now accumulated 4300 hours at 1000°F and 10^{-6} torr and 140 thermal cycles (300 to 1000°F at 6°F/min) during an additional 1700 hours for a total of 6000 hours of environmental testing. At the end of 4200 hours at 1000°F and 50 thermal cycles (total hours, 4900) these switches were removed from the vacuum-furnace and calibrated for the third time. No measurable changes were found in switch point or force vs plunger travel (spring) characteristics.

Two switches of the S8DS design were assembled, calibrated, and subjected to 5 thermal cycles and 50 hours at 1000°F in vacuum. A photograph of an assembled switch is shown in Figure 69. These switches will be operationally tested for 2200 hours in the S8DS vacuum-irradiation-temperature environment (HF-10).

The basic differences between the S8DS design and the developmental model switch have been described previously.* Additional modifications have been incorporated, consisting of: (1) a change in the method of staking the movable contact adjusting nut from a heliarc weld to a percussive arc weld and (2) a change in the material of the snap ring which maintains pre-load on the overtravel spring, for better compatibility with the operating temperature.

Improvements have also been made in assembly procedures, including (1) development of an optical comparator method of ensuring alignment of the graphite contact face and contact holder before the adjusting nut is tightened and (2) addition of a wear-in procedure, to remove excess dry-film lubricant inside the switch barrel, consisting of 25 manual operations of the switch followed by air-cleaning.

*C. E. Johnson, "SNAP 8 Progress Report, February-April 1965," NAA-SR-11092 (CRD), June 15, 1965

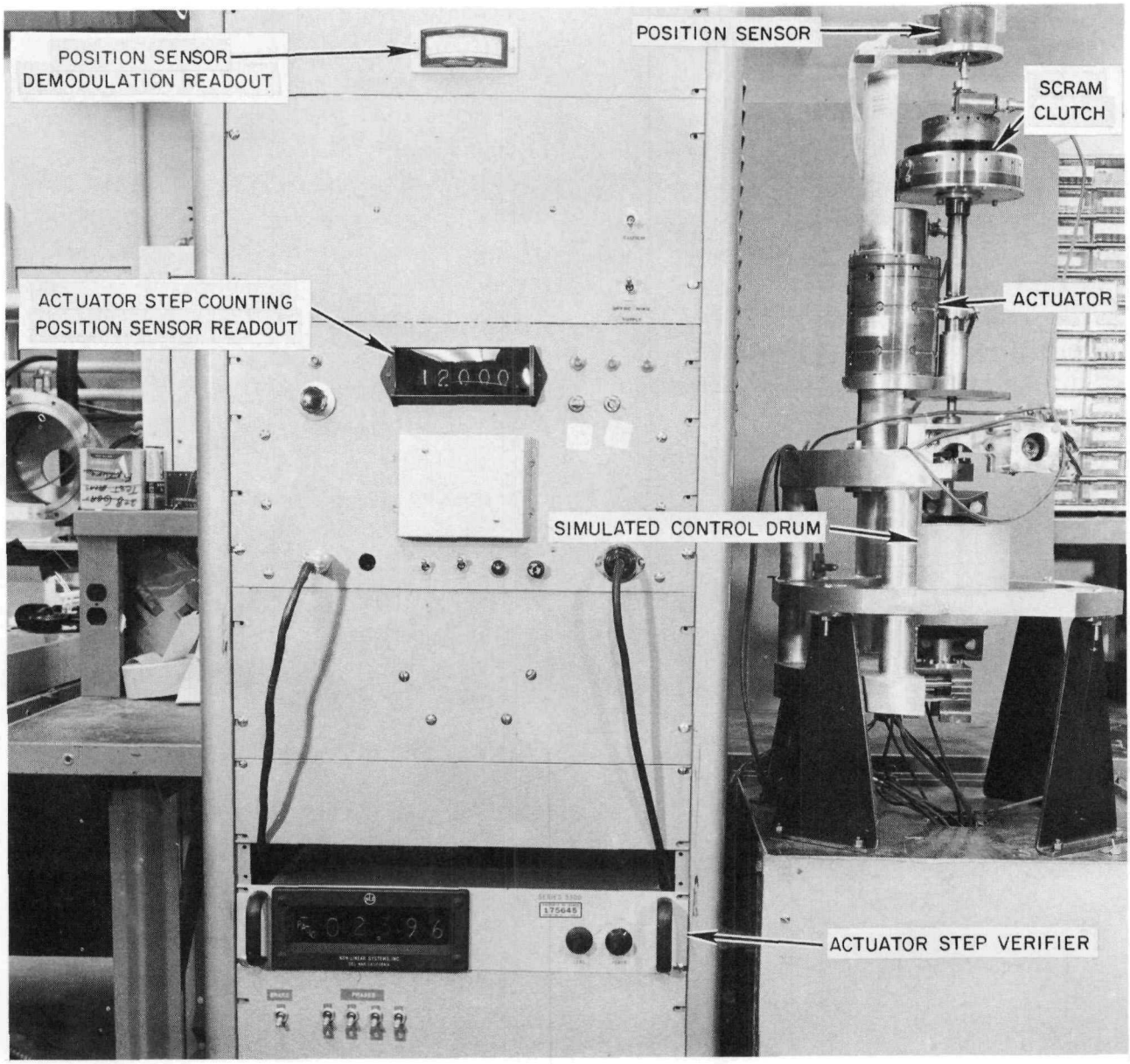

7-20-65

7568-551525A

Figure 70. Actuator Step-Counting and Verifying System Used During System Tests with S8DS Developmental Scram Kit

The S8DS design switches were found to exhibit higher contact resistance (~15 ohms) than the developmental switches (~2 ohms), apparently due to surface oxidation of the fixed contacts. Since the circuits in which they are used are of relatively high impedance, proper operation is expected. Also, a wear-in effect was observed in that the lower value of resistance was obtained after 100 operations of switching a 25-ma, d-c inductive load.

2. Precision Position Sensor

The S8DS system requires six precision drum-position-sensing channels for use in reactor experiments to be conducted throughout the reactor test. System accuracy of ±0.1° is desired.

The step counting and verifying system* utilizes a position sensor demodulator, and digital voltmeter to verify drum motion when the actuator is pulsed by the controller, and to provide a digital display of position by counting these steps.

Assembly of the prototype system was completed. Bench checkout of the electronics portion was completed, and system tests (using the developmental scram kit to simulate the control-drum drive system) were initiated. Time response measurements were made on the electronics portion and on the complete system.

Results of these tests indicated that the time response of the system is too slow to allow verification and counting of individual 0.13-degree steps. This would have to be accomplished in 400 milliseconds, the shortest time between steps for both the automatic and manual controllers. Also, the signal-to-noise ratio for minimum drum rotation for a single step (0.03°) was found to be marginal.

Good results were obtained in verifying and counting two-step groups (0.26° nominal per operation), such as are generated by the S8DS automatic controller. The system verified and counted 385 unidirectional two-step groups with only one error, and 47 groups at reversal of direction with no error. Figure 70 is a photograph of the step counting and verification system prototype and the S8DS developmental scram kit.

F. CONTROLS

1. Controller

The reactor controller is required to provide properly sequenced outputs to three control-drum actuators which in turn, control the reactivity of the reactor. The direction, rate, and order of control-drum rotation is controlled by the state of the input signals to the controller. The design goal for the controller is a minimum of 10,000 hours operation over which it will receive a significant total integrated radiation dosage. The primary purpose of this program is the development of a controller of reliable performance under these conditions.

The design approach selected utilized magnetic core-transistor circuitry. Five basic modules are required: a logic module, shift driver, oscillator, relay driver, and relay. The magnetic approach permits a reduction of greater than 50% in semiconductor devices as compared to an all-transistor approach. This is a very significant factor in increasing the overall reliability of the controller.

a. Prototype Controller

A modular core-transistor logic assembly was designed and constructed for use in an irradiation test. This assembly consists of an oscillator, a shift current driver, sixteen logic

*C. E. Johnson, "SNAP 8 Progress Report, November 1964-January 1965," NAA-SR-10792 (CRD), March 15, 1965

modules, seven relay drivers, and eight relays. The oscillator and six logic modules connected as binaries form a time base generator which every 5 seconds pulses a phase sequencer consisting of ten logic modules and seven relay drivers. This subassembly is capable of controlling one actuator and demonstrates all of the basic performance functions of a complete controller. The block diagram for this assembly is shown in Figure 71.

This assembly was irradiated in the AI shield test and irradiation reactor to approximately 4.4×10^{14} nvt, total dose. Only preliminary dosimetry and performance information is available at this time. The entire assembly operated satisfactorily up to 5×10^{13} nvt total dose. At the end of the test only the oscillator remained operative.

A laboratory test controller was constructed to check the operation of the reference design. Successful operation was achieved utilizing reference design packaged radiation-hardened modules, radiation-hardened relays, and printed circuit board interconnections.

The reliability test breadboard core-transistor logic assembly has operated without failure for 6500 hours. The purpose of this test is to obtain component performance data under actual operating conditions. There are seven of the basic core-transistor-logic modules in this assembly so that over 45,000 module-hours have been accrued without failure.

b. S8DS Controller

The S8DS controller is a nonflight, rack-mounted unit designed primarily for use in the S8DS system test. The unit provides four discrete stepping rates, three of which are variable over a wide range. The unit provides visual status information and a variable setpoint capability which is used to vary the point at which stepping rate changes are made. Manual rate

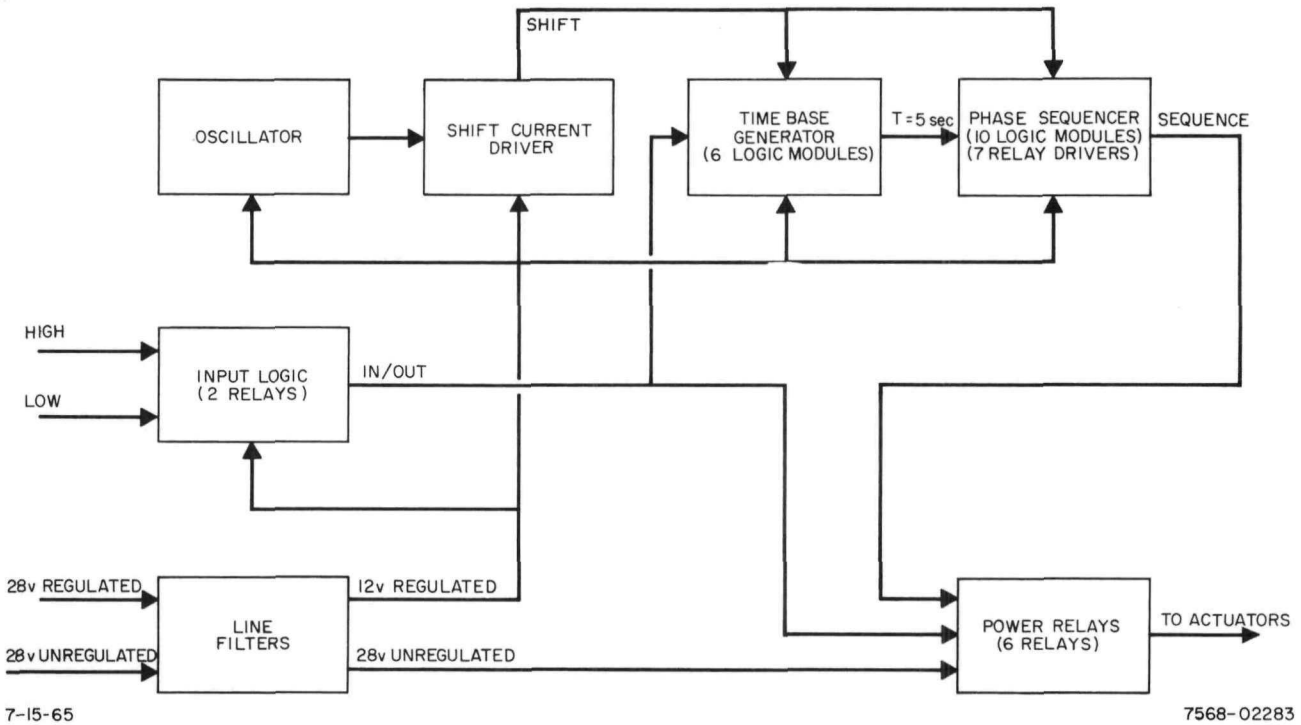

Figure 71. Modular Core-Transistor Logic Assembly Block Diagram

selection and manual overrides are included where required. This controller will be used to study and determine the optimum reactor startup cycle. The results from this study will provide the final performance requirements for a reference design.

Fabrication of this controller was completed. Final checkout has been initiated and minor corrections are being made as necessary to complete the acceptance test.

2. Temperature Detector

The temperature detector provides voltage signals to the temperature switch which are proportional to the reactor outlet coolant temperature. The detector, in conjunction with the switch, establishes the limits of the reactor deadband and commands the controller to drive the drums whenever the outlet coolant temperature passes outside this deadband.

a. Reference Design

The reference design is a platinum resistance temperature detector (RTD) which forms one leg of a three-wire Siemens bridge. As the resistance of the detector changes with temperature, the output of the bridge to the control winding of a high-gain magnetic amplifier in the switch varies accordingly. The bridge is adjusted to null at that detector resistance corresponding to the temperature at the middle of the deadband.

Thermal testing at 1300°F of evaluation RTD's continued. These detectors are continuously maintained at 1300°F to simulate long-term operating conditions. They are checked for drift every 500 hours by calibration in a triple point cell (0.01°C) utilizing precision laboratory resistance measuring techniques. Accuracy of this calibration converted to equivalent temperature at 1300°F is ±0.2°F. Five detectors out of an original 25 remain with acceptable limits (-4°F shift in 10,000 hours). Their drift in terms of equivalent setpoint shift is shown in Figure 72. All data is referenced to zero after an initial 1000-hour stabilizing period. This stabilization will be performed on all units prior to acceptance. Prototype detectors being procured are similar in design to the RTD's evaluated in these tests. RTD No. 6 exhibited a large decrease in resistance at 6500 hours and was removed from test. RTD No. 3 was previously damaged during handling.* RTD's No. 3 and No. 6 are shown for reference only.

Three prototype S8DS detectors were received and placed on long-term drift testing at 1335°F in air. Calibration procedures are as above. Approximately 500 hours of the initial 1000-hour stability test have been accumulated.

S8DS detectors are entering design verification testing which includes a 1000-hour stability test prior to acceptance and delivery.

The temperature detector NaK test loop was filled and preliminary operation at 1000°F established. The loop was flushed until plugging runs indicated that a purity of less than 50 ppm had been attained. The loop was then moved to the laboratory and hookup to utilities initiated. This loop will be used for thermal cycling and vacuum endurance tests of detectors.

b. Backup Design

The backup design is a thermocouple sensor which also operates into a high gain magnetic amplifier-switch. In addition, this design requires a reference potential source and an associated highly regulated, low voltage supply.

No effort was expended on this task and it has been deleted for GFY 1966.

*C. E. Johnson, "SNAP 8 Progress Report, February-April 1965," NAA-SR-11092 (CRD), June 15, 1965

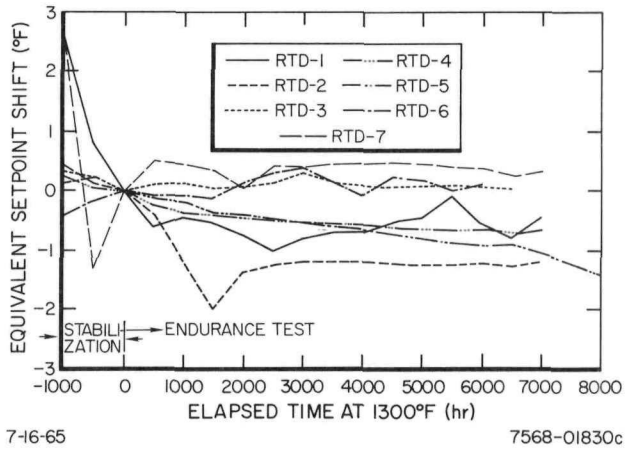

Figure 72. Resistance Temperature Detector Drift Data

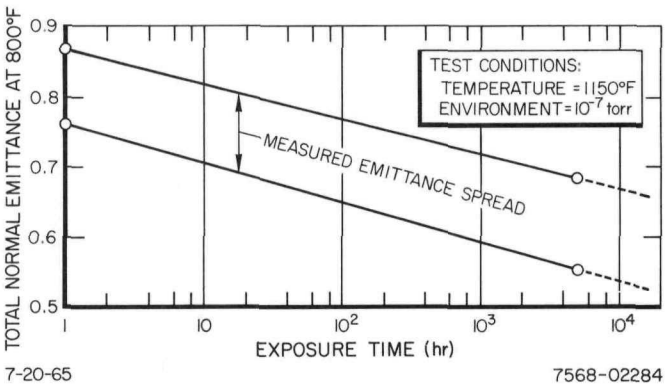

Figure 73. Anodized Beryllium Emittance Characteristics

TABLE 49

RESULTS OF LONG-TERM TESTS ON EMITTANCE COATINGS ON BERYLLIUM*

Number of Samples	Type of Coating	Initial Emittance	Total Test Time, (hr)	Final Emittance
10	Anodized Beryllium	0.76 to 0.87	5000	0.55 to 0.68
5	Anodized Beryllium	-	2000	0.53 to 0.58
3	Bare-Natural Tarnish only	0.15 to 0.23	2000	0.12 to 0.13
3	Fused Silicon Beryllium	0.63 to 0.84	3000	0.70 to 0.84
4	Graded, Plasma-Sprayed Chromium Oxide	0.88 to 0.90	2000	0.89 to 0.90

*Total normal emittance measured at 800°F.

3. Temperature Switch

The temperature switch receives the output from the RTD's and provides signals to the controller whenever the reactor outlet coolant temperature passes outside the deadband limits as defined by two preset points.

Two prototype S8DS switches were constructed and performance tested to confirm the design. Operation was within specification limits.

Procurement of parts for the S8DS switches is well underway. Preliminary acceptance tests were conducted on the first set of vendor-wound magnetic amplifiers prior to approval for final production.

G. MATERIALS

1. Environmental Testing

The objective of this study is the evaluation of coatings for the SNAP 8 beryllium neutron reflectors which will provide high infrared radiation emittance over long periods in high vacuum. The performance of several types of coatings is being tested by means of a long-term environmental test operated at 1150°F and 10^{-7} torr pressure. Emittance of coatings on beryllium samples has been measured periodically during the course of the test period. The test was terminated after 5000-hours exposure on the anodized beryllium samples.

A total of 25 beryllium samples was included in the environmental testing. The results are shown in Table 49. These data (also shown on Figure 73) indicate that the emittance of the anodized beryllium (the S8DS reference coating for the beryllium reflectors) degrades below acceptable values with high-temperature use. Under the above conditions, in 10,000 hours the minimum emittance is expected to degrade to less than 0.55 from an initial average of 0.82. Under current S8DS operating conditions, an emittance of 0.8 would result in beryllium temperatures of 1300°F, whereas an emittance of 0.5 would result in a temperature of 1400°F. Substitutes for the anodized coating are being investigated to find a coating of higher emittance which will not degrade with use.

2. S8DS Reflector Shim Coating

A review of possible alternates to the anodized coating was conducted. Two of the coatings evaluated were considered to be suitable candidates and additional testing and evaluation has begun. Both of these coatings have emittances better than 0.85 and appear to be stable. The two coatings are (1) the plasma-sprayed, three-phase, graded chromium-oxide coating which was used on the SNAP 10A reflector shims, but at much lower temperatures (~700°F), and (2) the aluminum-phosphate, chromium-nickel-cobalt oxide spinel, known as AI-90, which has received about 5000 hours of testing at 1450°F.

3. Post-Test Evaluation of Anodized Beryllium Samples Tested at 1300°F in Helium

Ten samples of anodized beryllium were exposed in an environmental test at 1300°F in a helium atmosphere containing 100 ppm oxygen and with a dew-point of less than -40°F. Five of these samples were exposed for 5709 hours and the other five for 3169 hours. This test was originally planned to evaluate the anodized coating performance under the S8ER operational conditions. The purpose of the coating on the S8ER reflector was to provide both oxidation protection of the beryllium and high emittance. The coating on these samples is being carefully examined to learn the mode of degradation of anodized coatings. Metallographic examinations are being made on both damaged and undamaged sections of the anodized coating. The emittance of the coating is about 16% lower than expected on the basis of the results from the

environmental testing discussed above. The more rapid degradation in tests is believed to be the result of slow oxidation from the 100 ppm oxygen in the test.

Table 50 summarizes the test data.

TABLE 50
EMITTANCE OF ANODIZED BERYLLIUM*

Number of Samples	Test Time (hr)	Emittance (at 800°F)	Emittance (at 1100°F)
5	3169	0.509	0.524
5	5709	0.525	0.535

*Tested at 1300°F, 100 ppm O_2, -40°F dew point.

H. SAFETY COMPONENTS

The electrically actuated band release device (EABRD) is a versatile electrically fired fusible link release actuator applicable to many reactor shutdown situations such as destruct charge shell release, reflector ejection, etc. Separation is accomplished by raising the temperature of the tubular structural housing with an internal helical resistance heater until the tube wall strength is exceeded by the tensile load applied to the housing.

Development of the EABRD has proceeded along several concurrent paths concerned with both the structural problems and the electrical energy restrictions.

1. Housing

Tensile tests and creep-rupture tests have been conducted to optimize the structural configuration and to establish design parameters to facilitate the sizing of actuators for a variety of uses. Tests have indicated that the short-term yield strength of the thin-walled (0.012-in.) tubular housings at 900°F is well below the long-term creep-rupture strength and should be utilized for design purposes.

2. Heater

Heater configuration and power density studies were initiated. Bobbins were fabricated to accommodate a number of variations in wire size, number of turns, and turn spacing. Ten heaters were assembled and are ready for test.

3. Assembly Test

Two EABRD assemblies (0.012-in. wall housing) were subjected to shock and vibration at the SNAP 8 component qualification test levels (35 g shock and 19 g maximum vibration). No external physical damage was observed and electrical resistance reading indicated no change in circuit continuity or insulation resistance degradation. Subsequently, performance tests showed the separation times and energy requirements agreed with test data from similar EABRDs not subjected to the launch loads. One EABRD heater bobbin parted on separation which might indicate that the bobbin was weakened or cracked during the shock and vibration sweeps. This condition will be investigated further.

I. SHIELD

1. Summary

The examination of the structural mockup (No. 1) was completed. Some buckling of the support legs and cracking in the legs near the perforation were noted and are attributed to tension loading during shock and vibration. These cracks did not, however, cause internal catastrophic failure during testing. The rib test specimen was destructively analyzed and showed an internal structure superior to previous shields as a result of using a criss-cross type of honeycomb matrix. The No. 3 mockup, a steel wool stabilizer and aggregate casting to evaluate pipe pass-through, was completed.

The reference tests to be used in evaluating thermal conductivity of insulation materials

were initiated. A test was assembled to determine the hydriding rates of lithium metal as a function of time, temperature, and surface area.

A 2000-hour test, to evaluate a brazing alloy as to compatibility with 1300°F lithium hydride (LiH), is in progress. Interaction tests between Li and LiH at 600, 900, and 1200°F for 4000 hours are in progress and another interaction test of 2000 hours duration at these conditions is reported below.

Tests were also run to evaluate the use of titanium as a container or coating of a container during casting of LiH to effect release from the container walls when the LiH is solidified. The initial tests gave very encouraging results.

2. Shield Structural Mockup No. 1*

Post-test examination of Mockup No. 1, was completed. The entire operation was conducted in the large shield examination drybox facility. After cleavage of the block of lithium hydride and removal of one support leg, as previously described,† the support leg was washed clean of lithium hydride and examined for damage. Partial buckling and flattening of the leg was observed on the side opposite the Z-ring, shown in Figure 74. Closer examination revealed cracks originating at the perforations in the leg. Figure 75 shows a close-up of a typical crack. These cracks are believed to be tension-induced fatigue cracks produced during vibration testing.

The remaining half of the block was washed clean of lithium hydride and it was found that the middle leg (No. 5 of Figure 76), 90° from the leg shown in Figure 74, had also suffered severe cracking at the perforations. The locations of these two legs coincided with the lateral planes in which the specimen had been vibration tested. Complete evaluation and reporting of test results is currently in progress.

3. Rib Test Specimen

The rib test specimen was fabricated to study the effect of rib thickness on bonding between the cast lithium hydride block and the internal ribs, to evaluate the use of the criss-cross matrix as a crack-controlling medium, and to study the effect of a casting cycle on the titanium dioxide porcelain enamel high emissivity coating.

Postcasting x-rays, including lateral views and end-on views, show the specimen to be free of large internal cracks and lacking in the centerline low-density area, which is characteristic of the unidirectional honeycomb matrix and the steel-wool matrix castings. The criss-cross matrix differs from the unidirectional honeycomb in that alternating layers of the matrix are rotated 90°, giving two-directional stability. The test assembly was subjected to two thermal cycles from room temperature to 1000°F. The temperature vs time data are being analyzed to determine the bulk thermal conductivity of the lithium hydride block. A void volume test was run on the rib test can showing 0.0673 ft^3 of void volume and a bulk density of 93.7%, which is in excellent agreement with the bulk density average of 93.9% ±1.1% for all previous shields cast.

Visual examination of the titanium dioxide coating after casting showed good adherence and darkening of the coating. Skin specimens were removed during postmortem examination and emissivity determinations are being made.

*C. E. Johnson, "SNAP 8 Quarterly Progress Report May-July 1964," NAA-SR-9992 (SRD), September 22, 1964
†C. E. Johnson, "SNAP 8 Progress Report, February-April 1965," NAA-SR-11092 (CRD), June 15, 1965

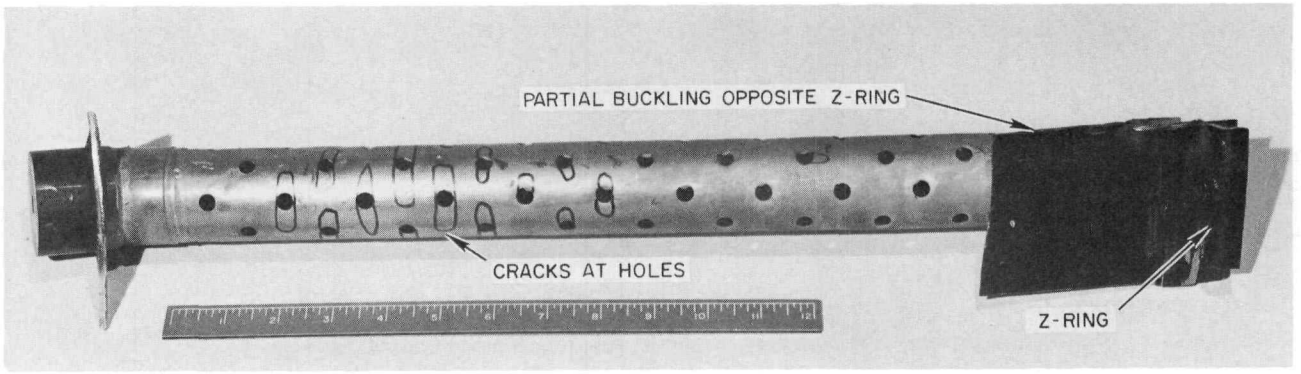

3-26-65 7568-551377A

Figure 74. Support Leg Removed and Cleaned of Lithium Hydride. Cracks are circled in black.

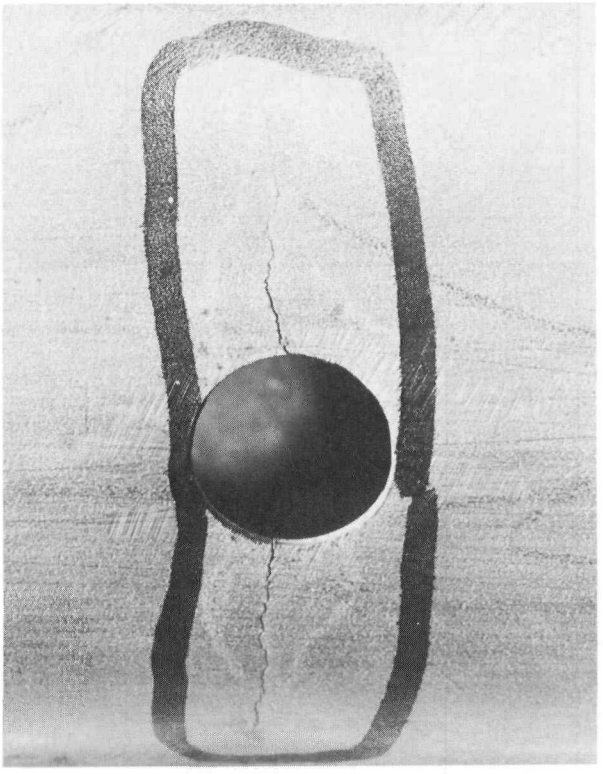

3-26-65 7568-551378

Figure 75. Closeup of Crack at Perforation in Leg

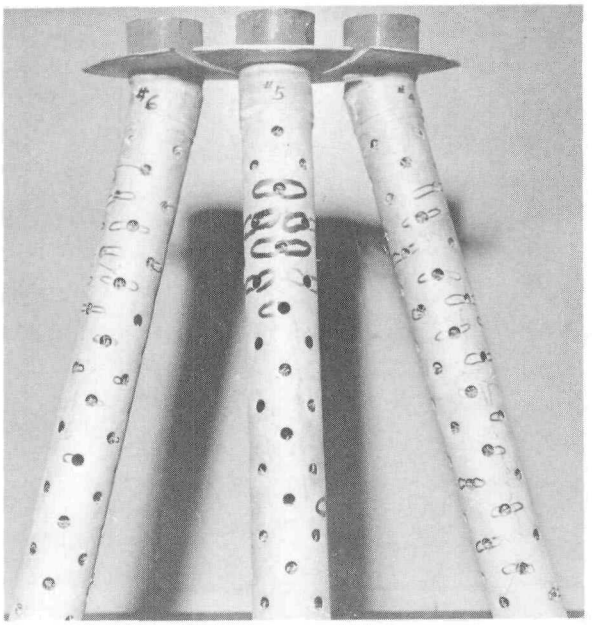

5-4-65 7568-56441

Figure 76. Trio of Support Legs Removed from Mockup No. 1, Showing Fatigue Cracks

The test assembly was dissected to allow visual evaluation of lithium-to-rib bonding, rib-to-casing-weld bonding, and performance of the criss-cross matrix. Examination of the hydride block (Figure 77), after removal of the can head and several vertical strips of casing, revealed extremely large LiH crystals throughout the entire block. The large crystals are due to a slow cooling rate during the casting cycle and result in poor bonding and low material strength. Large cracks along the crystal boundaries are also shown throughout the block.

Rib thicknesses studied were 0.005, 0.010, 0.015, and 0.020 in. The can contained two ribs of each thickness, 180° apart. One rib of each thickness was removed by making two vertical cuts, resulting in a pie-shaped piece of hydride surrounding each rib (Figure 78). Several light blows with a small hammer fractured the hydride completely and broke it loose along the full length of each rib. The low strength of the hydride was probably due to the large crystals and no quantitative analysis of bonding between the ribs and the hydride could be made nor could a relation between rib thickness and bonding be made.

After removal of the LiH from the ribs (Figure 79), visual examination of the ribs and the rib-to-can welds was made. Extensive warpage of the ribs was noted and the thinner ribs showed greater warpage than the thicker ones. No correlation between hydride bonding strength and warpage could be drawn. The tab welds between the ribs and the can showed excellent bonding and no indication of corrosion from the molten LiH during casting. Pull tests, to obtain quantitative values for weld joints strength, will be performed.

After removal of the four ribs from the test can, the LiH in the remaining portion of the can was washed out to enable visual inspection of the intact can and matrix assembly. The matrix showed some warpage, but had withstood the casting cycle without loss of shape and without loss of the spot-weld joints between layers of the matrix.

Evaluation of the criss-cross matrix was hampered by the presence of large crystals, but use of the matrix was highly successful in eliminating the centerline low-density area and the large cracks present in previous shields. Mechanical bonding of the matrix layers was excellent.

4. Shield Mockup No. 3

This mockup is designed to establish the feasibility of internal NaK lines and of casting a layer of tungsten aggregate within the lithium hydride.

The shield assembly was completed except for the actual casting of the lithium hydride. Figures 80 and 81 show the test shield in the final stages of assembly prior to welding on of the upper head. Figure 80 shows the layer of granular W – 2 wt % Mo alloy gamma shielding prior to covering with a layer of stainless-steel screen and stainless-steel wool mesh (Figure 81).

5. NaK Pipe Insulation Tests

As part of advanced shielding concepts the proposal to pass high-temperature fluids through the neutron shield raises the problem of heat transfer from the fluids to the lithium hydride and possibly raising the temperature of the LiH above its melting point. The NaK pipe insulation test was initiated to study superinsulation materials in high vacuum with a 1300°F heat source simulating a NaK flow.

A test assembly to evaluate insulation material was designed and fabricated. The test capsule consists of a 1-in. diameter x 10-in. long copper core, with hemispherical ends and an internal 50-watt heater. The core is surrounded with a 1/4-in.-thick wall copper jacket of 3 in. ID. The insulation material to be studied is

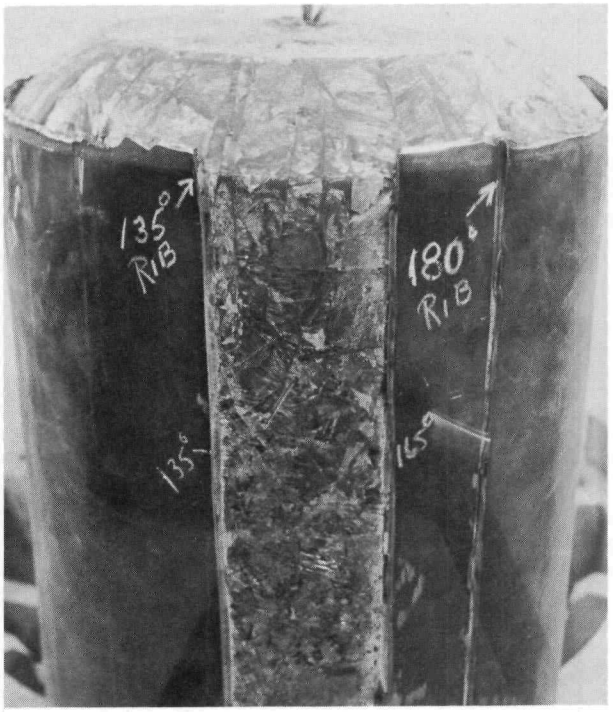

5-5-65 7568-56445

Figure 77. Rib Test Specimen – Head and Portion of Wall Removed to Show Lithium Hydride Crystal Structure

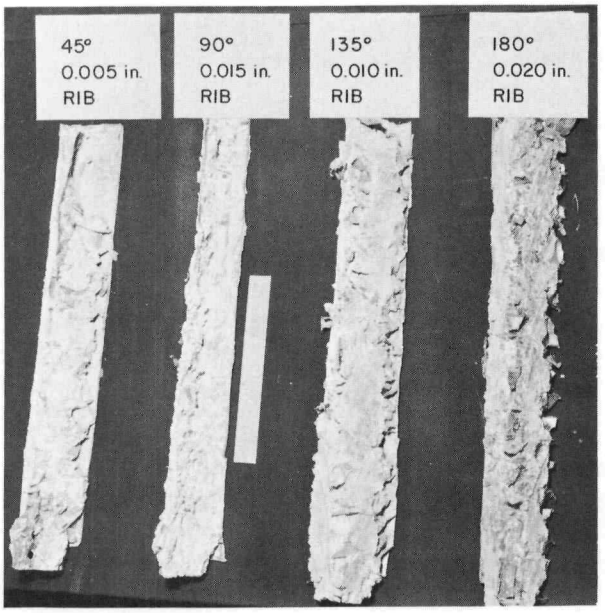

6-10-65 7568-56467A

Figure 78. Ribs Removed From Rib Test Specimen for Evaluation of LiH-to-Rib Bonding Strength

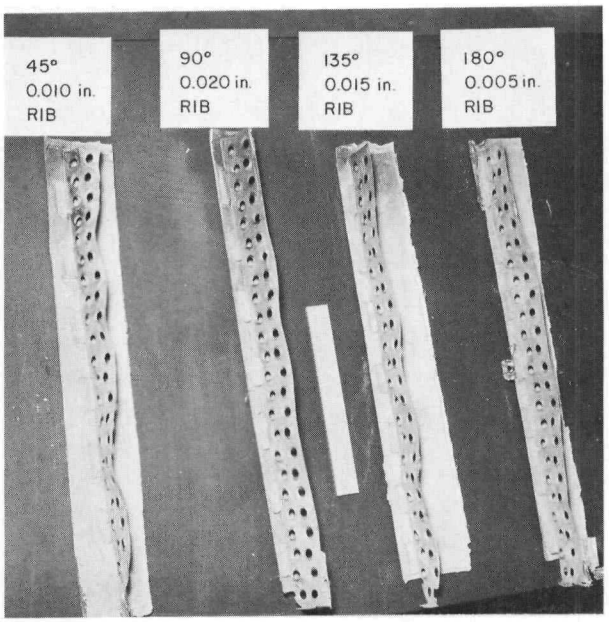

6-10-65 7568-56472A

Figure 79. Rib Removed From Rib Test Specimen Showing Warpage of Rib and Rib Tab-to-Can Bonding

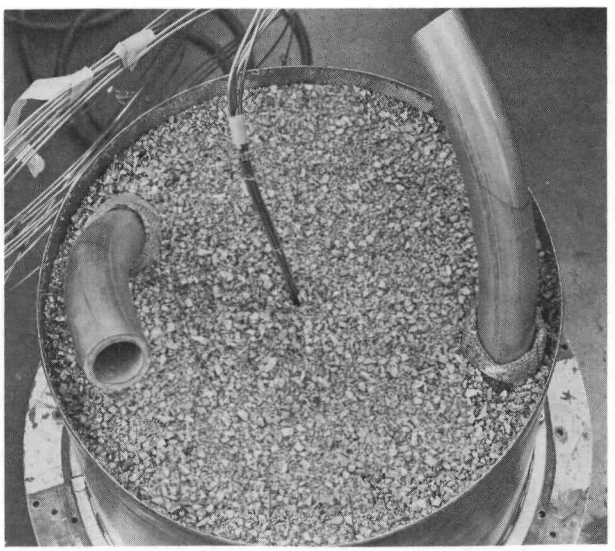

5-14-65 7568-56450

Figure 80. Mockup No. 3 Test Specimen with W– 2 wt % Mo Alloy Installed

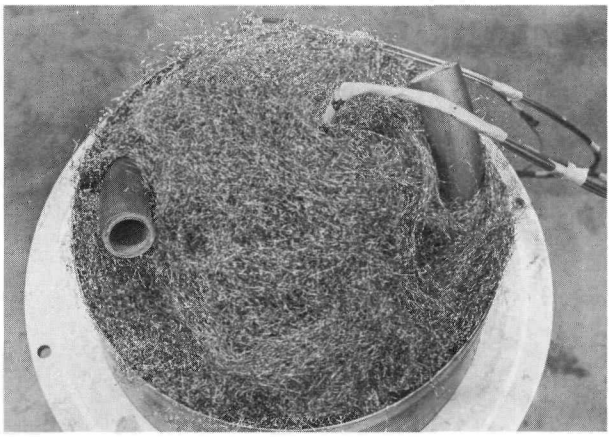

5-18-65 7568-56452

Figure 81. Mockup No. 3 Test Specimen Stainless-Steel Wool Mesh Prior to Welding of Upper Head

placed between the core and jacket. Chromel-alumel thermocouples, 0.003 and 0.005 in. diameter, are embedded at the ends and center of the jacket and core walls. The assembly is placed in an ion pump system and, after complete outgassing, a steady-state temperature difference is established between the core and jacket. The thermal conductivity of the insulation is then calculated on the basis of the temperature difference and the power input required to maintain the temperature difference. As a check, the thermal conductivity is recalculated, based on the time vs temperature decay curve, when the core heater is turned off and the centerline temperature allowed to reach equilibrium with the jacket temperature. A series of insulations are to be studied. An insulation tape with a known thermal conductivity is being used for system checkout. The tape was wrapped around the core until a snug fit with the jacket was obtained. The assembled test apparatus (Figure 82) was sealed in the ion pumped vacuum test chamber and outgassing was started with the core temperature at 1300°F and the

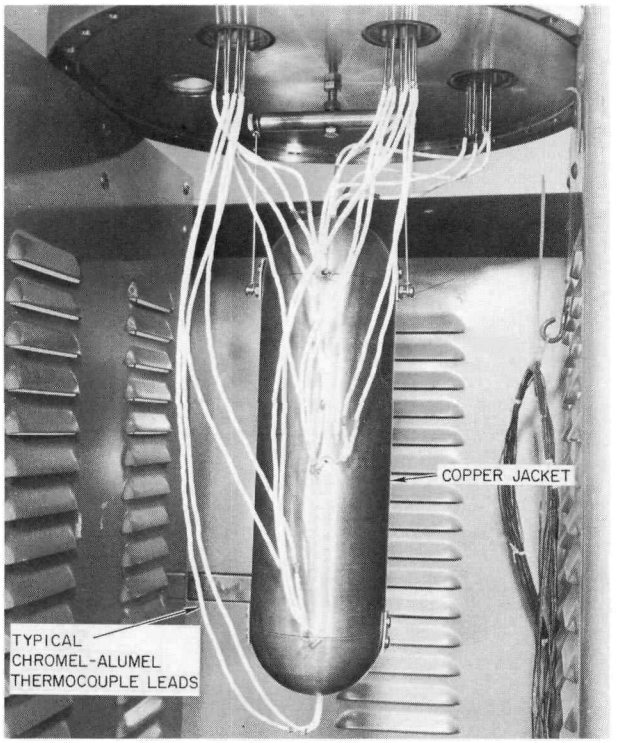

4-22-65 7568-4026

Figure 82. Insulation Test Apparatus

jacket temperature at 290°F. The system is operating under a vacuum of 5×10^{-8} torr. The test run will begin when outgassing is completed.

6. Lithium Hydriding Tests

A series of tests to determine the effective rate of hydriding lithium metal as a function of temperature, surface area, and hydrogen overpressure has been initiated in the Ainsworth vacuum balance system.*

The balance system was modified for the tests by addition of a new specimen suspension thermocouple and baffle plates and the incorporation of a pressure regulation system. The system will be capable of studying samples at temperatures up to 1400°F, pressures at 2 atm abs., and surface areas to 10 in.

*C. E. Johnson, "SNAP 8 Progress Report, November 1964-January 1965," NAA-SR-10792 (CRD), March 15, 1965, Figure 86, p 126

TABLE 51

OBSERVATIONS ON THE INTERACTION OF LITHIUM AND LITHIUM HYDRIDE

Temperature (°F)	Observations			
	500 hr	1000 hr	2000 hr	4000 hr
600	Li metal had drained clean when capsule was inverted at 600°F. LiH appeared unchanged although stuck to capsule.	Li metal drained from LiH sample. Apparently no change in the LiH pellet.	Li did not drain from Li H sample at 600°F.	In progress.
900	Li did not drain from LiH sample when inverted at 900°F. Surface of LiH appeared unchanged.	Same as 500-hour test although capsule was kept inverted at 600°F for 3 days.	Capsule leaked air — apparently corrosion of pinch-off tube at edge of lower pinch. The walls of the capsule were coated with a 1/8-in.-thick layer of hard material.	In progress.
1200	The Li-LiH apparently interacted to form a liquid which flowed when the capsule was inverted and drained at 1200°F.	The Li did not drain when inverted at 600°F. LiH sample completely interacted except for a small trace adhering to the capsule walls.	Only small flecks of LiH could be found in the Li matrix material. Did not drain at 600°F.	In progress.

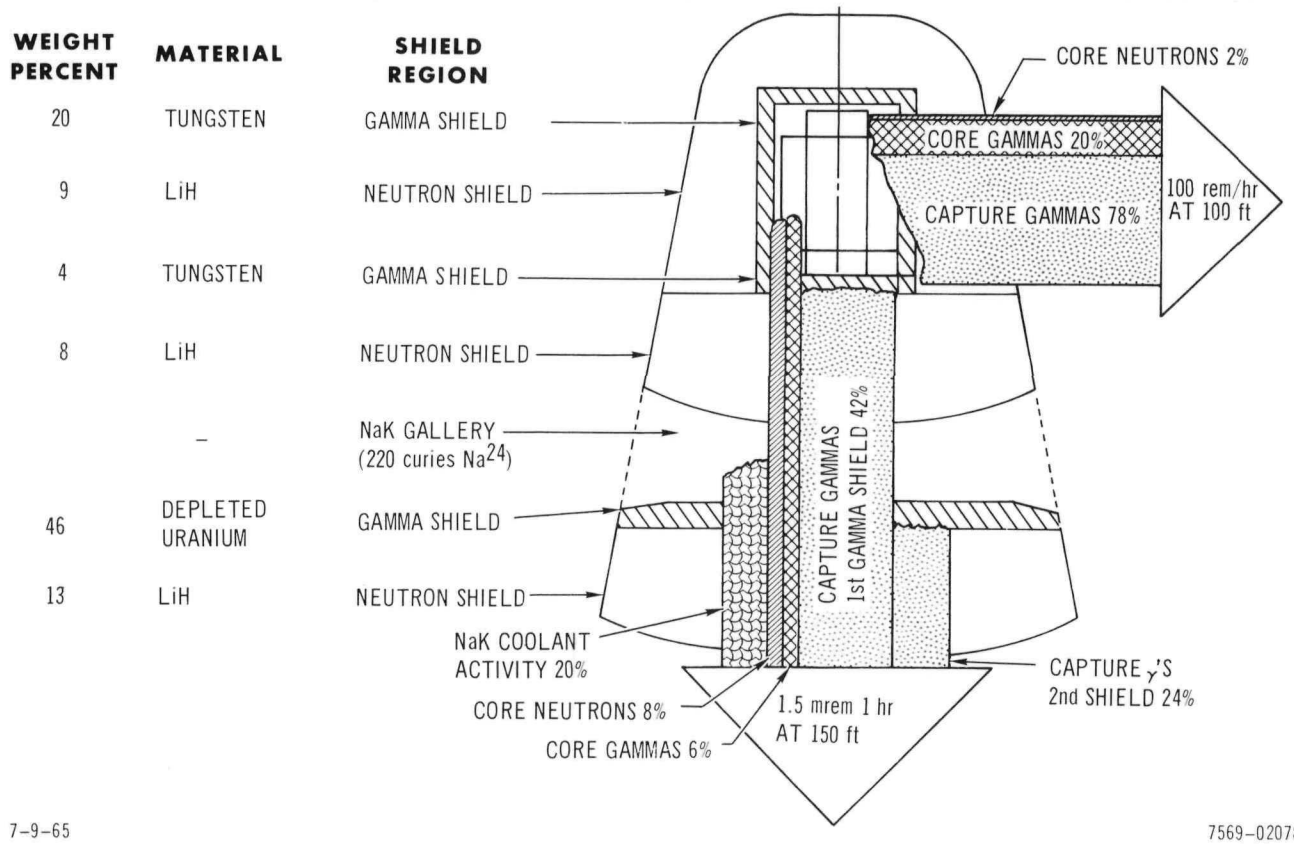

Figure 83. 4π Shield Weight and Dose Contributions

The system is now undergoing initial checkout, and hydriding tests will begin when the checkout is concluded.

7. Braze Compatibility with LiH

The search for a commercial braze alloy, compatible with molten lithium hydride (melting point about 1268°F or 686°C) during the shield casting operation, revealed that the Haynes Stellite 157 alloy (70.5 Co, 21 Cr, 4.5 W, 2.4 B, and 1.6 Si) possessed outstanding corrosion resistance for 100 hours.* A specimen is currently under test at 1300°F and will be examined after 2000 hours of exposure.

8. Li-LiH Interaction Study

The beneficial effect of the addition of Li metal on the cast LiH shield properties* dictated additional studies to define the long-term interaction of Li metal on LiH at elevated temperatures. Twelve stainless-steel capsules were prepared, each containing a small cylinder of cast LiH and an approximately equal volume of metallic Li. The cylinder of LiH was held in the bottom of the capsule by a stainless-steel screen to permit the molten Li metal to drain from the specimen when inverted. The capsules were outgassed, evacuated, backfilled with hydrogen to provide 1 atm internal pressure at the test temperature, and heliarc welded. The capsules were placed in a test furnace, heated for the specified time, and inverted. Table 51 summarizes the observations made when the capsules were sectioned lengthwise.

9. Gamma Shield Development

The production of capture gamma rays in gamma shielding materials, such as tungsten and depleted uranium, is an undesirable factor if minimum weight shields are to be achieved. This is illustrated in Figure 83 which shows a recent manrated shield layout with the poison-backed control-drum reflector. The rendezvous shield is tungsten while the gallery shield is depleted uranium. The figure indicates graphically what the significant sources are which make up the total dose behind the shadow shield and outside the rendezvous shield for this design. It is clear that a material with low capture-gamma-ray production can result in lower shield weights. This has directed attention to gamma shielding materials, such as lead or zirconium hydride, which have a low capture-gamma-ray production.

Four rendezvous shield concepts were analyzed to determine which would result in the lightest total shield weight. The results, shown in Figure 84, indicate that the liquid lead rendezvous shield results in a 23% weight saving over the tungsten rendezvous shield. Less weight saving was found for the zirconium hydride and the zirconium hydride/lithium hydride aggregate. For this comparison, the materials and region thickness of the shadow-shield portion were held the same.

Liquid lead shields used in various conceptual studies of manrated shields, both in the rendezvous shield portion and the shadow shield, have shown significant weight saving.

The low absorption cross section of pure lead reduces the capture-gamma-ray production by a factor of about 100 over materials such as tungsten or depleted uranium. Because lead does not have any resonances, the use of poisons, such as boron, can reduce the neutron captures even further. Liquid lead also has a reasonably high density of about 10.0 gm/cm^3, which is an advantage in shadow shields.

*C. E. Johnson, "SNAP 8 Progress Report, February-April 1965," NAA-SR-11092 (CRD), June 15, 1965

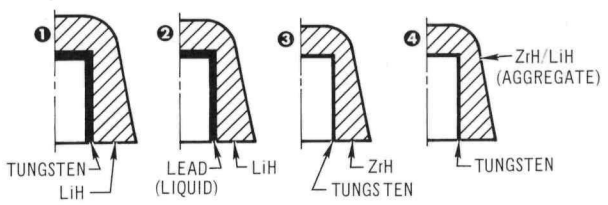

	1	2	3	4
GAMMA SHIELD	2.6 in.	2.3 in.	1.0 in.	1.0 in.
NEUTRON SHIELD	11.8 in.	9.6 in.	9.1 in.	9.7 in.
RELATIVE WEIGHT (INCLUDING SHADOW SHIELD)	100	77	91	87
ESTIMATED DEGREE OF DEVELOPMENT EFFORT	1.0	1.5	3.0	1.5
ESTIMATED UNIT PRODUCTION COST	1.0	0.9	2.5	0.95

7-12-65 7569-02100

Figure 84. Rendezvous Shield Concepts

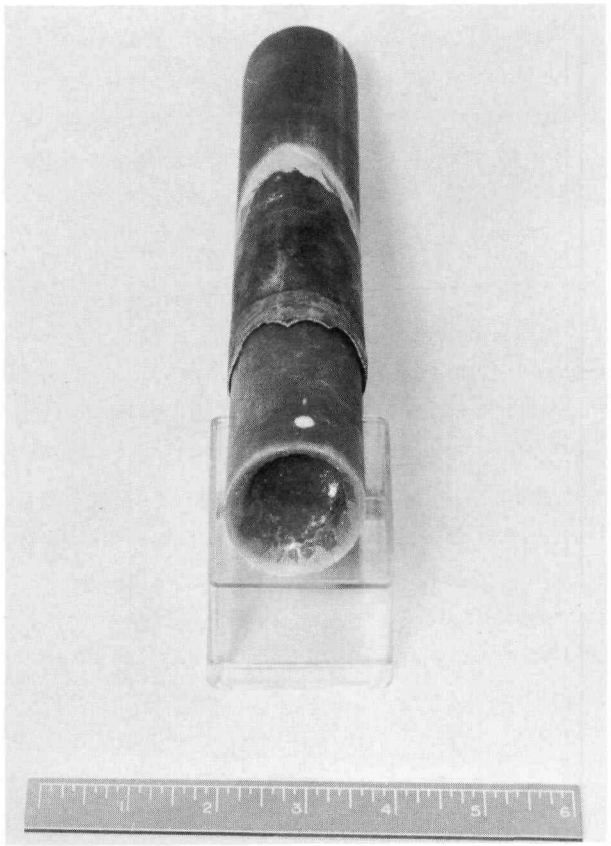

4-13-65 7568-47255

Figure 85. Lithium Hydride Cast in a Titanium Tube

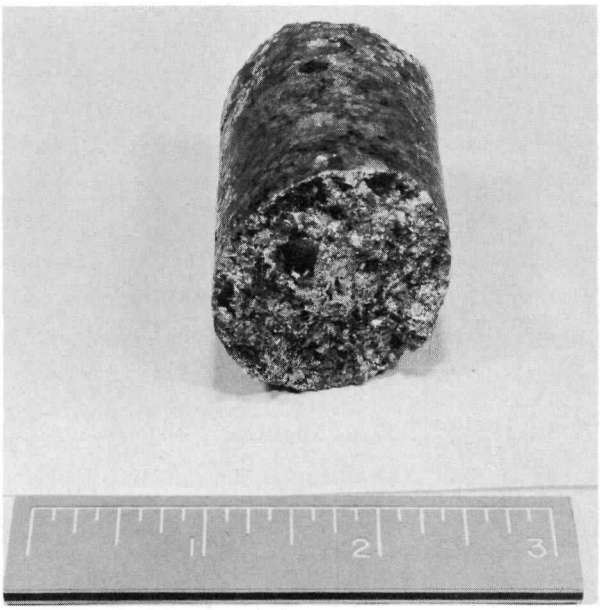

6-21-65 7568-56480

Figure 86. LiH-ZrH Aggregate Cast in a Titanium Tube

6-21-65 7568-56479

Figure 87. Released Casting and Titanium-Coated, Stainless-Steel Mold

Using current technology, a container can be designed that will accommodate the change of phase and thermal expansion of the lead during reactor startup. Lead has a low vapor pressure at high temperature (1.0 mm of Hg at 1809°F), so the shield will not be a pressure vessel. The corrosion properties of liquid lead are well documented. A particularly large amount of data available at 1800°F indicates that suitable corrosion-resistant container materials are available for liquid lead shield fabrications at this temperature.

Evaluation of the lead glass sample, cast in the laboratory, showed no weight saving advantage over a material such as depleted uranium for a manrated split shadow shield. The composition of the lead glass sample corresponded to $4PbO\text{-}1B_2O_3$ or about 11 wt % B_2O_3. The low density of the material (6.91 gm/cm^3), plus the amount of oxygen and boron which are inefficient gamma attenuating materials, offset the materials advantage of very low capture-gamma-ray production.

10. Mold Release Tests

When LiH is cast in stainless-steel containers, a bond is formed between the container and LiH mass. This bond has been utilized in shield casing and support structural design. On the other hand, it is sometimes advantageous to have the LiH mass released from the container wall when the casting cools. Examples are the casting of test bars or in casting blocks of LiH for use in sectional assembly of large shields. The ability to selectively control the bonding between lithium hydride and the shield casing and internal structure should be useful in optimizing the shield design.

Containers or coating materials that rapidly form brittle hydrides during the LiH casting process were chosen since the LiH will not bond to the hydride surface. Titanium and zirconium were the candidate materials and feasibility testing has been done with titanium. LiH has been cast under a hydrogen atmosphere in a titanium tube and found to release readily at room temperature (Figure 85). Transverse rupture tests resulted in a modulus of rupture of 4010 psi for one specimen, compared to 133 psi in published values. The higher values are probably due to absence of internal cracks usually formed during cooling of cast specimens in nonreleasing molds. A LiH-ZrH aggregate was also cast in a titanium tube and was easily removed (Figure 86).

Additional tests were conducted wherein titanium was deposited on stainless-steel and mild-steel mold surfaces by vapor deposition. These castings were also readily removed from the mold. Figure 87 shows the released casting and titanium-coated, stainless-steel mold.

One sample of LiH cast into a zirconium mold could not be easily removed.

BLANK

VI. SNAP 8 EXPERIMENTAL REACTOR (S8ER)

A. INTRODUCTION AND SUMMARY

The objectives of the S8ER are to demonstrate reactor operation and to determine reactor performance characteristics at both 450 and 600 kwt. The tests are required to verify the SNAP 8 design and to provide experimental data upon which to base the reference design.

The operational phase of the S8ER test program has been completed and all objectives have been accomplished. Presently, the system is undergoing disassembly and post-operations examination. Both the primary and secondary NaK systems have been disassembled. All components were visually screened upon removal. Selected components have been submitted for detailed metallographic examination. The results of preliminary examination performed to date indicate that components and piping of both NaK systems are in good condition.

B. SYSTEM DISASSEMBLY

Soon after final shutdown of the S8ER on April 15, 1965, the secondary coolant system was drained and disassembled. Circulation of the NaK primary coolant continued for six weeks after shutdown to remove shutdown decay heat, after which time the primary coolant system was drained and flushed twice with NaK to minimize radioactive contamination within the piping. The primary coolant system piping within the primary vault was then disassembled.

Disassembly of both primary and secondary piping proceeded in a similar manner, with the exception of the contamination control required in disassembly of the primary piping. First, insulation was removed and external surfaces and thermocouples were inspected. Pipes were then marked for identification and to indicate cut locations.

As pipe sections were cut and removed, they were inspected for abnormalities. They were then cleaned with an organic cleaner and packaged for more detailed examination if required. Visual examinations revealed that the piping was in satisfactory condition. During disassembly of the secondary piping two granular deposits (Figure 88) were discovered. The deposits had the visual appearance of NaK oxide. These deposits are now undergoing detailed chemical analysis. No such deposits were observed in the primary system.

Following primary piping disassembly in the vault, control-drum-drive motors, control-drum position indicators, and primary piping were removed from above the shutdown shield in the containment vessel.

C. CORE REMOVAL

A core lifting tool (Figure 89), to be used to engage the S8ER core as a unitized package for removal from the reactor vessel, was designed, fabricated, and tested with mockup equipment. The core will be lifted into the core transportation cask, shown in Figure 90 being fitted to the 14-in.-thick shield which will provide shielding and tool access during core removal. Rehearsals were conducted of core removal and of cask transportation to the AI hot laboratory where the core package will be disassembled and fuel elements will be examined.

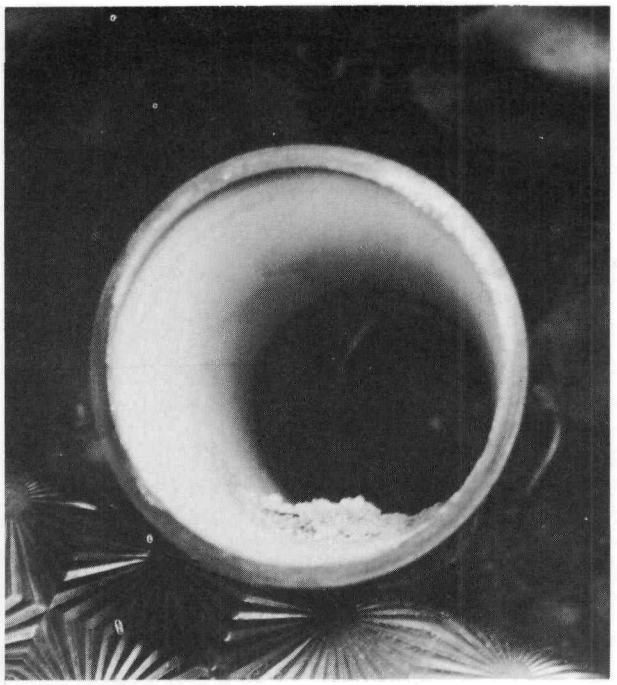

7-24-65 7568-02334

Figure 88. Granular Deposits in NaK Pipe

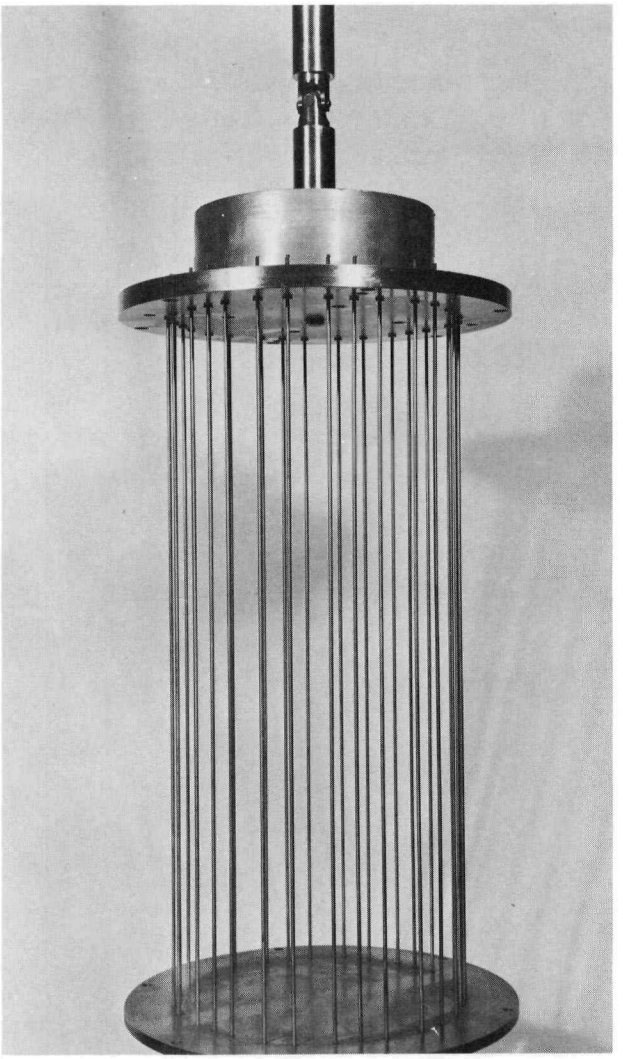

6-17-65 7568-18671

Figure 89. Core Lifting Tool

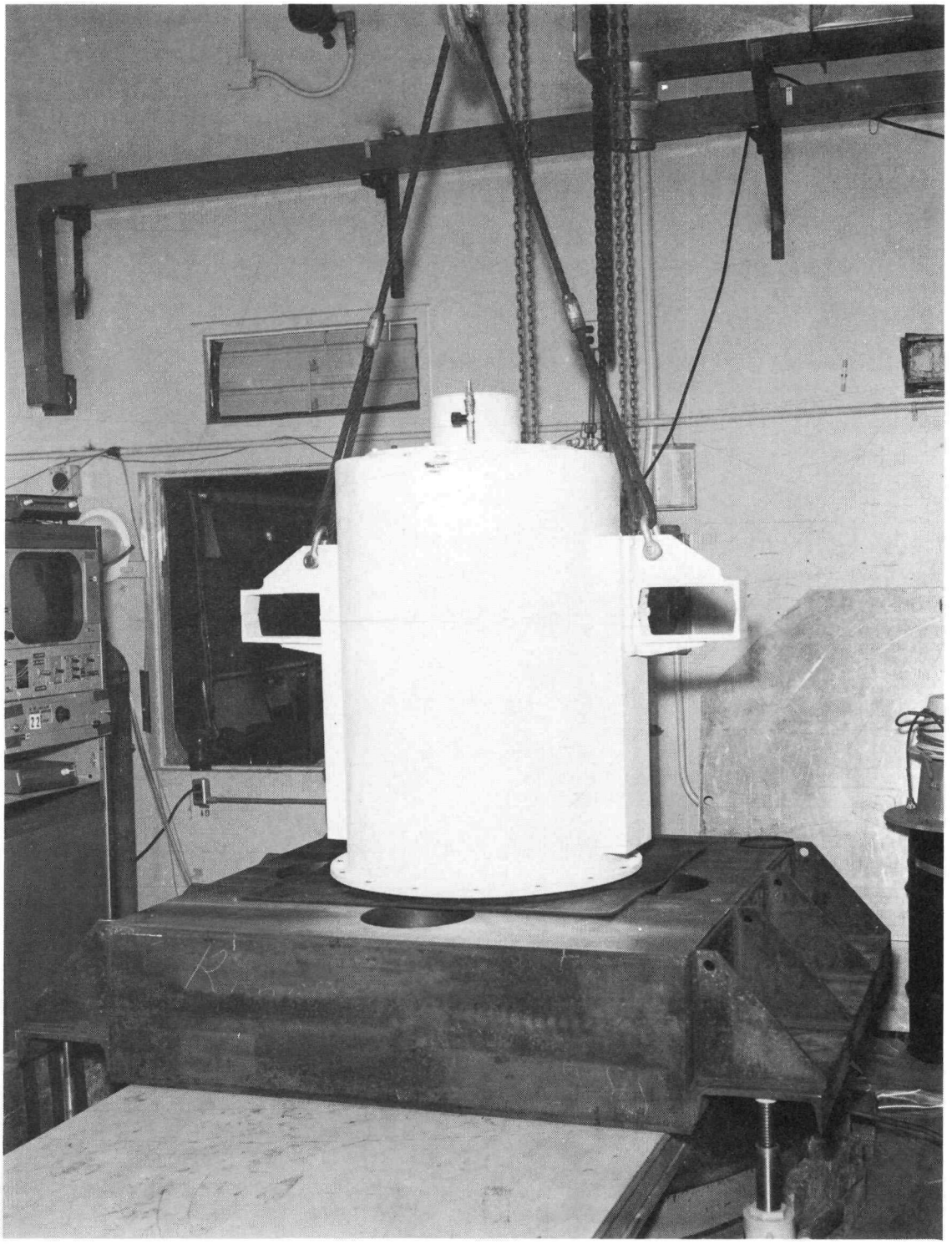

7-15-65 7568-56490

Figure 90. Core Transportation Cask

BLANK

VII. SNAP 8 DEVELOPMENTAL REACTOR MOCKUP (S8DRM-1)

A. INTRODUCTION AND SUMMARY

The SNAP 8 developmental reactor mockup (S8DRM-1) is a nonnuclear prototype system used to verify the reference design. As this system is the first attempt to verify the SNAP 8 nuclear system, some malfunctions are expected. Failed components are replaced or redesigned as necessary following the testing.

The main objectives of the S8DRM-1 program are to: (1) provide test information useful for the development of the reference components and reactor systems; (2) test the adequacy of the fabrication techniques of the reactor components; (3) develop and prove the reactor and system assembly and checkout procedures; and (4) demonstrate that the reactor and components can withstand the launch conditions and operate subsequently in simulated space environments.

The formal test program for the S8DRM-1 includes an assembly test, a startup reliability test, a prelaunch environmental test, a launch environmental test, an orbital startup test, and an endurance test under simulated space vacuum.

The test program has been completed through the launch environment test.* The modifications of the reactor to add revised components and to replace the failed components were completed. The designs and plans to modify the environmental test facility to maintain 10^{-9} to 10^{-10} torr pressure during endurance testing were also completed. At this point, the test program was terminated. The reactor system, shield, test equipment, and facility are being prepared for storage.

B. REACTOR COMPONENTS

The acceptance test of the modified design control drum actuators was successfully completed. The revised design incorporated the larger diameter field and brake coil wires (27 gage vs 30 gage) as well as other improvements† to increase the performance reliability.

A new set of cable harnesses was fabricated and acceptance tested. These cable harnesses utilized the latest technique of terminating the cable conductor to the connector pin as developed for the S8DS.§

C. REACTOR ASSEMBLY

The S8DRM-1 reactor assembly was completely rebuilt using the following parts of modified design: (1) control drum actuator, (2) cable harness, and (3) control-drum bearing.† Those parts which had been damaged during the launch environment test§ were also replaced. The comparison of the measured torques of the control drum with the old and the new control-drum bearings are shown in Table 52.

*C. E. Johnson, "SNAP 8 Progress Report, February-April 1965," NAA-SR-11092 (CRD), June 15, 1965
†C. E. Johnson, "SNAP 8 Quarterly Progress Report, May-July 1964," NAA-SR-9992 (SRD), September 22, 1965
§C. E. Johnson, "Progress Report, SNAP 8, August-October 1964," NAA-SR-10492 (SRD) December 23, 1965

TABLE 52

CONTROL-DRUM TORQUE DATA

Drum Number	Torque Out (in.-oz)		Torque In (in.-oz)	
	New Bearing	Old Bearing	New Bearing	Old Bearing
1	44	192	48	208
2	30	58	25	48
3	36	58	35	49
4	37	112	39	94
5	20	58	28	48
6	18	28	28	40

D. TEST FACILITY

A modified design of the NaK heater assembly used as an in-core-vessel heat simulator was completed. The fabrication of the new heater assembly is partially completed.

The endurance test vacuum system was modified by adding a 16-in. diffusion pump. The vacuum control console was also modified to add an alarm system as well as the control for the new pump. The plans to modify the vacuum test chamber further to obtain and maintain endurance test pressure of below 10^{-9} torr were completed. As shown on Figure 91, the modification consists of the addition of an ion pump, titanium sublimation getter pump, liquid nitrogen, cryogenic panel, and a new section of the vacuum vessel. The detail designs and the equipment specification to incorporate these modifications have been completed.

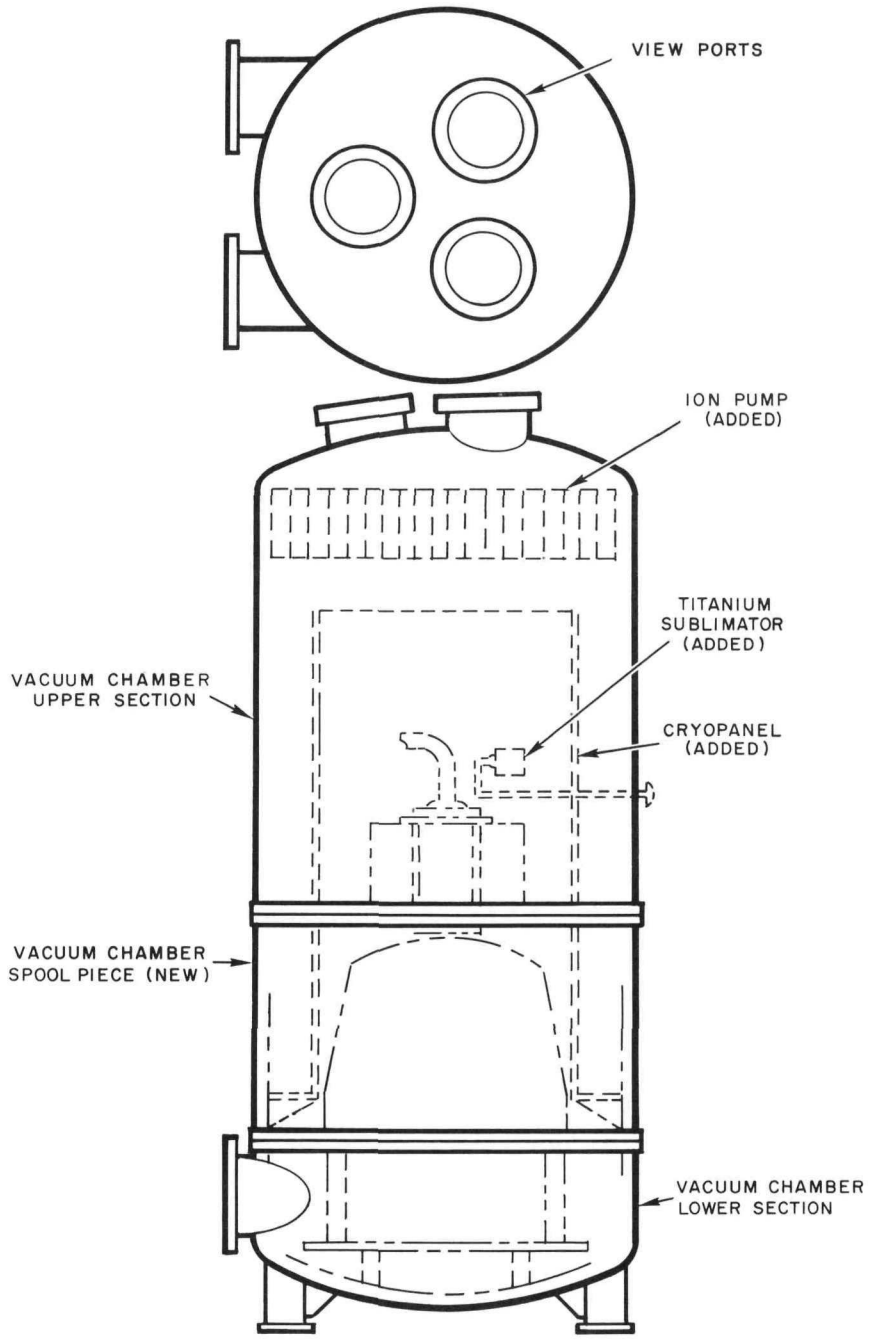

Figure 91. S8DRM-1 Vacuum Test Chamber Modification

BLANK

VIII. SNAP 8 GROUND PROTOTYPE (S8DS)

A. INTRODUCTION AND SUMMARY

The current objectives of the S8DS program are: to determine the steady-state and transient performance characteristics of a SNAP 8 reactor at a variety of operating conditions including higher-than-rated power and temperature; to demonstrate satisfactory operation of the improved fuel element design and the automatic reflector control features; to develop and demonstrate techniques of automatic startup and control; to determine the nuclear and thermal operating characteristics of SNAP 8 shielding materials in a typical radiation and temperature environment; and, if possible to test the reactor as a component of a nuclear electric power generating system.

Anodized beryllium test samples for the beryllium reflector yielded lower than design point emissivities which will increase the operating temperature of the reflector. Re-analysis of the as-built cable harness remote connector indicated that operating temperature could be higher than the design capability of the connector and the thermal effects of various design parameters are being evaluated to determine what modifications must be made to the connector design. The reactor core vessel fitup, completed scram kit, actuators, limit switches, and assembly and acceptance test fixtures are shown in a series of photographs.

B. THERMAL ANALYSIS

1. Component Temperatures

The S8DS component temperature analysis was revised to reflect more recent information on the as-built configuration of the S8DS reactor assembly.

Recent testing of S8DS anodized beryllium test samples indicated that the emissivity of the anodized beryllium reflectors would be significantly lower (ϵ = 0.5) than the value used in the original analysis (ϵ = 0.8). Measurements were also made on the vacuum chamber as installed for the S8DS test and it was found to have a room temperature emissivity of approximately 0.15. The reduced emissivity of the reflectors and high reflectivity of the vacuum chamber combined to produce temperatures 25 to 100°F higher than the nominal values previously reported.

In order to maintain component temperatures at approximately the same level as reported in the previous component temperature analysis, it is required that: (1) the S8DS vacuum chamber be coated to reduce its reflectivity and (2) that a special high emissivity coating be used on the exterior surface of the S8DS reflector shims. A comparison of temperatures corresponding to the original assumptions, the as-built configuration, and the recommended modified design is shown in Table 53.

2. Shield Temperatures

Initial analysis of the S8DS shield temperatures assumed vessel wall emissivity of 0.6. With the emissivity of the vessel wall ~0.2, the heat load on the side of the shield is significant due to thermal radiation from the core reflected from the low emissivity walls. A preliminary analysis taking these changes into account indicated that the maximum shield temperature for 600-kwt, 1300°F outlet coolant temperatures should be less than 900°F, indicating that no problems should exist due to shield temperatures. A survey of the shield temperatures for various core power levels and NaK temperatures is being analyzed.

TABLE 53

COMPONENT TEMPERATURE COMPARISON

Component Description	Previous Nominal Operating Temperature (°F)	Current As-Built Temperature (°F)	Temperature With Recommended Changes (°F)	Component Description	Previous Nominal Operating Temperature (°F)	Current As-Built Temperature (°F)	Temperature With Recommended Changes (°F)
Drive Actuator, Lower End Plate	930	1010	985	Maximum Beryllium Drum, Outer Face	1140	1265	1160
Actuator Rotor, Lower Shaft (at Bearing)	930	1035	1005	Lower Beryllium Stationary Reflector at Bearing Bracket	1105	1195	1160
Actuator Rotor (Center)	940	1040	1015	Upper Beryllium Stationary Reflector at Bearing Bracket	1205	1285	1240
Actuator Stator (Center)	885	990	965	Reflector System Hinge Pin Mounting Bracket	1130	1185	1160
Actuator Case	880	985	960	Lower Reflector Bearing Bracket at Reflector	1083	1155	1125
Actuator Upper End Plate	835	975	950	Lower Reflector Bearing Housing at Race	1006	1085	1055
Actuator Rotor, Upper Shaft (at Bearing)	905	1020	995	Lower Reflector Bearing Socket	1007	1085	1055
Actuator Brake Housing	780	900	870	Lower Reflector Bearing Ball	1023	1105	1075
Actuator Brake Teeth	880	1010	985	Lower Reflector Bearing Bushing	1023	1105	1075
Actuator Brake Spring	880	1010	985	Lower Reflector Drive Shaft	1072	1165	1120
Drive Pinion	905	1015	985	Lower Control Drum Bracket at Drum	1210	1310	1230
Drive Gear Teeth	860	985	955	Scram Kit Upper Drive Shaft Bearing	590	755	710
Drive Gear Shaft Bearing	855	980	945	Scram Clutch Coil Housing	730	855	835
Drive Bellows	875	1005	970	Scram Clutch Teeth	735	860	840
Upper Reflector Bearing Bracket at Reflector	1180	1260	1215	Scram Operating Spring	570	740	695
Upper Reflector Bearing Housing at Race	1025	1155	1120	Scram Clutch Coil (With Electrical Heating)	770	890	875
Upper Reflector Bearing Socket	1025	1155	1120	Position Sensor Shaft Coupling	605	790	745
Upper Reflector Bearing Ball	1030	1160	1120	Position Sensor Rotor	-	715	675
Upper Reflector Bearing Bushing	1030	1160	1120	Position Sensor Case	-	675	630
Upper Reflector Drive Shaft	1045	1170	1125	Position Sensor Lower Bearing	-	675	630
Upper Control Drum Bracket at Drum	1215	1310	1230				
Maximum Beryllium, Cusp	1295	1370	1315				
Maximum Beryllium Drum, Inner Face	1245	1340	1250				

3. Cable Harness Remote Connector Assembly

Re-analysis of the as-built S8DS cable harness remote connector assembly indicated that the maximum temperature could be over 500°F or 100°F higher than the design temperature (400°F). Preliminary calculations showed that the thermal radiation from the reactor exterior and the primary NaK pipes to the remote connector assembly was the principal heat source. The analysis of the remote connector temperatures indicated that the uncertainty in the surface contact heat transfer coefficient between surfaces in vacuum produced a large variation in the predicted maximum temperature and that the effect of thermal radiation transfer from the hot reactor exterior and NaK pipes could be significantly reduced by installing radiation barriers. By inserting two polished plates ($\epsilon \sim 0.2$) between the remote connector and the hot surfaces, the thermal flux to the remote connector can be reduced by approximately a factor of 3.

The surface contact heat transfer coefficient of the remote connector assembly is being determined experimentally by measuring the transient temperature response of various components of an S8DS remote connector heated in vacuum. The values of the surface contact heat transfer coefficients are obtained by comparing the transient temperature results at various times using an analog model simulation. The temperatures of the remote connector operating under various physical conditions are being determined using the same analog setup modified to simulate the reactor environment.

The effect of varying the following items is being investigated to determine their effect on the connector temperatures and to determine what modifications need to be made to the connector design: (a) thermal barrier, (b) redesigning certain components, (c) using ductile material to significantly increase conduction between surfaces, and (d) selectively coating component surfaces with high or low emissivity coatings.

C. REACTOR CORE VESSEL AND INTERNALS

The completed reactor core components are shown in Figure 92 and the trial fit-up of the core internals (with dummy fuel elements) is shown in sequence in Figures: 93 (flow baffle), 94 (lower grid plate), 95 (half core of internal reflectors and dummy fuel elements), 96 (full core), and 97 (upper grid plate). The trial fit-up of the reactor core and support structure is shown in Figure 98.

D. NEUTRON SHIELD

The shield void volume measured after casting the lithium hydride revealed a density of 94.1% of the theoretical maximum. The shield was subjected to a thermal cycle test; as a result, the conical section distorted slightly leaving a corrugation effect with the lower head bulged down. These distortions should have no effect on the end use. Radiographic examination of the shield revealed a low density region down the center consisting of multiple cracks and some separation of lithium hydride from the rib structure.

E. REFLECTOR AND DRIVES

The S8DS reflector design was modified to use a 3-in.-thick shim (a 2 in. increase). The initial system will utilize single 3-in.-thick shims and the standby reflector system will utilize three 1-in.-thick shims for a total shim thickness of 3 in. added to the 2-in. drum. This change was made to provide additional reactivity margin for increased life or for possible operation at higher-than-rated power and temperature (above 600 kwt, 1300°F). The new shims will have a special high emittance coating. A test and evaluation program of the high emittance coating has been initiated (see Section V-G).

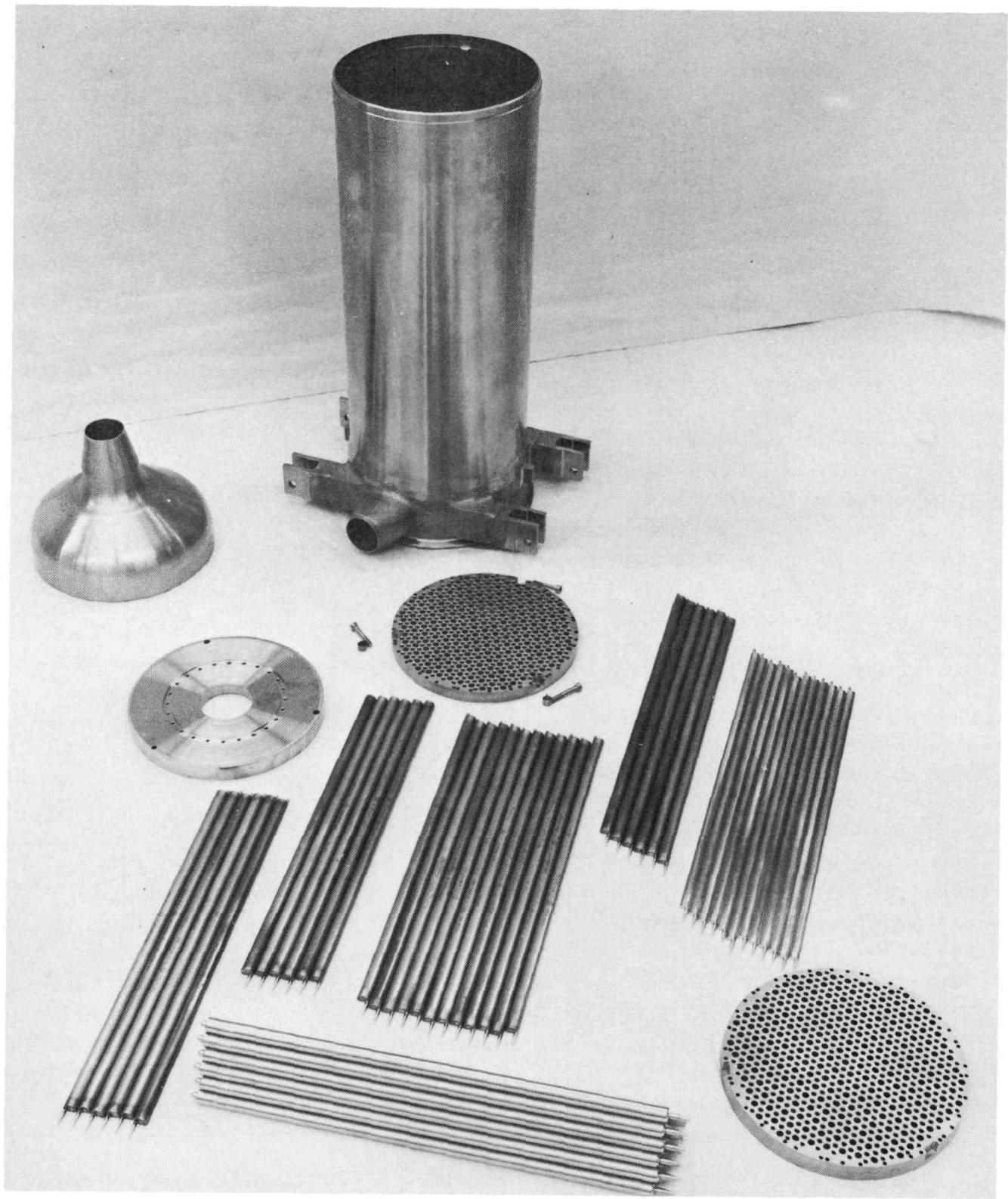

7-15-65

7568-12190

Figure 92. S8DS Reactor Core Components

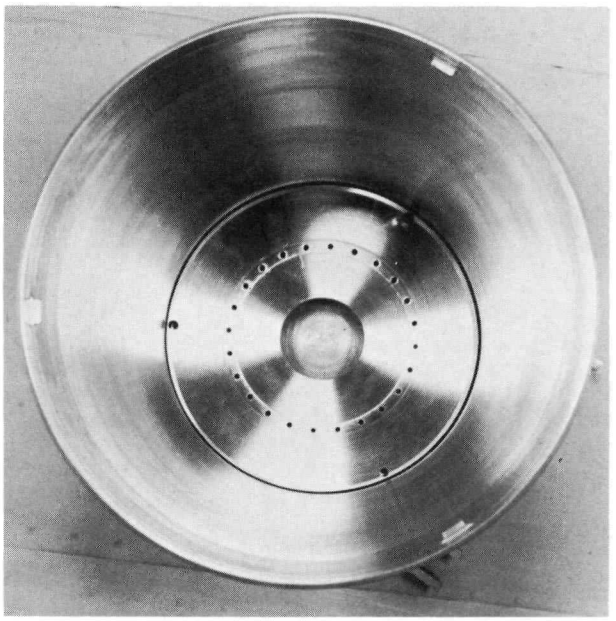

7-15-65 7568-12185

Figure 93. Interior of S8DS Core Vessel Showing Flow Baffle Plate

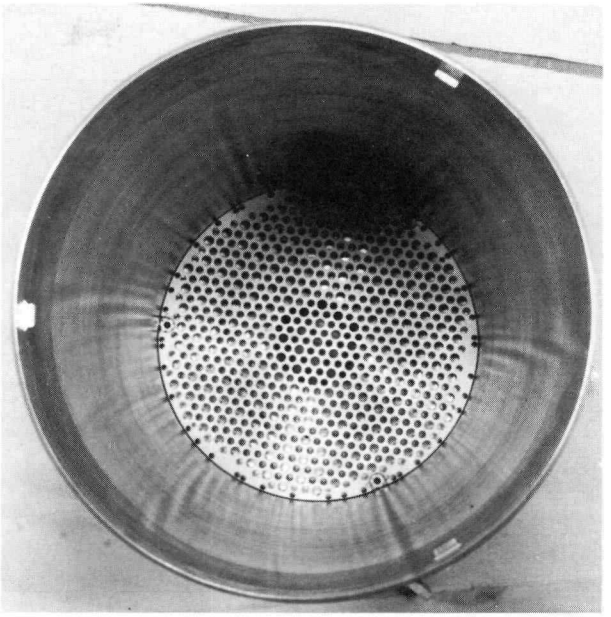

7-15-65 7568-12184

Figure 94. Interior of S8DS Core Vessel with Lower Grid Plate Installed

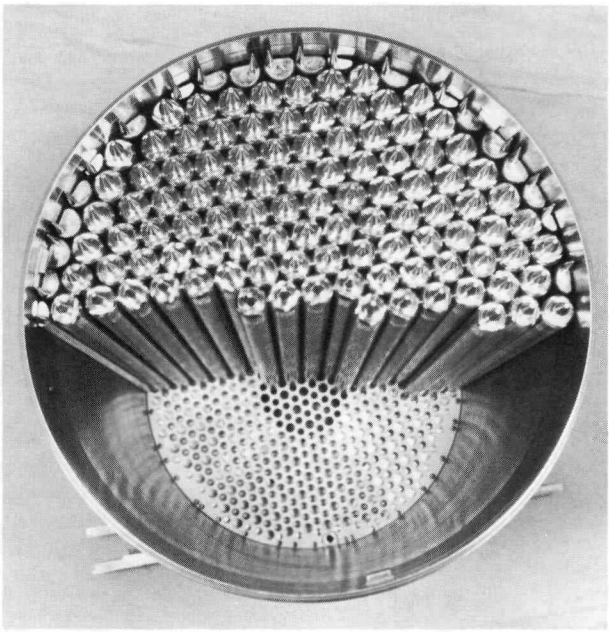

7-15-65 7568-12188

Figure 95. S8DS Core Vessel Partially Filled with Internal Reflectors and Dummy Fuel Elements

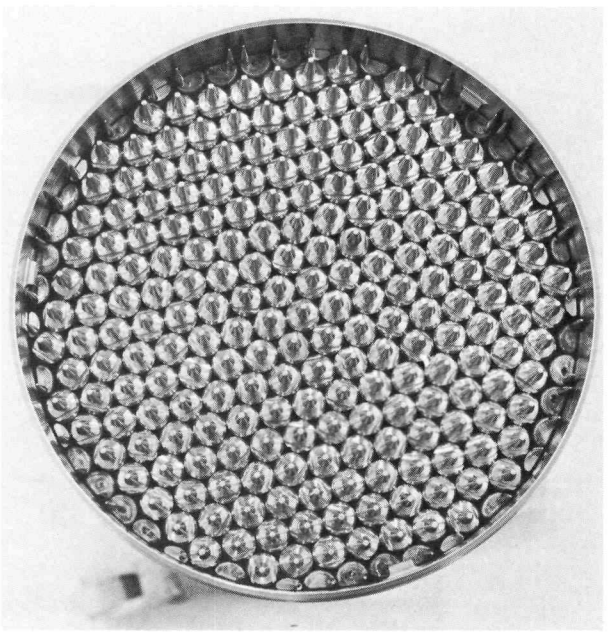

7-15-65 7568-12187

Figure 96. S8DS Core Fully Loaded with Internal Reflectors and Dummy Fuel Elements

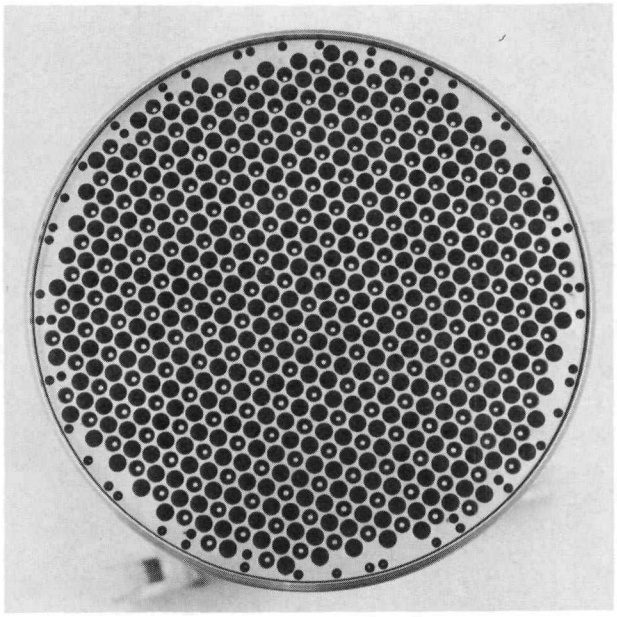

7-15-65 7568-12186

Figure 97. S8DS Core Vessel with Upper Grid Plate in Place

Three scram drive mechanisms (shown on clean bench in Figure 99 with 12 scram snubbers) have been assembled and have performed satisfactorily in preoperational tests. The preoperational tests included the measurements of the scram clutch holding force, pull-in force, and residual magnetic force. One of the scram drive mechanisms is shown in Figure 100. Figures 101 and 102 show one of the twelve S8DS snubbers and a drive gear assembly.

F. SYSTEM INSTRUMENTATION

Three actuators and 20 limit switches are shown on the clean bench in Figure 103 after completion of assembly.

G. ASSEMBLY AND ACCEPTANCE TESTING

The objective of this function is to assemble the S8DS reactor and to conduct nonnuclear component and assembly acceptance tests prior to delivery of the reactor to the Ground Proto-

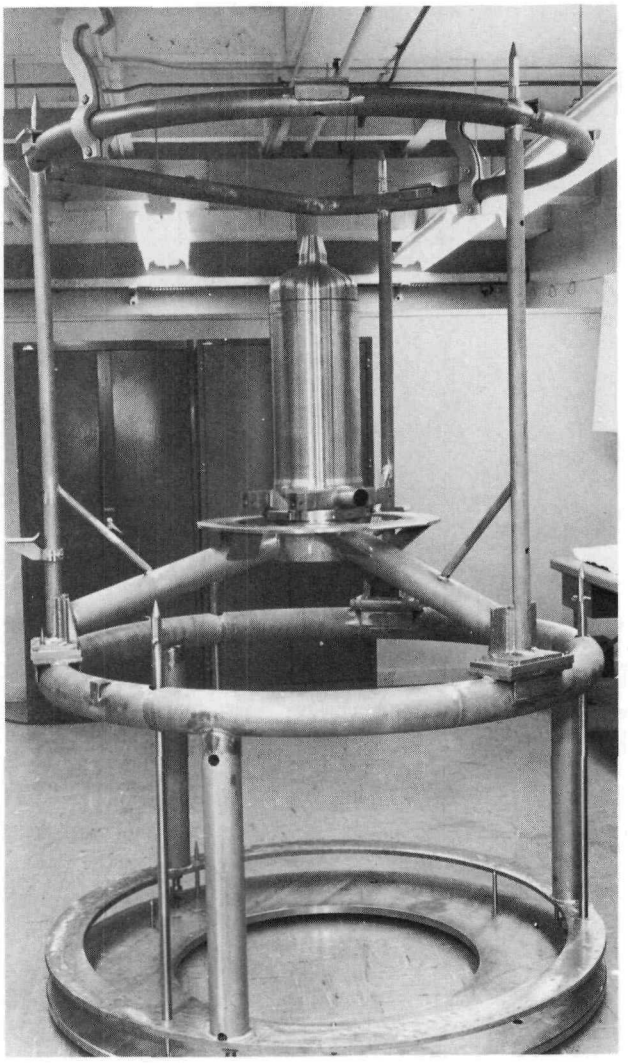

7-15-65 7568-12181

Figure 98. S8DS Reactor Core and Support Structure Fit-up

type Nuclear Test Facility. Acceptance testing includes thermal-vacuum tests to verify that the S8DS components and final assembly will perform in accordance with final design criteria.

1. Facility

All nonnuclear reactor assembly operations will be performed within a 20 ft by 28 ft prefabricated laminar-flow clean room (Figures 104 and 105). The room surpasses requirements of

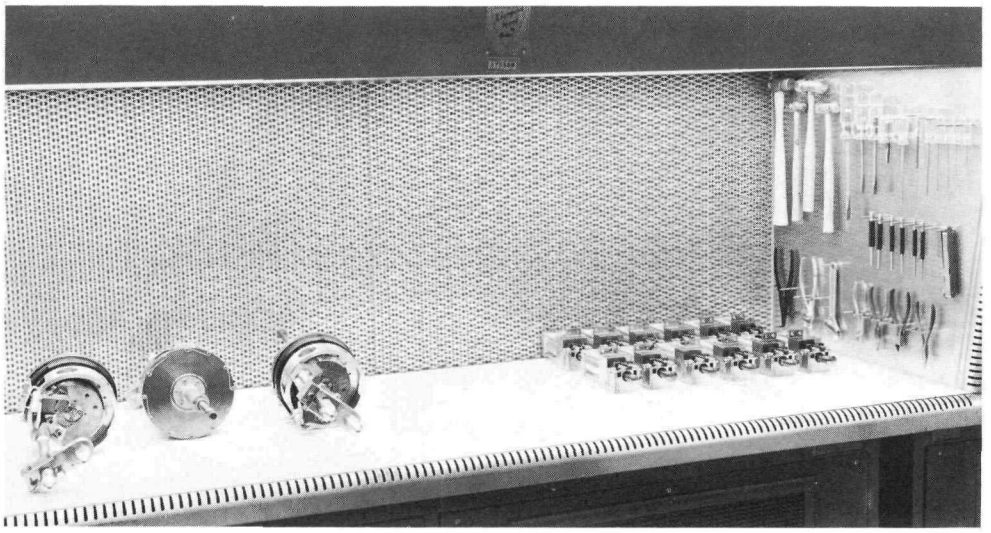

7-14-65 7568-12179

Figure 99. S8DS Scram Mechanisms and Scram Snubbers Assembled on Clean Bench

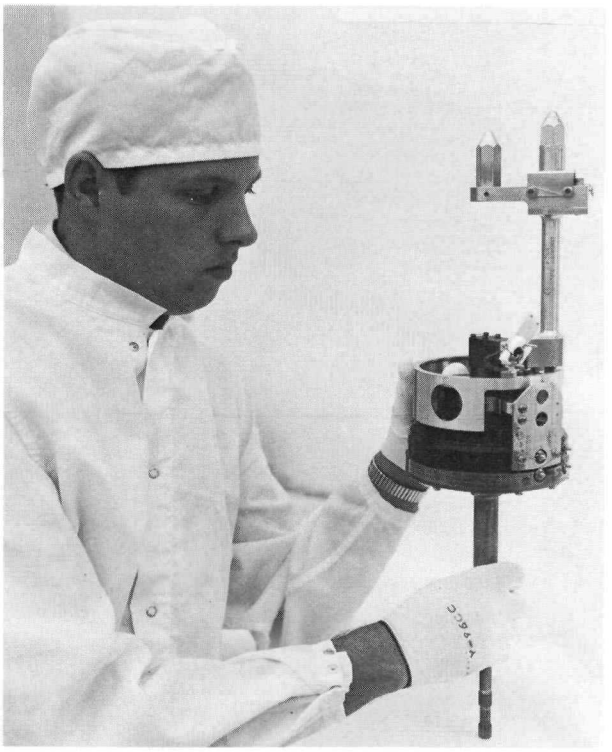

7-20-65 7568-55143

Figure 100. S8DS Scram Drive Assembly

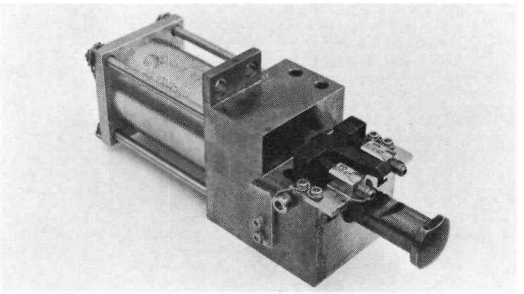

7-20-65 7568-551538

Figure 101. S8DS Snubber Assembly

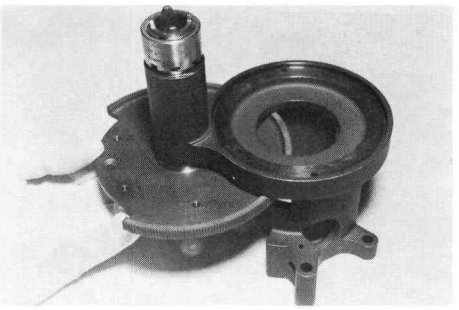

7-20-65 7568-55140

Figure 102. S8DS Gear Housing Assembly

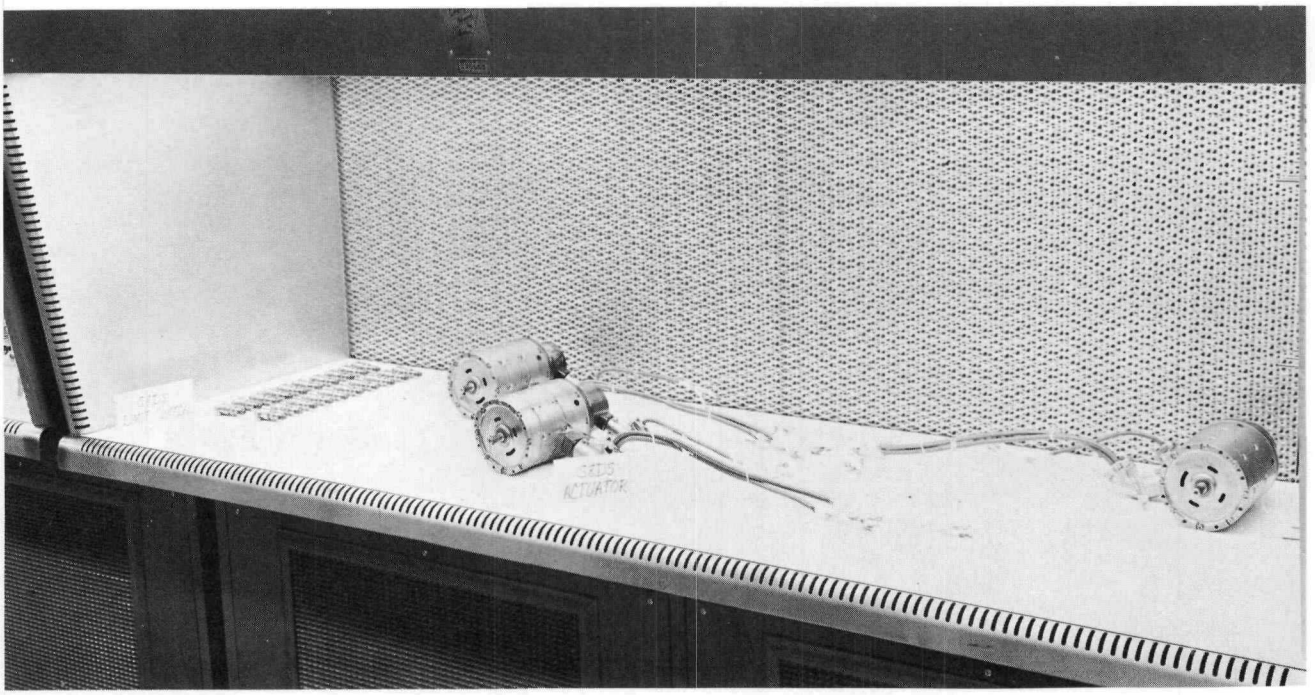

7-14-65 7568-12178

Figure 103. S8DS Limit Switches and Actuators Assembled on Clean Bench

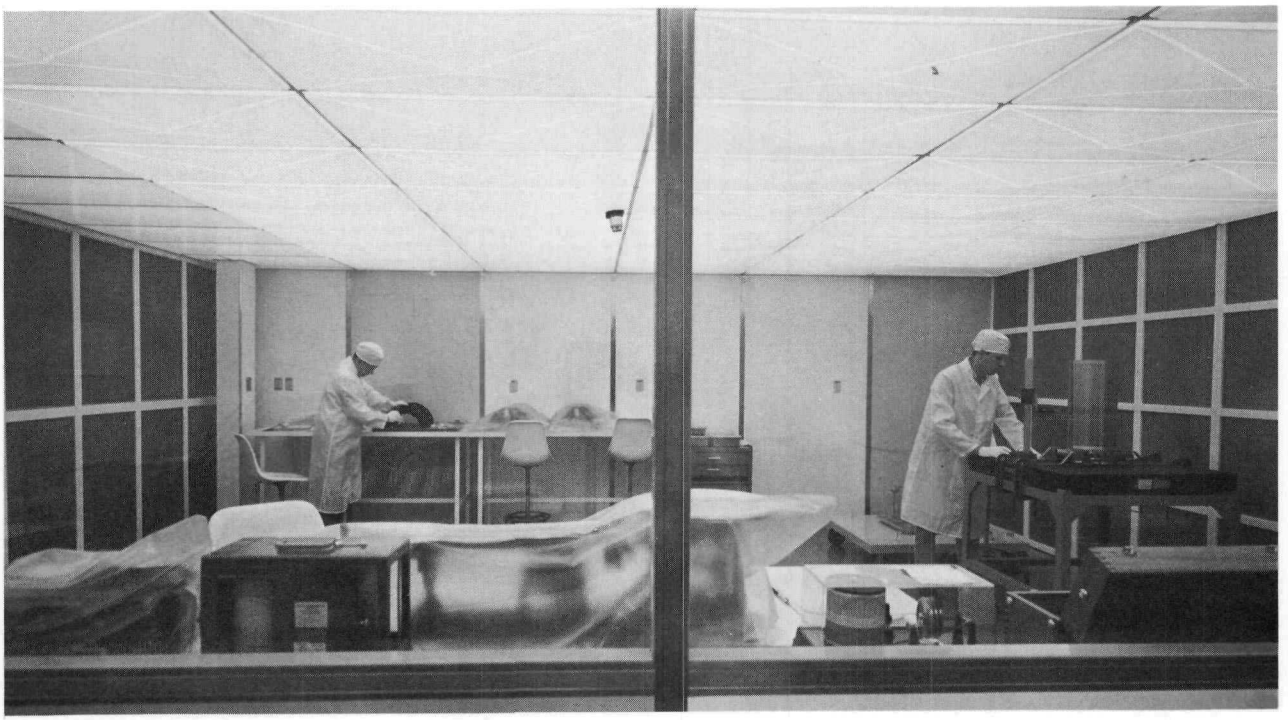

6-24-65 7568-52194

Figure 104. Prefabricated Laminar-Flow Clean Room

a Class 10,000 clean room (Federal Standard No. 209) as demonstrated during initial acceptance tests and subsequently during actual operations. The airflow is directed horizontally, at laminar velocities, across the room from one wall to the opposite wall (see Figure 106). This is achieved through the use of nine preassembled blower-filter modules which are bolted together to form one end wall. The opposite wall, which is the air exit wall, consists of a grid-type structure containing eighteen laminated screen prefilters. The prefilters are used to create air resistance to produce airflow uniformity within the clean room. A return-air plenum is located between the upper and lower ceilings.

6-24-65 7568-52196

Figure 105. Prefabricated Laminar-Flow Clean Room, Interior View

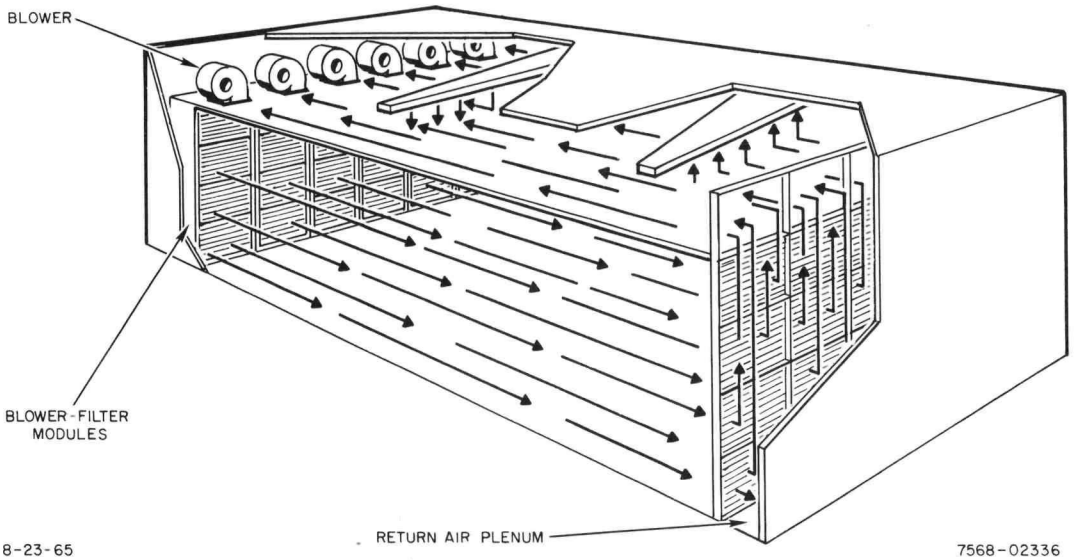

8-23-65 7568-02336

Figure 106. Horizontal Airflow Pattern in Laminar-Flow Clean Room

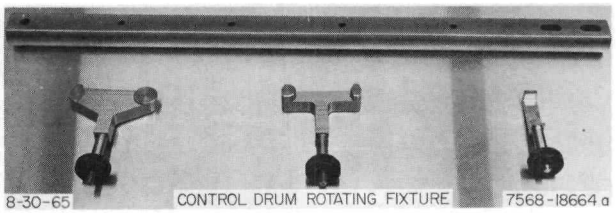

Figure 107. S8DS Control-Drum Rotating Fixture

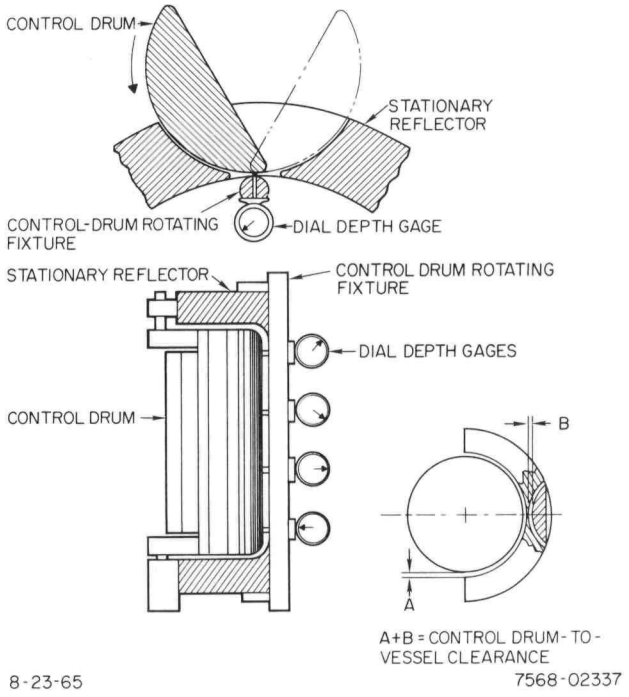

Figure 108. S8DS Control-Drum Gap Measurement Tool

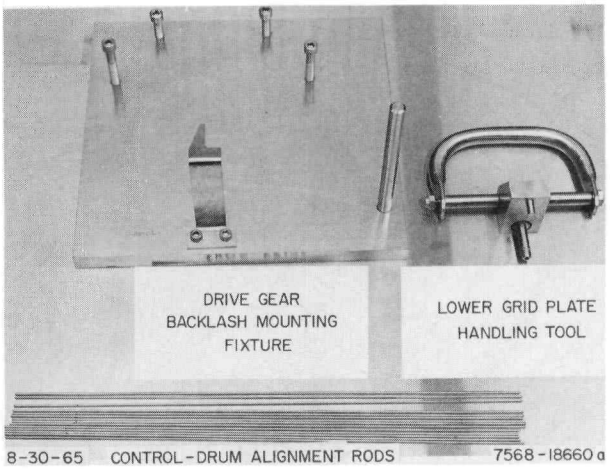

Figure 109. S8DS Drive Gear Backlash Mounting Fixture, Lower Grid Plate Handling Tool, and Control-Drum Alignment Rods

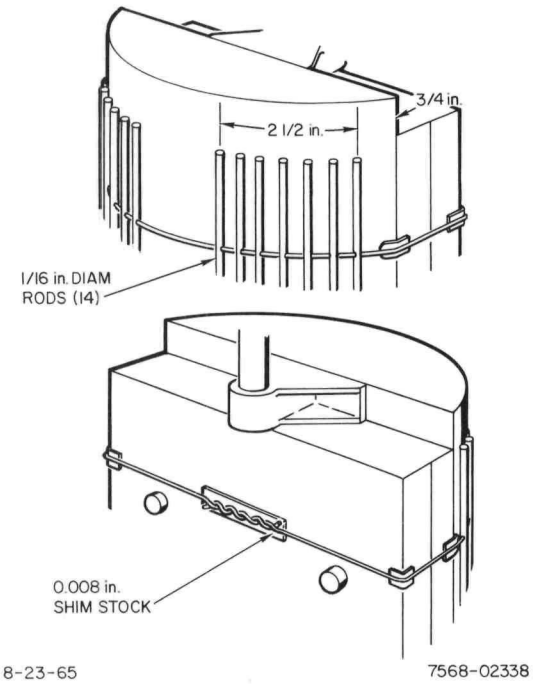

Figure 110. S8DS Control-Drum Gap Shims

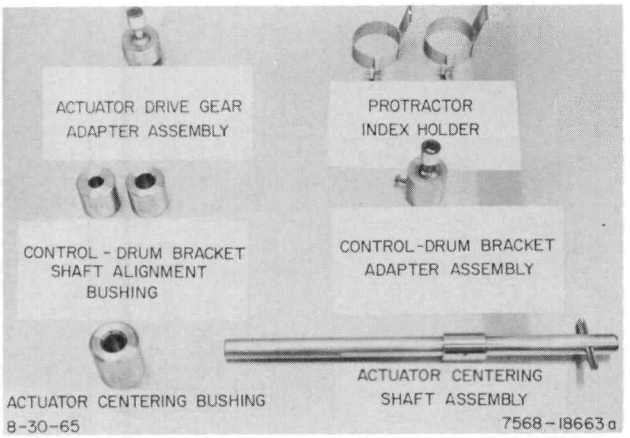

Figure 111. S8DS Assembly Tools

2. Assembly Tools

The tools fabricated for assembling the S8DS reactor and schematics depicting their functions are shown in Figures 107 through 117. The control-drum rotating fixture (Figure 107) is used to determine the physical clearance between a control drum and the reactor vessel (Figure 108). The lower grid plate tool (Figure 109) is used for inserting the grid plate into the reactor vessel and to align the grid plate with respect to the vessel. Control-drum alignment rods (Figure 109) establish the gap between a rotating reflector and a stationary reflector (see Figure 110).

The drive gear backlash mounting fixture (Figure 109) is used in conjunction with the protractor index holder (Figure 111) and the actuator drive gear adapter assembly (Figure 111) to determine drive gear-pinion backlash (see Figures 112 and 113). The control-drum bracket shaft alignment bushing (Figure 111) aligns the upper and lower control-drum shafts with respect to each other and the beryllium control drum (see Figure 114). The alignment of an actuator drive shaft pinion with respect to the control-drum drive shaft is accomplished by using the actuator centering bushing (Figure 111) in conjunction with the actuator centering shaft assembly (Figure 111) as depicted in Figure 115.

The control-drum bracket adapter assembly (Figure 111) locks onto the control-drum upper shaft spline. A torque gage is inserted in the socket end. The control drum is then rotated to determine bearing friction.

The half-reflector retaining clamp (Figure 116) locks the reflector assembly to the reactor vessel for half-reflector assembly and tests (see Figure 117). The reflector holding-fixture support assembly (Figure 116) is a safety device which, when used with the reflector holding fixture, prevents accidental tipping of a reflector during assembly operations. The position-sensor bracket centering fixture (Figure 116) is used to align the position-sensor drive shaft with respect to the scram drive assembly.

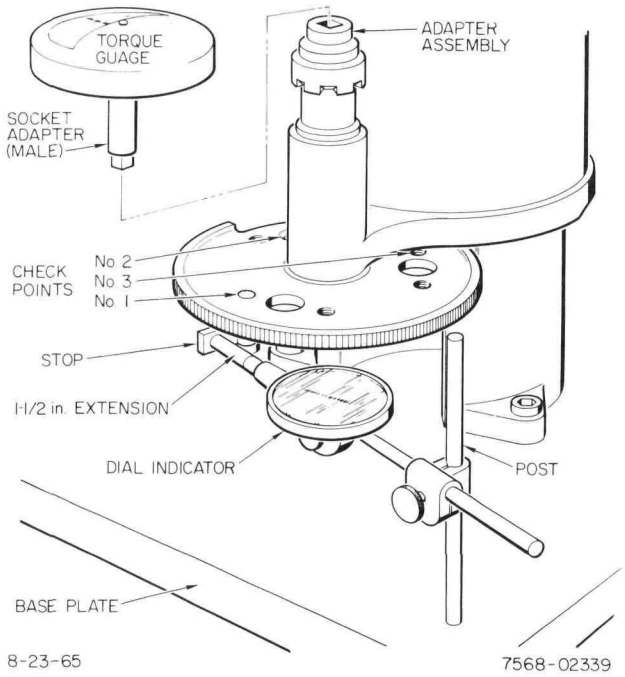

Figure 112. S8DS Scram-Drive Backlash Measuring Tool

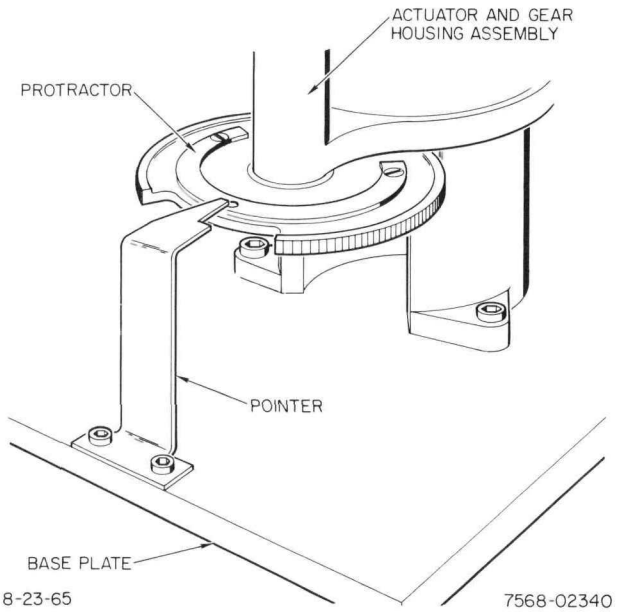

Figure 113. S8DS Control-Drum-Drive Position Measuring Device

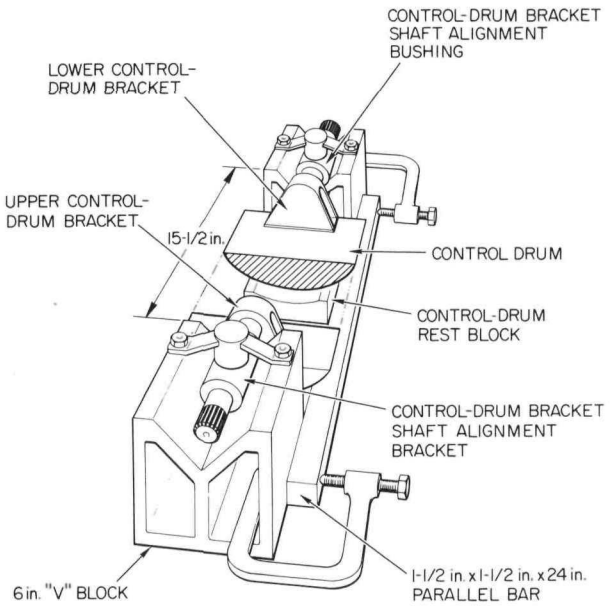

Figure 114. S8DS Control-Drum Bearing Assembly Tooling

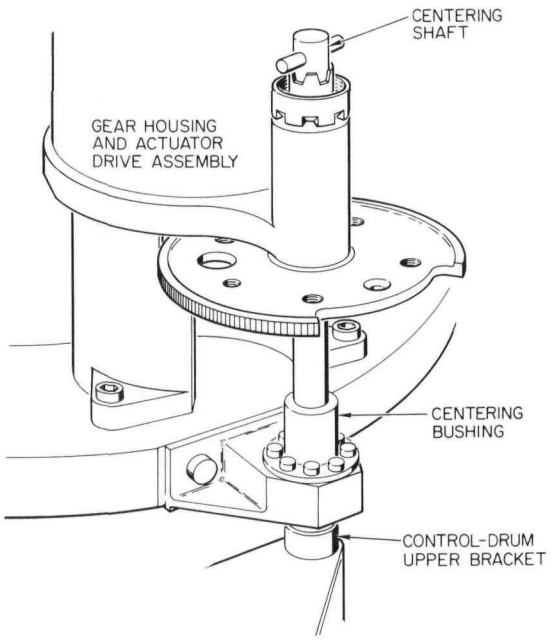

Figure 115. S8DS Scram-Drive Alignment Tool

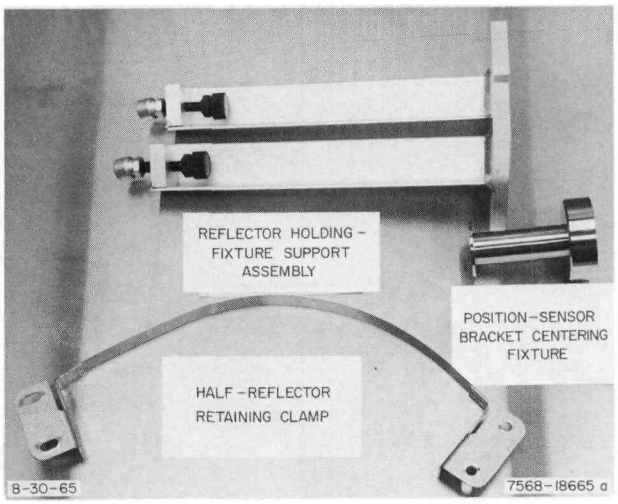

Figure 116. S8DS Reflector Holding Fixture Support Assembly, Position-Sensor Bracket Centering Fixture, and Half-Reflector Retaining Clamp

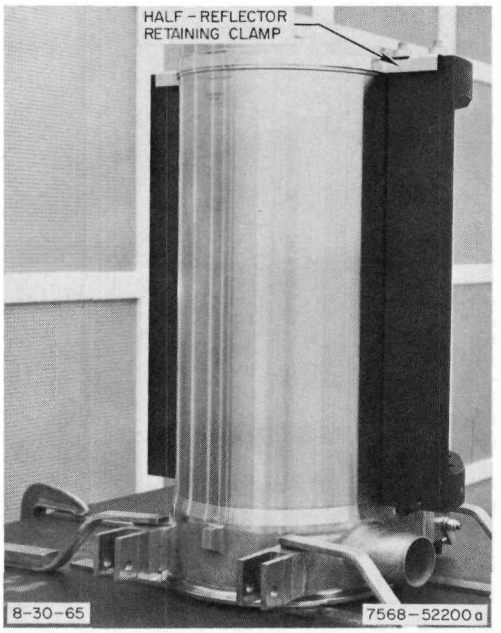

Figure 117. S8DS Tooling Vessel, Z-Half Reflector Clamped to Reactor Core Vessel

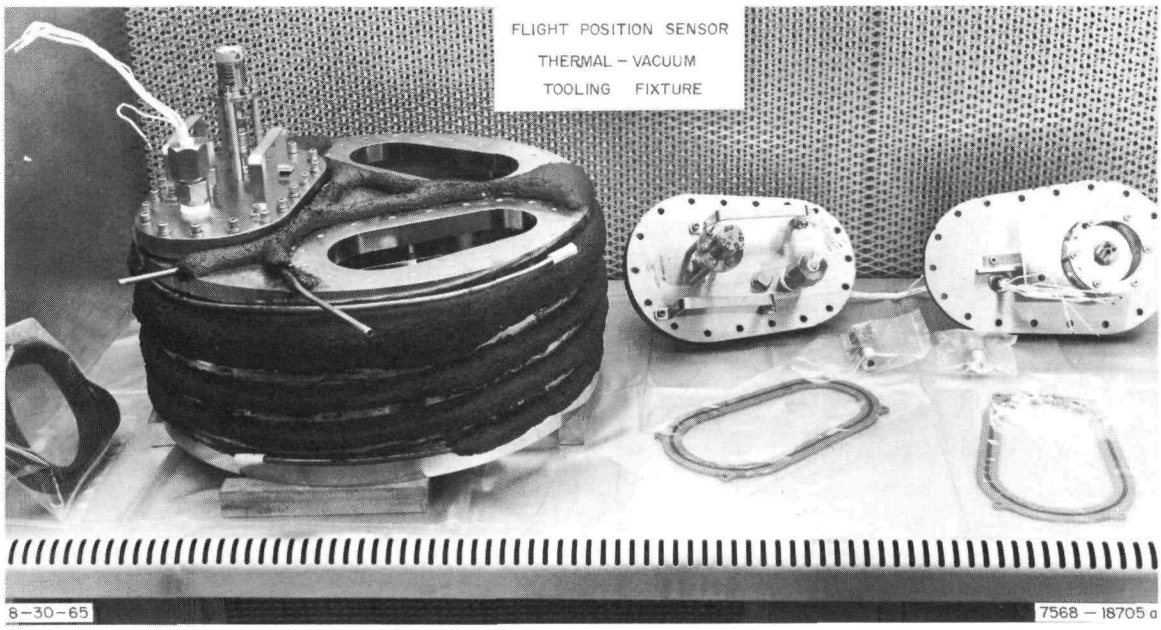

Figure 118. S8DS Flight Position Sensor Thermal-Vacuum Tooling Fixture

3. Component Acceptance Test Tools

Fixtures for acceptance testing S8DS Reactor components are shown in Figures 118 through 124.

Flight position-sensor accuracy, repeatability, dielectric properties, and bearing friction under ambient and thermal-vacuum conditions are determined on the fixture shown in Figure 118. The design of the fixture permits testing of three sensors simultaneously. The limit-switch ambient test fixture (Figure 119) is used to determine the following switch parameters under ambient conditions: (1) contact resistance, (2) dielectric properties under actuated and unactuated conditions, (3) switch pre-travel and overtravel, and (4) force required to depress the plunger to the actuation point. The control-drum actuator is tested on an actuator torque-displacement device (Figure 120) to determine stator phase characteristics; i.e., angular displacement vs torque output.

The snubber absorbs the kinetic energy of a control drum after a scram. The fixture shown in Figure 121 is used to determine snubber plunger compression loads and snubber pawl release force in ambient conditions.

The control-drum drive actuator is tested on the fixture shown in Figure 122, to evaluate torque and voltage-current characteristics, both static and dynamic. The holding capability of the actuator brake is also determined on this test fixture.

The function of the actuator thermal-vacuum fixture (Figure 123) is to test the actuator in temperature and vacuum operating conditions. The rotational accuracy, dielectric strength, and torque characteristics of each actuator are measured.

Limit-switch contact resistance and dielectric strength in thermal-vacuum conditions are determined on the fixture shown in Figure 124. The design of this fixture permits simultaneous test of ten switches.

The hinge and bracket assemblies installed on the first reflector half are shown in Figure 125. The tooling vessel used to establish vessel-reflector physical clearance (gap) is shown in Figures 126 and 117. The reflector half is shimmed to meet gap requirements in Figure 127.

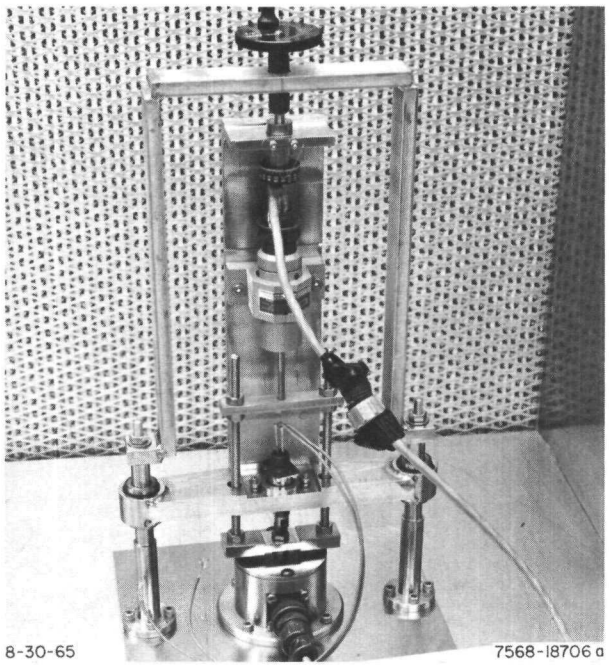

Figure 119. S8DS Limit Switch Ambient Test Fixture

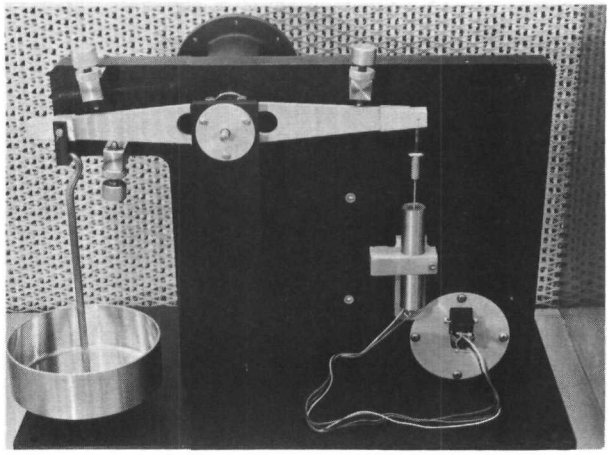

8-30-65 7568-18666a

Figure 120. S8DS Actuator Torque Displacement Device

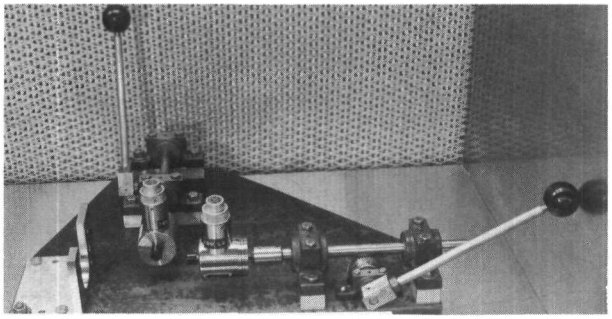

8-30-65 7568-18658a

Figure 121. S8DS Snubber Ambient Test Fixture

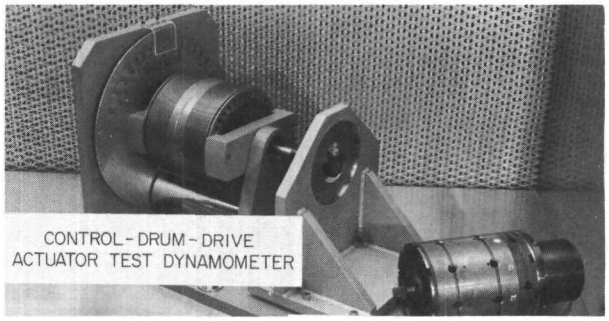

8-30-65 7568-18662a

Figure 122. S8DS Control-Drum-Drive Actuator Test Dynamometer

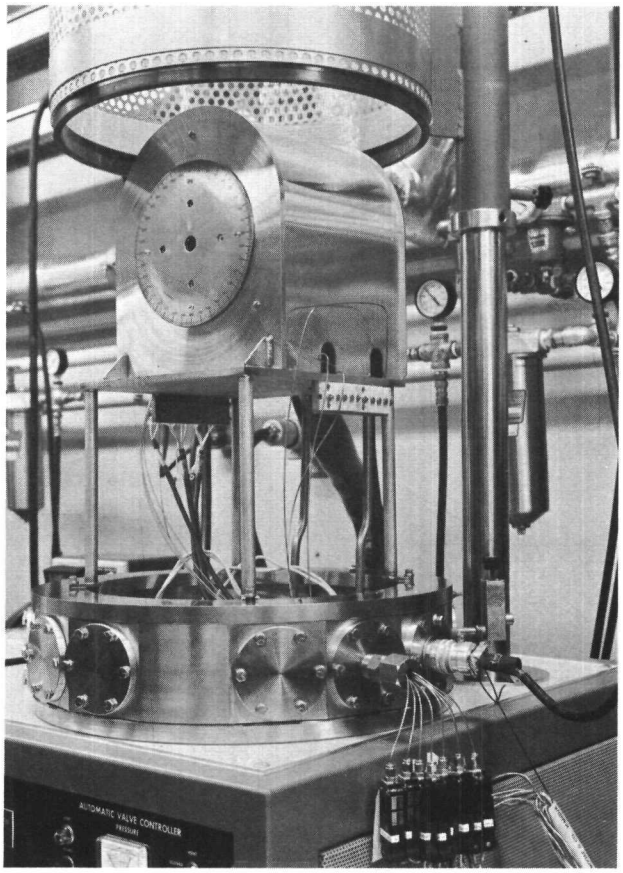

7-14-65 7568-18712

Figure 123. S8DS Actuator Thermal-Vacuum Test Fixture

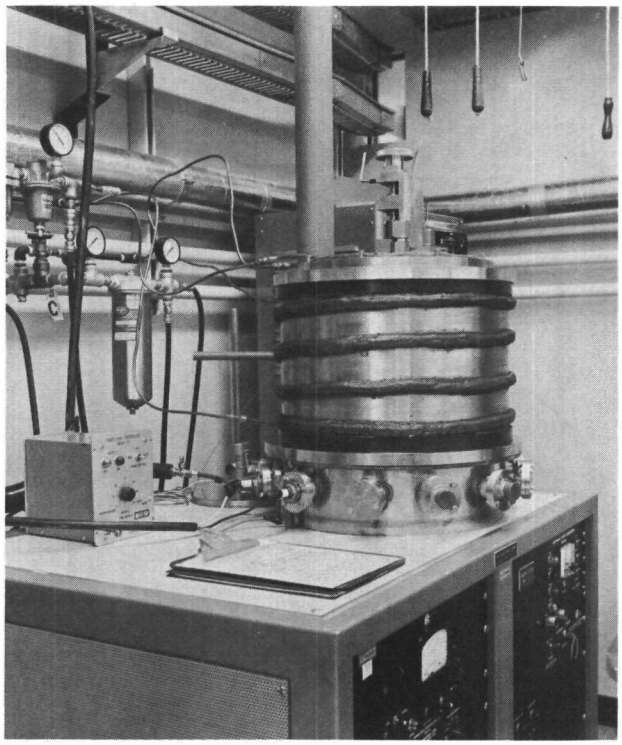

7-14-65 7568-18711

Figure 124. S8DS Limit Switch Thermal-Vacuum Test Fixture

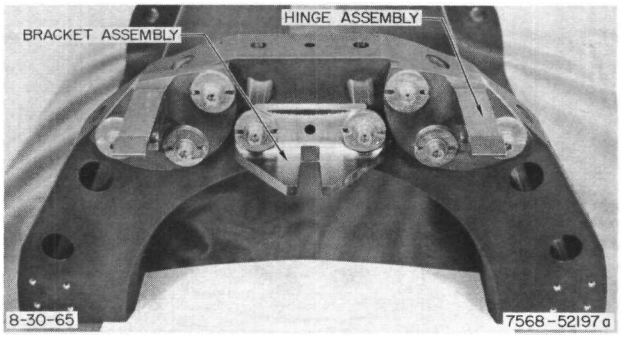

Figure 125. S8DS Reflector Half

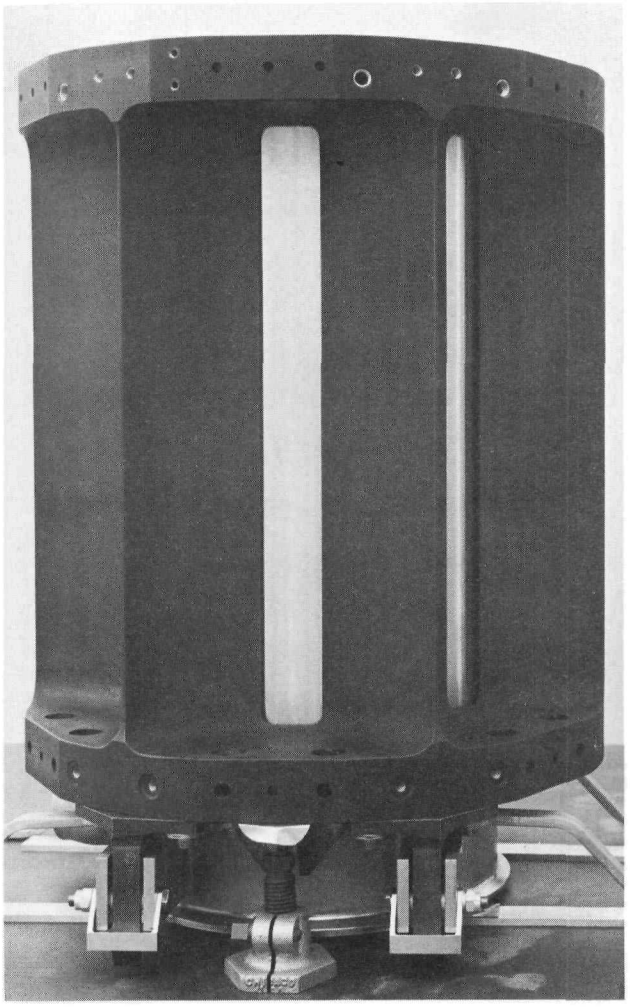

6-29-65 7568-52199

Figure 126. S8DS Tooling Vessel, Z-Half Reflector

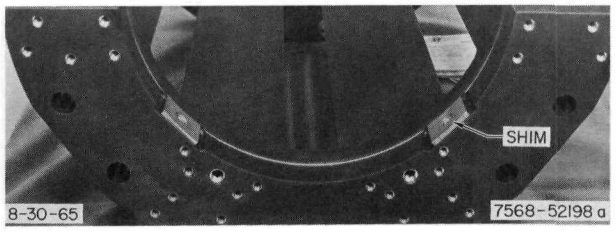

Figure 127. S8DS Half Reflector, Bottom View

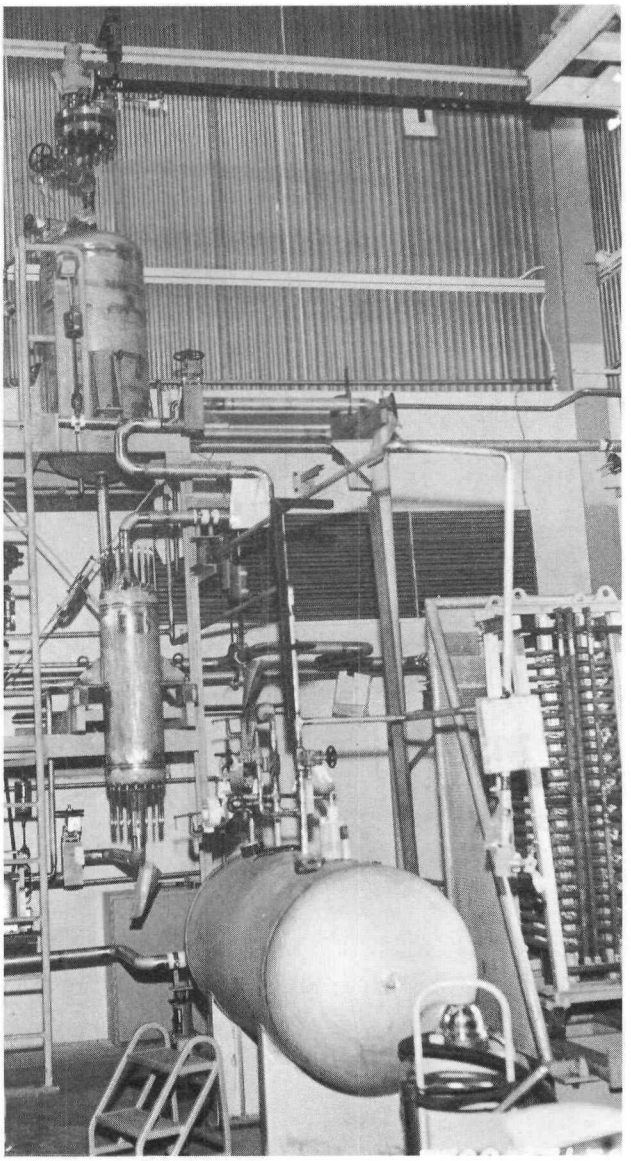

7-9-65 7568-57139

Figure 128. S8DS Secondary Heat Transfer System

H. TEST SUPPORT EQUIPMENT

1. Heat Transfer System

The spooling of the nuclear shakedown system is complete. Installation of equipment in Building 059 was started. The primary fill tank, the secondary cold trap support and blower, secondary support structure, secondary fill tank, secondary EM pump, and 22 supports have been installed in the high bay area. The secondary fill tank, the secondary pump and the secondary support structure, which includes the 150-kw heater and secondary surge tank are shown on Figure 128. The airblast heat exchanger and two supports have been installed on the outside pad. The vent gas storage tank and pressure relief holdup tank were welded in position in the vault. Figure 129 is a view of the vault. It shows the reactor containment vessel, the primary pallet, which consists of the primary surge tank, the intermediate heat exchanger, and the primary pump.

The primary surge tank has been replaced with a larger sized tank. The new surge tank is capable of accommodating expansion of NaK to a system operating temperature of 1400°F.

2. Instrumentation and Electrical

Wiring of the graphic panel and the console in Building 059 was started. Installation of the a-c power to the instrument cabinets continued. Interconnect wire is being installed in the underfloor wiring trays. The instrument wiring in the control room is progressing on schedule. The console, graphic panel, and some instrument racks can be seen on Figure 130.

I. FACILITY MODIFICATION

The contractor completed the installation of the vacuum system and other facility modifications on June 4, 1965.

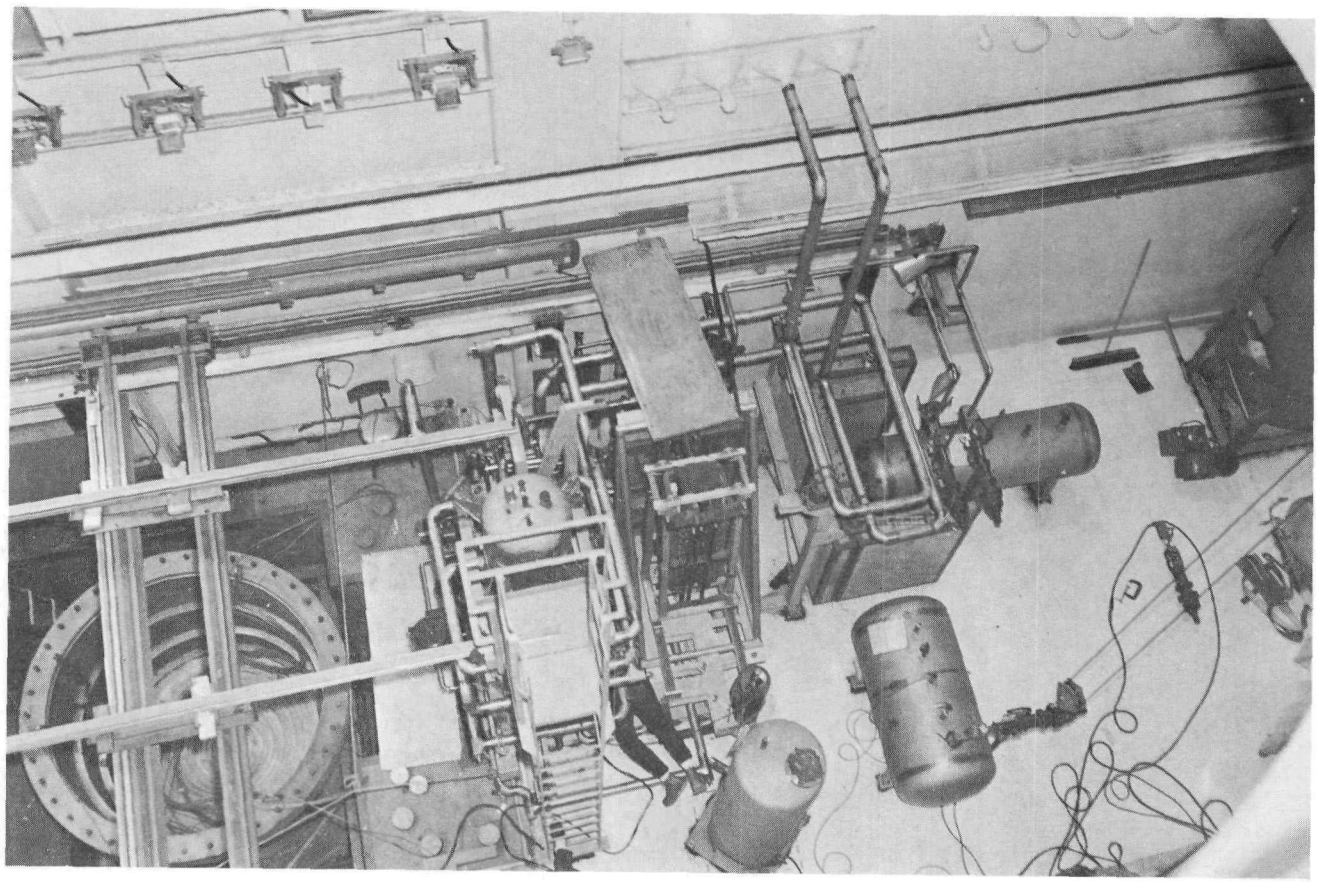

7-19-65

7568-57150

Figure 129. S8DS Vault

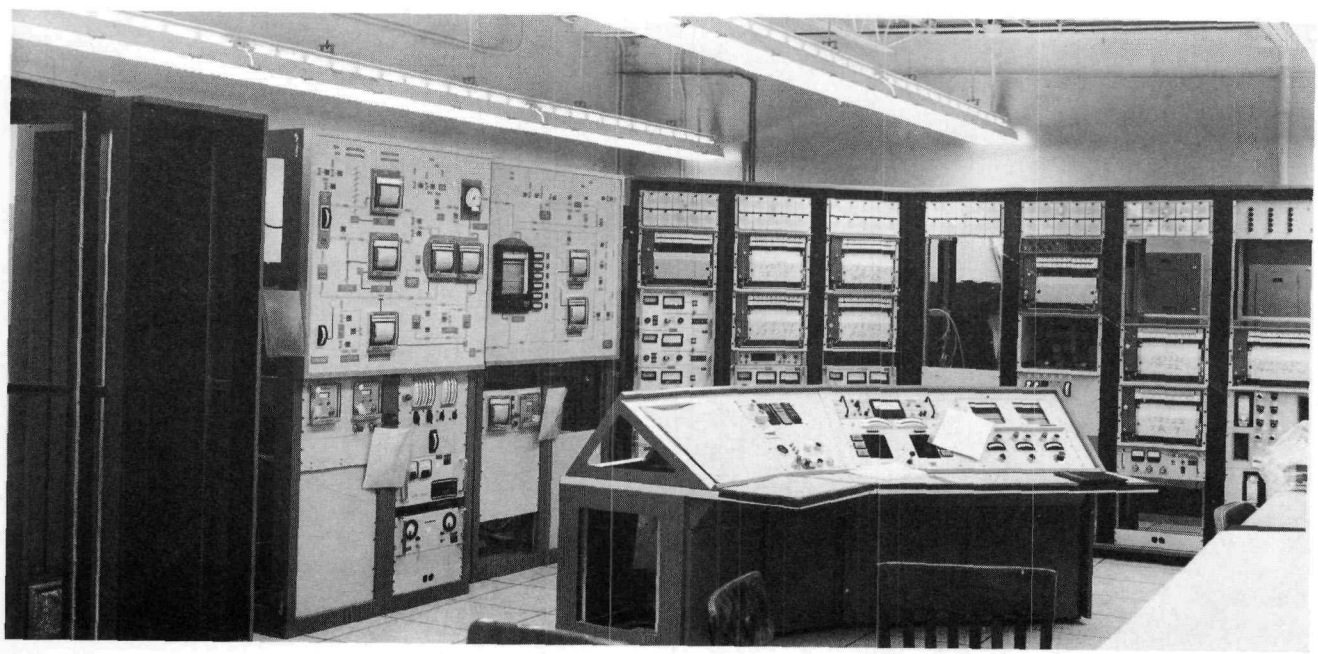

6/2/65

7561-5720

Figure 130. S8DS Console and Instrumentation